Identification of LHC beam loss mechanism : a deterministic treatment of loss patterns

Aurélien Marsili

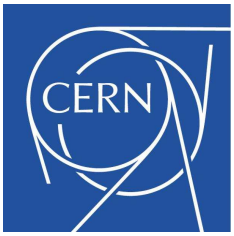

UNIVERSITÉ PARIS-SUD

ÉCOLE DOCTORALE: 534 MIPEGE

Laboratoire: CERN

PHYSIQUE

THÈSE DE DOCTORAT

soutenue le 21/11/2012 par

Aurélien MARSILI

Identification of LHC beam loss mechanism: A deterministic treatment of loss patterns

Directeur de thèse :	Patrick PUZO
Encadrante CERN :	Eva Barbara HOLZER
Composition du jury :	
Président du jury :	Achille STOCCHI
Rapporteurs :	Mike LAMONT
	Amor NADJI
Membre invité :	Jacques MARRONCLE

To Gen,
beacon of sanity in a storm of lunacy.

Acknowledgements

First of all, I would like to thank my girlfriend, Genevieve Steele, for helping to convince me to start a PhD in the first place. Without her incentive, I don't think I would have even started.

Then, amongst the people who allowed this PhD to take place, such as my section leader Bernd Dehning, I owe a lot to my university supervisor, Pr. Patrick Puzo, for accepting me as a PhD student in addition to his already busy schedule. He was the essential link between me and the university, saved me from a lot of administrative work, and above all was there for me every time I needed it. He was an excellent and reliable guidance for a PhD; the kind of supervisor every PhD student whishes to have.

I would like to address a specific thank to my supervisor, Barbara Holzer. She had the insight to let me test some of my ideas for sometimes several days on, with no guarantee of positive results; most of the tools developed for this PhD would have not existed without this freedom, and doing the work would have been much harder. But I am also very grateful for the many discussions of the results and the directions: every time a result was described as "interesting", I knew I was on the right path.

About one of these experiments, I am eternally beholden to my best friend Olivier Pernet. Sometimes two days messing with the right thing with the right people is worth more than an entire year of lessons. He made me moved to Python, which multiplied both creativity and efficiency; I remain convinced that none of this work would have been even possible without that original help.

One a related note, I need to thank people that saved weeks of my work by devoting to me half an hour of their time, by providing precise and efficient advise; and amongst these people are, each one with their own specialty:

Jorg Wenninger, Rhodri Jones, Jean-Jacques Gras, and my colleagues Mariusz Sapinski, Christos Zamantzas and Ewald Effinger.

The one person that helped me the most with all the technical details is with no doubt Annika Nordt. She provided the most help, developing and testing the new database access tool, and was the interface with the database people. Chris Roderick and Ronny Billen deserve a specific thought, for letting us mess with their databases, and for providing the access tools.

I would like to honor the memory of Shennong, the legendary Chinese emperor who discovered tea in 2737 BC. Without his discovery, and the massive trade developed by the United Kingdom in the 18^{th} century, none of this work would have happened.

On a different note, I'd like to thank all my past and present office mates, especially Christoph Kurfürst and Eduardo Nebot del Busto, for being such nice company, quiet when I was working and ready for a break when I needed it. I've never been so happy to go to work. This also includes my "thesis brother" Mohamed Koujili, and his wisdom.

Finally, I would like to thank Gen again for sharing my life all this time, and all the fun that was; for understanding the difficulties of a PhD by doing one herself; and for being always there for me, reliable as ever.

Summary

CERN's Large Hadron Collider (LHC) is the largest device ever built, with a total circumference of 26.7 km; and it is the most powerful accelerator ever, both in beam energy and beam intensity. The main magnets are superconducting, and contain the particles into two counter circulating beams which collide in four interaction points. CERN and the LHC will be described in *chap. 1*

The superconducting magnets of the LHC have to be protected against particle losses. Depending on the number of lost particles, the coils of the magnets could become normal conducting and/or will be damaged. To avoid these events a beam loss monitoring (BLM) system was installed to measure the particle loss rates. If the predefined safe thresholds of loss rates are exceeded, the beams are directed out of the accelerator ring towards the beam dump.

The detectors of the BLM system are mainly ionization chambers located outside of the cryostats. In total, about 3600 ionisation chambers are installed. Further challenges include the high dynamical range of losses (chamber currents ranging between 2 pA and 1 mA). The BLM system will be further described in *chap. 2*.

The subject of this thesis is to study the loss patterns and find the origin of the losses in a deterministic way, by comparing measured losses to well understood loss scenarios. This is done through a case study: different techniques were used on a restrained set of loss scenarios, as a proof of concept of the possibility to extract information from a loss profile. Finding the origin of the losses should allow acting in response. A justification of the doctoral work will be given at the end of *chap. 2*.

This thesis will then focus on the theoretical understanding and the implementation of the decomposition of a measured loss profile as a linear combination of the reference

scenarios; and the evaluation of the error on the recomposition and its correctness. The principles of vector decomposition are developed in *chap. 3*.

An ensemble of well controlled loss scenarios (such as vertical and horizontal blow-up of the beams or momentum offset during collimator loss maps) has been gathered, in order to allow the study and creation of reference vectors. To achieve the Vector Decomposition, linear algebra (matrix inversion) is used with the numeric algorithm for the Singular Value Decomposition. Additionally, a specific code for vector projection on a non-orthogonal basis of a hyperplane was developed. The implementation of the vector decomposition on the LHC data is described in *chap. 4*.

After this, the use of the decomposition tools systematically on the time evolution of the losses will be described: first as a study of the variations second by second, then by comparison to a calculated default loss profile. The different ways to evaluate the variation are studied, and are presented in *chap. 5*.

The next chapter *(6)* describes the gathering of decomposition results applied to beam losses of 2011. The vector decomposition is applied on every second of the "stable beams" periods, as a study of the spatial distribution of the loss. Several comparisons of the results given by the decompositions with measurements from other LHC instruments allowed different validations.

Eventually, a global conclusion on the interest of the vector decomposition technique is given.

Then, the extra chapter in *Appendix A* describes the code which was developed to access the BLM data, to represent them in a meaningful way, and to store them. This included connecting to different databases. The whole instrument uses ROOT objects to send SQL queries to the databases, as well as java API, and is coded in Python.

A short glossary of the acronyms used here can be found at the end, before the bibliography.

Résumé

Le *Large Hadron Collider (LHC)* du CERN, avec un périmètre de 26,7 km, est la plus grande machine jamais construite et l'accélérateur de particules le plus puissant, à la fois par l'énergie des faisceaux et par leur intensité. Les aimants principaux sont supraconducteurs, et maintiennent les particules en deux faisceaux circulants à contre–sens, qui entre en collision en quatre points d'interaction différents.

Ces aimants doivent être protégés contre les pertes de faisceau : ils peuvent subir une transition de phase et redevenir résistifs, et peuvent être endommagés. Pour éviter cela, des moniteurs de pertes de faisceau, appelés *Beam Loss Monitors (BLM)* ont été installés. Si les seuils de pertes maximum autorisées sont dépassés, les faisceaux sont rapidement enlevés de la machine.

Les détecteurs du système BLM sont en majorité des chambres d'ionisation situées à l'extérieur des cryostats. Au total, environ 3600 chambres d'ionisation ont été installées. Les difficultés supplémentaires comprennent la grande amplitude dynamique des pertes : les courants mesurés s'échelonnent de 2 pA jusqu'à 1 mA.

Le sujet de cette thèse est d'étudier les structures de pertes et de trouver l'origine des pertes de façon déterministe, en comparant des profils de pertes mesurés à des scénarios de pertes connus. Ceci a été effectué par le biais d'une étude de cas : différentes techniques ont été utilisées sur un ensemble restreint de scénarios de pertes, constituant une preuve de concept de la possibilité d'extraire de l'information d'un profil de pertes. Trouver l'origine des pertes doit pouvoir permettre d'agir en conséquence, ce qui justifie l'intérêt du travail doctoral.

Ce travail de thèse se focalise sur la compréhension de la théorie et la mise en place de la décomposition d'un profil de pertes mesuré en une combinaison linéaire des scénarios de référence ; sur l'évaluation de l'erreur sur la recomposition et sa validité.

Un ensemble de scénarios de pertes connus (e.g. l'augmentation de la taille du faisceau dans les plans vertical et horizontal ou la différence d'énergie lors de mesures de profils de pertes) ont été réunis, permettant l'étude et la création de vecteurs de référence. Une technique d'algèbre linéaire (inversion de matrice), l'algorithme numérique de *décomposition en valeurs singulières (SVD)*, a été utilisé pour effectuer cette décomposition vectorielle. En outre, un code spécifique a été développé pour la projection vectorielle sur une base non-orthogonale d'un sous-espace vectoriel. Ceci a été mis en place avec les données du LHC.

Ensuite, les outils de décomposition vectorielle ont été systématiquement utilisés pour étudier l'évolution temporelle des pertes : d'abord par la variation d'une seconde à l'autre, puis par différentes comparaisons avec un profil de pertes par défaut calculé pour l'occasion.

Puis, les résultats des décompositions ont été calculés pour les pertes à chaque seconde des périodes de "faisceaux stables" de l'année 2011, pour l'étude de la distribution spatiale des pertes. Les résultats obtenus ont été comparés avec les mesures d'autres instruments de faisceau, pour permettre différentes validations.

En conclusion, l'intérêt de la décomposition vectorielle est présenté.

Ensuite est décrit le code développé pour permettre l'accès aux données des BLMs, pour les représenter de façon utilisable, et pour les enregistrer. Ceci inclus la connection à différentes bases de données. L'instrument utilise des objets ROOT pour envoyer des requêtes SQL aux bases de données ainsi que par une interface Java, et est codé en Python.

Un court glossaire des acronymes utilisés dans cette thèse est disponible à la fin du document, avant la bibliographie.

Synthèse

Le *Large Hadron Collider (LHC)* du CERN, avec un périmètre de 26,7 km, est la plus grande machine jamais construite et l'accélérateur de particules le plus puissant, à la fois par l'énergie des faisceaux et par leur intensité. Les aimants principaux sont supraconducteurs, et maintiennent les particules en deux faisceaux circulants à contre–sens, qui entre en collision en quatre points d'interaction différents.

0.1 La protection du LHC

L'énergie totale contenue par un faisceau, 362 MJ à 7 TeV, correspond a l'énergie de 87 kg de TNT. Celle contenue dans les aimants, 10 GJ, correspond à 2.4 tonnes. En outre, les aimants supraconducteurs sont refroidis à l'helium liquide. Si une trop grande partie de cette énergie vient à être libérée en un seul endroit, les aimants peuvent subir une transition de phase de supraconducteurs à résistifs. L'énergie libérée et/ou l'augmentation de température peuvent causer des dommages importants (l'helium en phase gazeuse occupe un volume 750 fois plus important), et des temps d'arrêt de l'accélérateur. Celui-ci doit donc être protégé.

Pour cela, de nombreux systèmes ont été installés. Les systèmes dits passifs, commes les *collimateurs* et les absorbeurs, sont des éléments sur lesquels les particules les plus à risque peuvent être perdues de façon sûre. Les systèmes actifs contrôlent le maintient des faisceaux dans l'accélérateur. En cas de risque, les faisceaux sont rapidement extraits et dirigés vers un absorbeur; cette opération est appelée *beam dump*. Le système actif utilisé dans ce travail doctoral est l'ensemble des moniteurs de perte de faisceau *(*Beam Loss Monitors, BLM). Si les pertes dépassent les seuils maximum autorisés, un beam dump est déclenché

Les collimateurs sont des éléments composés de deux mâchoires parallèles au faisceau, qui peuvent être en Carbone, Cuivre ou Tungsten. L'écart entre les mâchoires est variable, contrôlé à 5 μm près, et est exprimé en unité d'écart-type du faisceau nominal, appelés σ. Un total de 88 collimateurs sont installés dans le LHC. La position des mâchoires dans les plans transverses (horizontale, verticale ou diagonale) a une place importante dans le rôle du collimateur.

Les différents types collimateurs (primaires, secondaires, absorbeurs, tertiaires) suivent une hiérarchie précise: les écarts entre les mâchoires sont de plus en plus importants *(cf. fig. 1)*. Les protons déviés par les collimateurs primaires seront absorbés par d'autres collimateurs plus ouverts. Les protons absorbés créent des gerbes de particules secondaires qui seront détectées par les moniteurs de perte de faisceau.

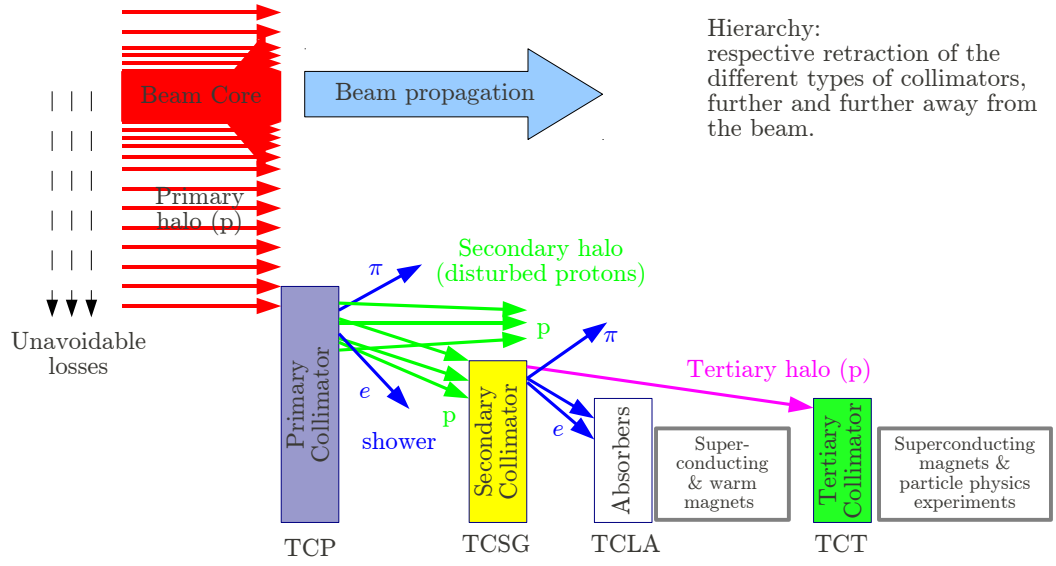

Figure 1: Schéma du système de collimation en plusieurs étages au LHC. Les materiaux sont: graphite renforcée à la fibre de carbone (CC), Cuivre (CU) aet Tungsten (W).

0.2 Moniteurs de perte de faisceau

Les détecteurs de pertes de faisceau du système BLM sont en majorité des chambres d'ionisation de 60 cm de long, situées à l'extérieur des cryostats. Les particules chargées

qui traversent les chambre ionisent le gaz, et le champ électrique appliqué sépare les ions des électrons, vers les électrodes de collection. Le signal est proportionnel à l'énergie déposée dans la chambre. Au total, environ 3600 chambres d'ionisation ont été installées. Les difficultés supplémentaires comprennent la grande amplitude dynamique des pertes : les courants mesurés s'échelonnent de 2 pA jusqu'à 1 mA.

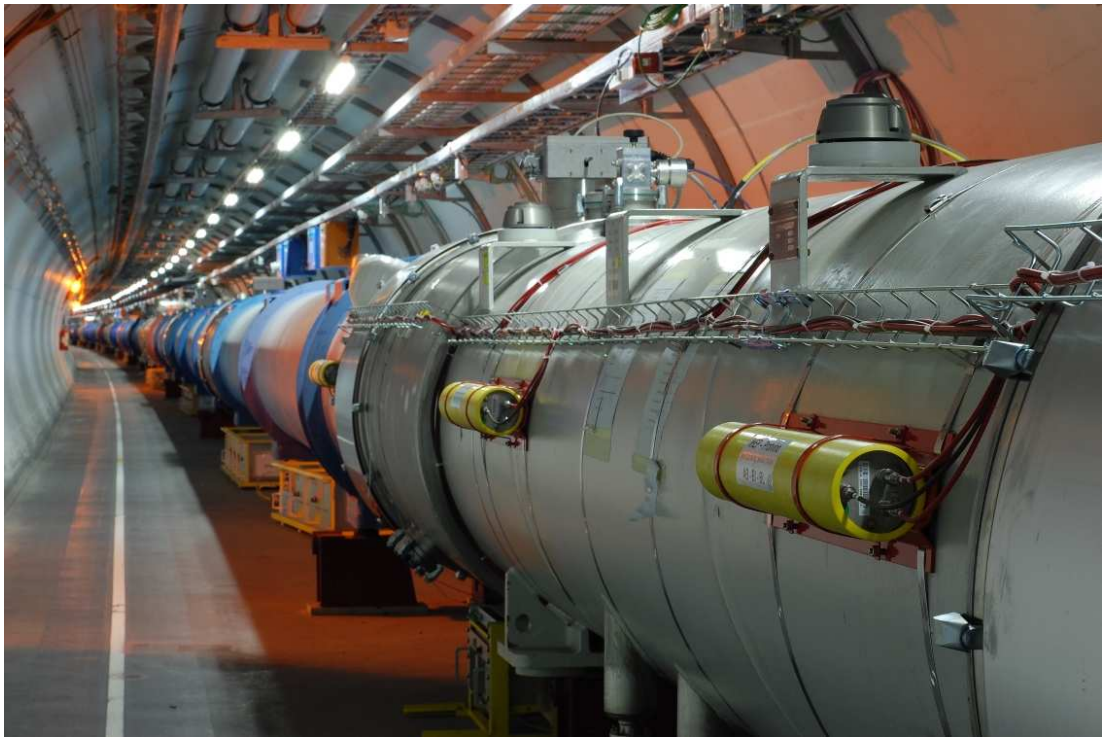

Figure 2: Exemple de l'installation de trois BLMs (chambres d'ionisation) sur le côté interne d'un quadrupole du LHC. Trois autres BLMs sont installés du côté externe. Les quadrupoles ont un cryostat de couleur grise, et les dipôles sont en bleu. (Photo D. Kramer.)

Dans le tunnel, la charge collectée dans chaque chambre est convertie en fréquence. Ce signal est ensuite analysé en surface par les comparateurs de seuil: si les pertes mesurées dépassent les seuils pré-établis, le faisceau est retiré du LHC.

La position des BLM autour des aimants découle de simulations d'interactions particules/matière, prenant en compte les positions des pertes les plus probables et le développement des gerbes secondaires dans les matériaux. En outre, de nombreux instruments de faisceau, comme les collimateurs, ont un BLM associé.

0.3 Intérêt du travail doctoral

Avant le début de ce travail doctoral, de nombreuses études des pertes avaient été effectuées à l'échelle locale: autour d'un élément. Cependant, aucune éude n'avait été effectuée à l'échelle globale, en considérant tous les moniteurs du LHC en même temps. La seule information donnée par un moniteur est la mesure des pertes à l'élément associé; mais une seule gerbe secondaire peut être détectée par plusieurs moniteurs; et certains des effets à l'orgine de pertes impliquent tout le LHC. Le nombre élevé de BLMs nécéssite un traitement automatique.

Le sujet de cette thèse est d'étudier les structures de pertes et de trouver l'origine des pertes de façon déterministe, en comparant des profils de pertes mesurés à des scénarios de pertes connus. Ceci a été effectué par le biais d'une étude de cas : différentes techniques ont été utilisées sur un ensemble restreint de scénarios de pertes, constituant une preuve de concept de la possibilité d'extraire de l'information d'un profil de pertes. Trouver l'origine des pertes doit pouvoir permettre d'agir en conséquence, ce qui justifie l'intérêt du travail doctoral.

Ce travail de thèse se focalise sur la compréhension de la théorie et la mise en place de la décomposition d'un profil de pertes mesuré en une combinaison linéaire des scénarios de référence ; sur l'évaluation de l'erreur sur la recomposition et sa validité.

0.4 Principe de la décomposition vectorielle

0.4.1 Espace vectoriel

Un profil de pertes est un ensemble de pertes mesurées par différents moniteurs (situés à différentes positions longitudinales le long du LHC) à un instant donné. On considère d'abord m moniteurs, et un espace vectoriel de dimension m associé. Chaque profil de pertes peut donc être représenté comme un vecteur de cet espace vectoriel, où chaque coordonnée j du vecteur est la perte mesurée au moniteur j. En outre, des pertes négatives n'ont aucune réalité physique: les coordonnées des vecteurs sont donc toutes positives, et on ne considère que la partie positive de l'espace vectoriel : $(\mathbb{R}^+)^m$. Les vecteurs sont tous normalisés pour avoir une norme de valeur 1.

On considère ensuite n profils de pertes de référence, et leurs vecteurs associés $(\vec{v}_i)$. Il est important de noter que $n < m$. Enfin, on considère un profil de pertes mesuré

appelé $\vec{X}$.

Le but de la décomposition vectorielle est de décomposer $\vec{X}$ en une combinaison linéaire des vecteurs $(\vec{v_i})$, c'est-à-dire de résoudre l'équation vectorielle:

$$\vec{X} = a \cdot \vec{v_1} + b \cdot \vec{v_2} + \cdots \quad \text{pour les } \{a, b, \ldots\} \tag{1}$$

Pour cela, deux techniques sont utilisées: par une succession de projections des vecteurs $(\vec{v_i})$ (non orthogonaux) dans l'espace vectoriel (procédé de Gram-Schmidt, G-S); et par des opérations matricielles. Puisque $n < m$, la matrice des vecteurs $(\vec{v_i})$ (notée M) n'est pas carrée, et son inversion n'est pas simple. On utilise donc l'algorithme de décomposition en valeurs singulières (*Singular Values Decomposition, SVD*).

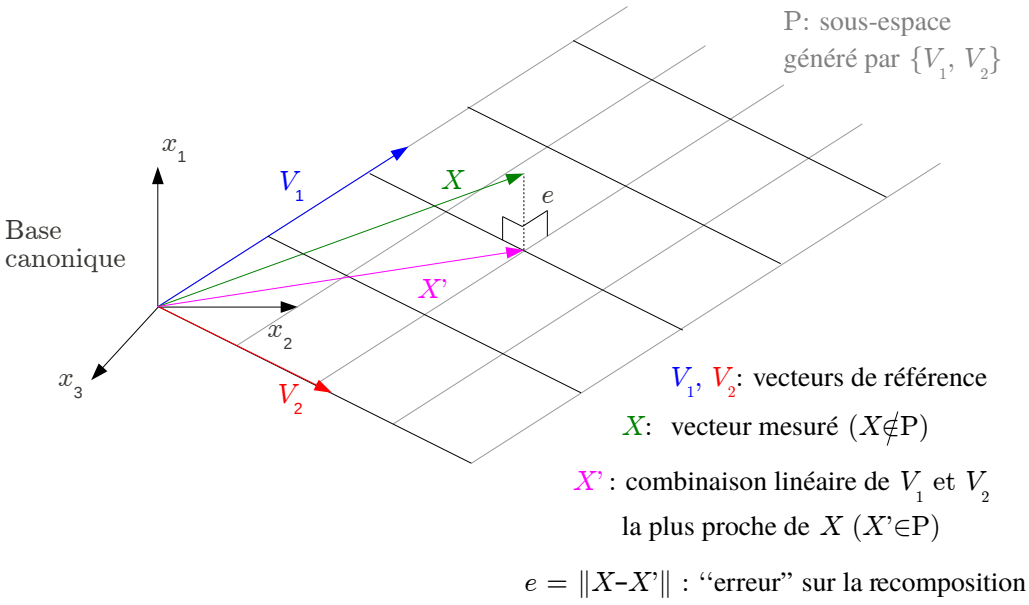

Figure 3: Exemple simplifié de décomposition vectorielle en 3 dimensions: $n = 2$, $m = 3$. Le vecteur $\vec{X}$ n'appartient pas au sous-espace P généré par $(\vec{V_1}, \vec{V_2})$. La recomposition $\vec{X}'$ correspond à la projection de $\vec{X}$ sur P. L'erreur sur la recomposition correspond a la norme euclidenne de la difference entre $\vec{X}$ et $\vec{X}'$.

Il est important de noter que le vecteur $\vec{X}$ n'appartient pas forcément au sous-espace généré par les vecteurs de référence $(\vec{v_i})$ *(cf. fig. 3)*. Pour évaluer la qualité de la décomposition, une erreur sur la recomposition e a été définie comme la norme euclidienne du vecteur de la différence entre le vecteur mesuré $\vec{X}$ et sa recomposition $\vec{X}'$.

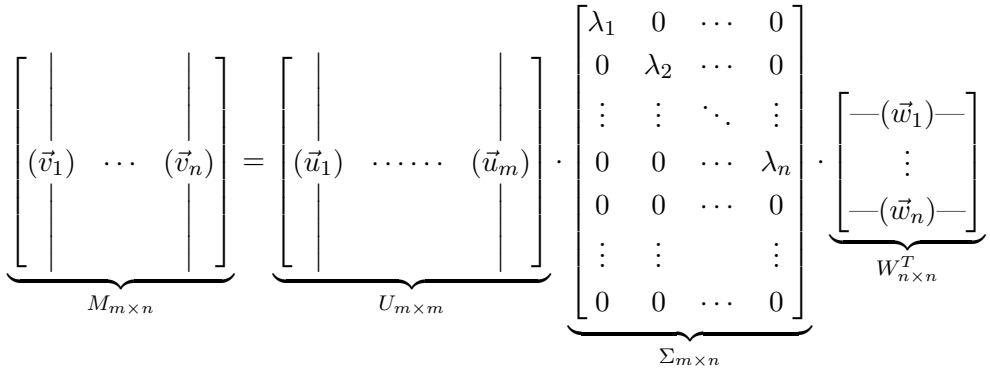

Figure 4: Structure des matrices utilisées dans la décomposition. M est la matrice de départ, composée des vecteurs $(\vec{v}_i)$; U et W sont les matrices des vecteurs singuliers à droite et à gauche respectivement. Σ une matrice diagonale (où $n < m$) contenant les *valeurs singulières*: toutes ses valeurs sont nulles sauf celles de la diagonale $\lambda_i = (\Sigma)_{i,i}$.

0.4.2 Décomposition en Valeurs Singulières (SVD)

L'équation vectorielle (1) peut s'écrire sous forme matricielle:

$$\vec{X} = M \cdot \vec{F} \tag{2}$$

où $\vec{F}$ est le vecteur formé par les coefficients {a, b, ...} et M est la matrice formée par les vecteurs $(\vec{v}_i)$.

La matrice M n'étant pas carrée, on utilise d'abord la décomposition en valeurs singulières (SVD, *cf. fig. 4*) pour pouvoir l'inverser ultérieurement:

$$M = U \cdot \Sigma \cdot W$$

La matrice inverse M^+ est calculé par:

$$M^+ \equiv W \cdot \Sigma^+ \cdot U^T$$

Le vecteur $\vec{F}$ est donné par:

$$\vec{F} \simeq M^+ \cdot \vec{X}$$

et la recomposition $\vec{X}'$ par:

$$\vec{X}' = M \cdot \vec{F} \simeq M \cdot M^+ \cdot \vec{X}$$

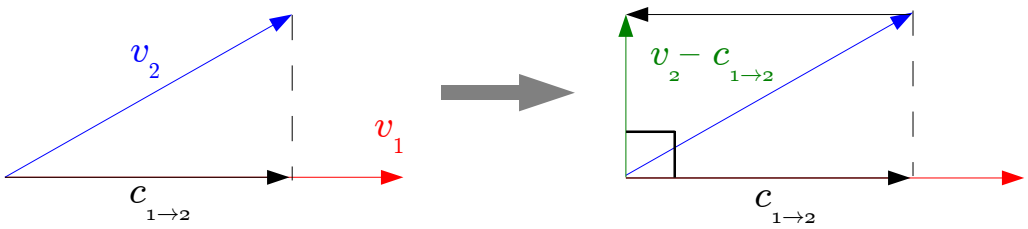

Figure 5: Première étape du procédé de Gram-Schmidt. On calcule la projection (en noir) de $\vec{v_2}$ (en bleu) sur $\vec{v_1}$ (en rouge), ce qui correspond à la contribution de $\vec{v_1}$ à $\vec{v_2}$. Puis on soustrait cette contribution pour obtenir un vecteur perpendiculaire a $\vec{v_1}$ (en vert). Cette opération est ensuite répétée avec le vecteur suivant.

0.4.3 Le procédé de Gram-Schmidt (G-S)

Le procédé de Gram-Schmidt (G-S) est un ensemble d'opérations vectorielles visant à créer une base orthonormale à partir d'un ensemble de vecteurs non orthogonaux *(cf. fig. 5)*. Une fois une base orthonormale créée, le vecteur $\vec{X}$ peut être projeté. Cependant, la base n'est pas unique: elle dépend de l'ordre dans lequel les vecteurs $(\vec{v_i})$ sont considérés. Les vecteurs sont donc ordonnés suivant leur distance (norme euclidenne de la différence) à $\vec{X}$.

0.5 Mise en place de la décomposition vectorielle

Un ensemble de scénarios de pertes connus ont été réunis, permettant l'étude et la création de vecteurs de référence. Ces scénarios correspondent à l'augmentation de la taille du faisceau dans les plans vertical et horizontal lors du passage de la résonnance 1/3 du tune du LHC, et à la différence d'énergie (plan longitudinal) lors de mesures de profils de pertes, pour chaque faisceau. Ces six scénarios correspondent aux collimateurs primaires du LHC.

L'ensemble des moniteurs significatifs (représentant les coordonnées des vecteurs) a été choisi suivant des règles spécifiques. Ces moniteurs devaient:

- présenter un écart–type très faible (négligeable devant la valeur moyenne) calculé

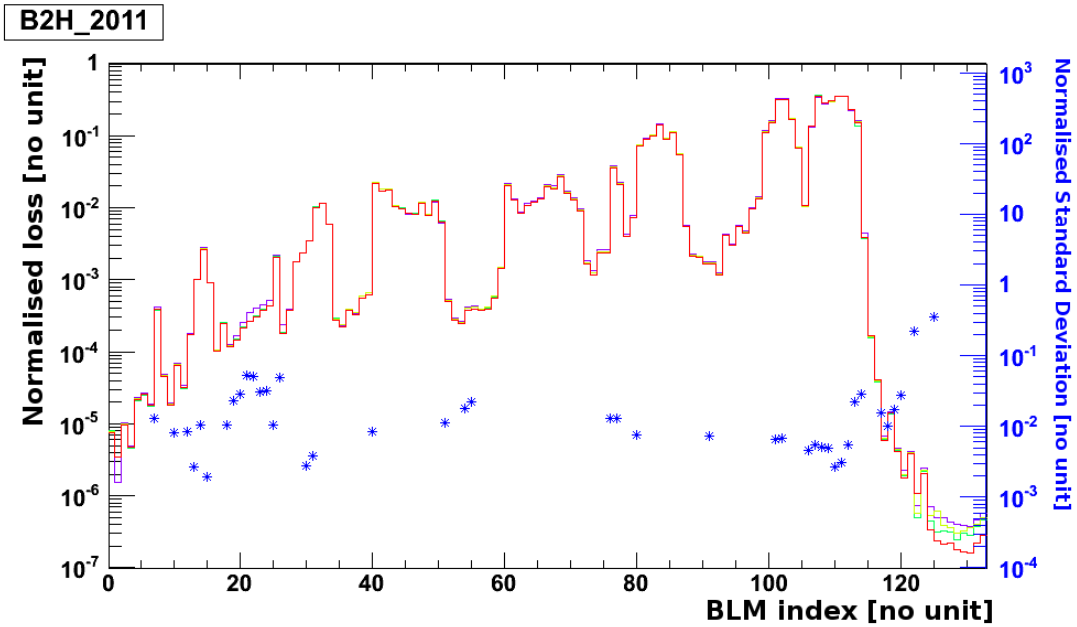

Figure 6: Exemple de sélection des profils de pertes après normalisation, pour les moniteurs du point 7, et le scénario correspondant au faisceau 2 horizontal. Les étoiles bleues correspondent à la valeur de l'écart–type normalisé pour les moniteurs sélectionnés. La qualité de la reproductibilité des mesures est visible par le fait que les profils sont presque indiscernables après normalisation; et par les valeurs d'écart-type, autour de 1% de la valeur moyenne pour chaque moniteur.

sur l'ensemble des mesures correspondant à un seul scénario (afin de s'assurer que le moniteur soit bien représentatif);

- présenter un écart–type important lorsque calculé pour les mesures des tous les scénarios possibles (afin de s'assurer que le moniteur soit bien discriminant d'un scénario à un autre).

La sélection finale des moniteurs pour le point 7 (plans transverses) est présentée dans la table *4.2*. Pour le plan longitudinal, la même technique de sélection a été utilisée, mais aucun profil de pertes n'est disponible pour un faisceau isolé car les deux faisceaux sont accélérés en même temps. Des profils de pertes on pu être recréés en assignant une valeur nulle aux moniteurs associés au faisceau non considéré. Les collimateurs tertiaires ont aussi été ajoutés, en leur associant le vecteur canonique correspondant, puisqu'aucun profil de perte n'est disponible.

Enfin, puisque la décomposition donne toujours un résultat, la justesse de la décomposition doit être évaluée, en utilisant l'erreur sur la recomposition *(cf. fig. 3)*. La décomposition

de profils de pertes connus correspondand à des scénarios connus permet de juger si le résultat de la décomposition est correct ou non. Les différents résultats ont permis d'établir des seuils dans la valeur de l'erreur: en-dessous de 0.1, la décomposition est correcte; au-dessus de 0.3, elle est incorrecte.

0.6 Evolution temporelle

Les outils de décomposition vectorielle ont été systématiquement utilisés pour étudier l'évolution temporelle des pertes. D'abord, la variation d'une seconde à l'autre du profil de perte contenant les 3600 moniteurs du LHC a été considéré, puis différentes comparaisons avec un profil de pertes par défaut calculé pour l'occasion. Ceci a montré que les différentes quantités considérées était bien équivalentes, mais que la plus représentative était bien la norme de la différence avec un vecteur fixe, comme pour l'erreur sur la recomposition.

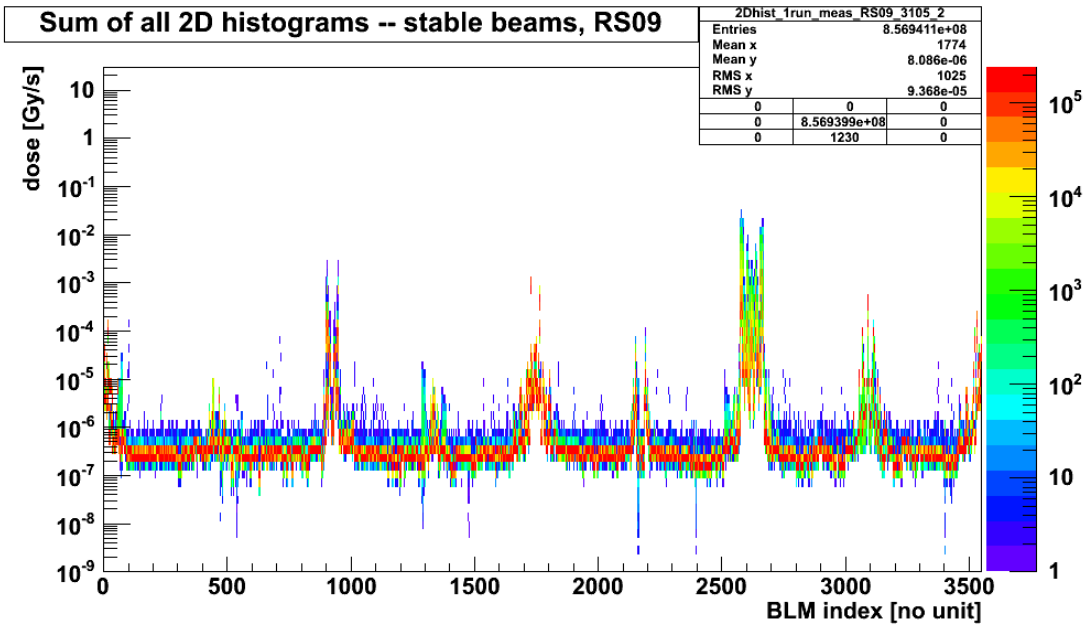

Figure 7: Profil de pertes par défaut, représenté par un histogramme a 2 dimensions, mesuré pendant $\simeq 70$ h. Chaque colonne correspond à un moniteur: l'indice du moniteur est indiqué sur l'axe horizontal, et la valeur de la perte à chaque seconde est reportée sur l'axe vertical. Le nombre d'entrées par case (pertes de même intensité) est représenté par l'échelle de couleurs. Les 8 arcs sont visibles, séparés par les régions d'insertion (pertes plus élevées).

Le profil de pertes par défaut, mesuré sur une centaine d'heures de faisceaux stable,

a apporté de nombreuses observations. Durant la période considérée, aucune perte n'a été enregistrée dans les arcs, et la résolution de la mesure est inférieur à un bit du système d'acquisition. Les seuls moniteurs pertinents pour cette étude sont ceux qui présentent une fluctuation importante, justifiant le choix des points 3 et 7, et des collimateurs tertiaires.

0.7 Décomposition spatiale

Les résultats des décompositions ont été calculés pour les pertes à chaque seconde des périodes de "faisceaux stables" de l'année 2011, pour l'étude de la distribution spatiale des pertes. Les facteurs sont présenté en fonction du temps, pour les deux techniques de décomposition; l'erreur sur la recomposition est aussi représentée sur le même graphe *(cf. fig. 8)*. Les facteurs associés au collimateurs tertiaires sont représentés sur un graphe à part. Ceci permet de visualiser quel type de pertes domine le vecteur mesuré à chaque seconde.

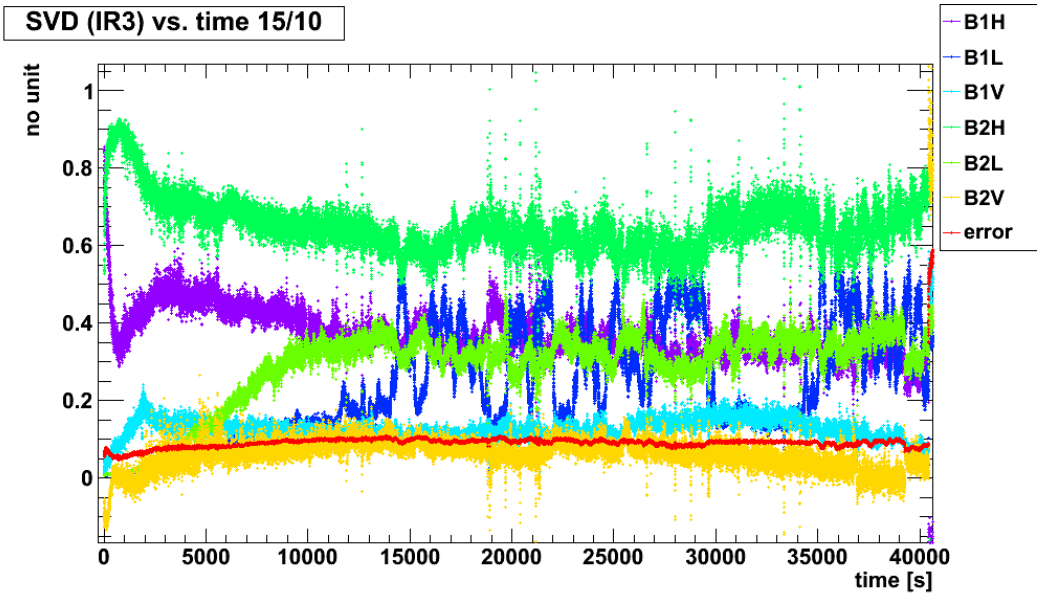

Figure 8: Exemple de représentation des résultats de la décomposition (SVD) en fonction du temps. La décomposition est dominée par le facteur du faisceau 2 horizontal. L'erreur sur la recomposition est représentée en rouge. Les pertes associées au plan longitudinal augmentent au cours des trois premières heures, puis se stabilisent (autour de 10 000 secondes).

Les résultats obtenus ont été comparés avec les mesures d'autres instruments de fais-

ceau, pour permettre différentes validations. Une première validation a été de vérifier que les pertes de faisceau se comportent bien comme la dérivée de l'intensité dans ce faisceau, lors d'une periode de faisceau stable où l'intensité diminuait plus rapidement dans le faisceau 1 que dans le faisceau 2.

La validité de la décomposition a aussi été vérifiée lors d'opérations sur les faisceaux pendant lesquels différents collimateurs sont refermés, créant des pertes importantes. Même lorsque deux collimateurs étaient déplacés en même temps, la décomposition est clairement dominée par un seul facteur; ceci est vérifié par les intensités dans les faisceaux, qui ne varient pas en même temps.

0.8 Conclusion & Appendices

En conclusion, l'intérêt de la décomposition vectorielle est présenté. Des structures spatiales de pertes ont été identifiées, et des techniques ont été développées pour permettre de les identifier dans un profil de pertes mesuré. La justesse de la décomposition a été évaluée, et les résultats vérifié grâce à d'autres instruments de mesure du faisceau. Un profil de pertes par défaut a aussi été mesuré pour étudier l'évolution temporelle des pertes.

L'outil de décomposition a depuis été adapté pour être utilisé en temps réel dans le centre de contrôle du LHC, et aider à l'opération de la machine et détecter des pertes inhabituelles. La validité des résultats dépend des vecteurs de référence. Les possibilités d'utilisation pourraient être étendue en créant de nouveaux vecteurs, pour d'autres scénarios, d'autres modes de faisceau; ou même en utilisant d'autres techniques de décomposition. L'outil pourrait même être utilisé dans d'autres machines où des profils de pertes peuvent être mesurés.

En appendice est décrit le code développé pour permettre l'accès aux données des BLMs, pour les représenter de façon utilisable, et pour les enregistrer. Ceci inclus la connexion à différentes bases de données. L'instrument utilise des objets ROOT pour envoyer des requêtes SQL aux bases de données ainsi que par une interface Java, et est codé en Python.

Un court glossaire des acronymes utilisés dans cette thèse est disponible à la fin du document, avant la bibliographie.

Contents

Chapter 1

The Large Hadron Collider and its protection

1.1 CERN

When CERN was founded in 1954, the name originally meant "Conseil Européen pour la Recherche Nucléaire", referring to a provisional body founded two years earlier. Its goal was to establish a world-class fundamental physics research organization in Europe. At the time, the most fundamental physics research was the study of the inside of an atom, thus the use of "nuclear" in the title of the new organisation: "European organisation for nuclear research". The name CERN was kept.

Today, the most fundamental physics studies concentrate on the basic constituents of matter: the fundamental particles. This is done by increasing the energy of particles in *accelerators*, and having the particles collide in *detectors* analysing these events. CERN's title is now the European laboratory for particle physics.

CERN is now the world's largest laboratory. It is run by 20 countries: Germany, France, United Kingdom, Italy, Spain, the Netherlands, Switzerland, Poland, Belgium, Sweden, Norway, Austria, Greece, Denmark, Finland, the Czech Republic, Portugal, Hungary, Slovakia, and Bulgaria. Many other countries, including Russia, Japan and the United States, are involved in the CERN programs.

The mission of CERN is clearly described in its convention:

"The Organization shall provide for collaboration among European States in nuclear research of a pure scientific and fundamental character (...). The Organization shall

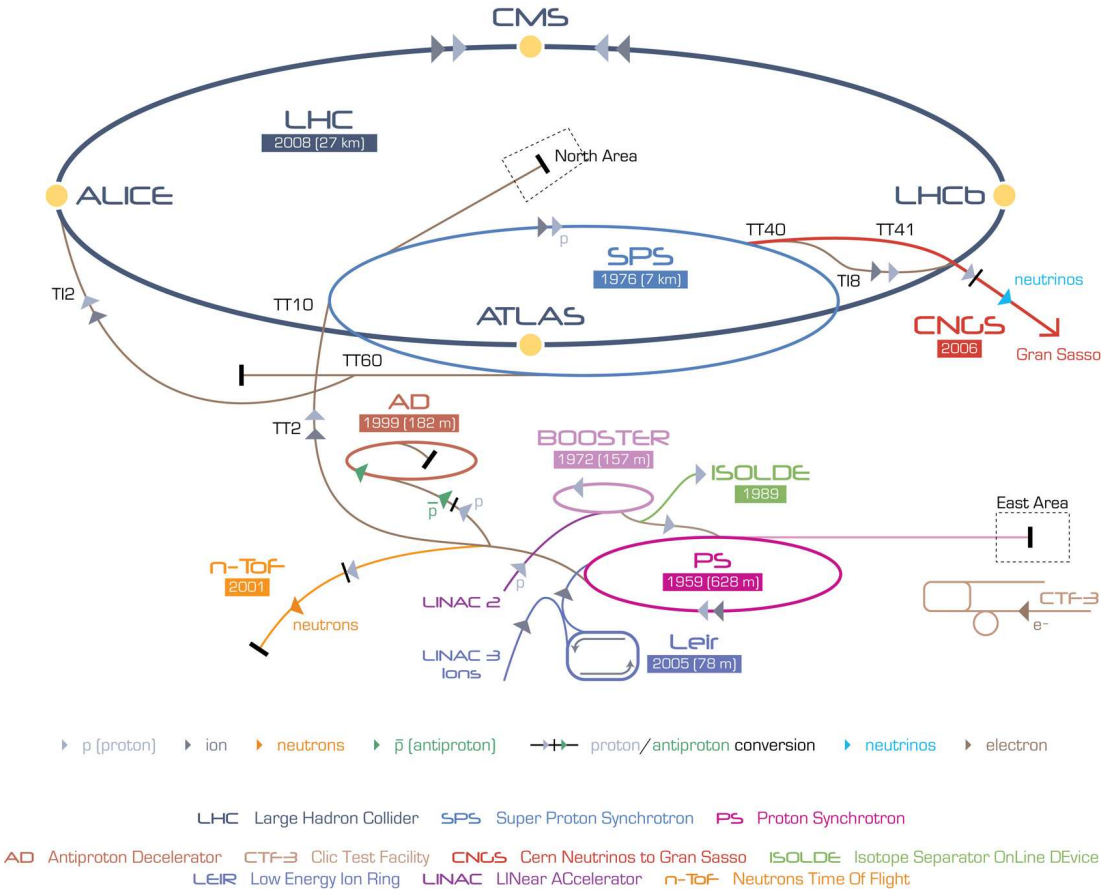

Figure 1.1: The chain of accelerators at CERN, from the linear accelerators to the detectors of the LHC, including all other CERN experiments and the different types of particles. LHC protons start at Linac 2, then are transfered successively into the Booster, the PS, the SPS and finally the LHC. The North Area is an extraction on fixed targets for mixed radiation field tests.

have no concern with work for military requirements and the results of its experimental and theoretical work shall be published or otherwise made generally available".

Around 3000 people are employed by CERN; in addition, another 6500 scientists from 500 universities and 80 countries work with CERN equipments or directly at CERN.

CERN's biggest and most famous accelerator is the *Large Hadron Collider (LHC)*, which hosts four main experiments: ALICE, ATLAS, CMS and LHCb. Each of them is the product of the collaboration of several thousands of people and a wide range of experimental facilities. CERN also operates many other different accelerators and experiments *(cf. fig. 1.1)*; however, these other experiments will not be described,

Circumference	26 659 m
Number of magnets	9593
Number of main dipoles	1232
Dipole operating temperature	1.9 K
Peak magnetic dipole field	8.33 T
Number of main quadrupoles	392
Number of RF cavities	8 per beam
Nominal energy, protons	7 TeV
Nominal energy per nucleon, ions	2.76 TeV
Design luminosity	$10^{34}\ \mathrm{cm}^{-2} \cdot \mathrm{s}^{-1}$
No. of bunches per proton beam	2808
No. of particles per bunch	$1.15 \cdot 10^{11}$ p
Nominal intensity	$3.2 \cdot 10^{14}$ p
Revolution frequency	11 245 Hz
Revolution period	88.924 µs
Min. bunch spacing	25 ns
Collision rate	600 MHz
Energy stored per beam (at 7 TeV)	362 MJ
Energy stored in the magnets (at 7 TeV)	10 GJ

Table 1.1: Nominal values of the main characteristics of the LHC, from (1), (9).

because they are not part of the scope of this work.

1.2 The Large Hadron Collider

1.2.1 Characteristics

The LHC is the largest machine ever built, with a total circumference of 26.7 km. Today, it is the biggest accelerator, but also the one with the highest energy, intensity and luminosity. Some of the most important characteristics of the LHC are given in *tab. 1.1.*

The role of the LHC is to increase the energy of the two counter-circulating beams of injected protons, and to make them collide in the four *interactions points* where the four experiments are installed. During a collision, the enormous amounts of energy lead to the creation of many other particle through the famous equivalence between mass

and energy. These newly created particles — and their decay products if they are not stable — can be detected by the experiments. The LHC can also accelerate lead ions nuclei.

The LHC itself is divided in eight straight *insertion regions (IR)*, separated by eight bending sections called *arcs* which form most of the LHC *(cf. fig. 1.2)*. In the arcs, the beams are simply transported. Each arc is made of 46 regular *cells*, which are composed of three 14.3 m dipole magnets and one 3.1 m quadrupole magnet. The cells are numbered from the middle of the IR towards the middle of the arc, left or right of the IR seen from the center of the ring. All interaction regions are also commonly referred to as "interaction points" (IP). Collisions only happen at the interaction points holding the experiments: ATLAS in IR1, ALICE in IR2, CMS in IR5 and LHCb in IR8. IR3 and 7 are dedicated to the cleaning of the beam; the acceleration by the radio-frequency chambers is done in IR4; and the extraction lines towards the beam absorber are situated in IR6.

Given the perimeter of the LHC and the corresponding frequency (for particles going at the speed of light), the space between bunches and the average number of collisions per bunch crossing, approximately 600 million collisions take place during one second. One of the challenges of the experiments was to have the processing power to deal with such an immense amount of information.

1.2.2 Experiments

Four of the 8 insertion regions of the LHC are dedicated to four big experiments: CMS, ATLAS, ALICE and LHCb.

CMS

The Compact Muon Solenoid (CMS), installed in IR5, is one of the two general-purpose experiments of the LHC. It has the standard structure of the previous general-purpose particle detectors in other accelerators. First (from the interaction point outwards) a silicon tracker, made of several layers of pixels, tracks the particle trajectories, giving their charge and momentum. Then, a homogeneous electromagnetic calorimeter measures the energy of particles sensitive to electromagnetic interactions, such as electrons and photons, by stopping them entirely. All their energy is deposited in the very dense

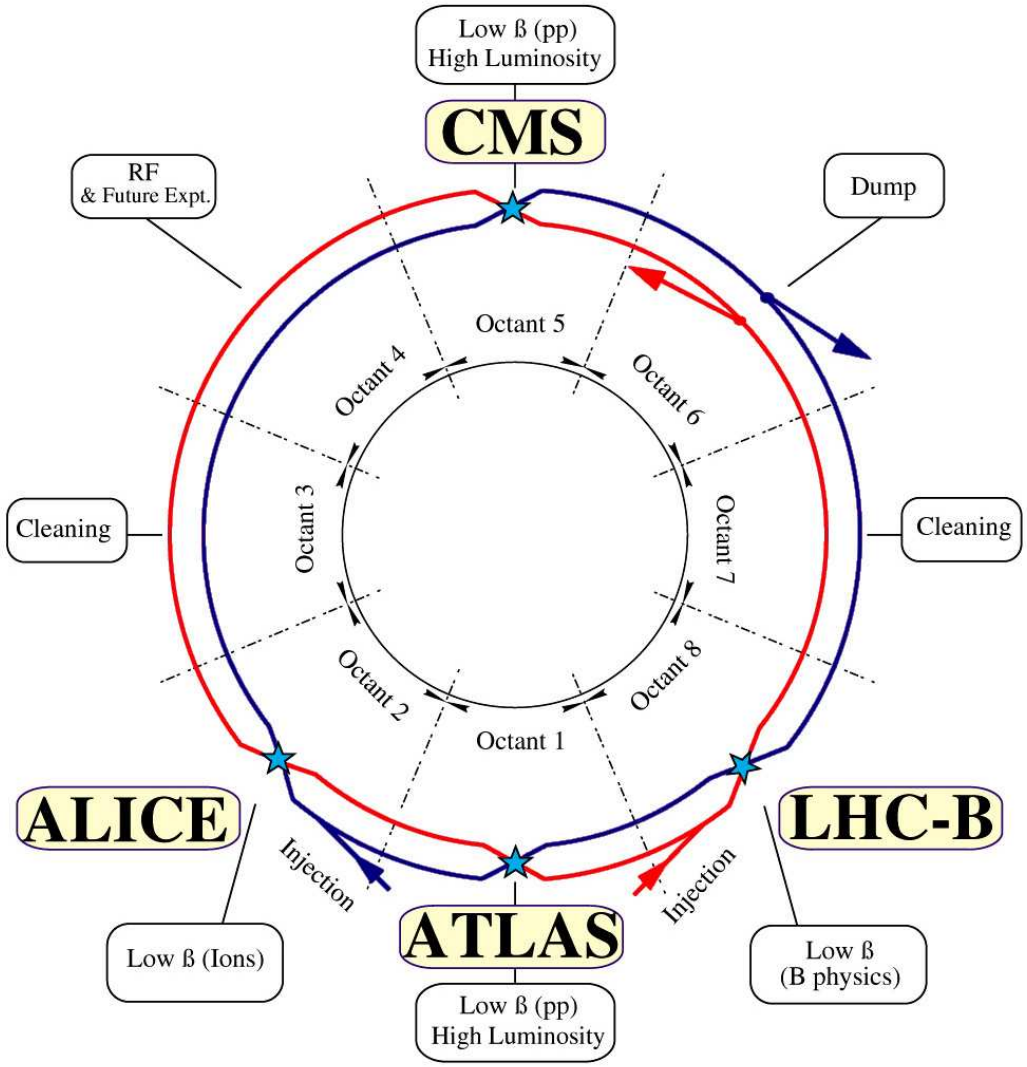

Figure 1.2: Schematics of the layout of the LHC, with the purpose of the different insertion regions. Beam 1 is represented in blue and goes clockwise, beam 2 is in red and goes anticlockwise. The collisions take place where the light blue stars are. The IRs are number clockwise starting at Atlas (IR1).

lead tungstate crystals. The next layer is a hadronic calorimeter, made of dense material such as brass and steel and plastic scintillators reading the signals. It is also homogeneous to try and deposit as much energy as possible before the next layer: the toroidal magnet.

In order to measure the charge and momentum of the created particles, their trajectories are bent by a magnetic field: these values are calculated from the curvature radius. The magnetic field of 3.8 T must be as uniform as possible, and is generated by a 6 m wide, 13 m long superconducting toroidal magnet. Outside the magnets are detectors dedicated to the only particles that can escape the calorimeters because of their higher mass: the muons. In total, CMS is 15 m wide, 21.5 m long and weights 12 550 t.

ATLAS

ATLAS, standing for "A Toroidal Lhc ApparatuS", is another general-purpose detector, installed in IR1. It has three trackers: the pixel detector, the semi-conductor tracker and the transition radiation tracker (made of drift tubes). The two calorimeters, electromagnetic and hadronic, are sampling calorimeters. They are made of two different-purpose materials: one creates the particle shower (lead and stainless steel for the electromagnetic calorimeter, steel for the hadronic one), the other measures the deposited energy (liquid argon and scintillating tiles respectively). In both cases, the total shower energy has to be estimated.

ATLAS has two magnets: an inner solenoid, situated around the inner trackers, creates a field of 2 T. The eight outer barrel toroid magnets are 20 m long, store 1.6 GJ of energy. These, as well as the end-cap toroidal magnet and their gear-shaped cryostats, give ATLAS' typical octagon shape. At the same location is the muon spectrometer installed, which is similar to the inner trackers, only not as precise but bigger. ATLAS is 46 m long, 25 m wide and weighs 7000 t.

ALICE

"A Large Ion Collider Experiment" (ALICE) is the LHC experiment dedicated to ion collisions, installed in IR2. One of the main goals of these collisions is to create a new state of matter called "quark-gluon plasma", at an equivalent temperature of ten

trillion degrees. This is thought to be the state of the universe during its first hundred microseconds.

The structure of ALICE is more complicated than the ones of the other experiments. It is made of nine sub-detectors, from tracking to time of flight and transitions measurements. Measurements in ALICE require ion beams in the LHC instead of protons. The top energy per nucleus is 2.76 TeV, which corresponds to 575 TeV per ion, and 1.15 PeV in the center of mass.

LHCb

LHCb, installed in IR8, is entirely asymmetric. It only measures particles created in a cone around the beam pipe on one side of the interaction point. The "b" in the name, standing for the b quark (*beauty* or *bottom*, the 3^{rd} generation quark with a charge of $-1/3\,\mathrm{e}$), gives the goal of this experiment: to study particles containing a b quark, called b-hadrons. These particles are predominantly created close to the beam pipe.

The point of these studies is to understand the predominance of matter over antimatter in the universe, which corresponds to a violation of the CP symmetry. Like other particle detectors, LHCb has trackers, electromagnetic and hadronic calorimeters, muon detectors and a magnet. It also has Cherenkov detectors, and a vertex detector which is one of the instrument getting the closest to the beam in the LHC, and can move away for protection reasons.

1.2.3 Chain of previous accelerators

The LHC does not accelerate the protons to their maximum energy alone: it is at the end of a chain of accelerators *(cf. fig. 1.1)*. The protons originally come from a bottle of hydrogen. The electrons are removed, leaving single charged protons. They are accelerated to a kinetic energy of 50 MeV by the linear accelerator called LINAC2, and injected into the Booster. The Booster is a synchrotron made of four superimposed rings which have a circumference of 78 m. The protons are accelerated to 1.4 GeV, and then injected into the Proton Synchrotron (PS), which has a circumference of 628.3 m. The energy of the protons is increased up to 26 GeV, and the 50 ns bunch structure is created. The protons are then injected into the Super Proton Synchrotron (SPS), which has a circumference of 6.9 km, and they are accelerated to 450 GeV, before being extracted to the LHC.

1.2.4 Beam optics & acceleration

The equipment used to accelerate particles are the *Radio Frequency (RF) cavities*. They provide an oscillating electric field that will accelerate the particles when they pass through the cavities, without disturbing them before and after the cavity (as a fixed field would). The radio frequency also creates the bunch structure of the beams and regulates the momentum. The particles circulate, passing through the RF many times, allowing a progressive acceleration.

The trajectory of the particles is bend in a circle by a vertical magnetic field constant with respect to the particle position, provided by dipoles called *Main Bending (MB)* magnets. However, this is not enough to keep the particles on a stable orbit. Elements which can focus the particle beam are needed: they are called *Main Quadrupoles (MQ)*.

They generate a magnetic field whose strength along one axis of transversal plane depends on the displacement of the particle on this axis: the further from the center the particle, the stronger the field.

The quadrupoles will then focus the particles in one direction, and defocus in the other. Particles with the highest displacement will experience the strongest field, which will inflect their trajectory and direct the particle back towards the center. In the arcs, only considering particle transportation, not beam instruments, the quadrupoles are the places where particles have the highest displacement, i.e. are closest to the beam pipe, and most likely to be lost. A succession of focusing and defocusing magnets (for one axis; successively defocusing and focusing for the other), separated by bending magnets, is needed to keep the particles going in a circle.

The envelop of all particle trajectories (i.e. the most outside ones) is called the *Beta function*. Other higher-order effects such as variations in momentum and periodic errors require higher orders magnets to insure a proper particle behaviour, such as sextupoles compensating for chromaticity.

1.2.5 Beam modes

The LHC has two particle beams circulating in opposite directions and behaving independently. Before producing physics data, the LHC goes through a series of preparation phases to bring the beams into collision. These phases are called *beam modes* (3).

The first step of a LHC run is the injection of a *pilot bunch* whose intensity is not dangerous for the machine, at injection energy: 450 GeV. Then, during the *injection* mode, more bunches are injected from the SPS into the LHC according to the current filling pattern. Once all required bunches have been injected, the *ramp* is started. In this phase, the protons are accelerated up to the collision energy (3.5 TeV at the time of writing). The current in the magnets is increased accordingly: protons with higher energy need a higher magnetic field to keep the same curvature radius, which is fixed (beam pipe).

Once the nominal energy is reached (flat top), the *squeeze* mode can start. The point is to decrease the value of the β function at the interaction points, bringing the circulating particle into the smallest possible area to maximise the number of collisions. The value is denoted $\beta^\star$, and this is achieved by the magnet triplets situated on each side of the interaction points.

Once the beams have been brought into collision (during the *adjust* mode) and are in collision, and the beam conditions (such as life time) are under control (3), the *stable beam* mode is set. This mode makes up the most part of a physics run, and is the one during which the physics data are taken.

1.3 Magnets

Part of the design of the LHC was imposed by the dimension of the pre-existing tunnel. The tunnel was the one of the Large Electron-Positron collider, which was operated between 1989 and 2000, then dismantled. The shape of the tunnel and the consequent curvature radius, together with the energy goal of 7 TeV for the particles, imposed strong requirements on the magnets. The value of the magnetic field needed for 7 TeV protons is 8.3 T, which requires a current of 12 500 A.

The choice was made to use superconducting magnets. They are made of superconducting coils which can carry electric current with no resistance. There is no heat dissipation, allowing to carry much greater currents for the same cable section, thus producing higher magnetic field. Due to cooling issues in resistive coils, and the saturation of iron yokes, the magnetic fields in non-superconducting magnets is limited to about 2 T.

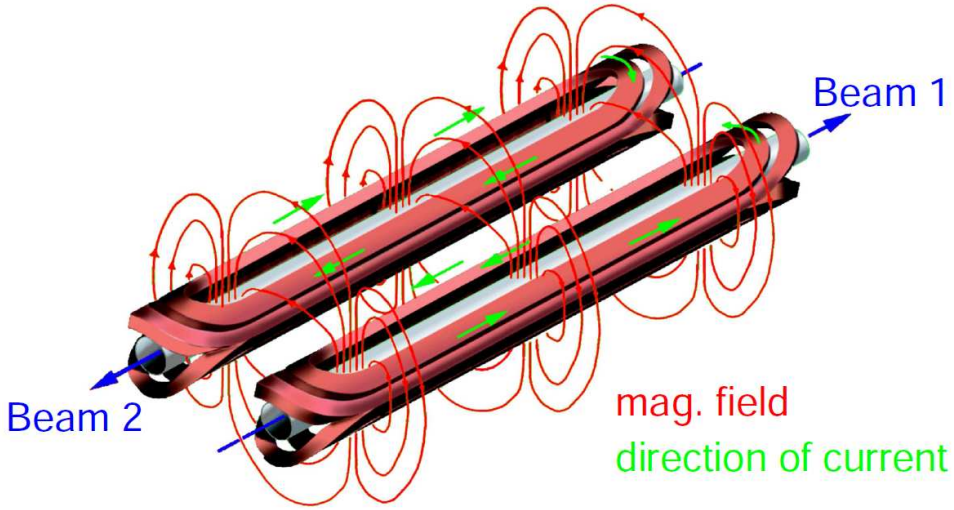

Figure 1.3: Geometry of the coils of the dipoles. The dipoles bend the proton trajectories in the horizontal plane. The magnetic field lines, in red, are shared between the two beams.

The 12 500 A can be carried in titanium-nobium wires of a section of a few square millimetres, instead of the 80 cm^2 which would be needed for normally conducting copper wires. Moreover, the current density in these copper wires would not be enough to create the requested magnetic field. The magnetic saturation of the material would prevent reaching such high fields. The absence of energy dissipation decreases the electric energy consumption, but increases the cost of cooling. The operating temperature of the LHC magnets is 1.9 K. This is achieved by cooling down the magnets with liquid helium.

The two beams of the LHC travel in separated beam pipes everywhere except at the collision regions. The two beam pipes are in the same cryostat, 194 mm away from each other. This is achieved by a two-in-one design. In a dipole, the four coils share the same yoke and some field line: part of the field for one beam is used by the other *(cf. fig. 1.3)*. This design is a way to decrease the energy consumption of the LHC.

1.4 Collimators

In this section, the collimation system will be presented.

1.4.1 Machine Protection

The energy of 362 MJ stored in each nominal beam of the LHC, at top energy of 7 TeV per beam, is unprecedented. It is enough to melt about 500 kg of copper, and the maximum stored energy exceeds by a factor 1000 all other existing accelerators *(cf. fig. 1.4)*.

A deposited energy as little as $1\,\mathrm{mJ/cm^3}$, or a few-turns loss of a portion of the beam as small as $3 \cdot 10^{-9}$ of the nominal intensity of $3 \cdot 10^{14}$ p *(cf. tab. 1.1)* is sufficient to quench a superconducting magnet; a portion of 10^{-6} could damage the equipment and lead to long downtimes (2).

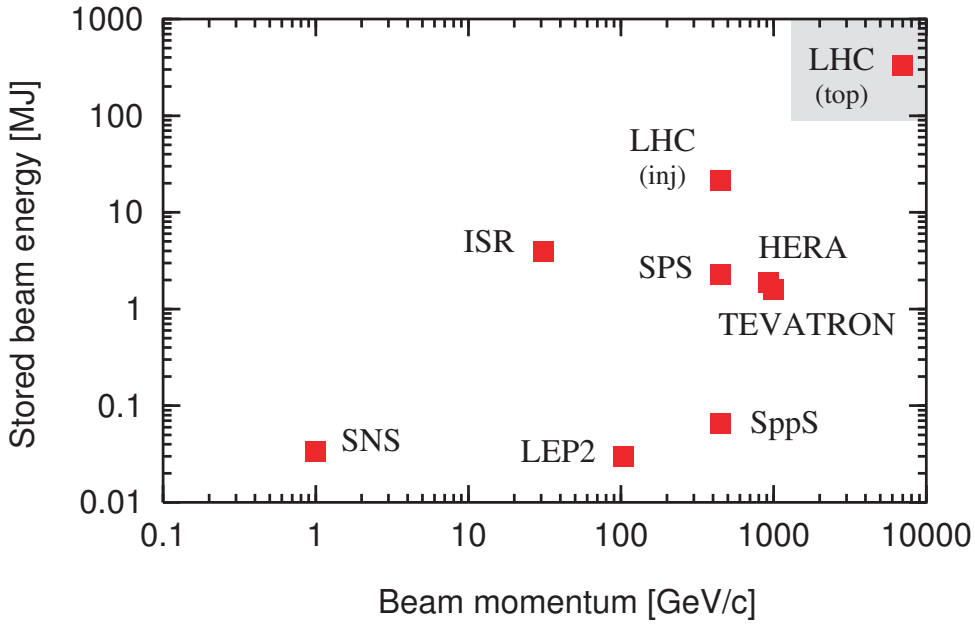

Figure 1.4: Energy stored in the beam versus beam momentum for past and present accelerators, from (5). The link between the two is the beam intensity. If the beam momentum is the most "visible" value for fundamental research (some decay channels can only happen above a certain energy), the machine protection challenges stand in the total energy stored in the beam.

Such losses must be avoided. The LHC is protected by *active* systems, which can detect dangerous situations and consequently remove the *beam permit* from the Beam Interlock System. This triggers a extraction of the beam from the machine towards an absorber in a process called *beam dump*. Around 140 active system are connected to the Beam Interlock System (4). Amongst the main ones are the *Beam Loss Monitoring*

(BLM) system and the Quench Protection System. The BLM system will be described in *chap. 2*. The Quench Protection System measures the voltage in the superconducting magnets, which should be zero for perfectly superconducting magnets (no resistance).

When the voltage drop across the magnets exceeds predefined thresholds, indicating an increase in resistance coming from a starting resistive transition (quench), quench heaters are triggered. They are thin resistive stripes, situated inside the superconducting coils. Their role is to heat the coil homogeneously so that the energy present in the magnet is not dissipated in only one point of the coil. The electric current is safely extracted from the magnet in the meantime. If all the energy was lost at the same point, the temperature increase would exceed the boiling temperature of helium, leading to an increase of volume by a factor $\simeq 750$. The temperature increase can be enough to melt the coil of the magnet.

Other systems, called *passive*, protect the LHC by providing dedicated places where the protons can be lost safely, without any danger for the equipment. Passive protection systems are *collimators* and *absorbers* installed in dedicated cleaning regions and in front of sensitive equipment. They are *aperture limitations*: the parts of the LHC that are the closest to the beam. When protons moves away from the nominal orbit, the first component encountered should always be a collimator.

1.4.2 Collimation

In circular accelerators, particles undergo transverse oscillations around the central orbit due to the successive focusing and defocusing, depending on their position and angle. They are called *betatron oscillations*. Depending on their phase advance compared to the accelerating radio-frequency cavities and their possible offset in energy or momentum, the particles will similarly perform longitudinal oscillations.

The limit for the oscillations of the particles is the aperture of the beam pipe. Any particle hitting material at an aperture limitation creates a secondary shower, and is lost from the beam. The point of the collimation system is to provide places and pieces of equipment on which the most external particles can be lost safely.

The collimators are robust beam elements designed to withstand the energy deposition of beam particles, while maximising dilution and absorption. Absorption depends

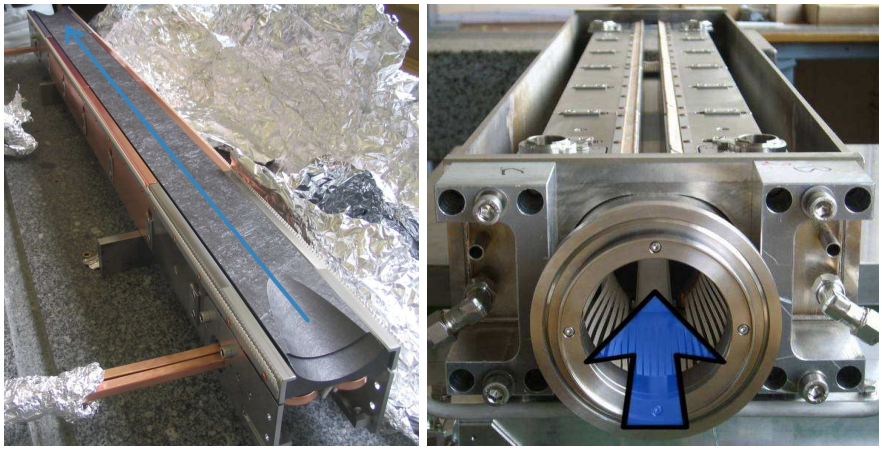

Figure 1.5: Left: picture of one collimator jaw made of CFC (graphite). Right: The two collimator jaws installed in the vacuum tank. The protons enter by the opening in the front of the vacuum tank and move parallel to the jaw. The blue arrows represent the trajectories of the particles. The collimator in the picture is horizontal.

on the inelastic interaction length of the material at the considered energies. Different material and functionalities were chosen depending on the required functionalities.

The collimators are made of two jaws, controlling the beam size in one plane of the beam optics *(cf. fig. 1.5)*. The jaws are moved by step motors, which have a precision of 5 μm and are remotely controlled (5). The gap between the jaws can vary between 0.5 and 60 mm, depending on the optics at the collimator position and the beam mode. It is often expressed in units of nominal σ, which is the standard deviation of the transversal proton distribution, assumed to be Gaussian. It is a measure of the width of the beam: $\sigma = \sqrt{\beta \cdot \epsilon}$, where ϵ is the emittance of the LHC, the value of the area covered by the particles in the phase space. At injection, the typical value at the primary collimator is $\sigma_{inj} = 1\,\text{mm}$; at top energy, $\sigma_{top} = 0.3\,\text{mm}$.

1.4.3 Types of collimators

The collimation system is a multi-stage scattering and absorbing scheme, with different types of collimators meeting different purposes *(cf. fig. 1.6)*. In total, 132 collimator locations have been reserved on the LHC. For the first phase of LHC operation, 88 collimators are installed and used. The main types of collimators are (5):

- *Primary collimators (TCP)*. Their jaws are made out of graphite reinforced by carbon fibers, called *CFC*. The goal of this low *atomic number (Z)* material is to

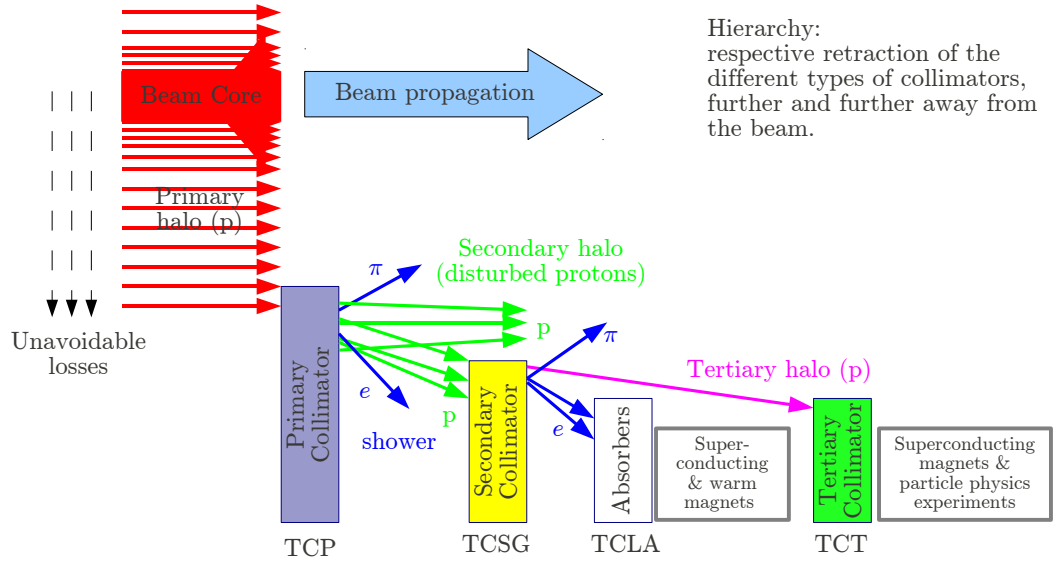

Figure 1.6: Multi-stage cleaning scheme of the collimation system of the LHC. The acronyms for the collimator names (TCT, TCSG, TCLS, TCT) are described in the text. The materials are carbon fiber-reinforced graphite (CC), copper (CU) and tungsten (W). More details about the installation of collimators are given in *fig. 1.7*.

scatter the protons from the beam halo: about 95% of the energy entering the jaw leaves it again. The jaw length is 60 cm, and the nominal jaw opening (at collisions at 7 TeV) for the transversal planes (IR7) is $6\,\sigma$ (6).

- Graphite *Secondary Collimators (TCSG)*, also made of CFC. They intercept the particle scattered by the primary collimators. Most of them are installed close to the corresponding TCP. The jaw length is 100 cm, and the nominal jaw opening (same conditions) is $7\,\sigma$ (6).

- *Tertiary Collimators (TCT)*. They are made of tungsten, which has a high atomic number, and are meant to protect the magnet triplets around the four experiments in the LHC. The jaw length is 100 cm, and the nominal jaw opening is $8.3\,\sigma$ (6).

- Long *absorbers (TCLA)*. They are made of tungsten or copper, and are meant to stop the tertiary halo. They are installed at the end of the two cleaning regions,

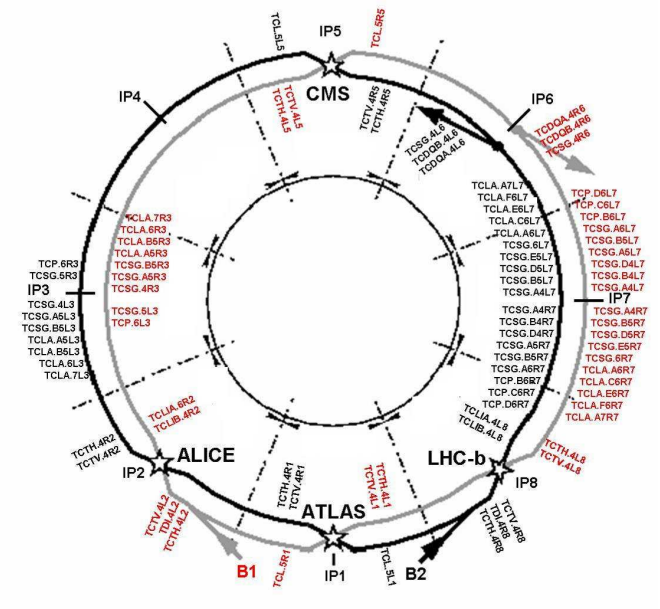

Figure 1.7: Installation of the collimators around the LHC (phase 1 of operation) (5). The red names correspond to beam 1; the black ones to beam 2. In a collimator expert name, the letters before the dot give the type of the collimator *(cf. text)*; the letters after the dot give the position of the collimator in the ring (including cell number). Most collimators for betatron cleaning are installed around IP7; most collimators for momentum cleaning are installed around IP3.

to protect the superconducting elements of the arcs.The jaw length is 100 cm, and the nominal jaw opening is $10\,\sigma$ (6).

Most collimators are installed in the two straight sections of the LHC that are dedicated to collimation *(cf. fig. 1.7)*: the *Insertion Regions (IR)* 3 and 7. IR3 holds the collimators for momentum cleaning, including the two primary collimators (for both beams). IR7 holds the collimators for betatron cleaning, including the 2 primary collimators per beam for the horizontal and vertical planes (4 in total), as well as skew collimators.

1.4.4 Performances & requirements

The performance of collimation in the LHC is quantified by the local cleaning inefficiency, which is the quantity of protons N_i lost at a location i of length L_i, over the total number of protons N_{tot} lost in the LHC :

$$\eta_{col} \equiv \frac{\frac{N_i}{L_i}}{N_{tot}} \tag{1.1}$$

The requirements for cleaning inefficiency is about $2 \cdot 10^{-5}\,\mathrm{m}^{-1}$ between the primary collimator and the highest loss in cold area, for a nominal intensity of $3 \cdot 10^{14}$ p per beam.

Another common value used to quantify the performance of collimation is the *cleaning efficiency* at the most critical superconducting element. This is the ratio between the highest loss at a collimator (usually a primary) over the highest loss at a superconducting element (the first superconducting magnets downstream the collimator). This number gives the ratio of particles lost in "adapted" areas over particles lost in "dangerous" areas.

The collimators must be able to withstand the energy deposited in their jaws (5) during regular beam losses (1% of a 7 TeV beam holding 360 MJ, lost over 10 s, corresponds to 360 kW) and accidental losses (3.6 MJ in a typical fast loss duration: 200 ns). The step motors must be radiation tolerant.

Another important point is that the total LHC impedance is dominated by the collimators. The collimators contribute to 60-70% of the total impedance of the LHC, thus limiting the maximum possible value of the intensity by the same amount.

Requirements on the mechanical parts include the roughness of the jaws (the size of the local microscopic asperities of the surface) which must be of the order of a micrometer; the flatness of the jaws (the overall bend) must be of the order of 40 µm. The position of the jaw must be controlled with a precision of 5 µm, and the angle of the jaw with a precision of 5 µrad.

1.4.5 Beam measurements involving collimators

All the way during the LHC commissioning, and during the progressing steps towards higher energy, intensity and luminosity, many tests and measurements were performed regularly on and with the collimators. A few example of these tests are presented in this section. Most of collimator operations rely heavily on the created losses being detected by the *Beam Loss Monitors (BLMs, presented in chap. 2).*

Direct shots

This type of measurement is done when there is no beam in the LHC. One of the jaws of the studied collimator is moved in fully, further than the middle position between both jaws. The other jaw is kept retracted. The first jaw covers the position where

most of the beam is supposed to be. This situation is of course not standard and can't take place while there is beam.

Then, a single pilot bunch is injected from the SPS into the beam to which the collimator is associated. The pilot goes along part of the ring, from the injection point (IP2 or IP8) to the collimator, where it is stopped by the jaw. The losses are recorded by the associated beam loss monitor.

The goal of this measurement is to study the behaviour of the collimator, and to calculate the value of the signal measured in the beam loss monitor per proton hitting the collimator jaw.

Collimator scraping

This measurement is performed when there is beam in the machine, usually at injection energy to limit the risk for the machine. While the beam is circulating, one jaw of the studied collimator is slowly moved in, step by step. Each step creates high beam losses, which quickly decrease as the collimator cleans that section of the transversal beam distribution *(cf. fig. 1.8)*. The collimator is then moved in another step.

This type of test gives precious information about the collimator's behaviour during high losses (for instance temperature increase); about the evolution and behaviour of the beam losses, how much they increase and how fast they decrease, which leads to a better understanding of beam losses and helps drawing conclusion for a better machine protection. The values of the abort threshold (losses above which the beam would be removed from the machine) can be tuned. Depending on the proportion of the beam lost on the collimator, some knowledge on the beam profile can be gained, and values of loss signal per proton can be calculated.

Resonance crossing

This type of measurement is done with beam in the LHC. It is the most relevant for this work, because it is the test that is the closest to the normal work of the machine. All collimators are supposed to be in their nominal position.

To perform this test, one of the tunes (vertical or horizontal) of one beam is moved across one resonance: a value of the inverse of an integer, for instance $1/n$. This means that every n turns, the particles will be at the same position of the accelerator with the same phase advance, same position and angle. Every little error in the lattice will be

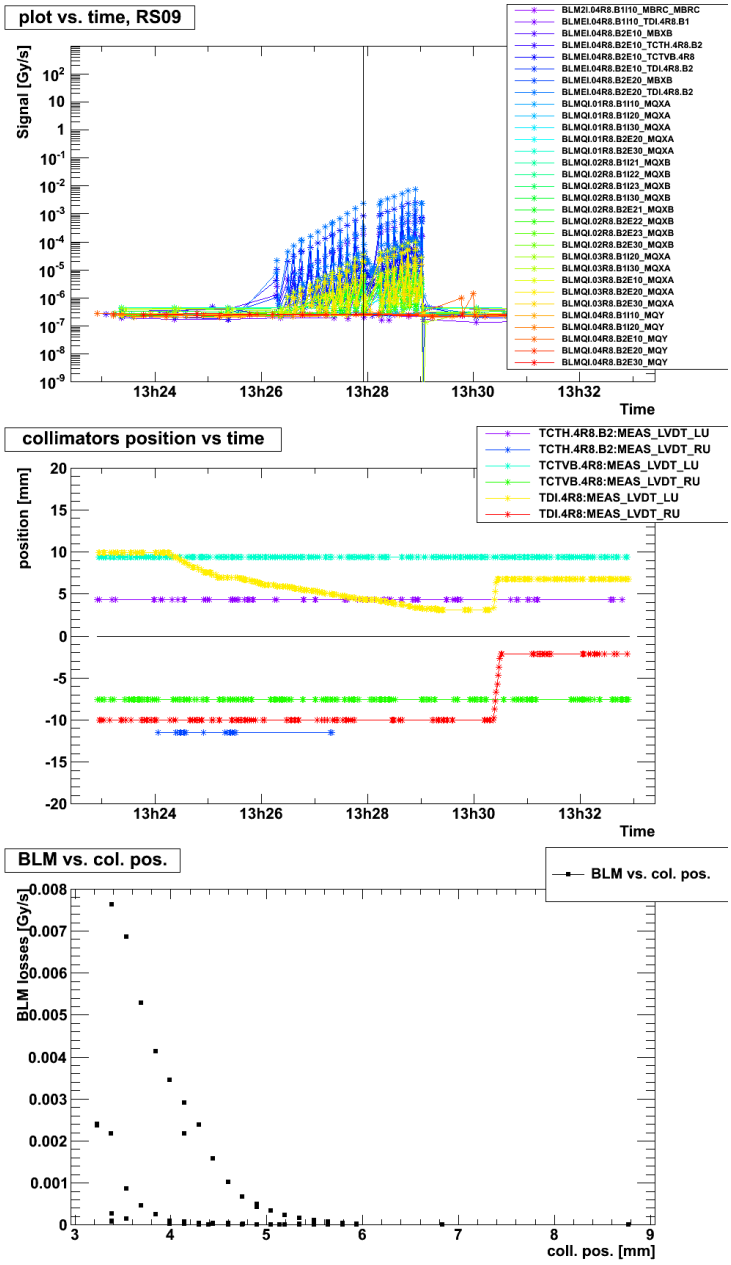

Figure 1.8: Top: Losses versus time, created during a scraping by a TDI (collimator at the junction of the injection line). Each colour corresponds to the signal of one beam loss monitor; the names are given in the legend. Center: Position of both jaws of the three collimators installed around the junction of the injection line. The beam was scraped with the left jaw of the TDI.4R8 (yellow). Bottom: Correlation between the loss at the collimator and the position of the jaw. The highest points, corresponding to the tip of the peaks, show the profile of the beam. The second profile corresponds to the losses measured one second after the movement (frequency of acquisition).

repeated every n turns. Consequently, the particle beam is not as controlled, and the beam size increases over few seconds. The beam will then graze a primary collimators and create losses.

The point of this measurement is to get a profile of the losses in the whole LHC. This gives information about the nominal settings of the collimators and the quality of the corresponding cleaning *(cf. § 1.4.4)*.

Collimator alignment

This procedure is part of normal LHC operation. The point is to align with respect to the beam, and to find the beam center at the collimator location. The collimator jaw is first moved out of the beam. Then, it is moved back in the beam slowly, while monitoring the level of the beam losses in the associated beam loss monitor (BLM). A specific application in the CERN control center controls the collimator movement and displays the losses at the same time. A sudden increase in the losses indicates that the collimator jaw is touching the outer part of the beam.

The same operation is done with the other jaw. Assuming a symmetric beam distribution in the considered plane, because of the movement of the particles in the transversal plane around the center position of the orbit, this center position can be calculated.

1.5 Conclusion

Most of the collimator operation rely on the measurements by the BLMs. They are one of the few system which give a direct insight on the reality of the machine, and play an important role in machine protection.

Chapter 2

The Beam Loss Monitoring System

In the LHC, the *Beam Loss Monitoring system (BLM)* protects the equipment from dangerous beam losses which could cause magnet quenches, stop the operation or damage the machine. When any loss exceeds the defined thresholds, the beam is removed from the machine. In this chapter, the design and installation of the BLM system will be described.

The main scope of this work is to study the signal of the Beam Loss Monitors. This work was performed in the Beam Loss Monitoring section (BL) of CERN, in the Beam Instrumentation (BI) group, part of the Beam (BE) department.

2.1 The monitors

In this section, we will describe the main type of monitors used by the BLM system in the LHC. Other types of monitors exist, but are not part of this work.

2.1.1 Ionisation Chambers

The main type of monitor used in the LHC are *ionisation chambers*. Around 3500 are installed all around the ring.

When protons are lost from the beam, they hit material (mainly collimators, but also the beam pipe) and create a *shower* of *secondary particles*. The chosen way to detect these secondary particles is an *ionisation chamber*, which is adapted to mixed radiation

fields. It is a 48 cm long cylinder containing 61 aluminium electrodes *(cf. fig. 2.1)* and filled with N_2 at 1.1 bar. The electrodes are held in place by six stainless steel rods, and they have a thickness of 0.5 mm, a diameter of 75 mm, and they are 5.75 mm apart. They are used alternately as bias electrodes and signal electrodes. A bias voltage of 1500 V is applied to the bias electrodes.

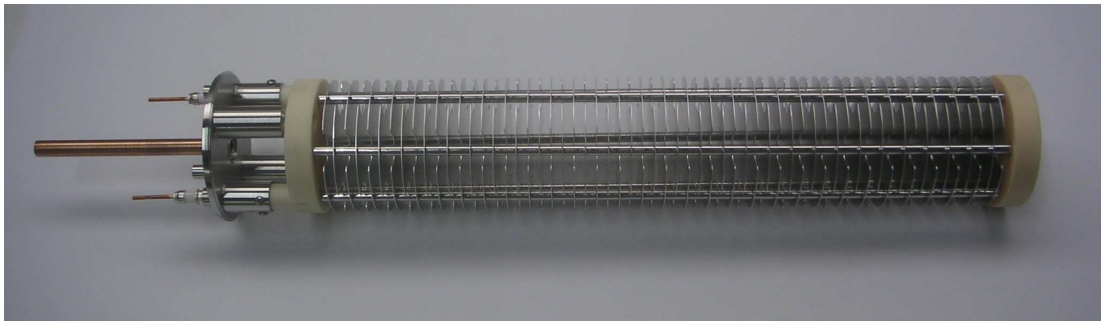

Figure 2.1: Inside view of an ionisation chamber used in the LHC BLM system, without the outside stainless steel tube. There are 61 aluminium electrodes; the insulation parts made of ceramic are visible (in white); the tube is filled with N_2 at 1.1 bar. (Picture courtesy of D. Kramer.)

The only electronic component directly next to the chamber are a resistor and a capacitor, forming a low-pass filter which smooths the bias voltage fluctuations. The monitors are radiation resistant: they can integrate up to 70 MGy per year and still keep their operational parameters unchanged (7).

When a charged particle passes through the chamber, it ionises the gas, creating ion/electron pairs. If this happens in the active volume of the chamber (the volume in which there is an electric field, the largest part of the chamber), the electrons and ions are separated by the electric field, until they reach the electrodes where they are collected (7).

In this operation regime, the ionisation chambers gives a current directly proportional to the energy deposited in the chamber.

2.1.2 Installation

The detector locations were determined from Monte Carlo simulations of the particle showers through the magnets (8). Most ionisation chambers are installed in the arcs, outside the cryostat of the quadrupoles *(cf. fig. 2.2)*, in the horizontal plane. This is were the physical beam size is the highest in the periodic lattice. The interconnection

between the quadrupoles and the dipoles is an aperture restriction in the arc. The simulation of the distributions of secondary particles depending on the loss location is shown in *fig. 2.3* (9).

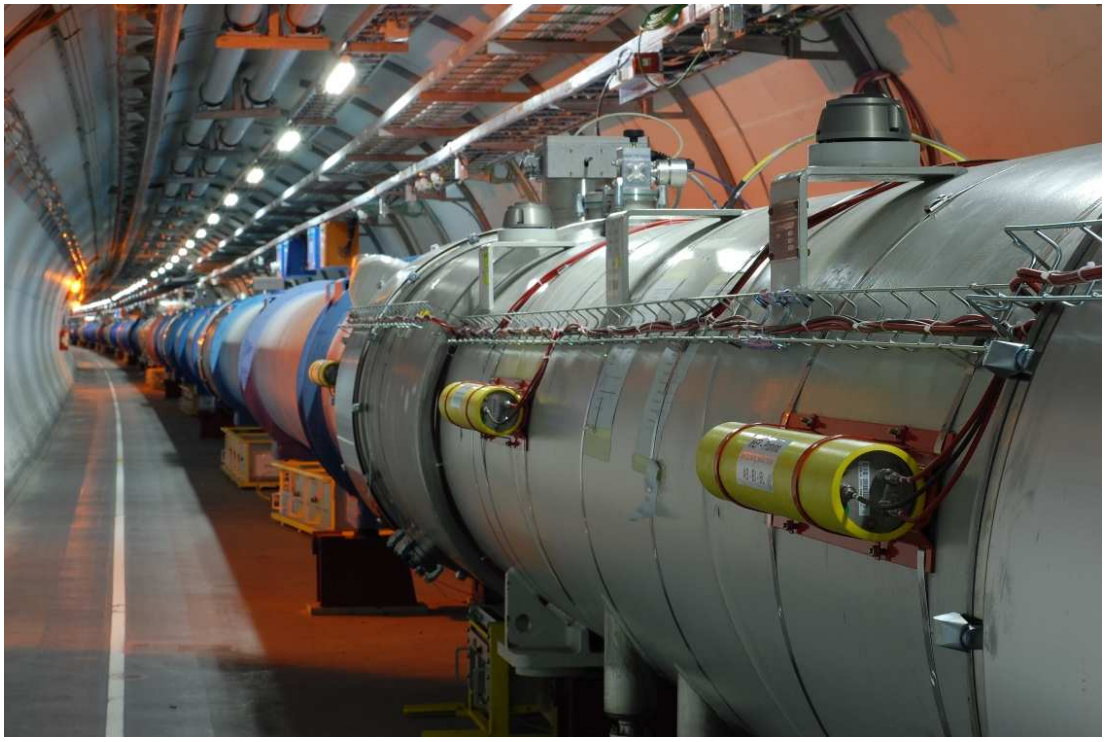

Figure 2.2: Example of installation of three BLMs (ionisation chambers) on the internal side of the LHC, on a quadrupole. Three other BLMs are installed on the other side (external). The quadrupoles have a white cryostat, whereas the cryostat of the dipoles is blue. The front-end electronics is installed under the cryostat, in the yellow crate. (Picture courtesy of D. Kramer.)

Most of the losses are meant to and likely to happen in chosen locations in the straight sections. This includes elements such as primary and secondary collimators, absorbers (for debris) and tertiary collimators before triplets, injection and extraction regions (septums, kickers and protection collimators). Each of these elements has one or more dedicated BLMs recording the losses.

2.2 Time Structure: Running Sums

The basic time structure for the collection of the charge in the ionisation chamber is the *basic integration window*, which lasts 40 μs. Every 40 μs (25.000 times per second),

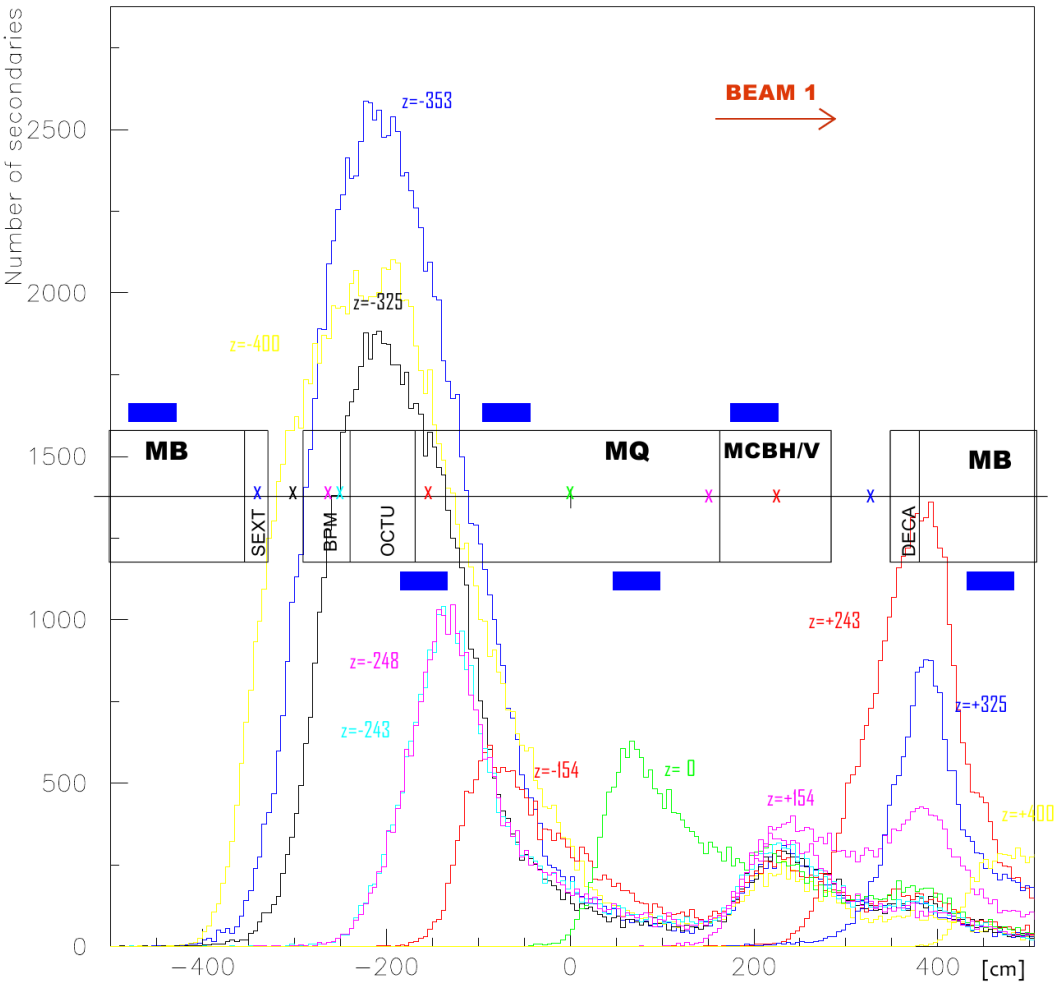

Figure 2.3: Longitudinal distribution of the secondary particles for likely loss locations for beam 1, from (9). The blue rectangles are the position of the monitors around the quadrupole; the monitors corresponding to beam 1 are the ones represented under the rectangles. The particles were scored outside the cryostat using Geant3 simulations. Each curve corresponds to a loss location marked by a 'x' on the magnet schematics, corresponding to aperture restrictions and likely loss locations. Courtesy of L. Ponce

the charge that has been deposited in the chamber is collected by the electronics.

A set number of these measurements *(cf. tab. 2.1)* are summed in a sliding window called *Running Sum (RS)*, and converted into a dose rate, expressed in Gy/s, by the corresponding calibration factors. Multiple running sums up to 84 s are calculated, allowing to keep a history of the data, and to quantify the typical time duration of the loss. A short loss contained in one 40 μs integration window will give a high value of the first running sums, but will be averaged in the longer ones. Conversely, long losses over numerous integration windows will sum up to a high value of the longer running sums.

Name	Number of 40 μs windows	duration
RS01	$2^0 = 1$	40 μs
RS02	$2^1 = 2$	80 μs
RS03	$2^3 = 8$	320 μs
RS04	$2^4 = 16$	640 μs
RS05	$2^6 = 64$	2.56 ms
RS06	$2^8 = 256$	10.24 ms
RS07	$2^{11} = 2048$	81.92 ms
RS08	$2^{14} = 16384$	655.36 ms
RS09	$2^{15} = 32768$	1.31 s
RS10	$2^{17} = 131072$	5.24 s
RS11	$2^{19} = 524288$	20.97 s
RS12	$2^{21} = 2097152$	83.89 s

Table 2.1: Name and duration of BLM running sums.

2.3 Electronics

In this section, the entire BLM electronics chain will be described, from the readout of the ionisation chambers signal to the beam dump decision and the publication of data.

2.3.1 In the tunnel

The output of the ionisation chamber is connected to the *front-end* electronics, typically via coaxial cables *(cf. fig. 2.5)*. In places where the front end has to be far away from the monitors (up to 800 m on the right side of the point 3 of the LHC), a twisted multi-wire cable is used. The chamber behaves like a capacitor discharging in an analog circuit called *Current to Frequency Converter (CFC) (cf. fig. 2.4)*.

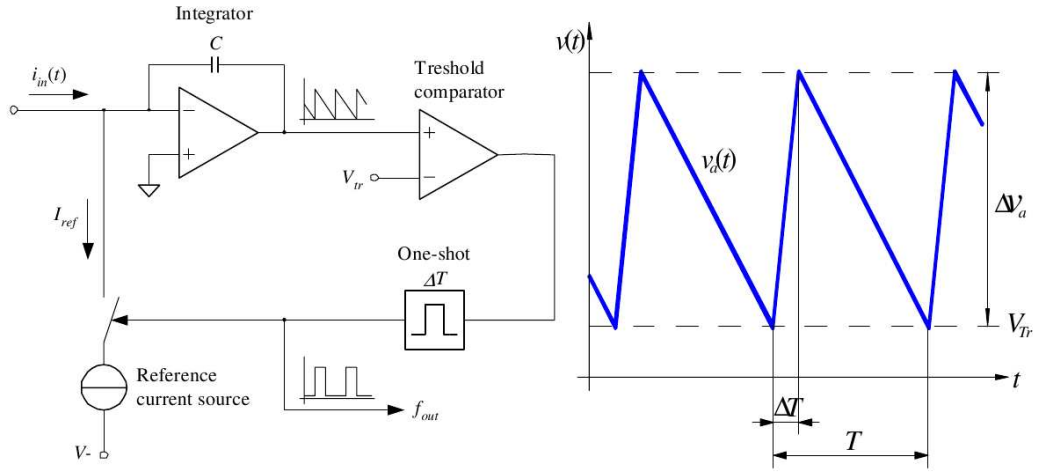

Figure 2.4: Left: schematics of the *Current to Frequency Converter (CFC)*. The input current $i_{in}(t)$ corresponds to the charge coming out of the ionisation chamber; the output is the frequency f_{out}. Right: output of the threshold comparator. The period T changes with time: $f_{out}(t) \equiv \frac{1}{T(t)}$.

The first part of the CFC is an integrator in which the charge is integrated into a current coded by a voltage. While the current is integrated, the voltage builds up, until it reaches the threshold. At this point, the integrator is quickly (with respect to the integration time) reset by sending in a reference current I_{ref} (the time needed to reach the original value is ΔT). This corresponds to one CFC count. The more charge comes out of the chamber, the more often the threshold is reached, and the higher the frequency of counts will be.

This circuit allows continuous operation by not having any dead time. Even if there is an input current during the reset of the integrator, it is measured: it decreases the reference current, meaning that the thresholds will be reached faster at the next "period", which will consequently be shorter (higher frequency).

During one period *(cf. fig. 2.4)*, the reference current I_{ref} can be seen as the slope of the voltage function during reset: after ΔT, the voltage has increased by ΔV_a:

$$\Delta V_a = I_{ref} \cdot \Delta T$$

If there is an input current during the reset, the reference current is decreased, and the equation becomes:

$$\Delta V_a = (I_{ref} - i_{in}) \cdot \Delta T \tag{2.1}$$

The same can be considered during the integration of the signal, which lasts $T - \Delta T$. The input current is the slope of the voltage function:

$$\Delta V_a = i_{in} \cdot (T - \Delta T)$$

$$T = \frac{\Delta V_a}{i_{in}} + \Delta T$$

$$(2.1 \Rightarrow T = \frac{(I_{ref} - i_{in}) \cdot \Delta T}{i_{in}} + \Delta T$$

$$T = \frac{I_{ref} \cdot \Delta T}{i_{in}} \tag{2.2}$$

The output frequency is calculated from there:

$$f_{out} = \frac{1}{T} = \frac{i_{in}}{I_{ref} \cdot \Delta T} \tag{2.3}$$

This circuit can't measure negative currents: this would lead to an increase of voltage in the comparator up to the saturation of the amplifier *(cf. fig. 2.4)*. In order to avoid this situation, the CFC is equipped with current source of 10 pA, injected constantly at the input. This value corresponds to the measured average noise value.

This has to be taken into account when considering low losses: no current smaller than 10 pA can be measured, and subsequently no loss corresponding to a current lower than 10 pA can be measured. In addition, if the amplifier stays in saturation mode for more than ~ 2 min, the CFC has a negative current compensation procedure (not represented), which increases the offset (up to 255 pA) until the measured current reaches 10 pA.

The output frequency is acquired and digitized by a Field Programmable Gate Array (FPGA), which controls an Gigabit Optical link Hybrid (GOH), sending the data back to the surface via optical fibres. In order to avoid any information loss, these optical links are redundant: two independent optical links send the same information.

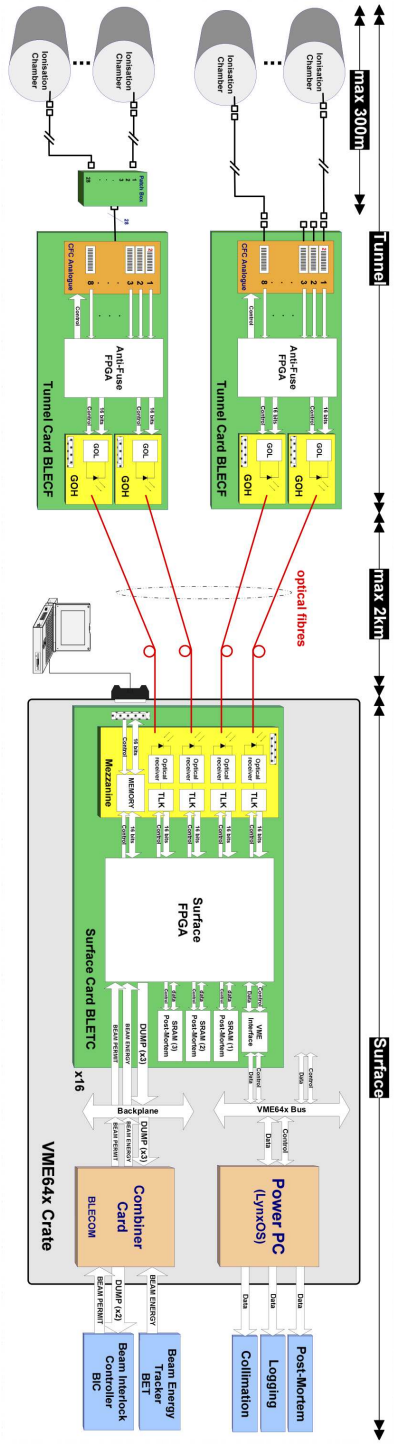

Figure 2.5: Schematics of the entire electronics chain of the BLM system. The locations and distances are indicated on the figure.

2.3.2 On the surface

The data processing and evaluation of the measured signal takes place in the *Threshold Comparator* cards, on the surface *(cf. fig. 2.5)*. The optical receivers are installed on a physically separated "mezzanine" card, which is directly plugged on the surface card. This allows easy replacement and checks.

The values are converted into dose rate (Gy/s) with the corresponding calibration factors and combined into running sums *(cf. tab. 2.1)*. All values are compared with the corresponding thresholds, which are different for every running sum and for every one of the 32 beam energy level, to follow the evolution of the beam in energy in the machine during the ramp. If any threshold is exceeded, a beam request is sent to the Beam Interlock System (BIS), and the content of the buffers is saved as *post-mortem* data.

Some of these measured running sums are saved in the LHC databases: one value per running sum is recorded every second. For all running sums shorter than one second (up to RS08), only one value is logged: the highest loss of all integration windows during the last second. For the longer running sums, the last in date at the time of logging is saved (10), even if the value is refreshed more than once per second.

2.4 Thresholds

In the threshold comparator cards, the different running sums are continuously compared with a set of predefined thresholds. If any of the thresholds is exceeded, a beam extraction is requested via the Beam Interlock System (BIS). The abort thresholds can be set separately for each BLM, and there are 12 running sums $\times$ 32 energy levels.

The threshold for a specific BLM depends on different factors, such as its position with respect to the beam line and the element it protects, and this element itself. The setting of the thresholds depends largely on empirical measures, and cannot be fully verified by automatic test procedures (11). The BLM *master thresholds* represents the best knowledge of quench or damage levels. It can be written as:

$$Th(E_b, \Delta t) = Q_{BLM}(E_b) \times N_p(E_b, \Delta t) \tag{2.4}$$

where E_b is the energy of the beam, Δt is the loss duration, Q_{BLM} is the signal observed in a BLM due to a single lost proton, and N_p is the maximum number of protons that can be lost in the protected element.

The time dependence comes from the considerations on loss durations: e.g., some energy deposited over a long time in one point of a superconducting magnet will have time to dissipate by conduction, and will be removed by the helium cooling; the same energy, lost over a very short period, could damage the magnet before the cooling has any effect. Many other considerations are taken into account, depending on the time scale of the loss at the considered element. From shorter to longer, the considered effects are: the heat reserve of the cable, the heat flow between the cable and the Helium, the Helium heat reserve and the Helium heat flow.

The energy dependence comes from the development of the hadronic shower, which depends on the energy of the protons. In addition, the superconductivity of a magnet depends on a set of three interdependent parameters: temperature, current and magnetic field. For increasing beam energies, the magnetic field and the current need to increase as well, leading to tighter limits on the temperature value.

Both Q_{BLM} and N_p rely strongly on Monte Carlo simulations and therefore include theoretical uncertainties. Security margins are set to account for these uncertainties, and they are corrected by analyzing data from the standard operation of LHC and by performing measurement with specific beam, for instance during machine development periods.

The values set in the electronics are called *applied thresholds*, and are always lower than or equal to the master thresholds:

$$th(E_b, \Delta t) = MF \times Th(E_b, \Delta t) \tag{2.5}$$

where the Monitor Factor MF is chosen lower than one (typically 0.1). It can be chosen independently for each monitor.

2.5 Justification of the doctoral work

As described in *§ 2.1.2*, the installation locations of the BLMs were carefully selected. Each one of them is associated with a specific element and an expected loss location within an element. There are many BLMs around the LHC ring, nearly 4000 in total, including 3600 ionisation chambers.

Nevertheless, each BLM gives just one "local" value: the loss that occurred at the location where the BLM is installed. In order to gain knowledge about the origin of a loss, one must consider the element protected by the BLM. For instance, losses at collimators are to be expected, as it is the role of collimators to create a safe location for losses.

The collimator characteristics would then help describing the specifics of the loss: from which plane it originated, if the particles are primary or secondary, and other similar information. As another example, a signal in the BLM associated to a quadrupole would point towards the likely loss location associated to this BLM. The local development of a loss, up to the scale of a quadrupole, is fairly well studied.

However, the BLM signals had never been considered on a global scale: that is, how would a loss develop over dozens of BLM and hundreds of meters. Considering many BLMs at the same time, and the respective signals in these BLMs, supplementary information about the origin of the loss can be extracted.

The point of this doctoral work is to try to define what information can be gained from a more global approach to the losses, and to evaluate the possibilities and the qualities of these various extractions. Different patterns were used in this work, as well as different techniques to extract these patterns from the loss profiles. The patterns included the time evolution of the losses, as well as the spatial distribution – always considering several monitors at a time.

The feasibility of such a global scale study of the LHC beam losses was evaluated, and the different techniques fulfilling the goal were developed and tested on real data. The theory, the implementation and the conclusions on the results will be presented in the next chapters.

Chapter 3

Principle of Vector Decomposition

In this chapter, we will explain the need for vector decomposition, and present the different techniques used in this work.

3.1 Principle

3.1.1 Motivation

The goal of this PhD is to understand the cause of beam losses in the LHC by studying the loss patterns. One way to achieve this is by reverse engineering: to try to recognize some well-known *loss scenarios* in a *measured loss profile*, and to decompose the measured loss profile as a *linear combination* of known scenarios. The quality of the recomposition must be evaluated.

3.1.2 Vector space

Let's consider an ensemble of m monitors, and a vector space of dimension m. Each monitor is associated with one dimension (one coordinate) of the vector space. The ensemble of monitors corresponds to the canonical basis of the space. Any *loss profile* can then be expressed as a *vector* on this space: each of the m coordinates of this vector is the value of the loss recorded by the corresponding monitor. The losses are only positive: "negative" losses are not physical. The vector will thus have only positive coordinates.

Let's consider a group of n known loss scenarios, and the corresponding n vectors $(\vec{v_i})$ expressed on the m-dimensional vector space. In this work, there are only a few loss scenarios for many monitors: $n < m$. If the situation was inverted, and there were more vectors than monitors ($n \geq m$), the vectors could be combined to create a square matrix, that could then be analytically inverted rather simply. It is not the case here: the vectors only span a subspace of the original m-vector space. They form a spanning set of the subspace. They are a basis of the n-vector space: typically, they are independent (this is checked by calculating the determinant) but not orthogonal.

Let's also consider a *measured loss profile*, and the corresponding measured vector $\vec{X}$.

In order to compare the different vectors, and to make all linear algebra operations easier, the choice was made to normalize the vectors so that they all have an euclidean norm equal to 1 in the m-vector space. A vector $\vec{v}$ of the vectors $(\vec{v_i})$, is simply divided by the value $\|\vec{v}\|$ of its euclidean norm, calculated as:

$$\|\vec{v}\| = \sqrt{\sum_{j=0}^{m} v_j^2} \tag{3.1}$$

where the scalars (v_j) are the coordinates of the vector $\vec{v}$.

3.1.3 Vector decomposition

The idea here is to find a linear combination of the vectors $(\vec{v_i})$ that will recompose the vector $\vec{X}$:

$$\sum_{i=0}^{n} f_i \cdot \vec{v_i} \approx \vec{X} \tag{3.2}$$

where the *factors* (f_i) are the scalars of the linear combination. They form a vector of dimension n, noted $\vec{F}$. Note that the recomposition is not exact, because the reference vectors $\vec{v_i}$ are not a basis of the m-vector space. The idea is to find some "typical loss scenarios" that would compose the considered loss. "Subtracting" a typical loss scenario from the overall loss is not physical, so the factors have to be positive: $\forall i, f_i \geq 0$.

The series of operations needed to find a set of factors recomposing the vector $\vec{X}$ is called *vector decomposition*. It can be achieved through *projections*, or *matrix inversion*, or some dedicated algorithm. Projections and matrix inversion will be quickly introduced; then, the corresponding technique used here will be described into greater details.

3.1.4 Projections

One way to achieve the vector decomposition (to find the factors of the linear combination) would be to project the measured vector $\vec{X}$ on the vectors $(\vec{v}_i)$. However, the vectors $(\vec{v}_i)$ are not in sufficient number ($n < m$): they don't form a basis of the m-vector space. They form a basis of the n-vector space, and the orthogonal projection of $\vec{x}$ on this space can be calculated. This is the vector part of the n-vector space which is the closer to $\vec{X}$.

One of the simplest processes that can create an orthogonal basis from a non-orthogonal set of vectors is called the *Gram-Schmidt process (cf. § 3.3)*. It uses no matrix inversion, no transformation, only simple operations (projection and subtraction) on the vectors. It can be seen as a geometrical process.

3.1.5 Matrix inversion

Another way to achieve the vector decomposition (to find the factors of the linear combination) would be to express the equation *3.2* as a matrix equation:

$$M_{m\times n} \cdot \vec{F}_n \simeq \vec{X}_m \tag{3.3}$$

where $M_{m\times n}$ is the matrix of size $m \times n$ formed by the n known vectors $(\vec{v}_i)$, and where we want to find $\vec{F}_n$, the n factors of the decomposition. The matrix M needs to be inverted such that:

$$\vec{F}_n \simeq M^{-1}_{n\times m} \cdot \vec{X}_m \tag{3.4}$$

Note that the M^{-1} notation is abusive: it is not exactly an inverse matrix, since it is not square. The matrix M^{-1} is the "left inverse" of M: it satisfies $M^{-1} \cdot M = I_n$ but can not satisfy $M \cdot M^{-1} = I_m$ (where I_n is the unitary matrix of size $n \times n$). Note that the inversion is exact; only the recomposition is not: $\vec{X}$ has no reason to belong to the subspace generated by the vectors of M.

Once M is inverted and $\vec{F}$ is calculated, the *recomposition* can be estimated. The inversion was exact, but the recomposition is not exactly $\vec{X}$: it is noted $\vec{X}'$ and belongs to the subspace, whereas $\vec{X}$ doesn't. It is calculated by:

$$\vec{X}' = M \cdot \vec{F} \tag{3.5}$$

The *error on the vector decomposition* can be estimated by calculating the norm of the difference between the original vector $\vec{X}$ and its recomposition $\vec{X}'$:

$$e \equiv ||\vec{X} - \vec{X}'|| \tag{3.6}$$

3.2 Singular Value Decomposition (SVD)

The *Singular Value Decomposition (SVD)* is the generalisation of the diagonalization of a square matrix, for a non-square matrix. It is a *matrix* decomposition technique (into singular values) that allows a simpler inversion of the matrix M than calculating M^{-1} directly. The goal is to do a *vector* decomposition of the vector $\vec{X}$ (finding the factors).

3.2.1 Principle

The diagonalization of a square matrix is the idea that a diagonalizable square matrix M can be expressed as the product of three matrices:

$$M = U \cdot S \cdot U^{-1}$$

where U is the matrix of eigenvectors; and S is a diagonal matrix where the values are the eigenvalues associated to the eigenvectors in U, in the same order.

A non-square matrix can be decomposed into singular values. It is called *Singular Value Decomposition (SVD)*, and is calculated by a computational technique (algorithm) of high precision *(cf. § 4.6)*. The decomposition is exact only to the precision of the algorithm, but we will assume here that it is exact.

$$M_{m\times n} \equiv U_{m\times m} \cdot \Sigma_{m\times n} \cdot W^T_{n\times n} \tag{3.7}$$

where:

- M is the original matrix, of size $m \times n$;
- U is an orthogonal unitary matrix, of size $m \times m$;
- W is an orthogonal unitary matrix, of size $n \times n$;
- Σ is a non-square diagonal matrix, of size $m \times n$.

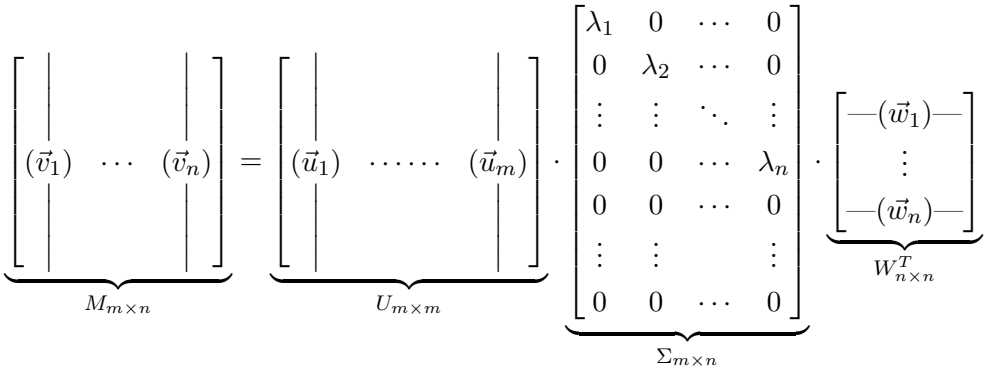

Figure 3.1: Structure of the matrices in the decomposition. M is the original matrix, made of the vectors $(\vec{v}_i)$; U and W are the matrices of the left and right singular vectors respectively. Σ is a diagonal matrix (with $n < m$) holding the *Singular Values*: all values are null, apart from the diagonal $\lambda_i = (\Sigma)_{i,i}$.

Σ is such that only the diagonal elements are non-null, and there are n in total. These values (λ_i) are unique and are called *singular values*.

U and W are orthogonal matrices: they generate an orthogonal basis of the corresponding N-vector space ($N = n$ or m). They satisfy $U \cdot U^T = I_N$. The vectors of U are called *left singular vectors*, and the ones of W are *right singular vectors*. These vectors are not unique for the SVD of one matrix M.

The transformation associated to the matrix M is decomposed by the SVD into three steps: a rotation (matrix W), a stretching (matrix Σ) and another rotation (matrix U) (12).

3.2.2 Advantages

The Singular Value Decomposition calculates the singular vectors U and W as well as the values λ_i of Σ. The vectors of U, of dimension m, are orthonormal and form a basis of the m-vector space, in which the losses are decomposed. Moreover, only the n first vectors at most are used: there are only n values λ_i. All vectors $(\vec{u}_j)$ for $j > n$ are associated with a zero in Σ during the matrix multiplication.

The singular values in Σ are sorted in decreasing order. The lower λ_i, at higher i, can be ignored for faster recomposition at the price of a small error. In this work $n \ll m$, so no λ_i are omitted. The first vectors (u_i) of U, associated to the λ_i of

higher value, will have a strong contribution in the recomposition; the ones with higher i ($i < n$) will have a small contribution (λ_i of smaller value); the ones with $i > n$ will have no contribution.

3.2.3 Important observations

In this section, we will give the exact expression of the coefficients of M as calculated by the SVD. The coefficients of the matrices are written in their standard form: (w_{ij}) for the matrix W, where i is the line number and j the column number, both varying between 0 and n. Note that the vector $(\vec{w}_1)$ will then have the coefficients (w_{1j}).

The product between the matrices $C_{m\times n}$ and $D_{n\times p}$, the result is a matrix of coefficients (e_{ij}) expressed as:

$$\forall i, j : e_{ij} \equiv \sum_{k=1}^{n} c_{ik}\, d_{kj} \tag{3.8}$$

Let's start by the multiplication $U_{m\times m} \cdot \Sigma_{m\times n}$. The elements will be called (s_{ij}) and are:

$$s_{ij} = \sum_{k=1}^{m} u_{ik}\, \lambda_{kj}$$

The elements λ_{kj} are null for all $k > n$ and all $j \neq k$, so the intermediate result is:

$$s_{ij} = \sum_{k=1}^{n} u_{ik}\, \lambda_{kj} = u_{ij}\, \lambda_j$$

Now, let's consider the multiplication of $(U\Sigma)_{m\times n}$ by $W_{n\times n}$. *Eq. 3.8* gives:

$$m_{ij} = \sum_{k=1}^{n} s_{ik}\, w_{kj} = \sum_{k=1}^{n} u_{ik}\, \lambda_k\, w_{kj}$$

$$m_{ij} = \sum_{k=1}^{n} \lambda_k\, u_{ik}\, w_{kj} \tag{3.9}$$

The most important point here is that only the first n vectors $(\vec{u}_k)$ are used. The coefficients of M are decomposed into the equivalent of a matrix product of the first n vectors of U and the vectors of W, but each term of the sum is weighted by a factor λ_k.

As a consequence, the vectors (u_k) for $k > n$ do not take part of the decomposition; so they are left by the algorithm as canonical vectors: the k^{th} coordinate is 1 and all the others are zero.

3.2.4 Pseudoinverse

Once the matrix $\Sigma_{m\times n}$ has been created, the *pseudoinverse* can be created. It is noted Σ^+ and has a size of $n \times m$. All values are null, apart from the diagonal ones which are $(\Sigma)_{i,i} = \frac{1}{\lambda_i}$ for $\lambda_i \neq 0$. This matrix is called pseudoinverse because it only satisfies $\Sigma^+ \cdot \Sigma = I_n$; the product $\Sigma \cdot \Sigma^+$ is a matrix of size $m \times m$, with only the n first diagonal elements are 1; all the others are zero.

The pseudoinverse of M is then:

$$M^+ \equiv W \cdot \Sigma^+ \cdot U^T \tag{3.10}$$

and satisfies:

$$\begin{aligned} M^+ \cdot M &= (W \cdot \Sigma^+ \cdot \underbrace{U^T) \cdot (U}_{I_m} \cdot \Sigma \cdot W^T) \\ &= W \cdot \Sigma^+ \cdot \Sigma \cdot W^T \\ &= W \cdot W^T \\ M^+ \cdot M &= I_n \end{aligned}$$

Note that it is different for $M \cdot M^+$: for the same reason as $\Sigma \cdot \Sigma^+$, it is a matrix of size $m \times m$, with only the n first diagonal elements are 1; all the others are zero.

3.2.5 Recomposition

Once the pseudoinverse has been calculated, the factors can be calculated (vector decomposition). The result is not exact, because the vector $\vec{X}$ is generally not part of the subspace generated by the vectors of M.

$$\begin{aligned} M \cdot \vec{F} &\simeq \vec{X} \\ M^+ \cdot M \cdot \vec{F} &\simeq M^+ \cdot \vec{X} \\ \vec{F} &\simeq \underbrace{W \cdot \Sigma^+ \cdot U^T}_{M^+} \cdot \vec{X} \\ \vec{F} &\simeq M^+ \cdot \vec{X} \end{aligned}$$

The recomposition $\vec{X}'$ is then calculated by:

$$\begin{aligned} \vec{X}' &= M \cdot \vec{F} \\ \vec{X}' &= M \cdot \underbrace{W \cdot \Sigma^+ \cdot U^T}_{M^+} \cdot \vec{X} \end{aligned}$$

3.2.6 Limitations

Accuracy of the recomposition

Given the matrix M, the SVD algorithm will always calculate a matrix decomposition $M = U \cdot \Sigma \cdot W^T$. Once the pseudoinverse M^+ calculated, the set of factors $\vec{F}$ can always be calculated, as well as the recomposition $\vec{X}'$. This recomposition is the combination of the vectors $(\vec{v_i})$ which is the closest to $\vec{X}$, and belongs to the subspace generated by the vectors of the loss scenarios. However, it doesn't mean that the recomposition $\vec{X}'$ will actually be close to $\vec{X}$; it can even be null. An example of such a situation is:

$$M = \begin{bmatrix} 1 & 1 \\ 0 & 1 \\ 0 & 0 \end{bmatrix} \qquad \vec{X} = \begin{bmatrix} 0 \\ 0 \\ 1 \end{bmatrix}$$

No set of factors can recompose $\vec{X}$: the projection of $\vec{X}$ on the subspace generated by the vectors of M is the point of coordinates $(0, 0, 0)$.

Without a proper evaluation of the accuracy of the vector decomposition, the factors are meaningless.

Negative factors

In the standard $\mathbb{R}^m$ vector space, each factor f_i can take any value in $\mathbb{R}$. However, there are physical limitations. The factors (f_i) represent the contribution of the different "standard" loss profiles (vectors $(\vec{v_i})$): negative values are not physical, nothing would "remove" a loss profile. Moreover, the losses are only positive: again, negative losses make no sense. The vectors $(\vec{v_i})$ are in $(\mathbb{R}^+)^m$: the space generated by the positive half of the field of real numbers (noted $\mathbb{R}^+$) considered m times.

A negative factor in the vector decomposition indicates that the corresponding vector can not contribute to the reconstruction of the vector $\vec{X}$. This means that the corresponding vector can not take part of the decomposition. It often points to a problem in the decomposition, for example that the chosen loss scenarios are not exactly adapted to the problem, and that the measured vector has other components than the selected vectors $(\vec{v_i})$.

One way to deal with this effect would be to remove this vector from the matrix M: the matrix would then have a size $m - 1$. The SVD could be calculated again; the

decomposition would be less accurate, but wouldn't have the negative factor any more (it would be zero). Here, this is not applied: when a factor is negative, it is never the most important one; in most cases, it is compensating for another factor being higher than one.

3.3 Gram-Schmidt process

The Gram-Schmidt process is a technique used to create an orthonormal set of vectors from another set of non-orthogonal vectors *(cf. 3.1.4)*. Once an orthogonal set of vectors is established, the vector decomposition can be achieved on this set, and is unique.

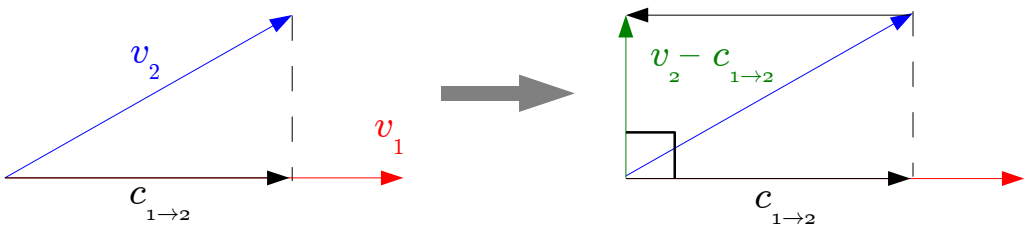

Figure 3.2: First step of the Gram-Schmidt process. The projection (black) of $\vec{v_2}$ (blue) on $\vec{v_1}$ (red) is calculated, corresponding to the contribution of $\vec{v_1}$ in $\vec{v_2}$. Then, this contribution is subtracted from $\vec{v_2}$ to obtain a vector perpendicular to $\vec{v_1}$ (green). This step is then repeated with the next vector.

3.3.1 Technique

The first step of the technique to make a vector orthogonal to another is to remove the contribution of the second vector to the first one. The contribution is the projection of the vector on the other, calculated with a scalar product. The algorithm is the following:

- take the second vector $\vec{v_2}$;
- calculate the projection of $\vec{v_1}$ on $\vec{v_2}$; the value of the contribution is $\|\vec{v_2}\| \cdot \cos\alpha$

where $\vec{v_1} \cdot \vec{v_2} = \|\vec{v_1}\| \cdot \|\vec{v_2}\| \cdot \cos\alpha$ and $\cos\alpha = \dfrac{(\vec{v_1} \cdot \vec{v_2})}{\|\vec{v_1}\| \cdot \|\vec{v_2}\|}$ so the contribution of $\vec{v_1}$ in $\vec{v_2}$ is: $\dfrac{(\vec{v_1} \cdot \vec{v_2})}{\|\vec{v_1}\|} \cdot \dfrac{\vec{v_1}}{\|\vec{v_1}\|}$ *(cf. fig. 3.2)*

- subtract the contribution of $\vec{v_1}$ from $\vec{v_2}$: $\vec{v_2}' = \vec{v_2} - (\vec{v_1} \cdot \vec{v_2}) \cdot \dfrac{\vec{v_1}}{\|\vec{v_1}\|^2}$

The result is a vector having no contribution on $\vec{v_1}$, i.e. orthogonal to $\vec{v_1}$:

$$\begin{aligned}
\vec{v_1} \cdot \vec{v_2}' &= \vec{v_1} \cdot \left[\vec{v_2} - (\vec{v_1} \cdot \vec{v_2}) \cdot \frac{\vec{v_1}}{\|\vec{v_1}\|^2}\right] \\
&= \vec{v_1} \cdot \vec{v_2} \; - \; (\vec{v_1} \cdot \vec{v_2}) \cdot \frac{\vec{v_1} \cdot \vec{v_1}}{\|\vec{v_1}\|^2} \\
&= \vec{v_1} \cdot \vec{v_2} \; - \; (\vec{v_1} \cdot \vec{v_2}) \cdot \underbrace{\frac{\|\vec{v_1}\|^2}{\|\vec{v_1}\|^2}}_{=1} \\
&= \vec{v_1} \cdot \vec{v_2} \; - \; \vec{v_1} \cdot \vec{v_2} \\
\vec{v_1} \cdot \vec{v_2}' &= 0
\end{aligned}$$

This must be repeated for each vector. Every time, the contribution from all precedent vectors must be subtracted:

$$\vec{v_i}' = \vec{v_i} - \sum_{j=1}^{i-1} (\vec{v_j} \cdot \vec{v_i}) \cdot \frac{\vec{v_j}}{\|\vec{v_j}\|^2} \tag{3.11}$$

Only the first vector is left unchanged.

The result is a set of vectors $(\vec{v_i'})$ where all vectors are orthogonal to the others. Once this set is created, the measured vector $\vec{X}$ can be decomposed.

3.3.2 Importance of the order of the vectors

During the Gram-Schmidt process, only the first vector is left unchanged. If all vectors are "close" to each other, as in our case (in the same $\frac{1}{2^m}$ subdivision of $\mathbb{R}^m$, that is $(\mathbb{R}^+)^m$), then the main factor f_i in the vector decomposition will be the first one:

$$\vec{X} \simeq \vec{v_1} \;\Rightarrow\; \vec{X} \cdot \vec{v_1} \simeq 1$$

All other vectors of the orthogonal set have to have some negative coordinates in order to be orthogonal to the first vector (which has only positive coordinates). If the second

vector $\vec{v_2}$ only had positive coordinates, it would give a strictly positive scalar product:

$$\forall i,\ v_{1i} > 0,\ v_{2i} > 0 \quad \Rightarrow \quad \sum_{i=0}^{m} v_{1i} \cdot v_{2i} > 0$$

proving that some negative elements in $\vec{v_2}$ are needed to compensate for all strictly positive elements of $\vec{v_1}$. In short, if all coordinates of $\vec{v_1}$ and $\vec{v_2}$ are strictly positive, the two vectors can't be strictly orthogonal. (In this study, this is particularly true for vectors corresponding to the same beam and transversal planes, e.g. B1H and B1V; less so for vectors of different beams).

The contribution of the other vectors in the recomposition will then be small. This can be expressed as:

$$\vec{v_2}' \perp \vec{v_1} \text{ and } \vec{v_1} \simeq \vec{X} \ \Rightarrow \ \vec{v_2}' \cdot \vec{X} \simeq 0$$

This is a broad simplification, and the results showed that the factors can have other values than 1 or 0. But the conclusion is that the order in which the vectors $(\vec{v_i})$ are considered when creating the orthogonal set $(\vec{v_i}')$ influences the result of the decomposition.

Since the order of the vectors is chosen, the choice was made to order the vectors $(\vec{v_i})$ by "closeness to $\vec{X}$" (in the sense of the scalar product) *before* the Gram-Schmidt process. The vector $\vec{v_i}$ which is the "closest" to $\vec{X}$ (i.e. the one that maximizes $\vec{X} \cdot \vec{v_i}$ for all i) will give the highest factor of all (f_i): it will also be the highest contribution in the recomposition $\vec{X}'$.

3.4 MICADO

MICADO (standing for "MInimisation des CArrés d'Orbite") is an iterative algorithm that doesn't involve any projection or matrix inversion: it calculates the factors (f_i) (vector $\vec{F}$) directly (13).

The algorithm starts with an arbitrary set of factors (f_i) (vector $\vec{F}$); calculates the recomposition $\vec{X}' = M \cdot \vec{F}$; and evaluates the quality of the recomposition $\|\vec{X}' - \vec{X}\|$. Then, it varies the factors, and checks that the new recomposition is closer to the original vector than the first recomposition. These iterations carry on until the algorithm converges.

3.5 Recomposition and error

3.5.1 Motivation

All the algorithms presented here, when given a set of vectors and a measured vector, will always return a decomposition of the measured vector on the vector set *(cf. § 3.2.6)*. A recomposition of the original vector as a linear combination of the basis vectors can always be calculated *(cf. eq. 3.5)*. This recomposition is the projection of the original vector on the subspace generated by the reference vectors, and is the "closest" possible to the original vector.

However, the recomposition has no reason to be actually close to the original vector: it depends only on the vector set. In some cases, the recomposition can be null *(cf. § 3.2.6)*.

A way to evaluate the error on the recomposition is needed, in order to know how accurate the decomposition was.

3.5.2 Evaluation of the error

As seen before *(cf. § 3.1.2)*, all vectors are in $(\mathbb{R}^+)^m$ (the space generated by the positive half of the field of real numbers ($\mathbb{R}^+$) considered m times) which means that they are "close" to each other in the sense of the scalar product: $\forall\, \vec{v_a}, \vec{v_b} \in (\vec{v_i}),\ 0 < \vec{v_a} \cdot \vec{v_b} \leq 1$. In order to evaluate how close two vectors are in the m-vector space, the choice was made to consider the *norm of the difference* (subtraction) between the two vectors *(cf. fig. 3.3)*:

$$(eq.\ 3.6) \quad e = \|\vec{v_a} - \vec{v_b}\|$$

Note that no claim is made here that this choice is the best; some other ways to evaluate this difference can be considered, such as normalizing to the highest monitor instead of normalizing to the vector length; or using different norms than the euclidean norm ($\|x\|_2 = \sqrt{\sum x_j^2}$), for instance: $\|x\|_1 = \sum |x_j|$ or $\|x\|_\infty = max(x_j)$.

The error on the recomposition is evaluated by calculating the norm of the difference between the original vector and its recomposition. Since the two vectors are in $(\mathbb{R}^+)^m$, the recomposition error has to be between 0 (when the two vectors are equal) and $\sqrt{2}$ (when the two vectors are orthogonal).

For SVD, the recomposition is straightforward *(cf. § 3.2.5)*, and has a physical meaning. The reference vectors are actual loss profiles, and the understanding of the

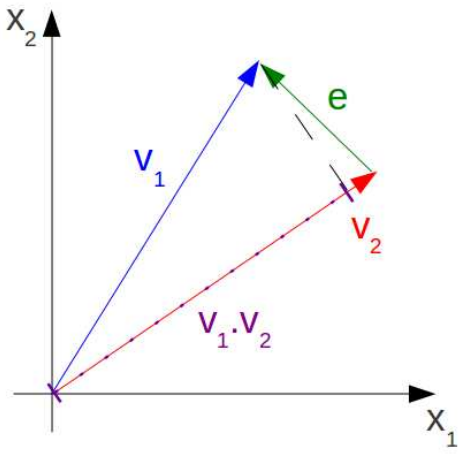

Figure 3.3: Example of the calculation of the error on the recomposition between two vectors $\vec{v_1}, \vec{v_2}$, in a space where $m = 2$. Note that this is always valid, because two vectors always generate a plane in a m dimensions vector space. The purple dash represent the scalar product $\vec{v_1} \cdot \vec{v_2}$. The *error on the recomposition* is the length of the vector $\vec{e}$.

factors is mathematically exact: they are the coefficients of the linear combination of loss profiles.

For the Gram-Schmidt process, the recomposition is not as straightforward. The returned factors are associated to the orthogonalised vectors (after the process) and not to the reference vectors. The orthogonalised vectors don't have a direct physical meaning: they are a reference vectors minus their projections on other reference vectors *(cf. § 3.3)*. Moreover, the recomposition calculated with the orthogonalised vectors is exactly the same vector as the recomposition from SVD: it is the projection of the original vector on the subspace. The error on the recomposition would be exactly the one calculated for the SVD.

Instead, the choice was made to calculate the error on the recomposition with the original *reference* vectors (before orthogonalisation) instead of the orthogonalised vector used to calculate the decomposition. This choice was motivated by the values of these errors, which only differ by around 1%. An example of distributions of the errors on recomposition will be presented in *fig. 4.20*.

The error on the recomposition for Gram-Schmidt (G-S) is not mathematically exact – the exact value is given by the one for SVD – but carries a physical meaning (linear combination of the reference vectors), at the cost of a small error.

3.6 Conclusion

The theories of the different techniques of vector decomposition and a way to evaluate the difference between the original vector and the recomposed vector were presented. The next chapter will explain the practical details of the implementation of these decompositions: which monitors and which vectors were chosen.

Chapter 4

Implementation of Vector Decomposition

This chapter will present the implementation of vector decomposition: the choice of the known loss scenarios, and the selection of the BLMs that generate the vectors.

4.1 Creation of the default vectors

In this section, the creation of the *reference vector set* will be presented: which loss scenarios are used, and how they were gathered.

4.1.1 Choice of beam loss scenarios

The goal of this work is to try to recognize *patterns* in the LHC beam losses; to adapt and implement algorithms achieving a decomposition of *measured loss profiles* into a sum of *known loss scenarios* (used as patterns); and to evaluate the *quality* of these different decompositions.

The choice was made to start with the typical loss scenarios in the point 7 of the LHC. It is the place where the primary and secondary collimators for *transversal* (*horizontal* and *vertical*) cleaning are installed, creating the highest losses in nominal running conditions (this will be described in the next chapter, *fig. 5.1*, the default loss profile in the LHC during nominal operation).

The chosen loss scenarios are the resonance crossings for both planes and both beams *(cf. fig. 4.1)*. They are the verification measurements of collimation cleaning.

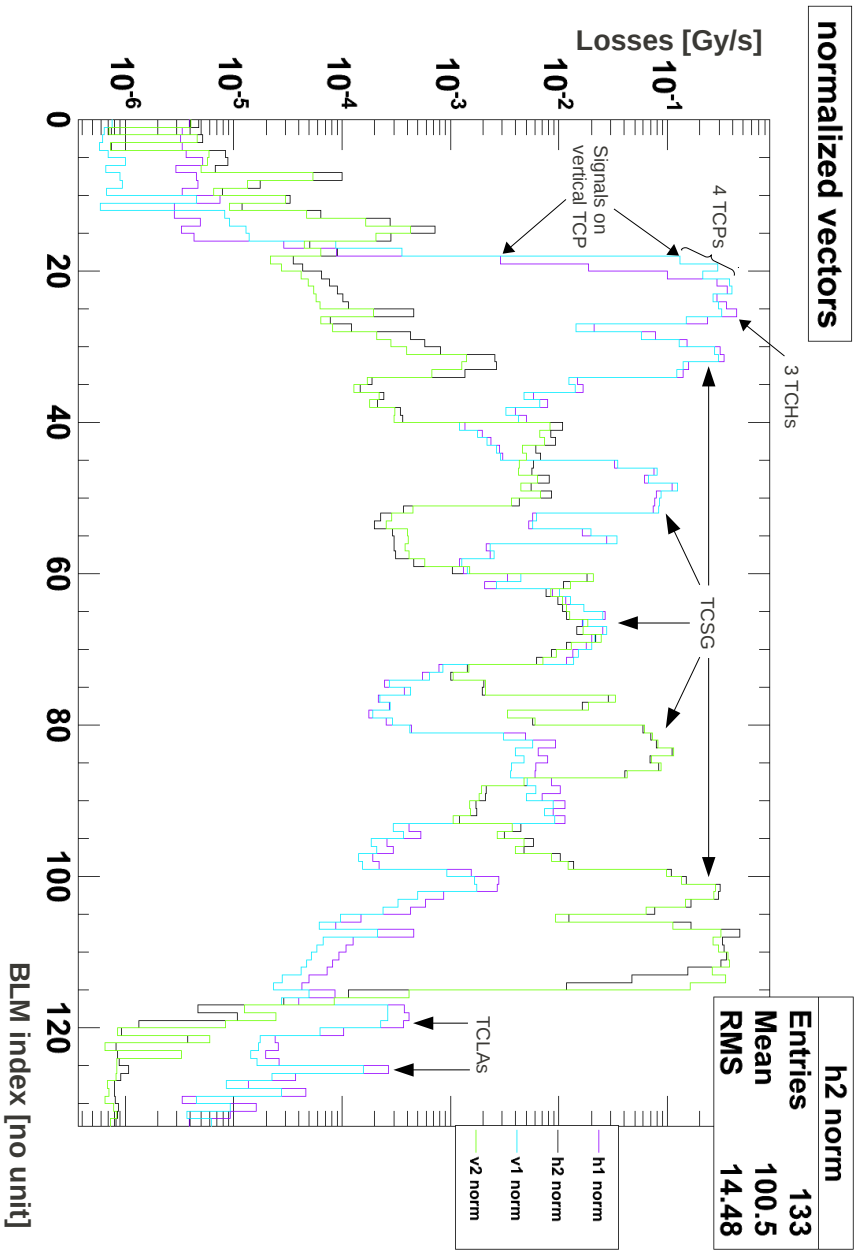

Figure 4.1: Example of one set of the 4 transversal loss scenarios for the 4 resonance crossings (2 planes and 2 beams) measured in the point 7 of LHC. The horizontal axis gives the index of the BLM, and the vertical axis gives the measured losses for each profile. This set was measured the 9^{th} of September 2010 *(cf. tab. 4.1)* and is not used in the final decomposition. All vectors are normalised so they have a length 1 in the m-vector space. Only the relative position (order) of the monitors is respected (same as in the LHC), not their absolute position (DCUM). Note that only a few BLMs present a different signal between horizontal losses and vertical losses (such as the BLM associated to the vertical TCPs: #18 and #118).

Each of these verifications is called a *loss map*. The operator changes the tune Q of one plane such that it crosses the resonance $Q = \frac{1}{3}$: the beam size in the corresponding plane suddenly increases up to the point of touching the primary collimators jaws. The collimators being in their nominal position, the measured loss map is nominal.

Later, more reference vectors were added. In order to have a more complete understanding of the collimation cleaning in the LHC, two *transversal loss scenarios* were added, corresponding to the *momentum cleaning*. This way, the complete set of primary collimators in the LHC are taken into account. However, the momentum cleaning is achieved in the point 3 of the LHC, meaning that extra monitors will be added later.

It was also decided to add the BLMs associated to all the tertiary collimators out of interest. All these monitors were added at the same time, when recalculating the "longer" vectors (with more coordinates). The choice of monitors and loss maps for IR3 will be presented separately.

The transversal (horizontal & vertical) loss scenarios have the advantage of presenting very different cases. The difference between both beams is very obvious (purple and blue profiles for Beam 1, black and green profiles for Beam 2 on *fig. 4.1*), because the corresponding primary collimators are far away from each other. On the other hand, the horizontal and vertical scenarios are very entangled. The difference is visible on the two first primary collimators *(cf. fig. 4.1, #18 and #118)*; the signals downstream correspond mainly to disturbed particles and/or secondary showers, which are very complex. These secondary showers don't follow the optics of the LHC, and their propagation on the downstream monitors is similar for both beams.

4.1.2 Dates of measurement

The first transversal loss maps used were all measured in 2010 *(cf. tab. 4.1)*. The dates of these loss maps were found first by being in the CERN Control Center when they were measured, and by searching the LHC logbook (14). These dates were cross-checked in collaboration with members of the Collimation Working Group (CWG) (15). One date had to be removed because of wrong collimator hierarchy, and two other dates that had been missed were added. Due to the low number of loss maps, they were all kept and used.

Date	Time	Loss scenario
2010/03/28	15:25:52	B1V
2010/03/28	15:28:38	B1H
2010/03/28	15:32:16	B2V
2010/03/28	15:35:00	B2H
2010/10/04	14:28:52	B1V
2010/10/04	14:29:49	B1H
2010/10/04	14:30:52	B2V
2010/10/04	14:31:47	B2H
2010/09/19	21:49:18	B1V
2010/09/19	21:51:31	B1H
2010/09/19	21:52:58	B2V
2010/09/19	21:54:07	B2H
2010/06/18	00:29:22	B2V
2010/06/18	00:39:54	B1V
2010/06/18	00:49:47	B1H
2010/06/18	00:52:15	B2H
2010/06/04	15:35:20	B1V
2010/06/04	15:48:45	B2V
2010/06/04	16:07:38	B1H
2010/06/04	16:41:11	B2H
2010/04/30	23:20:12	B2H
2010/04/30	01:27:56	B1V
2010/04/30	02:22:00	B1H
2010/04/30	02:34:05	B2V
2009/12/10	22:58:49	B1H
2009/12/10	23:03:06	B2H
2009/12/10	23:25:29	B1V
2009/12/10	23:28:40	B2V

Loss scenario	Date & time
B1H	2011-05-15 06:52:37
	2011-05-18 20:03:11
	2011-04-04 19:10:11
	2011-04-12 02:54:54
B2H	2011-05-15 06:44:04
	2011-05-18 20:14:31
	2011-04-04 19:13:10
	2011-04-12 03:03:57
B1V	2011-03-12 20:23:44
	2011-03-09 00:06:05
	2011-03-11 17:43:32
	2011-06-24 01:43:45
B2V	2011-03-12 20:29:56
	2011-05-07 21:48:28
	2011-03-09 00:08:55
	2011-06-24 01:49:53
B1L	2011-03-09 00:17:13
	2011-03-11 17:48:32
	2011-05-15 05:58:45
B2L	2011-04-18 18:13:59
	2011-05-07 22:09:52
	2011-06-24 01:54:39

Table 4.1: Left: Dates and times of the 2010 loss maps, and the corresponding loss scenarios. These loss maps are not used in the decompositions presented. Right: Dates and times of the selection of the 2011 loss maps used in the decompositions, for each loss scenarios. Times are UTC.

Later, in 2011, more loss maps were measured in different conditions, allowing a finer selection. The different conditions, their effect on the loss maps and the selections are discussed in *§ 4.3*. The final selection is presented in *tab. 4.1*.

4.1.3 Normalisation

The overall loss depends on many factors. The most important of them is the beam intensity, but the losses also depend on the optics: focusing errors are amplified during the crossing of the $^1/_3$ resonance, leading to an increase of the transversal beam size. Particles will then be lost on places where the beam envelop is close to the aperture. The intensity of the overall loss is different for every vector of every set: the vectors must be normalized before comparison.

The choice was made to normalize the vectors to an euclidean norm of 1 in the m-vector space: that is, to divide the vector by its length in the sense of the euclidean norm (the standard norm in a vector space). This is motivated by the concept of an orthonormal base of the sub-space: here the vectors are not orthogonal, but still have a norm equal to 1 *(cf. fig. 4.2)*. In most cases, the norm of the vector is dominated by one or few coordinates, so this is similar to normalising to the highest signal.

4.1.4 Effect of the BLM offset

Even when no particle is lost from the beam, there is always a minimum signal in the BLMs. This is part of the design: a 10 pA current is permanently sent in the reading electronics, avoiding the situation where there is no charge to collect *(cf. § 2.3)*. This can be seen in *fig. 4.2, top*: all BLMs above index #125 have the same signal for all dates, even though the losses had different amplitudes. The explanation is that no loss was recorded at these position, only the offset current. It corresponds to $1.8 \cdot 10^{-7}$ Gy/s for RS09.

When the vector is normalised, the offset is divided by the value of the euclidean norm of the corresponding vector. It results in various artificial increases of the offset, as seen in *fig. 4.2 bottom* for all BLMs above index #125. This could have an effect on the decomposition: during a globally low loss, the affected monitors would present a normalised signal higher than for a globally high loss, even if their signals were originally equal (and null).

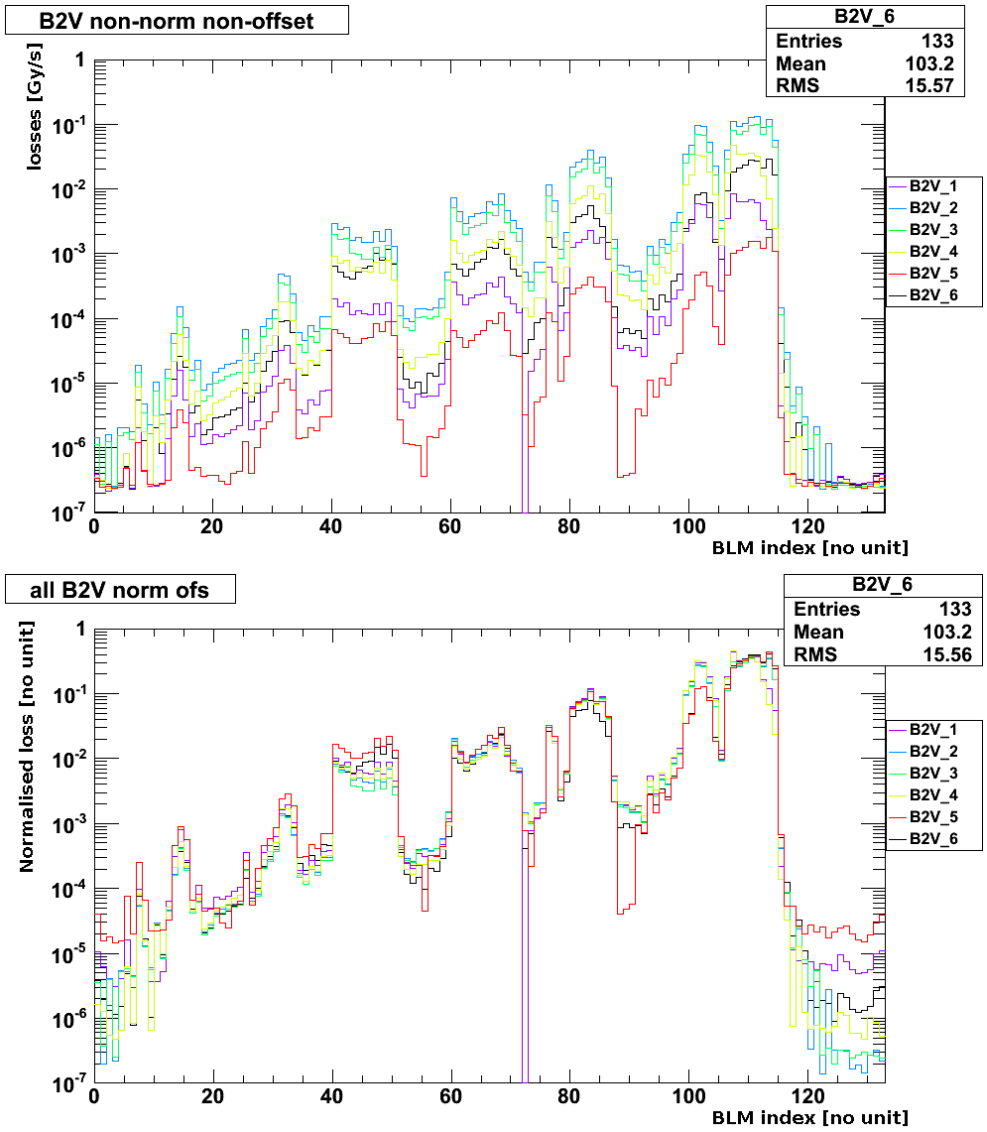

Figure 4.2: Example of the effect of the normalisation. Both plots show the loss maps (measured at different dates in 2010) of one loss scenario: the vertical resonance crossing of beam 2. These specific loss maps are not used in the decomposition. Top: the vectors are not normalized. The "shapes" (the respective values of the coordinates) are similar, but the euclidean norm is different. Bottom: all vectors have a euclidean norm equal to one. The "shapes" are similar for all vectors. The BLMs on the right (above #125) show the effect of normalisation on the offset: they had the same signal ($1.8 \cdot 10^{-7}$ Gy/s) for all curves before normalisation *(top)*, but show different normalised signals *(bottom)*. Therefore, the value of the offset is subtracted from all BLM signals before normalisation.

In order to avoid this phenomenon, the value of the offset ($1.8 \cdot 10^{-7}$ Gy/s for RS09) is systematically removed from all monitors when constructing the vectors, before normalisation.

4.2 Choice of the list of BLMs

This section will present the selection of the m BLMs from IR7 composing the coordinates of the transversal loss vectors expressed in the m-vector space. The selection of monitors of IR3 will be presented separately.

4.2.1 Problem

In this work, each coordinate of the loss vectors corresponds to the signal of one BLM. They must be selected following specific criteria. Beforehand, these criteria themselves must be established.

The influence of each BLM signal — each vector coordinate — on the whole vector depends only on the intensity of the loss, and BLMs with high losses will have a higher weight in the decomposition. In addition, the point of this work is to separate different loss vectors (loss scenarios). From this point of view, there are three main types of monitors:

1. BLMs that have a low signal in all loss scenarios;
2. BLMs that have a high signal in all loss scenarios;
3. BLMs that have different signals in different loss scenarios.

It is obvious that the most interesting BLMs, when discriminating between scenarios, will be the BLMs of the third type.

BLMs with low signal in all scenarios

When calculating one of the vector decompositions, the BLMs of the first type have no influence. They do not carry information on the nature of the loss: if added to the vectors, they only "dilute" this information. If they are included, the vector will have a higher dimension for the same information.

It is better to ignore these BLMs. Tests on simple examples show that they don't drastically change the result of a decomposition. Typically, for SVD, one of the left eigenvectors will have zeros everywhere, and a one at the position of the BLM: it will be a vector of the canonical basis. The corresponding singular value will be very low, or there will be no singular value associated to that vector: the index of the vector will be higher than n. The vector will either be ignored or have only a negligible contribution. This was checked by running the SVD with all monitors in IR7, then plotting all the left singular vectors of matrix U *(cf. § 3.2)*.

BLMs with high signal in all scenarios

The case opposite to BLMs of the first type are the BLMs that show, in every case, a signal higher than most other BLMs of the vectors. This case is more critical because such BLMs, even if they cannot be used for discriminating between loss scenarios, have a strong influence on the decomposition: the higher the signal of the BLM relative to the others, the higher the influence on the decomposition. Only a small variation on the contribution of such BLMs can be bigger than the signal of some other BLMs, and lead to a change in the recomposition result.

If possible, such BLMs should be removed from the list, as they do not carry discriminating information: their signal is high in all scenario. They could lead to wrong decomposition. The concept of the decomposition is to match vectors. Between all coordinates, the highest ones have the highest influence on the decomposition. Matching such a coordinate (even if it carries no information) to the detriment of a another smaller coordinate (which could carry information) will lead to a smaller error on the decomposition for the wrong information. The vector would have been matched to the "wrong" coordinate.

BLMs that have different signals in different scenarios

This third case is the most relevant one. These BLMs can be used for simple discrimination "by eye" between scenarios. They are the BLMs carrying the information about the differences between the loss scenarios.

The selected BLMs were the ones that were at the same time in the list of BLMs with highest signals, and in the list of BLMs with the highest variations from one loss

scenario to another. The ways to evaluate this variation are presented in the next section.

4.2.2 Selection technique

The list of chosen BLMs, selected after sorting by different criteria, was produced by following several steps.

Distributions of the signal of each BLM

For the BLM selection, all loss scenarios were considered together. All the occurrences (loss maps) of all the loss scenarios were gathered. Each loss map is a verification measurement of collimation cleaning. These measurements are done on a regular basis in the LHC, meaning that several are available.

The average signal and the standard deviation of each BLM were calculated considering all loss maps of all scenarios together, after normalisation. The standard deviation gives a quantification of the variation of the signal from one loss scenario to another.

Beforehand, the check was made that the signal of one BLM doesn't change much between loss maps of the same scenario *(cf. § 4.1.1)*. The standard deviation of the signal of a BLM within one loss scenario is small: less than 5% of the average signal, for 2010 and 2011 loss maps. Conversely, the standard deviation between scenarios is big *(cf. fig. 4.3)*: same order of magnitude as the average; that is, much bigger than the standard deviation within one scenario.

Variations of BLM signal between scenarios

The first way to evaluate the variation of one BLM signal from one scenario to another was to calculate the difference between the highest and the lowest signal for all loss maps. However, this doesn't take into account all loss maps, only the two loss maps with highest and lowest signal. The way to consider all loss maps is to use standard deviation.

However, both the standard deviation and the difference between minimum and maximum signals are proportional to the mean value of the signal. When ordering the monitors by decreasing standard deviation, the results are extremely similar as a simple "ordering by signal" *(cf. tab. 5.1)*. The relevant quantities here are the *Relative*

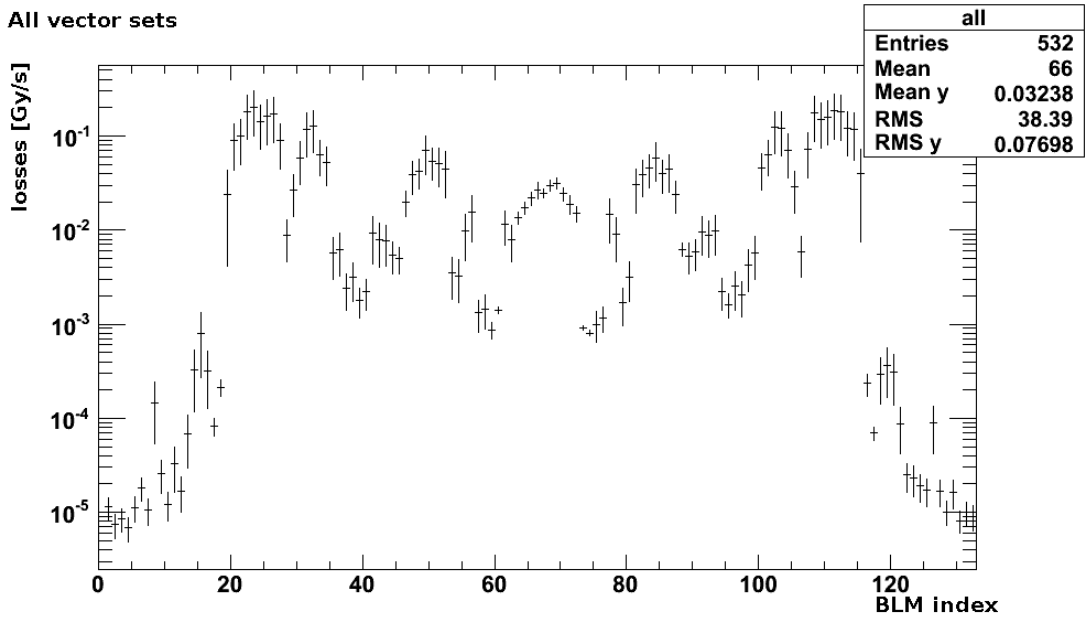

Figure 4.3: Distributions of all BLMs of point 7 when considering all loss scenarios at the same time, for the loss maps of 2010. Averages and standard deviations are calculated for all 28 measurements (4 scenarios × 7 dates) at the same time. These specific loss maps are not used in the decomposition, but the selection is the same. BLMs are displayed with the same relative order as they have in the LHC, but DCUM is not respected. The BLMs showing the bigger error bars are the most relevant ones.

Standard Deviation (RSD); and the *min/max ratio*, which corresponds to the "length of the error bar" in log scale *(cf. fig. 4.3)*.

These two quantities gave very similar results, and the monitors with the highest values were selected *(cf. tab. 4.2)*.

Symmetry beam 1 / beam 2

The physical implementation of components and instruments in the LHC is nearly always symmetric for beam 1 and beam 2 around the interaction points. It is the case for the collimators in point 3 and 7. In order to follow this symmetry, every time a monitor was selected for one beam, the symmetric monitor was added to the list as well. This is validated by the fact that in most cases, both monitors were already in the selection.

The results are presented in *tab. 4.2*.

Index	BLM left of IP 7	Symmetric BLM right of IP 7	Index
018	BLMEI.06L7.B1E10_TCP.D6L7.B1	BLMEI.06R7.B2I10_TCP.D6R7.B2	114
019	BLMEI.06L7.B1E10_TCP.C6L7.B1	BLMEI.06R7.B2I10_TCP.C6R7.B2	113
020	BLMEI.06L7.B1E10_TCP.B6L7.B1	BLMEI.06R7.B2I10_TCP.B6R7.B2	112
021	BLMEI.06L7.B1E10_TCP.A6L7.B1	BLMEI.06R7.B2I10_TCP.A6R7.B2	111
022	BLMEI.06L7.B1E10_TCHSV.6L7.B1	BLMEI.06R7.B2I10_TCHSV.6R7.B2	110
023	BLMEI.06L7.B1E10_TCHSH.6L7.B1	BLMEI.06R7.B2I10_TCHSH.6R7.B2	109
024	BLMEI.06L7.B1E10_TCHSS.6L7.B1	BLMEI.06R7.B2I20_TCHSS.6R7.B2	108
026	BLMEI.06L7.B1E10_MBW.B6L7	BLMEI.06R7.B2I10_MBW.B6R7	106
030	BLMEI.06L7.B1E10_TCSM.A6L7.B1	BLMEI.06R7.B2I10_TCSM.A6R7.B2	100
054	BLMEI.04L7.B1E10_TCSG.D4L7.B1	BLMEI.04R7.B2I10_TCSG.D4R7.B2	77
055	BLMEI.04L7.B1E10_TCSM.D4L7.B1	BLMEI.04R7.B2I10_TCSM.D4R7.B2	76
007	BLMEI.07L7.B2I10_TCLA.A7L7.B2	BLMEI.07R7.B1E10_TCLA.A7R7.B1	125
010	BLMQI.06L7.B2I20_MQTL	BLMQI.06R7.B1E20_MQTL	122
012	BLMQI.06L7.B2I10_MQTL	BLMQI.06R7.B1E10_MQTL	120
013	BLMEI.06L7.B2I10_TCLA.D6L7.B2	BLMEI.06R7.B1E10_TCLA.D6R7.B1	119
014	BLMQI.06L7.B1E30_MQTL	BLMQI.06R7.B2I30_MQTL	118
015	BLMEI.06L7.B2I10_TCLA.C6L7.B2	BLMEI.06R7.B1E10_TCLA.C6R7.B1	117
028	BLMEI.06L7.B2I10_TCLA.B6L7.B2	BLMEI.06R7.B1E10_TCLA.B6R7.B1	107
031	BLMEI.06L7.B2I10_TCLA.A6L7.B2	BLMEI.06R7.B1E10_TCLA.A6R7.B1	101
040	BLMEI.05L7.B2I10_TCSM.E5L7.B2	BLMEI.05R7.B1E10_TCSG.E5R7.B1	91
051	BLMEI.05L7.B2I10_TCSM.A5L7.B2	BLMEI.05R7.B1E10_TCSM.A5R7.B1	80

Table 4.2: List of selected BLMs of IR7. The index corresponds to the BLM index in the figures showing the signal distributions, such as *fig. 4.1, fig. 4.2* and *fig. 4.3*. The monitors were selected to have the highest relative standard deviation, or to be the symmetric of such a monitor. In the naming convention, the part after the underscore "_" is the name of the element associated to the BLM; the part before describes the BLM and its position.

4.3 Final loss map selection

In 2011, following the experience acquired in 2010, the settings of the collimators were changed, and in the first months of 2011, many loss maps were measured. The first observation were that these loss maps were different from the ones measured in 2010. They also show differences in shape one to another.

4.3.1 Dependency on energy

The settings (opening of the jaws) of the collimators being dependent on the energy, the loss profiles will be different depending on the energy. Within all loss maps measured in 2011, two different beam energies were used. The loss maps were sorted according to

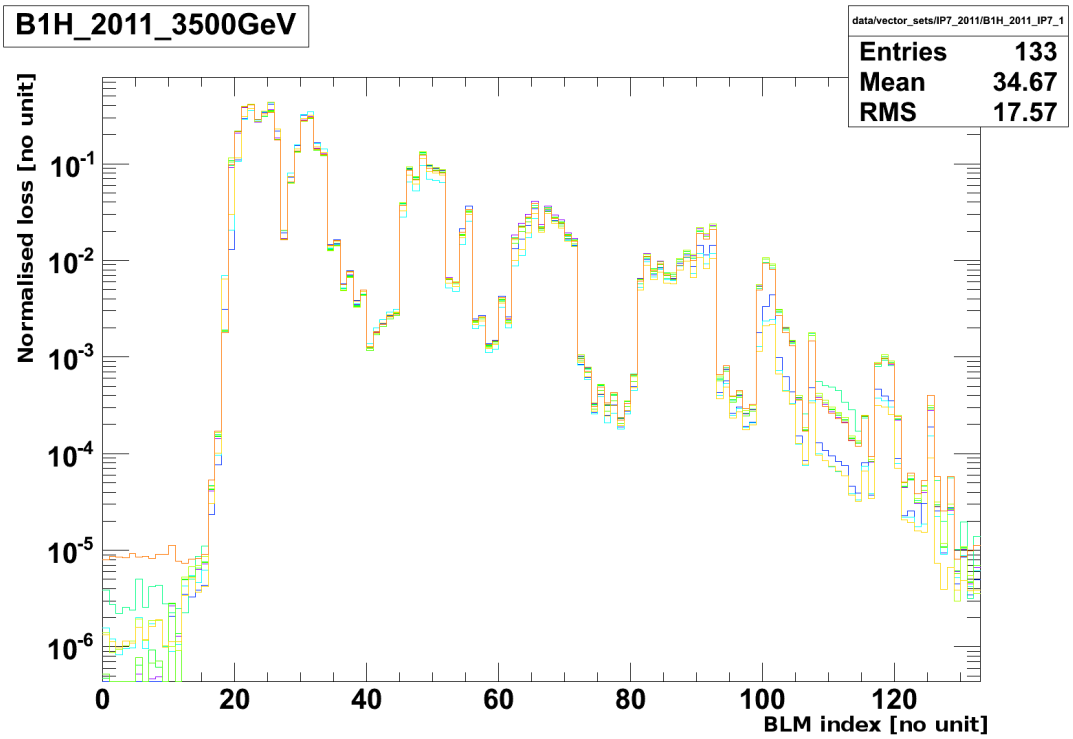

Figure 4.4: All 2011 loss maps (at the time of the study) for Beam 1 horizontal, normalised. Note that even though the overall shapes are similar, critical monitors such as the ones associated to primary collimators give "inconsistent" results: the loss at the vertical collimator (#18) in one loss map can be the same as the value at the horizontal collimator (#19) in another loss map.

whether the loss map was measured at injection energy (450 GeV) or collision energy (3.5 TeV at the time). One example for the loss scenario B1H is shown in *fig. 4.4*.

However, even after sorting by energy, the results are still "inconsistent": even though the overall shapes are similar, the variations of the loss recorded in one BLM within one loss scenario are in some cases higher than the signal of the BLM. For instance, the BLMs at index #18 and #19 can have similar values from one loss map to another. Sorting by energy is not enough.

The loss maps must be sorted according to another criterion: the order in which they were measured.

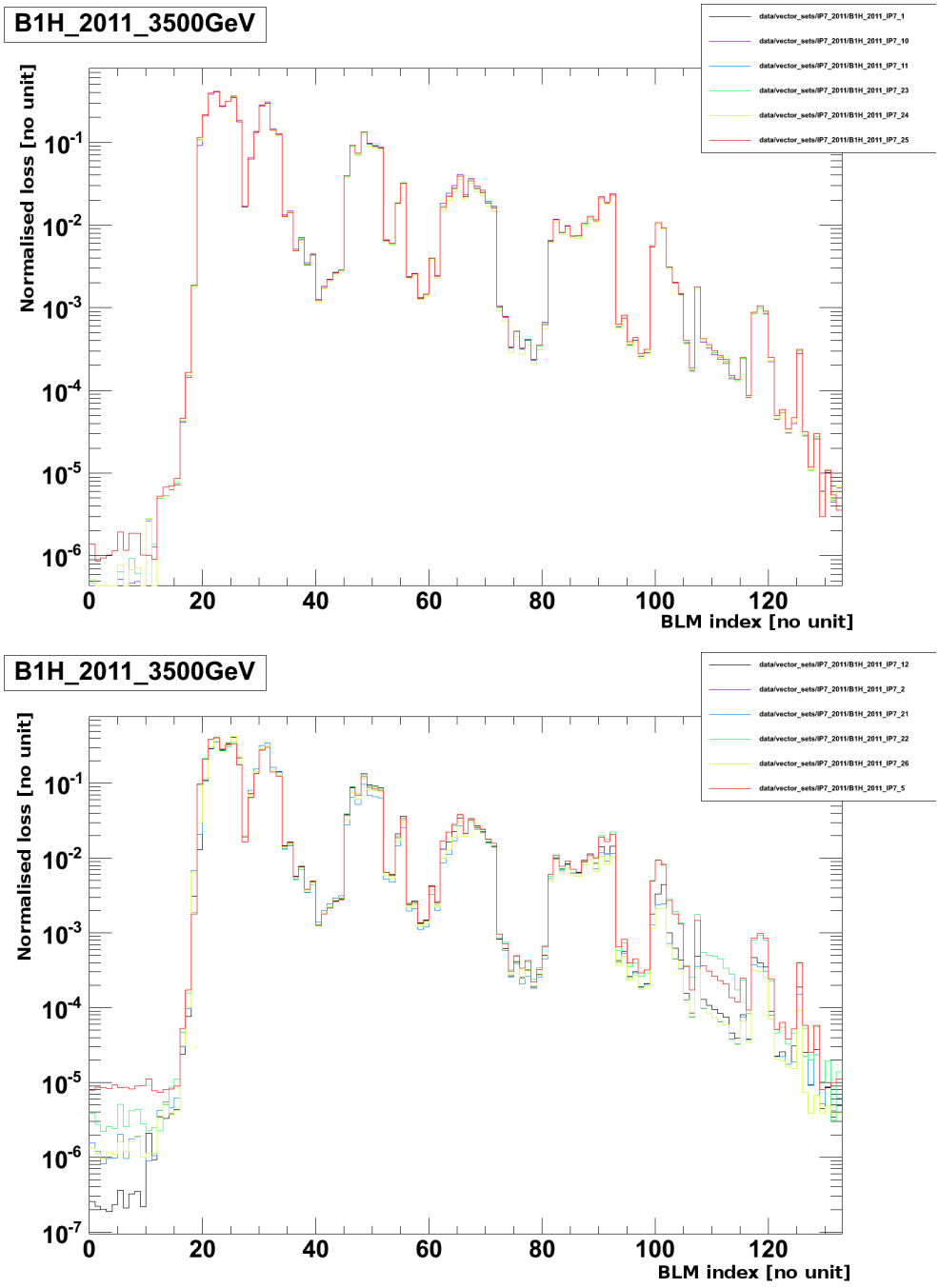

Figure 4.5: Top: 2011 loss maps for B1H measured *before* the loss maps for B1V. Bottom: 2011 loss maps for B1H measured *after* the loss maps for B1V. Each colour correspond to a different loss map. Note how the spread is different: the normalised losses for one BLM are very close in the first case, and further apart in the second. Quantitative values of standard deviation are given in *Fig. 4.6*.

4.3.2 Order of the loss maps

As described in *§ 4.1.1*, the loss maps are measurements of losses during the crossing of the resonance of the tune for one of the transversal planes. The measurement for the other plane is done directly afterwards: the beam is not extracted, and no new beam is injected.

However, the resonance crossing and the cleaning by the collimators perturb the beam. Even though it is supposed to affect only one plane, both planes see an effect, even if it is only due to the coupling between them. This means that the loss maps corresponding to the plane measured first will give very consistent and reproducible results, whereas the loss map measured secondly will be perturbed.

This effect is shown in *fig. 4.5*. The loss maps all correspond to the same loss scenario (beam 1 horizontal), and they are sorted according to the following criterion: whether the loss maps were measured *before* or *after* the other loss scenario for the same beam (beam 1 vertical). The difference can already be estimated visually: there is more variation within the values of one monitor when the loss maps were measured in second position *(cf. fig. 4.5 bottom)*.

4.3.3 Reproducibility for IR7

Quantitative result are given in *fig. 4.6*. It shows the loss maps for beam 2 horizontal which were measured before the loss maps for beam 2 vertical. For each of the selected monitors, the standard deviation was calculated and normalised by the average signal. The results are shown in blue: most monitors have a standard deviation corresponding to 1% of the average signal.

These loss maps were measured over the course of three months, showing that during this period, the standard deviation of the BLM signal (after vector normalisation) is around 1% of the average signal *(cf. fig. 4.6)*.

4.4 Adding more cases: longitudinal scenarios and TCTs

Once the standard vectors for the insertion region 7 were assumed to be correct, the decision was made to extend the analysis by adding information about the third beam plane: the longitudinal cleaning of the beam. The collimators for longitudinal cleaning are installed in insertion region 3.

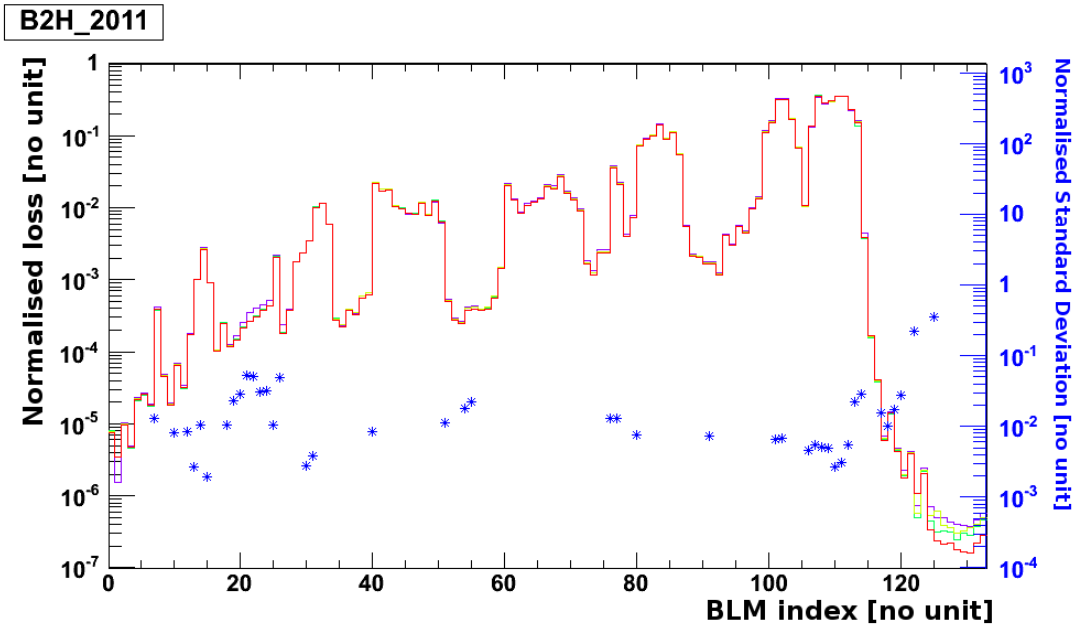

Figure 4.6: Values of signals in all monitors of IP7 for the B2H loss maps of 2011, and values of the normalised standard deviation of the signal of the selected BLMs (in blue), for all loss maps of the loss scenario B2H taken *before* the loss maps for B2V. All scenarios and the final selection of monitors will be presented in *fig. 4.11, fig. 4.12* and *fig. 4.13*. Most of the standard deviations are around 1% of the value of the average. The two higher values (#122 and #125) appear because the average value of the signal for this scenario is small and close to the offset, and the effect of the noise gives a high standard deviation. These monitors were selected by symmetry and are not relevant for B1 scenarios; the symmetric monitors, which are used in this scenario, are at index #7 and #12, and have a normalised standard deviation around 1% as well.

In this section, we will present the different problems which arise when adding the longitudinal loss scenarios to the decomposition, and the consequent choices made. The addition of the *tertiary collimators (TCTs)* will also be described.

4.4.1 Longitudinal loss maps

The situation in IR3 is much simpler than the one in IR7, because the losses only come from one plane of the beam. There are only two primary collimators in IR3, one per beam.

Similarly to the transversal loss scenarios, the point of adding the two longitudinal loss scenarios to the decomposition is to be able to separate the longitudinal losses originating from B1 or B2 from the transversal (horizontal and vertical planes) losses

for B1 and B2. However, the main problem is that there is no loss map for only one beam in IR3 at 3.5 TeV. The selection technique used for IR7 monitors is not applicable.

The longitudinal losses correspond to losses created by off-momentum particles. During the loss maps measurements, off-momentum particles are created by changing the frequency of the radio frequency cavities, usually by $\pm 500\,\mathrm{Hz}$. These particles are then lost on the primary collimators in IR3.

In the case of the 2011 transversal loss maps, it was shown that only the loss maps performed first should be kept. This was not possible here: not enough longitudinal loss maps were measured separately. Usually, they are measured just after the transversal ones, without dumping the beam and injecting a new one.

The consequence is that there were no longitudinal loss maps available for a single beam. Several operations were necessary to recreate them.

4.4.2 Intensity derivative

For every loss map in the available list, the two beams were considered at the same time. Most of the loss maps are *mixed*: the level of the losses are similar for both beams *(cf. fig. 4.7)*. However, sometimes one beam can be more sensitive than the other to the change in frequency. It is a purely empirical result; the frequency of the RF chambers for both beams have exactly the same frequency. From one second to the next, the loss profile can be dominated by one beam or the other.

A tentative study of the intensity was done to try to identify times at which a loss map might be dominated by one beam. The numerical derivative of the intensity in a beam, as given by the *fast Beam Current Transformers*, was calculated. However, even if the derivative of the intensity was clearly dominated by one beam at a given second, it did not correlate clearly with the measured loss profile. One of the reasons could be that particles are lost in other places than the monitors of IR3, especially in IR7.

Several seconds around the time of the loss map were investigated manually, for each loss map. They were separated between the ones clearly dominated by one beam (at least by a factor 10 in the monitors specific to one beam) and the mixed ones. Wrong profiles, for which the losses in IR7 are higher than in IR3, were discarded.

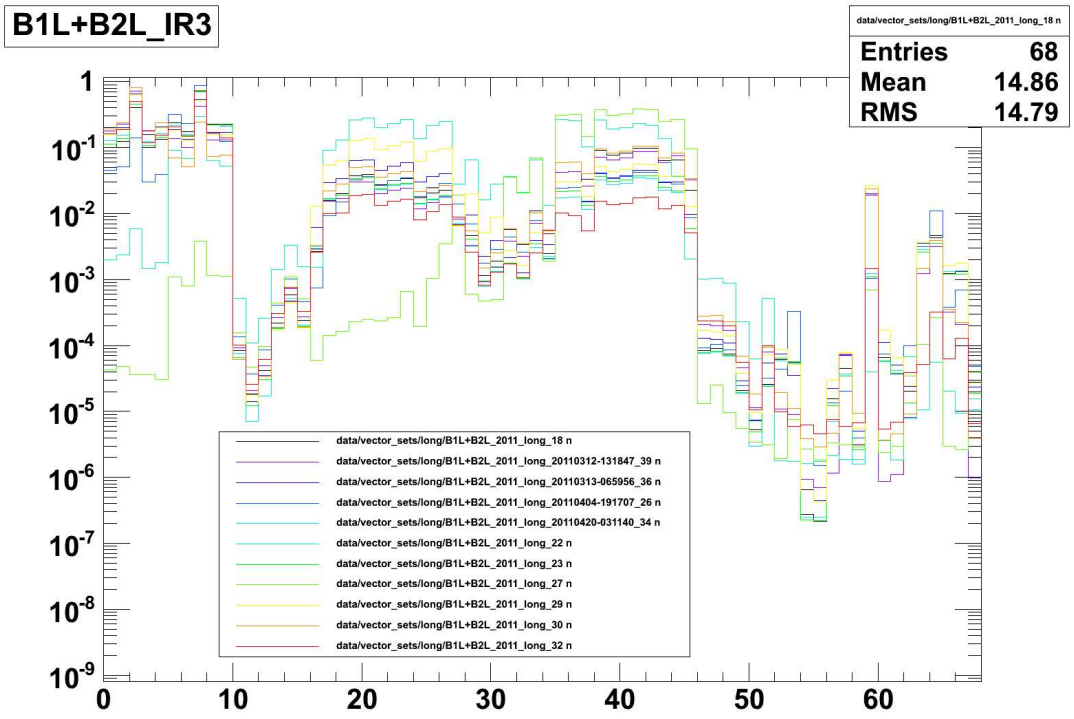

Figure 4.7: Example of several mixed loss maps represented on the same graph (normalised). The ten first monitors are from IR3; the sixteen last ones are associated to tertiary collimators; the rest is from IR7. In this example, the isolated light blue curve is the only loss map clearly dominated by one beam (B2) in IR3. The full list of monitors is given in *tab. 4.5*.

4.4.3 Choice of the monitors

In order to get a finer selection, it was suggested that the signal of one monitor S_i could be reconstructed as a linear combination of the derivatives of the two intensities:

$$S_i = \alpha \frac{dI_1}{dt} + \beta \frac{dI_2}{dt}$$

This was tried with a χ^2 fit for the data ± 6 seconds around the time of each loss map; for all loss maps together; and with a cut for only significant values of the intensity derivative. The fit gave reasonable results but the model wasn't precise enough: the error on the recalculated signal was too big, of the order of magnitude of the signal itself.

Consequently, the selection of monitors given by this technique (monitors for which $\alpha \gg \beta$ or $\beta \gg \alpha$) were the same as the ones selected by the same selection technique

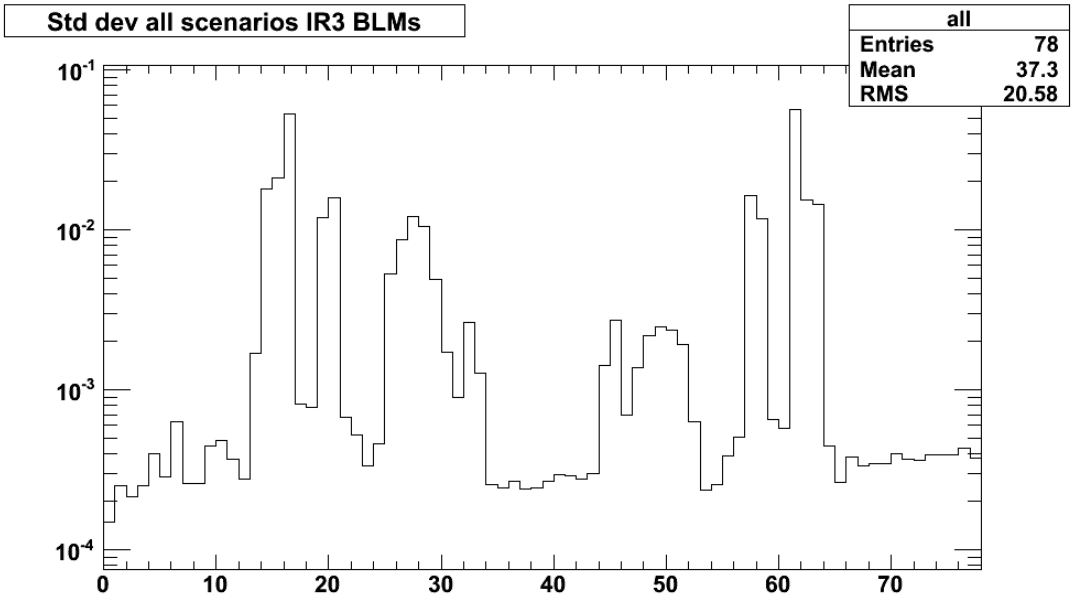

Figure 4.8: Relative Standard Deviation (RSD) of all monitors in IR3, for all loss maps. The BLM index corresponds to the position of the monitor in IR3 and will not be used anywhere else. The selected monitors are the ones giving the highest RSD for all loss maps *(cf. § 4.2.2)*.

as for IR7 *(cf. § 4.2.2)*.

The monitors with the highest relative standard deviation over all loss maps were selected *(cf. fig. 4.8)*. The results were obvious: the BLMs associated to the primary collimator (TCP), and 4 other BLMs around them. The first (in beam order) and more important losses happen there; and these BLMs are far away from the TCP for the other beam. The selection of monitors for IR3 is given in *tab. 4.3*

4.4.4 Creation of the longitudinal vectors

The longitudinal loss maps were sorted by beam manually: the monitors associated to one beam had to dominate the ones for the other beam (by at least a factor 10). After that first selection, the average and standard deviation were calculated for each monitor. The outlying loss maps (values of the monitor signal being more than three standard deviations away from the average) could then be removed. The validity of the suppression was verified by checking that the new standard deviation had a value similar to the previous, and that all signals were within three standard deviations of the average. The final selections of loss maps will be presented later, in *fig. 4.13*.

Index	BLM name
0	BLMEI.06L3.B1I10_TCP.6L3.B1
1	BLMEI.06L3.B1I10_TCHSH.6L3.B1
2	BLMEI.06L3.B1I10_TCAPA.6L3.B1
3	BLMEI.05L3.B1I10_TCSG.5L3.B1
4	BLMEI.05L3.B1I10_TCSM.5L3.B1
5	BLMEI.05R3.B2E10_TCSM.5R3.B2
6	BLMEI.05R3.B2E10_TCSG.5R3.B2
7	BLMEI.06R3.B2E10_TCAPA.6R3.B2
8	BLMEI.06R3.B2E10_TCHSH.6R3.B2
9	BLMEI.06R3.B2E10_TCP.6R3.B2

Table 4.3: List of selected BLMs of IR3. The index corresponds to the BLM index in the loss maps *(cf. fig. 4.7)*. The BLMs were selected to have the highest relative standard deviations *(cf. fig. 4.8)*.

The fact that the loss maps are always "mixed" (losses always come from both beams) means that the effect of the cross-talk between the two beams can not be evaluated. In order to compensate for this, it was suggested that the monitors associated to the other beam should be set to zero. This was cross-checked on the loss maps: these monitors have lower signals. Both vectors are represented in *fig. 4.9*.

In order to evaluate the validity of the choice and quality of the recomposition with these vectors, they were cross-checked with the mixed loss maps. The two longitudinal vectors showed in *fig. 4.9* were summed and normalised to a euclidean norm of 1; then, the error between the measured mixed loss maps and the recreated sum of vectors was calculated *(cf. fig. 4.10)*. It was also calculated for the average of all the mixed loss maps, which gives the best agreement.

4.4.5 Tertiary collimators

It was decided to add the *tertiary collimators (TCT)* to the vectors, in order to know what part of the BLM signal is due to the collimation cleaning, and what part of the signal has a different origin.

The TCTs are part of the collimation hierarchy *(cf. fig. 1.6)*, but they are installed close to the interaction points. All the losses measured at the TCT at the time of a loss map are assumed to come from the primary and secondary collimators. There are no collisions at the time of the loss maps. During nominal operation, the debris from the collisions can reach the TCTs.

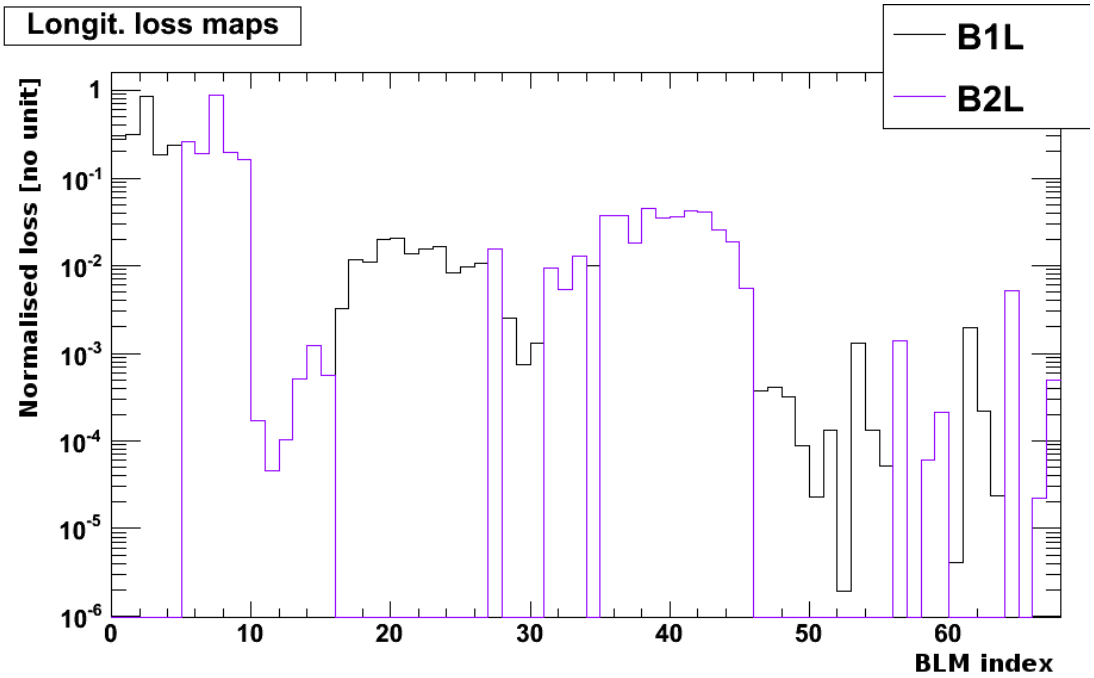

Figure 4.9: Reference vectors for the longitudinal loss scenarios. Beam 1 is in black, Beam 2 in purple. The full list of monitors is given in *tab. 4.5*. The non-null coordinates of one vector correspond to the BLMs associated with the beam considered. For the other vector, the situation is inverted.

No loss maps were associated to the TCTs. The choice was made to add one canonical vector per TCT. All losses coming from collimation are reconstructed by the transversal and longitudinal vectors; what is left is given by the factor associated to the canonical vector. This is equivalent to calculating the difference between the loss recalculated by the decomposition and the current loss at the TCT.

4.4.6 Final loss maps — reproducibility

Once the lists of monitors and loss maps were established, the values could be extracted (for all monitors, for each loss map) and the averages were calculated.

In the figures *4.11, 4.12 and 4.13*, all loss maps of each scenario are shown. The coordinates of the corresponding reference vector is the average over all loss maps.

The calculated values of relative standard deviation show how well the measures could be reproduced. In order to compare the quality of the loss maps against each other, all the Relative Standard Deviations were gathered on the same plot *(cf. fig. 4.14)*.

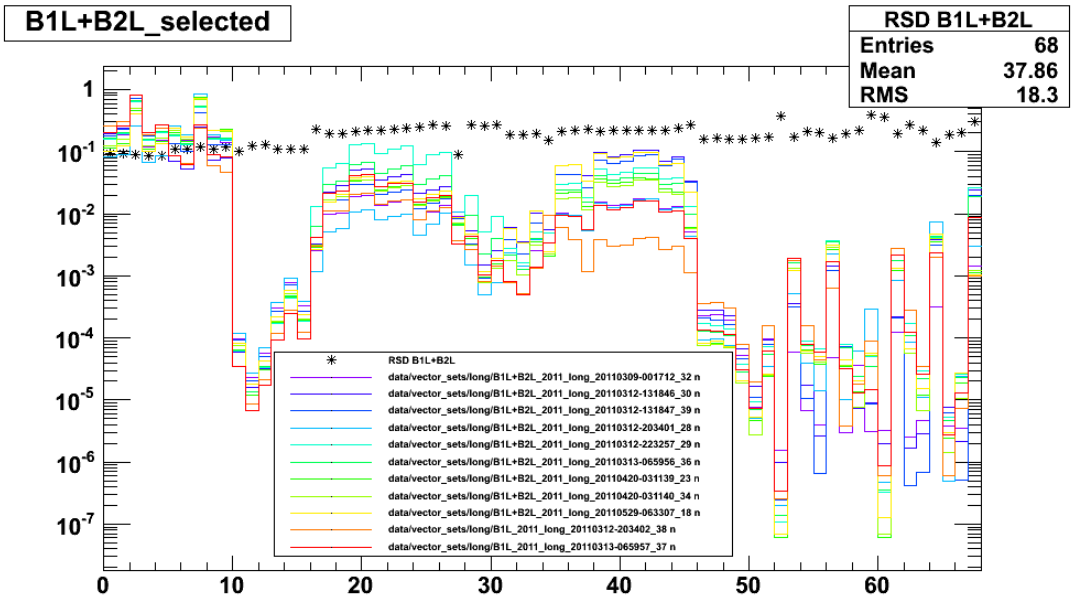

Name of loss map	Error
B1L+B2L_2011_long_20110420-031140_34	0.2148
B1L_2011_long_20110312-203402_38	0.4926
B1L+B2L_2011_long_20110312-131847_39	0.2932
B1L+B2L_2011_long_20110420-031139_23	0.2715
B1L+B2L_2011_long_20110313-065956_36	0.1853
B1L+B2L_2011_long_20110309-001712_32	0.1670
B1L+B2L_2011_long_20110312-131846_30	0.5135
B1L+B2L_2011_long_20110312-203401_28	0.4859
B1L+B2L_2011_long_20110312-223257_29	0.3248
B1L_2011_long_20110313-065957_37	0.4645
B1L+B2L_2011_long_20110529-063307_18	0.3545
average of loss maps	0.1284

Figure 4.10: Top: selection of "mixed" longitudinal loss maps, for which the losses for both beams were of similar level. The stars indicate the relative standard deviation calculated over all loss maps. Bottom: Error calculated between each "mixed" loss map and the sum of the two vectors *(cf. fig. 4.9)*. The last line is the same error, calculated between the average of all these loss maps and the sum of the two vectors B1L and B2L used in the decomposition. Most values are high w.r.t. the conclusion on the "correctness" of a decomposition *(cf. § 4.7)*, but the same error calculated for the average of all these loss maps is lower. This shows a good agreement between the vectors chosen to represent the longitudinal loss maps, and the vectors measured as mixed loss maps.

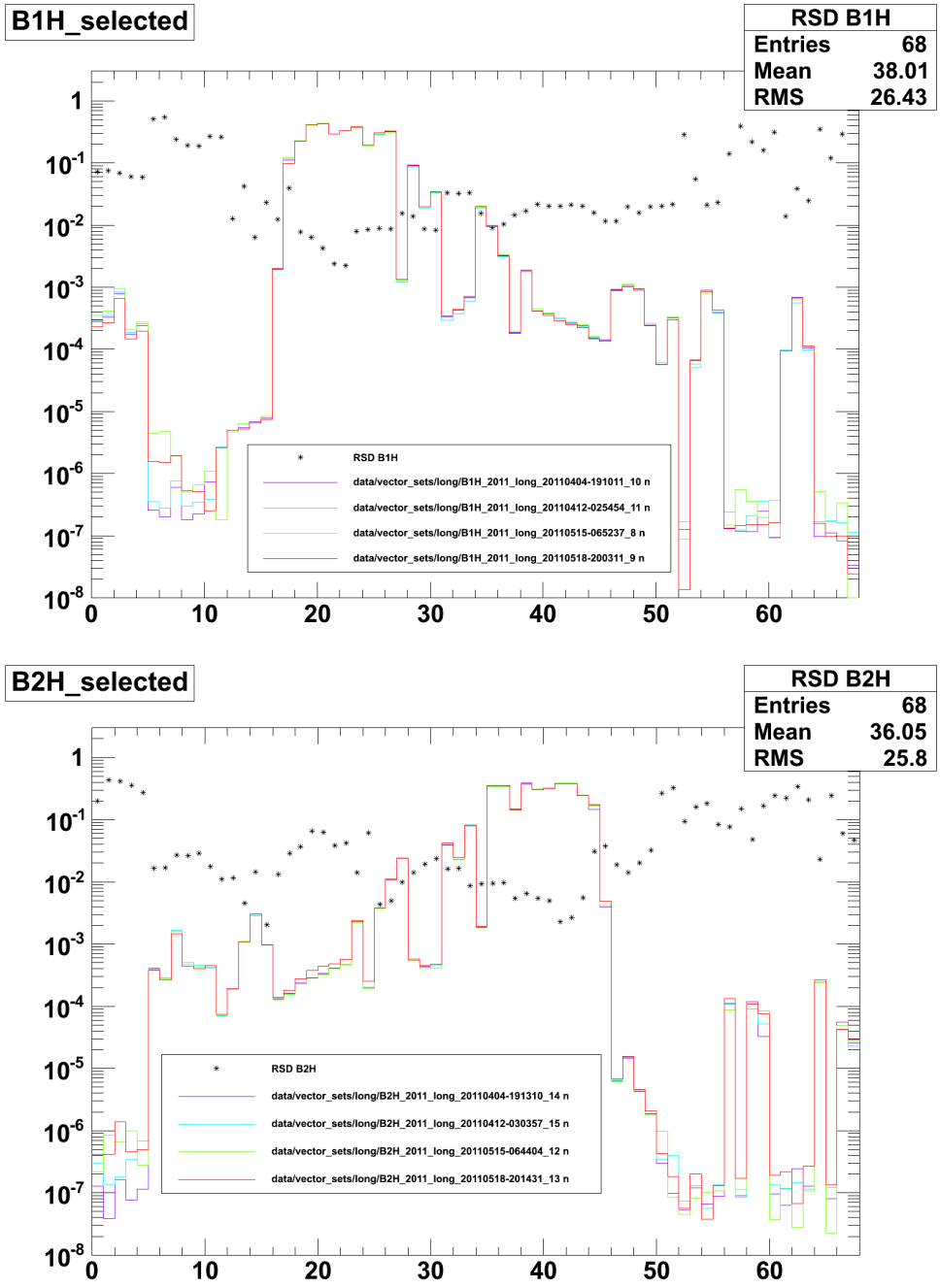

Figure 4.11: Selection of horizontal loss maps of 2011, used in the decomposition. Top: beam 1, bottom: beam 2. The stars represent the relative standard deviation for each monitor. The average (not represented) is the value used in the corresponding reference vector. The full list of monitors is given in *tab. 4.5*.

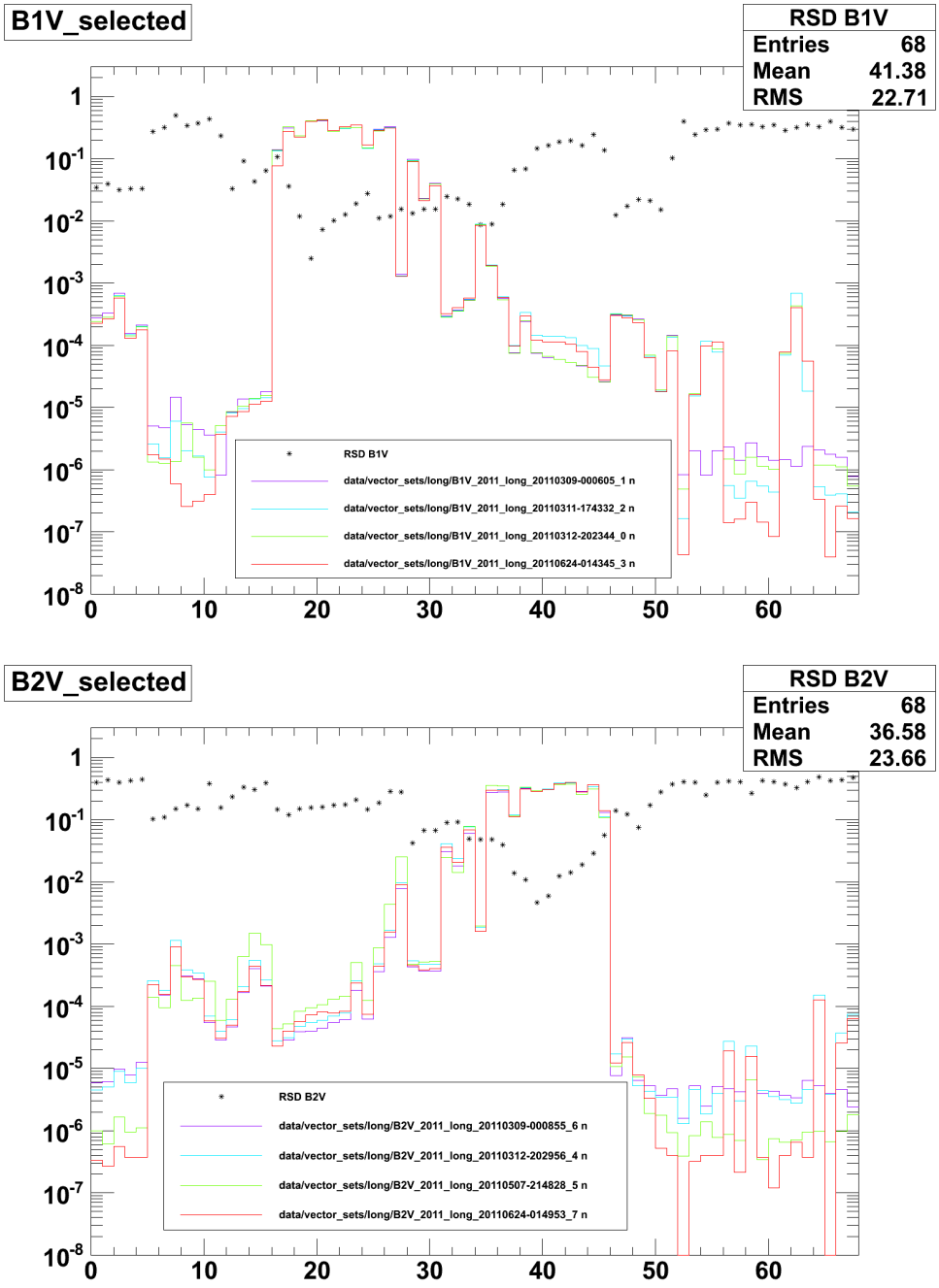

Figure 4.12: Selection of vertical loss maps of 2011, used in the decomposition. Top: beam 1, bottom: beam 2. The stars represent the relative standard deviation for each monitor. The average (not represented) is the value used in the corresponding reference vector. The full list of monitors is given in *tab. 4.5*.

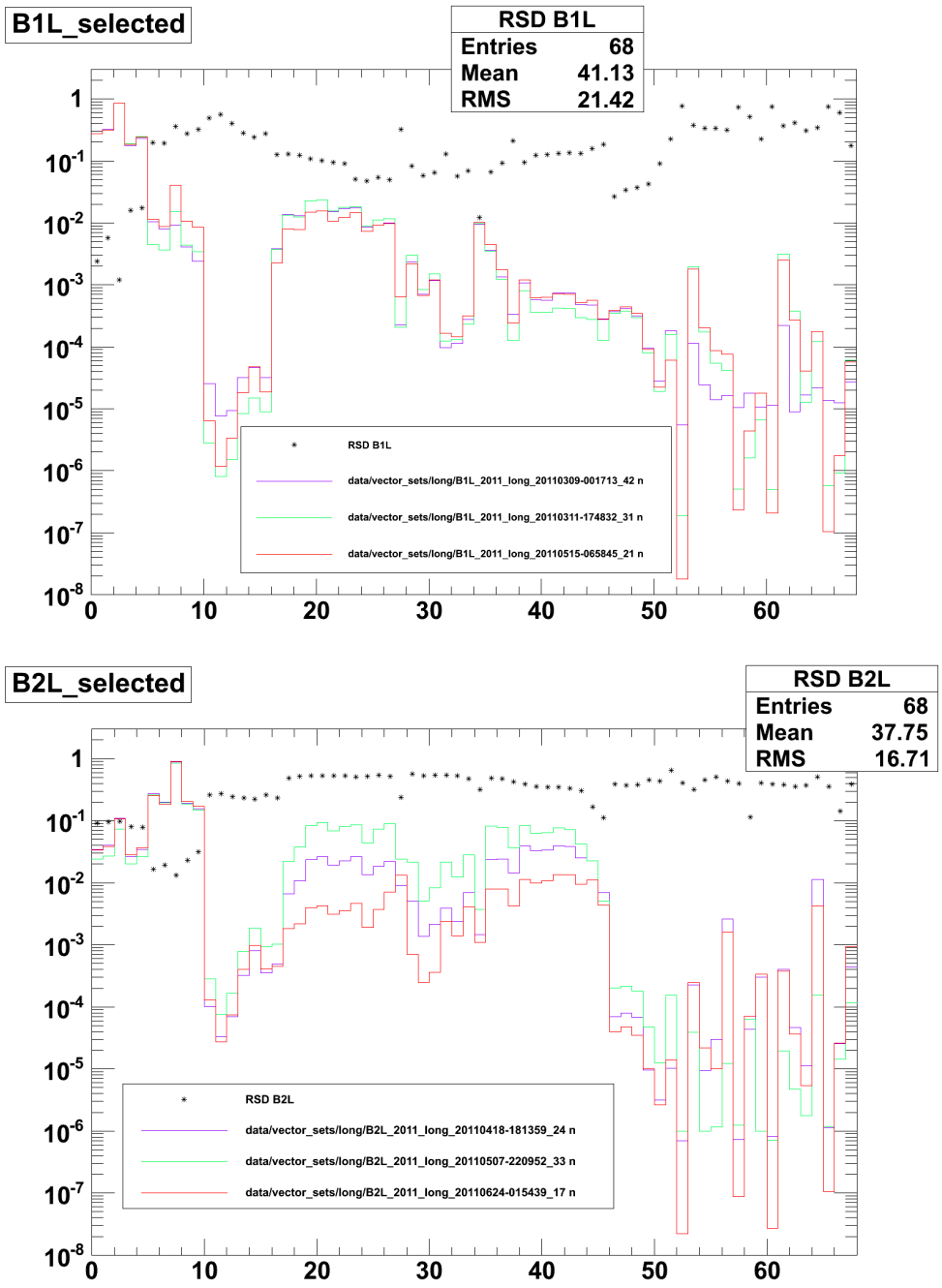

Figure 4.13: Selection of longitudinal loss maps of 2011, used in the decomposition. Top: beam 1, bottom: beam 2. The stars represent the relative standard deviation for each monitor. All loss maps are dominated by one monitor: its signal is nearly 1 after normalisation, and it has consequently the lowest RSD. The average (not represented) is the value used in the corresponding reference vector. The full list of monitors is given in *tab. 4.5*.

Index	BLM name	Scenario
52	BLMEI.04L2.B1E10_TCTH.4L2.B1	B1H
53	BLMEI.04L5.B1I10_TCTH.4L5.B1	
54	BLMEI.04L8.B1E10_TCTH.4L8.B1	
55	BLMEI.04L1.B1I10_TCTH.4L1.B1	
56	BLMEI.04R1.B2I10_TCTH.4R1.B2	B2H
57	BLMEI.04R2.B2E10_TCTH.4R2.B2	
58	BLMEI.04R5.B2I10_TCTH.4R5.B2	
59	BLMEI.04R8.B2E10_TCTH.4R8.B2	
60	BLMEI.04L2.B1E10_TCTVB.4L2	B1V
61	BLMEI.04L5.B1I10_TCTVA.4L5.B1	
62	BLMEI.04L8.B1E10_TCTVB.4L8	
63	BLMEI.04L1.B1I10_TCTVA.4L1.B1	
64	BLMEI.04R1.B2I10_TCTVA.4R1.B2	B2H
65	BLMEI.04R2.B2E10_TCTVB.4R2	
66	BLMEI.04R5.B2I10_TCTVA.4R5.B2	
67	BLMEI.04R8.B2E10_TCTVB.4R8	

Table 4.4: List of all TCT BLMs of the LHC. The index corresponds to the BLM index in the loss maps *(cf. fig. 4.7)*. The TCTs are sorted by type: B1H, B2H, B1V, B2V; then by position within one type.

Most of the monitors of IR7 give a RSD around 10^{-2} for the transversal loss maps. This shows the level of reproducibility of the measures for the transversal loss maps.

Some of the highest values are explained by the fact that they correspond to monitors associated to one beam, when the corresponding loss map is of the other beam. The monitor has a low signal leading to a high RSD. However, low signals do not influence the results of the decomposition. Some of the high RSD monitors, such as the first and last monitors of IR7, are not essential to the result of the decomposition, and could have been removed from the selection.

All the TCTs give a worst standard deviation than the other monitors; but they always have a signal lower than the other monitors, and thus will not influence the decomposition.

All the longitudinal loss maps present higher RSD than the transversal ones, which is a consequence of the different problems presented in *§. 4.4.1.*

Index	BLM name
0	BLMEI.06L3.B1I10_TCP.6L3.B1
1	BLMEI.06L3.B1I10_TCHSH.6L3.B1
2	BLMEI.06L3.B1I10_TCAPA.6L3.B1
3	BLMEI.05L3.B1I10_TCSG.5L3.B1
4	BLMEI.05L3.B1I10_TCSM.5L3.B1
5	BLMEI.05R3.B2E10_TCSM.5R3.B2
6	BLMEI.05R3.B2E10_TCSG.5R3.B2
7	BLMEI.06R3.B2E10_TCAPA.6R3.B2
8	BLMEI.06R3.B2E10_TCHSH.6R3.B2
9	BLMEI.06R3.B2E10_TCP.6R3.B2
10	BLMEI.07L7.B2I10_TCLA.A7L7.B2
11	BLMQI.06L7.B2I20_MQTL
12	BLMQI.06L7.B2I10_MQTL
13	BLMEI.06L7.B2I10_TCLA.D6L7.B2
14	BLMQI.06L7.B1E30_MQTL
15	BLMEI.06L7.B2I10_TCLA.C6L7.B2
16	BLMEI.06L7.B1E10_TCP.D6L7.B1
17	BLMEI.06L7.B1E10_TCP.C6L7.B1
18	BLMEI.06L7.B1E10_TCP.B6L7.B1
19	BLMEI.06L7.B1E10_TCP.A6L7.B1
20	BLMEI.06L7.B1E10_TCHSV.6L7.B1
21	BLMEI.06L7.B1E10_TCHSH.6L7.B1
22	BLMEI.06L7.B1E10_TCHSS.6L7.B1
23	BLMEI.06L7.B2I10_TCLA.B6L7.B2
24	BLMEI.06L7.B1E10_MBW.B6L7
25	BLMEI.06L7.B1E10_TCSM.A6L7.B1
26	BLMEI.06L7.B2I10_TCLA.A6L7.B2
27	BLMEI.05L7.B2I10_TCSM.E5L7.B2
28	BLMEI.05L7.B2I10_TCSM.A5L7.B2
29	BLMEI.04L7.B1E10_TCSG.D4L7.B1
30	BLMEI.04L7.B1E10_TCSM.D4L7.B1
31	BLMEI.04R7.B2I10_TCSM.D4R7.B2
32	BLMEI.04R7.B2I10_TCSG.D4R7.B2
33	BLMEI.05R7.B1E10_TCSM.A5R7.B1

Index	BLM name
34	BLMEI.05R7.B1E10_TCSG.E5R7.B1
35	BLMEI.06R7.B1E10_TCLA.A6R7.B1
36	BLMEI.06R7.B2I10_TCSM.A6R7.B2
37	BLMEI.06R7.B2I10_MBW.B6R7
38	BLMEI.06R7.B1E10_TCLA.B6R7.B1
39	BLMEI.06R7.B2I10_TCHSS.6R7.B2
40	BLMEI.06R7.B2I10_TCHSH.6R7.B2
41	BLMEI.06R7.B2I10_TCHSV.6R7.B2
42	BLMEI.06R7.B2I10_TCP.A6R7.B2
43	BLMEI.06R7.B2I10_TCP.B6R7.B2
44	BLMEI.06R7.B2I10_TCP.C6R7.B2
45	BLMEI.06R7.B2I10_TCP.D6R7.B2
46	BLMEI.06R7.B1E10_TCLA.C6R7.B1
47	BLMQI.06R7.B2I30_MQTL
48	BLMEI.06R7.B1E10_TCLA.D6R7.B1
49	BLMQI.06R7.B1E10_MQTL
50	BLMQI.06R7.B1E20_MQTL
51	BLMEI.07R7.B1E10_TCLA.A7R7.B1
52	BLMEI.04L2.B1E10_TCTH.4L2.B1
53	BLMEI.04L5.B1I10_TCTH.4L5.B1
54	BLMEI.04L8.B1E10_TCTH.4L8.B1
55	BLMEI.04L1.B1I10_TCTH.4L1.B1
56	BLMEI.04R1.B2I10_TCTH.4R1.B2
57	BLMEI.04R2.B2E10_TCTH.4R2.B2
58	BLMEI.04R5.B2I10_TCTH.4R5.B2
59	BLMEI.04R8.B2E10_TCTH.4R8.B2
60	BLMEI.04L2.B1E10_TCTVB.4L2
61	BLMEI.04L5.B1I10_TCTVA.4L5.B1
62	BLMEI.04L8.B1E10_TCTVB.4L8
63	BLMEI.04L1.B1I10_TCTVA.4L1.B1
64	BLMEI.04R1.B2I10_TCTVA.4R1.B2
65	BLMEI.04R2.B2E10_TCTVB.4R2
66	BLMEI.04R5.B2I10_TCTVA.4R5.B2
67	BLMEI.04R8.B2E10_TCTVB.4R8

Table 4.5: List of all selected BLMs. The index corresponds to the BLM index in the loss maps *(cf. fig. 4.7)*. BLMs are separated by IR3, IR7, and TCTs.

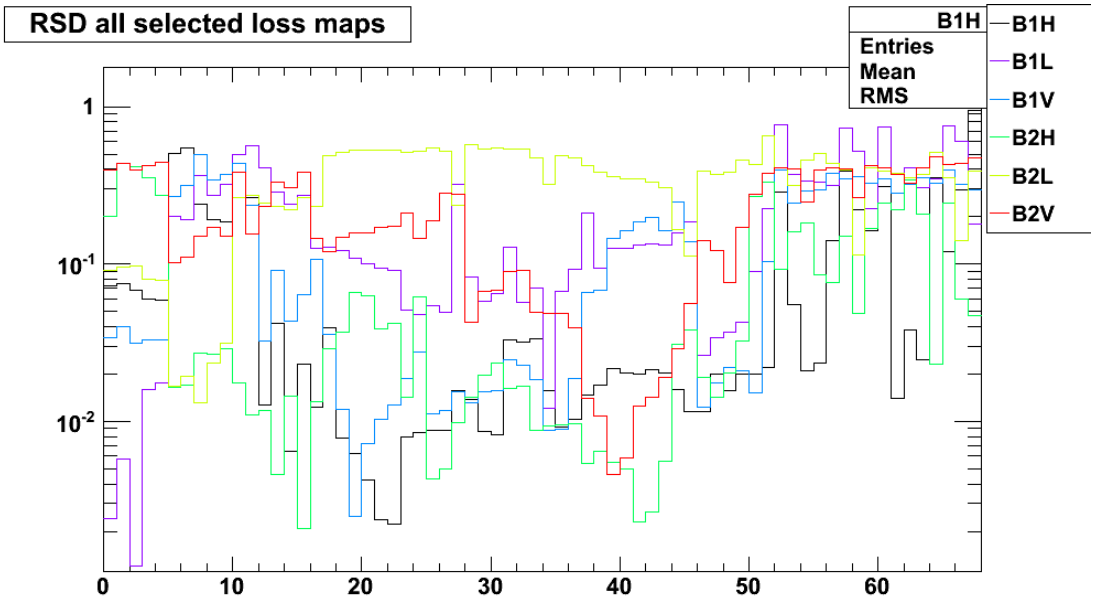

Figure 4.14: All Relative Standard Deviations for each reference vector used in the decomposition. The full list of monitors is given in *tab. 4.5*.

4.5 Validation of results: Centers of Mass

In this section, an easy way to separate between the four transversal loss scenarios will be presented.

4.5.1 Motivation

The different algorithms return the decomposition of a given loss vector. The calculated error tells how close a recomposition is to the original vector. It is still desirable to have a way to find which loss scenario corresponds to a given vector without doing any decomposition, to gain confidence in the procedure and implementation. Afterwards, it can be applied to other loss profiles, where simple verification might be more difficult.

The choice was made to use the normalized difference between the losses at primary collimators. It is also called *Center of Mass*, and for two signals a and b, is calculated as:

$$c = \frac{a-b}{a+b}$$

c represents the proportion of each signal: for $a \gg b$, $c \simeq 1$; for $b \gg a$, $c \simeq -1$; for $a \simeq b$, $c \simeq 0$. For the same overall loss $S \equiv a + b$, both a (for fixed b) or b (for fixed a)

depend linearly of c:

$$c = \frac{a-b}{S} \text{ and } b = S - a$$

therefore:

$$a = \frac{S}{2} \cdot c + \frac{S}{2}$$

for b, the result is:

$$b = -\frac{S}{2} \cdot c + \frac{S}{2}$$

This shows that for a fixed (or normalised) total loss S, each signal depends linearly on the center of mass if the other one is fixed: the center of mass gives the relative proportion of the signals.

The centers of mass also have the advantage to be able to be combined: a and b can be any combination of signals that we want to compare against each other. For instance, a can be the sum of the signals at the vertical collimators, and b the sum of the signals at the horizontal collimators.

4.5.2 Implementation and verifications

The values used for the centers of mass are the combinations of the signals at the four primary collimators *(cf. tab. 4.6)*.

Expert name	Beam & plane	BLM index	Loss
`TCP.D6L7.B1`	B1 vertical	18	v_1
`TCP.C6L7.B1`	B1 horizontal	19	h_1
`TCP.C6R7.B2`	B2 horizontal	114	h_2
`TCP.D6R7.B2`	B2 vertical	113	v_2

Table 4.6: List of primary collimators of IP7 used in the Centers of Mass.

The centers of mass used for discrimination between beam 1 and beam 2 is:

$$CoM_{1|2} \equiv \frac{(h_2 + v_2) - (h_1 + v_1)}{h_1 + v_1 + h_2 + v_2} \tag{4.1}$$

It always varies between -1 and $+1$. In this case, -1 means that the measured loss profile is made only of beam 1 scenarios, and $+1$ means that the measured loss profile is made only of beam 2 scenarios. A center of mass of 0 means that both beams give the same contribution to the overall loss.

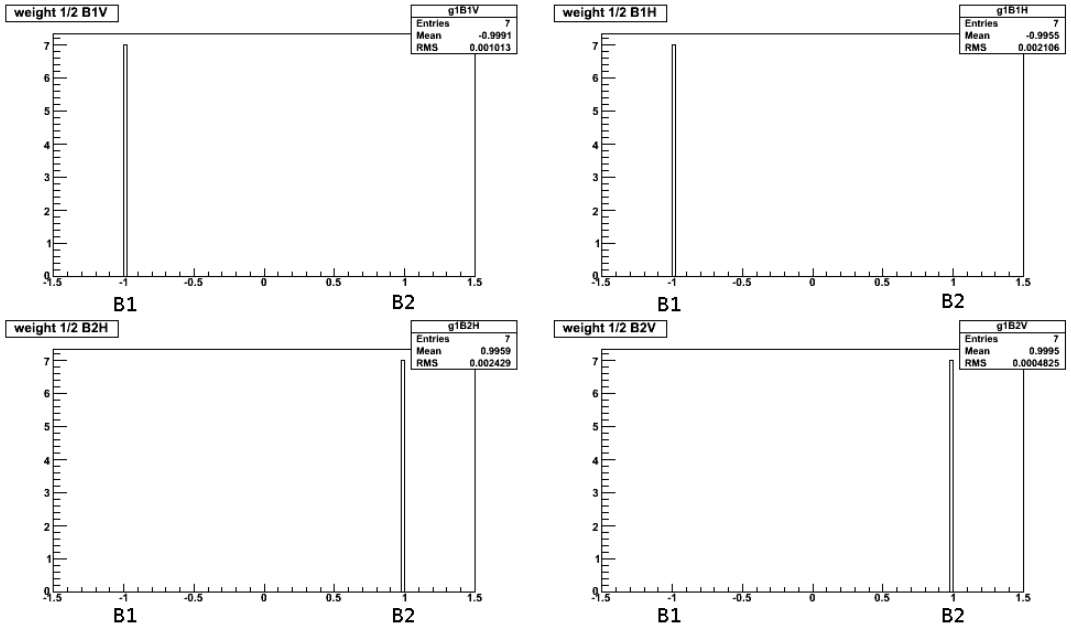

Figure 4.15: Distributions of the results of $CoM_{1|2}$ *(cf. eq. 4.1)*. Each one of the 4 plots corresponds to a loss scenario (known before the calculation), given in the title of each plot. There are 7 different loss maps for each scenario (28 in total). The results of the centers of mass match perfectly the type of every single vector. This is because the primary collimators for beam 1 are installed far away from the collimators for beam 2, and the signals at the corresponding BLMs are well separated: on *fig. 4.1*, the primary collimator for beam 1 are around index 20, whereas the ones for beam 2 are at index 116.

For horizontal and vertical cases, the center of mass is:

$$CoM_{H|V} \equiv \frac{(v_1 + v_2) - (h_1 + h_2)}{h_1 + v_1 + h_2 + v_2} \tag{4.2}$$

In this case, the center of mass varies between -1 when it is dominated by signal from the horizontal collimators and $+1$ when it is dominated by the signal from the vertical collimators. Again, a center of mass of 0 shows that the losses from both planes are equal.

In order to evaluate the correctness of the centers of mass, they were first calculated for all 28 loss maps of 2010 (4 scenarios $\times$ 7 dates). The results are presented in *fig. 4.15*. For beam discrimination, they match exactly the dominating beam (1 or 2) of every single vector.

However, the results for the centers of mass are not as good for the separation between horizontal and vertical loss maps *(cf. fig. 4.16)*. They are separated, but do

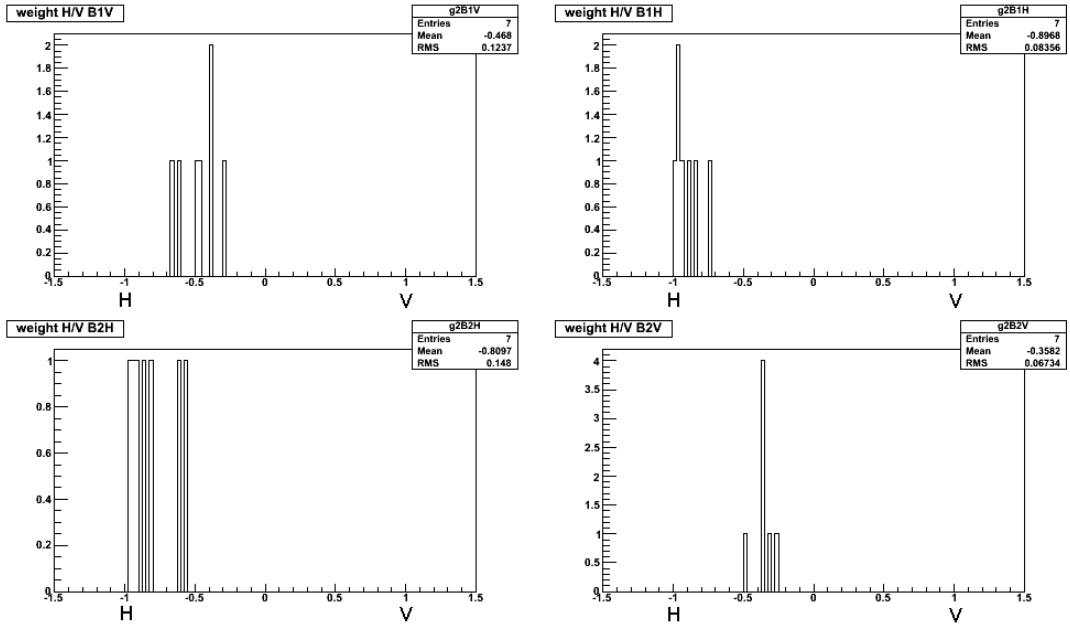

Figure 4.16: Distributions of the results of $CoM_{H|V}$ *(cf. eq. 4.2).* Each one of the 4 plots corresponds to a scenario (known before the calculation), given in the title. There are 7 different loss maps for each scenario (28 in total). The centers of mass have different values depending on the scenarios, but they vary between -1 and -0.5, instead of varying between -1 and 1.

not give the expected results: instead of varying between -1 and 1, the results vary between -1 and -0.5. This could be reproduced with the selected loss maps of 2011 used in the decomposition, and with all loss maps of 2011 for statistics *(cf. fig. 4.17).* The $CoM_{1|2}$, giving always correct results (all values are $+1$ or -1), are not represented.

In addition to varying in an interval smaller than expected, some of the 2011 loss maps give a "wrong" (opposite to the expected value knowing the associated loss scenario), e.g. -0.5 instead of -1 for some of the B1H loss maps of 2011 *(cf. fig. 4.17, right column, third plot down).* This is not an issue: these loss maps were not selected and are not used in the decomposition. Again, no loss map gives a $CoM_{H|V}$ bigger than zero.

This is due to the relative position of the corresponding collimators: the horizontal collimators sits downstream and next to the vertical one. The secondary shower produced when the protons hit the vertical collimator will also be detected by the horizontal collimator: part of the signal seen by the horizontal collimator comes from the vertical one.

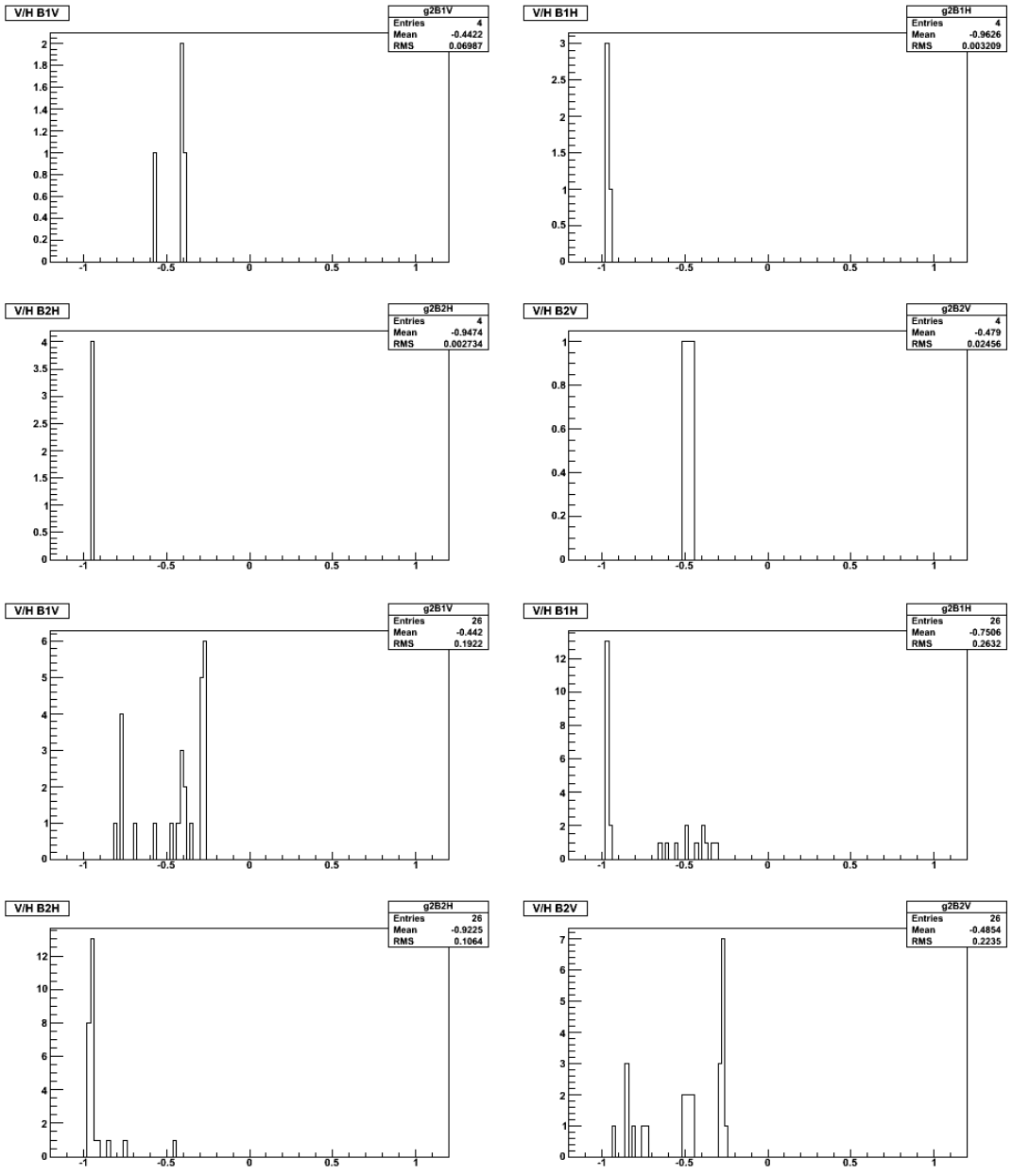

Figure 4.17: Distributions of the results of $CoM_{H|V}$ *(cf. eq. 4.2).* Each one of the 8 plots corresponds to one scenario (known before the calculation), given in the title; in each distribution, there is one entry per loss map of the considered scenario. Top 4: loss maps of 2011 used in the decomposition. There are 4 loss maps per scenario, given in *tab. 4.1.* The results of the centers of mass are separated and vary between -1 and -0.5. Bottom 4: all loss maps of 2011. Most of the entries for B1V and B2V are above -0.5; the lower values indicate "wrong" loss maps.

Several corrections were considered, such as subtracting the signal of the vertical collimator from the horizontal one, or stretching the variation interval.

Implementing the first method showed that a factor of roughly two times the vertical signal had to be subtracted in order to get a correct variation interval; but this created a pole for the function $(h, v) \mapsto (h - \alpha \cdot v,\ v)$, i.e. a value for which the function would diverge to infinity. Arbitrarily stretching the variation interval, corresponding to the precedent method with no pole and a correction factor of higher value, led to the problem of some values of the centers of mass being higher than one, in cases where the cross-talk between the two monitors is overestimated.

Eventually, the choice was made to keep the centers of mass uncorrected, knowing that the horizontal/vertical one would vary between -1 and -0.5.

4.6 Choice of the algorithm

In this section, the reasons to use or not the different decomposition algorithms will be discussed.

SVD

The Singular Value Decomposition has the drawback of sometimes returning negative factors, which have no physical meaning. However, it is the algorithm which gives the results closest to the original vector in the sense of the norm of the difference vector: the difference was calculated to be of the order of 10^{-16} to 10^{-18} for simple examples with 3×4 matrices. The choice was made to keep this decomposition technique, even if some results are not physical.

MICADO

The implementation and the first results of MICADO showed that the results are extremely close to the results of the Singular Value Decomposition: the difference is of the order of 10^{-16} to 10^{-18}. Both SVD and Micado give the closest possible recomposition. The choice was made to use only the SVD.

Gram-Schmidt

The Gram-Schmidt decomposition returns mainly one vector, and is then not as close to the original vector (in the sense of the norm of the difference). However, the results are always physical. The choice was made to keep this decomposition technique as well.

4.7 Evaluation of the correctness of a decomposition

4.7.1 Correct and incorrect decompositions

Several verifications were made in order to evaluate the quality of each loss map. It allowed to get some statistics on the results of the different algorithms. Additionally, one extra vector was decomposed on each set: it is a way to cross-check the loss maps using a common reference. Every time, the error between the chosen vector and its recomposition was calculated, allowing the comparison between sets of loss maps.

Then, every loss map of every set was decomposed on all the other sets. This way, loss maps giving bad results — that is, leading to wrong decompositions on every other vector set — could be removed.

The error on the recomposition, presented in *§ 3.5*, evaluates the difference between a vector and its recomposition in the m-vector space, but gives no information on how *correct* the decomposition is. For a vector corresponding to a known scenario, an *incorrect* decomposition (wrong linear combination of vectors) could produce a recomposition closer to the vector than the correct one.

The point of this section is to try to show a link between the value of the error on the recomposition and the correctness of this recomposition. It could for instance be expressed as a threshold value of the error, below which the decomposition is considered as correct.

4.7.2 Method and results

Different series of cross-checks were done: all the loss maps were decomposed on different vector sets, and the errors on the recompositions were calculated. The scenario associated to the loss maps being of course known, the decomposition could be sorted as *correct* or *incorrect*. In case of factors bigger than one (SVD), the decomposition was considered as correct if the highest factor was the correct one.

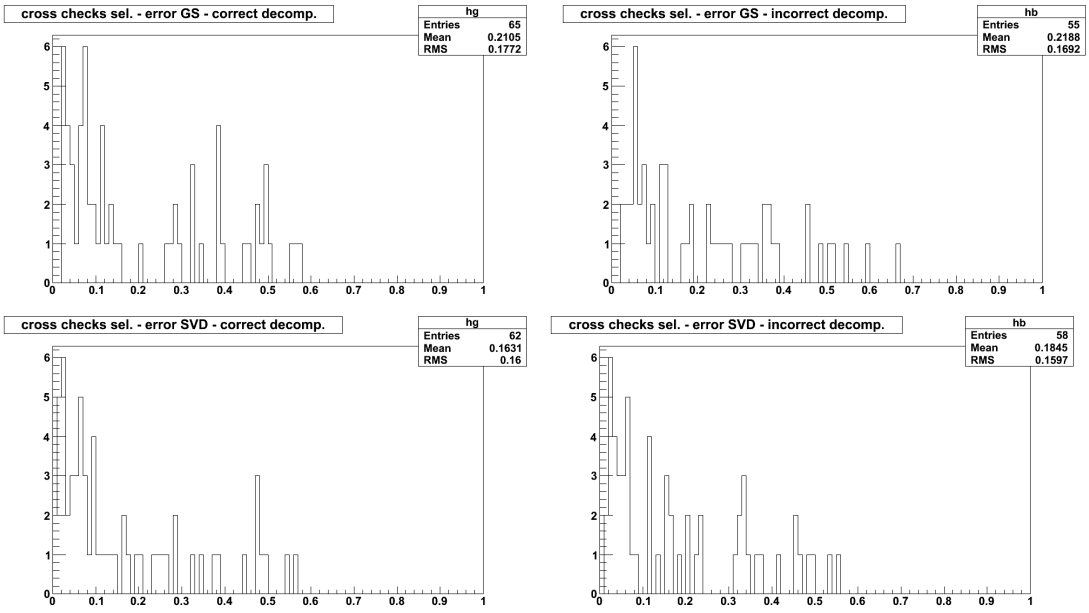

Figure 4.18: Distributions of correct (left) and incorrect (right) decompositions for G-S (top) and SVD (bottom) of every loss map of 2010 on every vector set (of the same loss maps). There are 120 decompositions in total. The averages are lower for the SVD (better recompositon), and the correct and incorrect are close to each other. See text for more observations.

Then, the distributions of the errors for correct and incorrect decompositions were ploted, and their averages calculated. The more separated these two averages are, the better the discrimination between correct and incorrect decompositions will be.

The first cross-checks were done with the loss maps of 2010 *(cf. tab. 4.1)*, both for SVD and G-S. Every loss map of each vector set is decomposed on all the other vector sets: there are 120 decompositions in total. The results are presented in *fig. 4.18*. The averages for correct and incorrect are, for G-S : 0.2105 and 0.2188; for SVD: 0.1631 and 0.1845. They are too close to each other to allow a good separation; there is an important overlaps between the two distributions.

Another observation is that every distribution is separated into two groups: many values are under 0.15, corresponding to *true positives* for the correct decompositions, but *fake positives* for the incorrect ones: the recomposition is incorrect, but close to the original vector. Similarly, a group of values seems to be centered around 0.45, especially for the correct GS decompositions. There are *true negatives* for the incorrect SVD decompositions. The similar values, for the correct decompositions, are *fake*

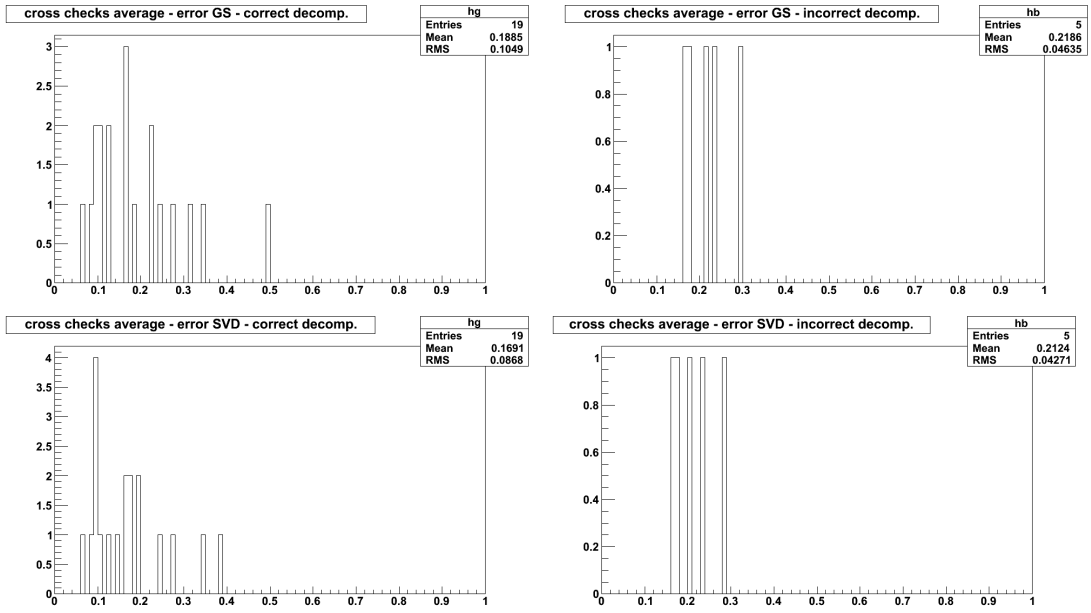

Figure 4.19: Distributions of correct (left) and incorrect (right) decompositions for G-S (top) and SVD (bottom) of every loss map of 2010 on the average vector set. There are 24 decompositions in total. The averages are lower for the SVD (better recomposition), and the correct and incorrect are still too close to each other to allow a good separation. See text for more observations.

positives: far from the original vector, yet correct.

A second cross-check was done by decomposing every loss map of 2010 on the average vector set (only for H and V): 24 decomposition in total *(cf. fig. 4.19)*. The first observation is that there are more correct decompositions than incorrect. However, there is still some overlaps, and the averages are still too close to each other to allow a good separation (0.1885 and 0.2186 for G-S; 0.1691 and 0.2124 for SVD). This is because the loss maps of 2010 were not sorted like the 2011 ones, following the order in which they were measured and the energy. The importance of these differences was only understood later.

4.7.3 Distributions of the error for the 2011 loss maps

In this case, all loss maps of 2011 were decomposed on the average set of selected loss maps *(cf. § 4.3)*, which is the set used in real data decompositions. In these, the majority of correct and incorrect decompositions are clearly separated.

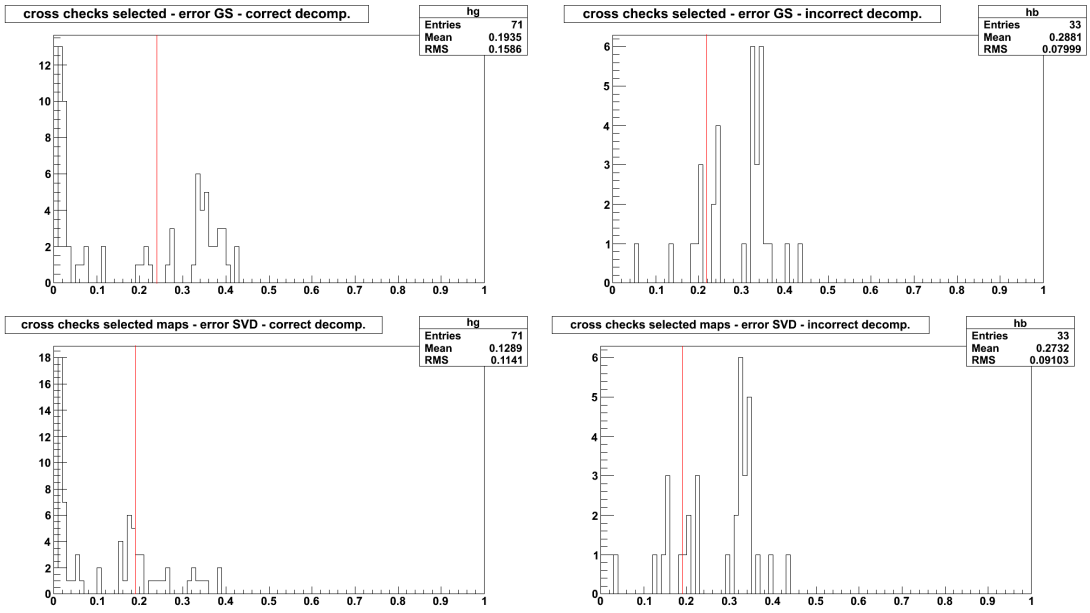

Figure 4.20: Distributions of correct (left) and incorrect (right) decompositions for G-S (top) and SVD (bottom) of every loss map of 2011 on the set of selected loss maps. There are 104 decompositions in total. The red lines represent the value of the geometrical mean between the means for correct and incorrect decompositions (see text). The majority of correct and incorrect decompositions are now clearly separated, even though there is still some fake negatives: distributions that are correct but far away from the original vector, and some fake positives.

For SVD, the averages for the correct decomposition is 0.1289 and 0.2732 for incorrect *(cf. fig. 4.20)*. The arithmetic mean between these two values is 0.201, and the geometric mean is 0.187 (the geometric mean is often preferred here, because it takes better into account the fact that there are many low values). Using 0.19 as a threshold, there are 51 entries below this value for the correct decomposition, corresponding to 72% true positives; and 20 entries above mean represent 28% fake negatives. For the incorrect decompositions, there are 26 entries above mean (79% true negative) and 7 below (21% fake positives).

For GS, the "correct" average is 0.1935, and the "incorrect" is 0.2881. The arithmetic mean between them is 0.236, and the geometric mean is 0.241 (there is no difference between arithmetic and geometric mean at the precision of 0.01 used in the distribution). For the correct decompositions, there are 38 entries below mean (54% true positives) and 33 above (46% fake negatives); for the incorrect decompositions, 24 above (73% true negatives) and 9 below (27% fake positives).

4.7.4 Conclusion on the values of the error

From these observations (especially on the distributions for 2011, which were selected much more carefully than the ones from 2010, keeping only the ones measured first), it appears than using only one value as a threshold would not separate correct and incorrect decompositions clearly. Considering different "cuts" would lead to a better separation into three categories. All errors below 0.1 are assumed to be correct decompositions; between 0.1 and 0.3, the result is undefined; and above 0.3, the decomposition is considered as wrong. This suppresses nearly all fake positives, but still leaves some fake negatives.

4.8 Application to LHC data

This section will present how the different decompositions are applied to LHC data, by opposition to the specific loss maps that were used for cross-checks, and the choices that were made. The results will be presented in *chapter 6*.

4.8.1 Implementation

After trials and cross-checks on different loss maps, the decompositions were calculated during physics beams of 2011. More specifically, the periods during which "stable beams" had been declared: most of the beam characteristics are left unchanged, and physics collisions are measured in the experiments.

Losses are studied at each second; the ensemble of losses at one second is called *current loss profile*. This specific frequency corresponds to the frequency at which data are recorded in the *measurement database (cf. §. A.2.3)*. In addition, a *default loss profile* corresponding to the average loss in nominal condition was created.

Beam losses are by definition not very high during stable beams: the losses are considered safe and are lower than the loss thresholds. If they get bigger, they lead to a "beam dump", and this case is not considered here; and the high losses not leading to a beam dump are rare. Consequently, a few non-stable beam periods were also studied, especially the LHC modes preceding stable beams periods, such as injection, ramp, squeeze and adjust.

4.8.2 Evolution of losses

The first check to do on the losses is to evaluate the evolution of the losses from one second to the other: that is, the "difference" between the loss profile at the current second and the loss profile at the previous second. Both loss profiles are considered as vectors with all ionisation chambers in LHC (N_{BLM} coordinates).

Several techniques can be used here, showing different aspects of the evolution of losses: the euclidean norm of the difference between the two vectors; the euclidean norm of the vector itself; the scalar product of the two vectors; the sum of all coordinates.

Euclidean norm of the difference

The first value calculated here is the norm of the difference (subtraction) between the normalised vector representing the losses at one second and the normalised vector representing the losses at the previous second *(cf. fig. 4.21)*:

$$\left\| \frac{\vec{X}(t+1)}{\|\vec{X}(t+1)\|} - \frac{\vec{X}(t)}{\|\vec{X}(t)\|} \right\| \tag{4.3}$$

Both vectors are normalized before calculating the subtraction: thus, this value depends only on the shape of the two vectors. As an illustration, let's consider the case where losses appear in one part of the LHC at one second; then, at the next second, losses of the exact same intensity (normalisation) appear in a different part of the LHC. Even if the norm of the corresponding vectors is the same for both seconds, the norm of the difference will give a high result. It is sensitive to changes of shape even if the norms of both vectors are strictly equal, which is the case after normalisation.

Norm of the vector

Calculating the euclidean norm of the vector is a good way to evaluate the magnitude of the overall losses in the LHC *(cf. fig. 4.21)*. It is the standard norm on a vector space. It is written:

$$||\vec{X}|| = \sqrt{\sum_i x_i^2} \tag{4.4}$$

where the (x_i) are the coordinates of the vector $\vec{X}$.

Scalar product

The scalar product considered here is the product of the vector representing the losses at one second and the vector representing the losses at the previous second *(cf. fig. 4.21)*:

$$\vec{X}(t) \cdot \vec{X}(t-1) = \sum_i x_i(t) \cdot x_i(t-1) \tag{4.5}$$

It combines information from the two previous cases (norm of vector and norm of difference). The vectors are of course not normalised. The norm can also be written as:

$$\|\vec{X}(t)\| \cdot \|\vec{X}(t-1)\| \cdot \cos(\text{angle}(\vec{X}(t),\ \vec{X}(t-1))) \tag{4.6}$$

where the contribution of the norm is obvious, and the angle between the two vectors is directly linked to the change of shape aforementioned. In addition, the norm of the vectors is several orders of magnitude higher than the "change of shape" *(cf. fig. 4.21)*. The change of shape corresponds to a variation of signal of only a few BLMs out of the total ($\simeq 3600$), and the variation is typically several orders of magnitude smaller than the average signal. Only a few BLMs out of the total see a real loss: most of the arc BLMs have a signal corresponding to the electronics offset. Thus, the scalar product is dominated by the effect of the norm and evolves like the norm.

Sum of all losses

The sum of all losses is another way to evaluate the overall intensity of the losses, by summing them *(cf. fig. 4.21)*:

$$||\vec{X}||_1 = \sum_i |x_i| = \sum_i x_i \tag{4.7}$$

where the (x_i) are the coordinates of the vector $\vec{X}$, and are all positive. The vector is not normalised. It is the more intuitive way to evaluate the overall loss.

Considerations on high losses

Let's assume that a very important loss happens in monitor j at the time t.

$$\exists\, j \in [\![\, 0, N_{\text{BLMs}} \,]\!],\ \forall i \in [\![\, 0, N_{\text{BLMs}} \,]\!], i \neq j,\ x_j(t) \gg x_i(t) \tag{4.8}$$

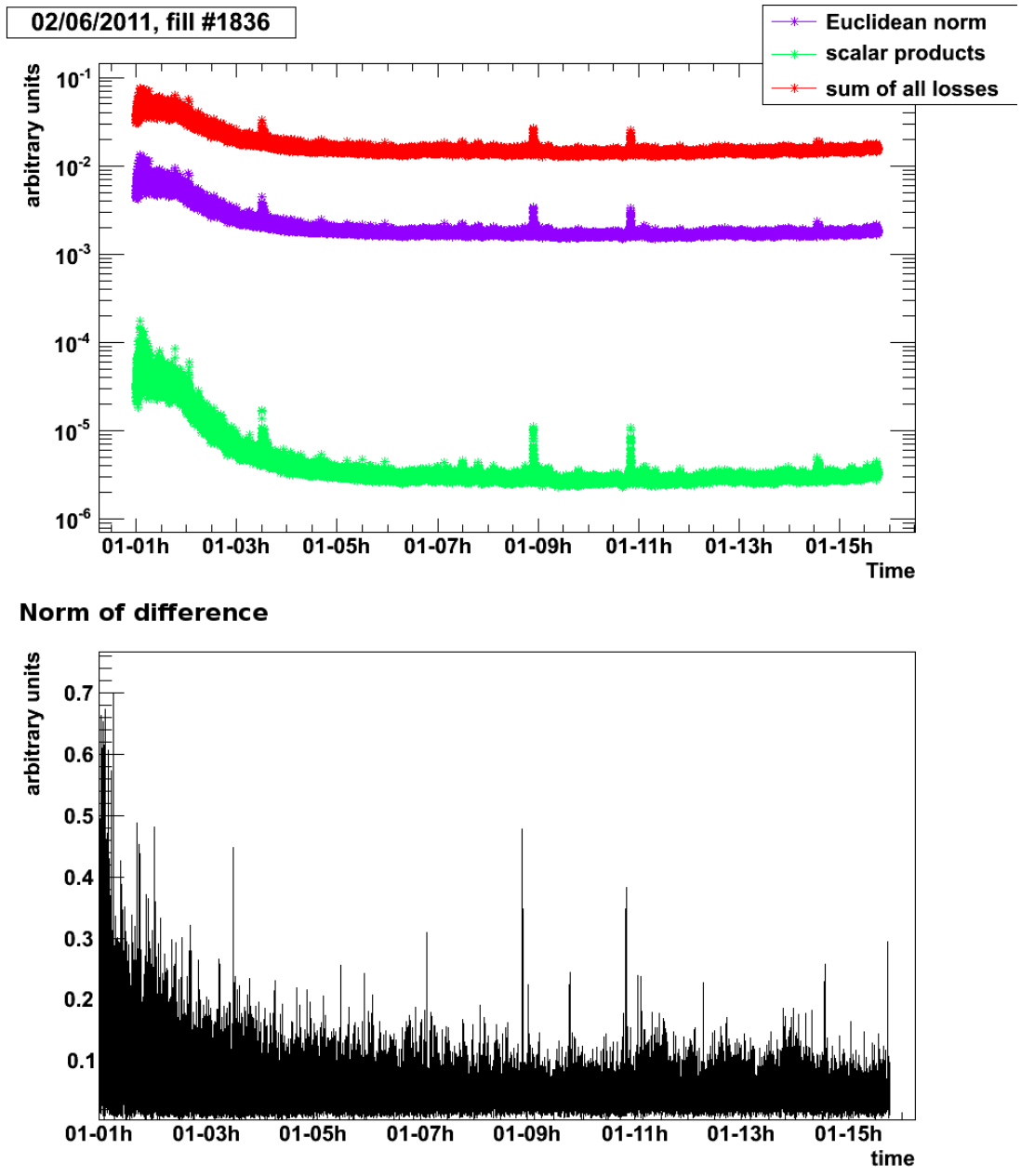

Figure 4.21: Top: values of the Euclidean norm of the current loss profile (purple), the scalar product of two consecutive loss profiles (green), the sum of all losses in the current loss profile (red). Bottom: values of the euclidean norm of the difference between two consecutive loss profiles. Note that the three top plots are very similar: they show similar information. The norm of difference displays a different information, but still relates to the others: the highest values appear at the same time.

where the (x_i) are the coordinates of the vector $\vec{X}$. This assumption is not realistic for only one monitor; however, it is for valid for the sum of the signals of a few monitors (such as the ones around a primary collimator in IR7). It has been observed in the LHC, where their losses can be several orders of magnitude higher than the default loss level. For simplicity, the equations will be written with only one x_j:

$$x_j(t) + x_i(t) \sim x_j(t)$$

We want to assume that the high loss x_j is higher than the sum of all losses in the LHC:

$$x_j(t) \gg \sum_{i \neq j} x_i(t) \tag{4.9}$$

This requires that the high loss is at least four orders of magnitude higher than the default loss level, because there are 3600 monitors considered here. Assuming that all (x_i) for $i \neq j$ have roughly the same value, the default (low) loss level, x_j needs to satisfy:

$$x_j(t) \gg 3600 \times x_i(t)$$

Again, this assumption is not realistic for one monitor (this situation happens only rarely). However, the same observation could be done for several monitors recording high losses satisfying *eq. 4.8*; in this case, their sum will satisfy the previous equation. For simplicity, the equations will be written with only one x_j. We can then write:

$$(4.9) \;\Rightarrow\; x_j(t) + \sum_{i \neq j} x_i(t) \sim x_j(t) \;\Rightarrow\; \sum_i x_i \;\simeq\; x_j \;\Rightarrow\; \|\vec{X}\|_1 \simeq x_j \tag{4.10}$$

This corresponds to the intuitive idea that all losses are smaller than and negligible compared to the loss in monitor j, and also that the sum of all losses for $i \neq j$ is smaller than and dominated by the loss in monitor j.

The equivalent arguments can be applied to the euclidean norm; at first order:

$$(4.8) \;\Rightarrow\; x_j^2(t) + \sum_{i \neq j} x_i^2(t) \simeq x_j^2(t) \;\Rightarrow\; \sum_i x_i^2(t) \simeq x_j^2(t)$$

$$\Rightarrow\; \|\vec{X}(t)\| \simeq x_j(t) \tag{4.11}$$

For the scalar product, we need to introduce a second vector. Let's consider a vector $\vec{X}(t+1)$ that is assumed to be nominal. All losses at the time $t+1$ will be negligible compared to the loss in monitor j at the time t:

$$\forall i \in [\![0, N_{\text{BLMs}}]\!],\ x_i(t+1) \ll x_j(t) \tag{4.12}$$

Especially: $x_j(t+1) \ll x_j(t)$.

The scalar product considered here is expressed as:

$$\vec{X}(t) \cdot \vec{X}(t+1) = \sum_i x_i(t) \times x_i(t+1)$$

Multiplying both sides of *eq. 4.8* by $x_i(t+1)$ gives:

$$x_j(t) \times x_i(t+1) \gg x_i(t) \times x_i(t+1)$$

and this is true for all $x_i(t+1)$, including $x_j(t+1)$. Thus:

$$x_j(t) \times x_j(t+1) \gg x_i(t) \times x_i(t+1)$$

With the same assumption as in *eq. 4.9* (the sum of all 3600 losses for $i \neq j$ is dominated by the loss in monitor j), we get:

$$x_j(t) \times x_j(t+1) \gg \sum_{i \neq j} x_i(t) \times x_i(t+1)$$

$$\Rightarrow\ \vec{X}(t) \cdot \vec{X}(t+1)\ \simeq\ x_j(t) \times x_j(t+1)$$

$$\vec{x}(t) \cdot \vec{x}(t+1)\ \propto\ x_j(t) \tag{4.13}$$

The results (4.10), (4.11) and (4.13) (the proportionality factor being different in each case) show that in case of a high loss, the norm, the sum of all losses and the scalar product will all behave similarly *(cf. fig. 4.21 top)*.

This conclusion can be broadened by considering, instead of the monitor $\#j$, the k highest monitors dominating the others. This corresponds to the idea that the distribution of signals is not uniform: there are a lot of monitors with low signal (around offset), several monitors with high signals (orders of magnitude above offset) and very few in between. The euclidean norm, the sum of all losses and the scalar product all behave like the k dominating monitors. This is visible in *fig. 4.21*.

4.8.3 Default Loss Profile

Another point of going through the losses in the LHC every second is to calculate a *Default Loss Profile* for the stable beams in the LHC. It is achieved by taking the average of the losses of each monitors during several stable beams periods. It can be done with a 2D histogram, showing the distribution of signal on one dimension, all monitors being displayed on the other dimension. It is then easy to extract the mean and standard deviation for each monitor.

After that, the variation between the current loss profile and the default loss profile can be calculated at each second. It will be presented in the next chapter.

Chapter 5

Time evolution of the beam loss in the LHC

The work presented in this chapter concentrated on studying the time evolution of the Beam Loss Monitors signals during nominal operation. These losses are considered as a vector, as presented in *chap. 4*, but this time all monitors are considered together.

The point is to learn how the losses evolve; check where important losses occur, and which parts of the LHC are free from losses. It will also give a better understanding of the behaviour of the vectors, and what information can be extracted from their time evolution.

5.1 Default Loss Profile

5.1.1 Interest

The *default loss profile* can be used to evaluate how much the current loss profile differs from normal. It is the average loss measured in each monitors. It is purely empiric and comes only from measurements: all the losses of all the BLMs in the LHC were recorded for all seconds of several *stable beam* periods of the running of the machine. The "stable beam" flag in the LHC indicates that the machine has reached its maximum energy (3.5 TeV at the time), that the beams are colliding, and that none of the main settings of the machine (energy and β*, the value of the beta function at the interaction point) will be changed.

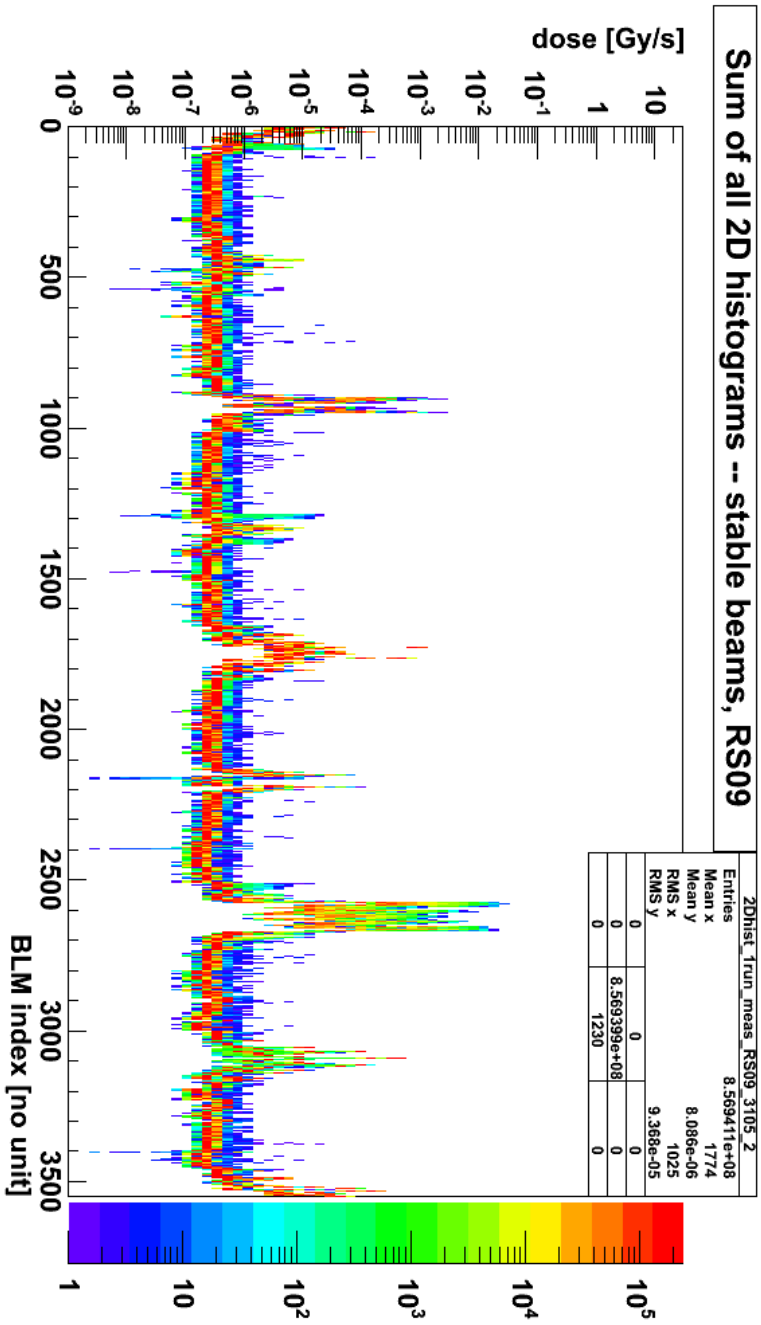

Figure 5.1: Default loss profile. The entries are the losses measured in each monitor in the LHC, cumulated during more than 300.000 seconds. One histogram was created per "stable beams" period, and they were all summed to obtain this result. A logarithmic scale is used for the loss value, and also for the number of entries (coded in colours). The 8 insertion regions are visible, separated by the arcs. See text for more observations.

The default loss profile is not normalised: the real value of the average loss in each monitor is kept, in order to give a good overview of what the nominal losses are in the LHC. These signal distributions show which monitors record a near constant signal (most entries in the same bin), and where the intensity of the loss for one monitor varies even during stable beams (entries spread over several bins).

5.1.2 Creation

The losses are gathered in a two dimensional histogram. The horizontal axis corresponds to the index of the BLM sorted by position (DCUM). The vertical axis gives the value of the integrated dose: the loss, in Gy/s. The dynamic range of the BLMs for running sum 9 — from 10^{-9} Gy/s to 23.7 Gy/s — was divided following an exponential scale. The bin height is constant in logarithmic scale. Every second, one entry per monitor is added. The result is that each "column" corresponds to the 1-dimension logarithmic distribution of the signal in this BLM, for all the hours of measurement *(cf. fig. 5.1)*.

5.1.3 Observations

Several observations show that the presented default loss profile described accurately the "default loss" in the LHC; and show that further processing would not modify the profile.

- Most BLMs have the majority of their signals within one bin: $\sim 2 \cdot 10^5$ entries out of the $\sim 2.45 \cdot 10^5$ total entries per monitor are within the same bin. This shows how constant the loss is: the standard deviation is smaller than the average value *(cf. § 5.2.1)*.

- For arc monitors, no signal significantly above the electronics offset (10 pA, *cf. § 2.3*) was recorded for the whole period of measurement. The value of this offset for RS09 corresponds to $1.8 \cdot 10^{-7}$ Gy/s; most of the entries are between 2 Gy/s and 4 Gy/s. This is the value of the offset in the arcs and the fluctuations of the signal measured when there is no beam in the machine, just above the electronics offset.

- The only higher signals (the isolated purple bins) always correspond to only 1 event. This means that, within the precision of the BLM system (if there were real losses, they were lower than the noise), and taking into account the offset of the electronics, there was no real loss recorded.

- The BLMs that show more fluctuation are situated at the 8 interaction regions, where the optics is different from the rest of the ring, where all collimators and absorbers are installed, and where luminosity induced losses can appear. All noticeable losses (above noise level) happen in very few specific places in the LHC; the losses only appear where they should.

- These monitors, recording high losses, do not show any signal at the offset level (level of the arc monitors), as they would if there was no beam in the machine. This means that the level of loss observed there is constant. All recorded signals correspond to particle lost during operation; if signals had been recorded when there is no beam in the machine, these monitors would show signal at the level of the offset (like the arc monitors).

- A few monitors corresponding to the neutral beam absorbers (TANs) at IR1 and IR5 have most of their signal in a very high bin (e.g. isolated red bin around index 20 and 1700). This is due to the luminosity induced losses, the debris (protons of lower energy and other particles produced during collision). The level of debris and the luminosity were approximatively constant during the time of study.

5.1.4 Comparisons of the loss in the LHC with the default loss profile

Once the average loss value of each BLM during "stable beams" was extracted from the histogram, comparisons were done between the *current loss profile* and the *default loss profile*, using the same techniques as for the comparison with the *previous second (cf. § 4.8.2)*: that is, scalar product *(cf. fig. 5.2, bottom left)* and norm of the difference *(cf. fig. 5.2, bottom right)*.

In this case, the scalar product gives a result similar in shape to the *euclidean norm* $\sqrt{\sum x_i^2}$ and the *sum of all losses* $\sum |x_i|$ *(cf. fig. 5.2)*. Reasons for this were discussed in *§ 4.8.2*. The correlation between the scalar product of the loss vector at one second

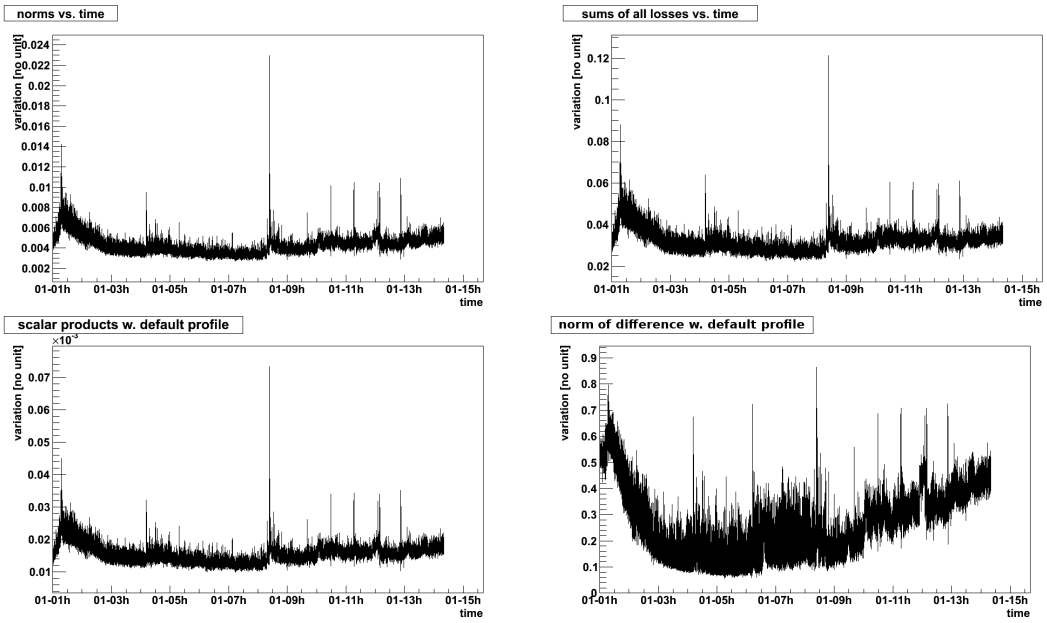

Figure 5.2: Top left: Norm of the current loss profile. Top right: sum of all losses at current second. Bottom left: scalar product of current loss profile with default loss profile. Bottom right: norm of the difference between the current loss profile and the default one. All plots represent a 13–hours long "stable beam" period from the 12^{th} of June 2011 (fill #1865). Note how the 4 plots display similar information (higher losses at the beginning of the run, high loss peaks at the same time) but the norm of difference emphasizes the smaller variations *(cf. § 4.8.2)*.

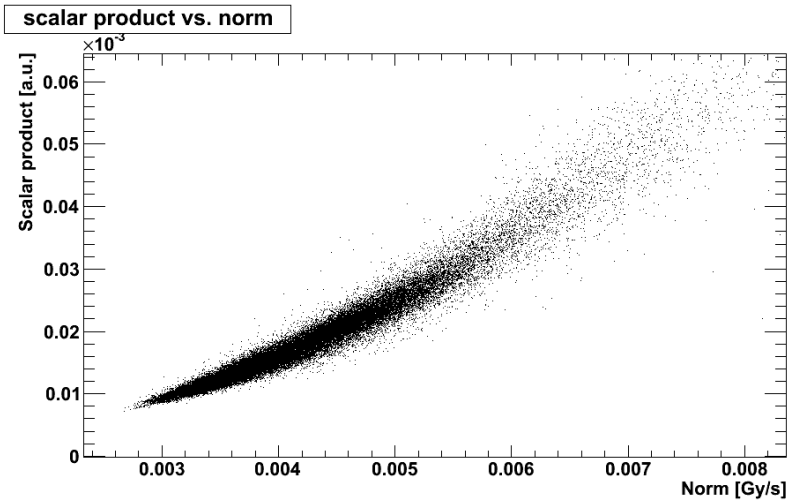

Figure 5.3: Correlation between the scalar product of the current loss vector and the loss vector at the previous second *(cf. fig. 5.2 bottom left)*, and the norm of the current loss profile *(cf. fig. 5.2 top left)*. This illustrates the point discussed in *4.8.2*; it shows that this scalar product is not a good estimation of the variation of the losses, because it is always dominated by one vector.

and the loss vector at the previous second, and the norm of the loss vector, is shown in *fig. 5.2*.

The scalar product of the loss vector at a time $x(t)$ with the default loss profile y is written:

$$\vec{x}(t) \cdot \vec{y} = \sum_i x_i(t) \cdot y_i$$

where $x_i(t)$ is the loss measured by the monitor i at t and y_i is the calculated average loss for this monitor.

Every second, the loss $x_i(t)$ is multiplied by a constant y_i: the scalar product with the default profile can be seen as a strictly monotonic (increasing) application. It will describe the overall loss in a similar way to the norm of the loss vector.

The norm of the difference is:

$$|\vec{x}(t) - \vec{y}| = \sqrt{\sum_i (x_i(t) - y_i)^2}$$

As shown in *§ 3.5* and *§ 4.8.2*, this value is better than the others to quantify the relative variations of two vectors close to each other.

Some effects were observed on all stable beam runs which were investigated. Even when the beams are declared "stable", the current loss profile is different from the default loss profile: the subtraction is never equal to zero *(cf. fig. 5.2)*. The current profile gets closer to the default profile (the norm of the difference decreases), and after about two hours, it is at the closest to the default profile (minimum of the difference). Then, several hours later, the difference starts increasing again. The current loss profile gets more and more different from the default one.

5.2 Individual evolution of the signal of a BLM

In this section, we will study the evolution of the signal of one monitor considered independently, for different types of monitors.

5.2.1 Arc monitor — low signal

The distributions of all losses *(cf. § 5.1.2 and fig. 5.1)* showed that the monitors from the arc have an extremely narrow distribution, with a standard deviation of $\sim 2 \cdot 10^{-8}$ Gy/s

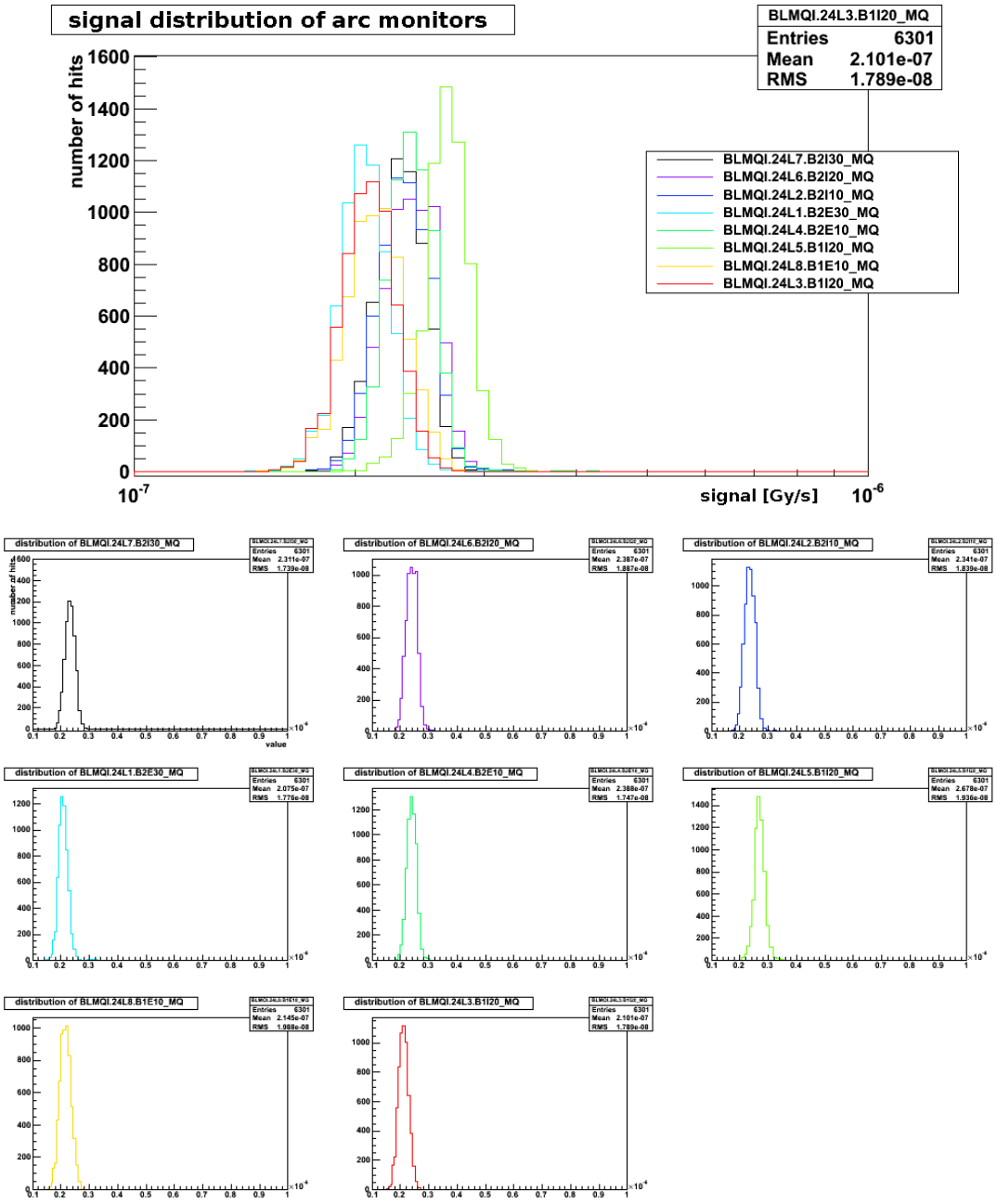

Figure 5.4: Top: Distributions of the signal of arbitrary arc monitors, from the 8 arcs of the LHC, for RS09. This figure shows how similar the distributions are, in shape and value, even for monitors situated far away from each other. The 10 pA electronics offset corresponds to $1.8 \cdot 10^{-7}$ Gy/s, which is within the variations of signal. The BLMs see no loss. Bottom: Separated distributions of the signal of arbitrary arc monitors. These figures give the values of average signal and standard deviation.

(compared to the dynamic range of 10^8) for roughly 300.000 entries. The signal of these monitors was studied in detail.

The BLMs were arbitrarily selected and taken from the 24^{th} cell on the left of each interaction point, which is far away from the interaction points. The figure *5.4 top* shows that the distributions are similar in shape and in value. Most arc monitors behave the same way, and the selected ones are a representative sample as seen in *fig. 5.1.* All the values of average and standard deviation of the different signal distributions, calculated numerically, are given by *fig. 5.4 bottom*: average is around $2.3 \cdot 10^{-7}$ Gy/s, and standard deviation around $1.8 \cdot 10^{-8}$ Gy/s for running sum 9.

The values of the average signal are very close to the value of the 10 pA current offset permanently sent in the tunnel electronics. It corresponds roughly to a value of 65 expressed in bit units, and $1.8 \cdot 10^{-7}$ Gy/s for running sum 9. The smallest step, one bit unit, is worth $2.76 \cdot 10^{-9}$ Gy/s.

Moreover, the signal of these monitors was checked during times when there was no beam in the machine, and the signal distributions showed the same average. This shows that the arc monitors record no signal coming from deposited charges, and the signal measured over the offset level is only due to noise. There are no detectable losses in the arcs during normal operation.

5.2.2 Variations of the signal of a monitor

After studying the distribution of the low-signal BLMs, the next step was to study the variations of these signals. It was done by calculating the distribution of the difference between the signal of one BLM at one second and the previous second *(cf. fig. 5.6).* This allows to study the effect of the noise.

The first observation is that the distribution of variation is similar for all chosen monitors, and has an mean value of zero at the precision of the measurement of the loss: the size of one bin corresponds to the value of one electronics bit. Then, the distribution can be fitted with a Gaussian *(cf. fig. 5.5).* The values of the mean and standard deviation given by the fit agree with the numerical average and standard deviation of the distributions *(cf. fig. 5.6)* to a precision higher than one electronics bit. The quality of the fit, including the errors, is given by the value of χ^2 over the number of degrees of freedom, and was calculated to be $\simeq 0.82$.

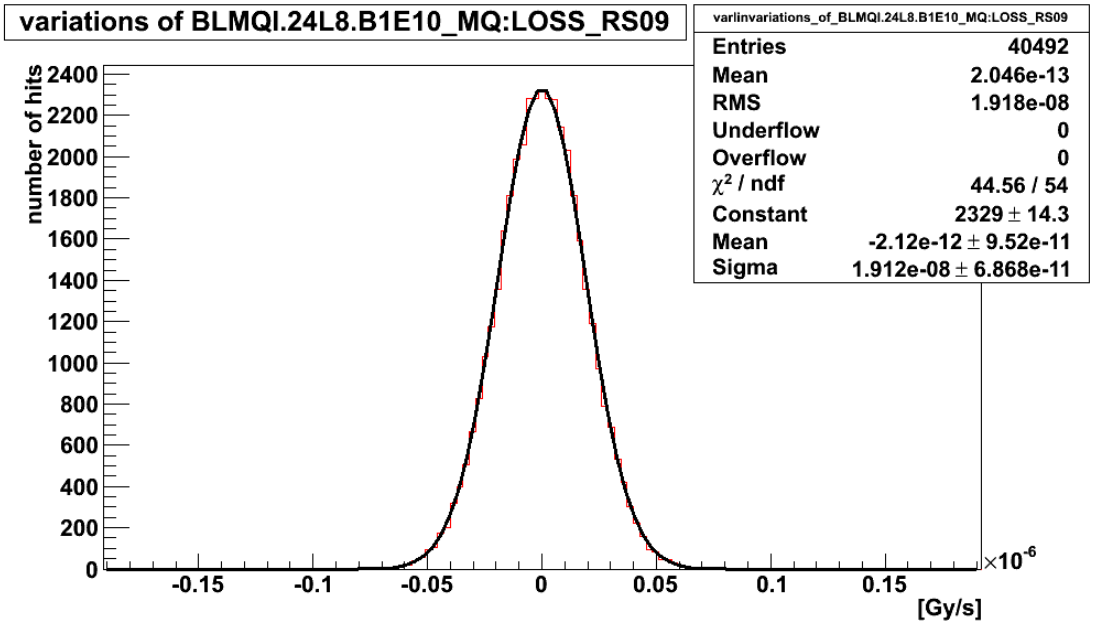

Figure 5.5: Example of a Gaussian fit of the distribution of the signal variation of an arc monitor. The values of the σ and μ parameters of the gaussian agree with the numerical average and standard deviation to a precision higher than one electronics bit (width of one histogram bin).

To the level of precision of the loss measurement, the variations of the signal are Gaussian.

BLM expert name	Location
`BLMEI.04R1.B1E10_TANAR.4R1`	Right of IR1
`BLMEI.04R1.B2I10_TCTVA.4R1.B2`	Right of IR1
`BLMEI.04R7.B1E10_TCSG.A4R7.B1`	Right of IR7
`BLMEI.03L5.B1I10_MQXA`	Left of IR5
`BLMEI.03R1.B1E30_MQXA`	Right of IR1
`BLMEI.04R7.B2I30_MQWA.A4R7`	Right of IR7

Table 5.1: Lists of monitors showing a high average signal (around 10^{-4} Gy/s) in the default loss profile. The names are given in the same order as in *fig. 5.7 top*.

5.2.3 IP monitors — high signal

The same study was done for monitors showing a permanently high signal *(cf. fig. 5.7)*. BLMs having some of the highest average signals (around 10^{-4} Gy/s) were selected.

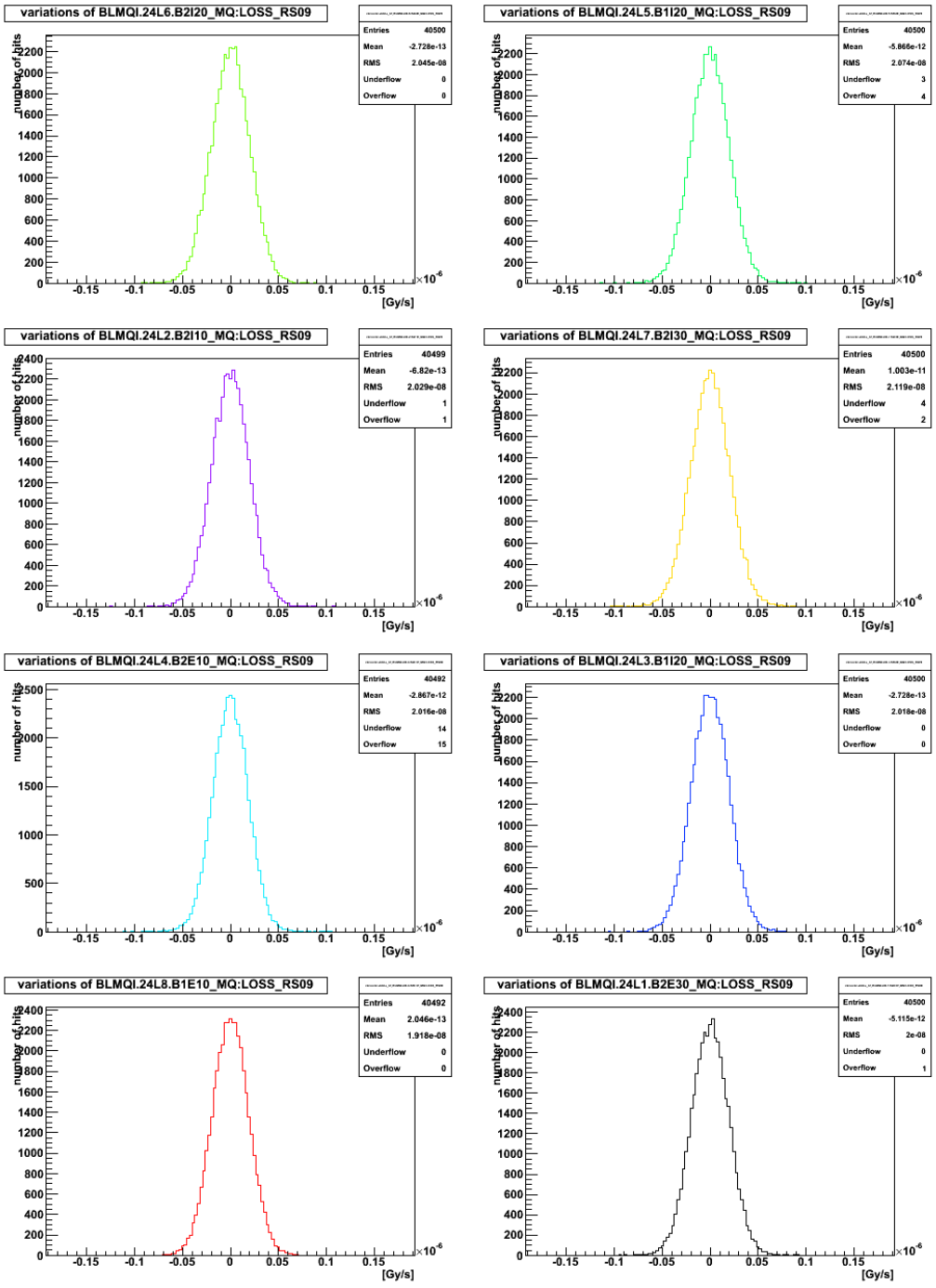

Figure 5.6: Distributions, for selected BLMs of the arcs, of the differences of the signal at one second and the signal at the previous second, during the stable beam of the 23^d of July 2011. The difference is a discrete number of bits; each bin covers exactly one value of the difference, and is the size of one electronics bit: $2.76 \cdot 10^{-9}$ Gy/s.

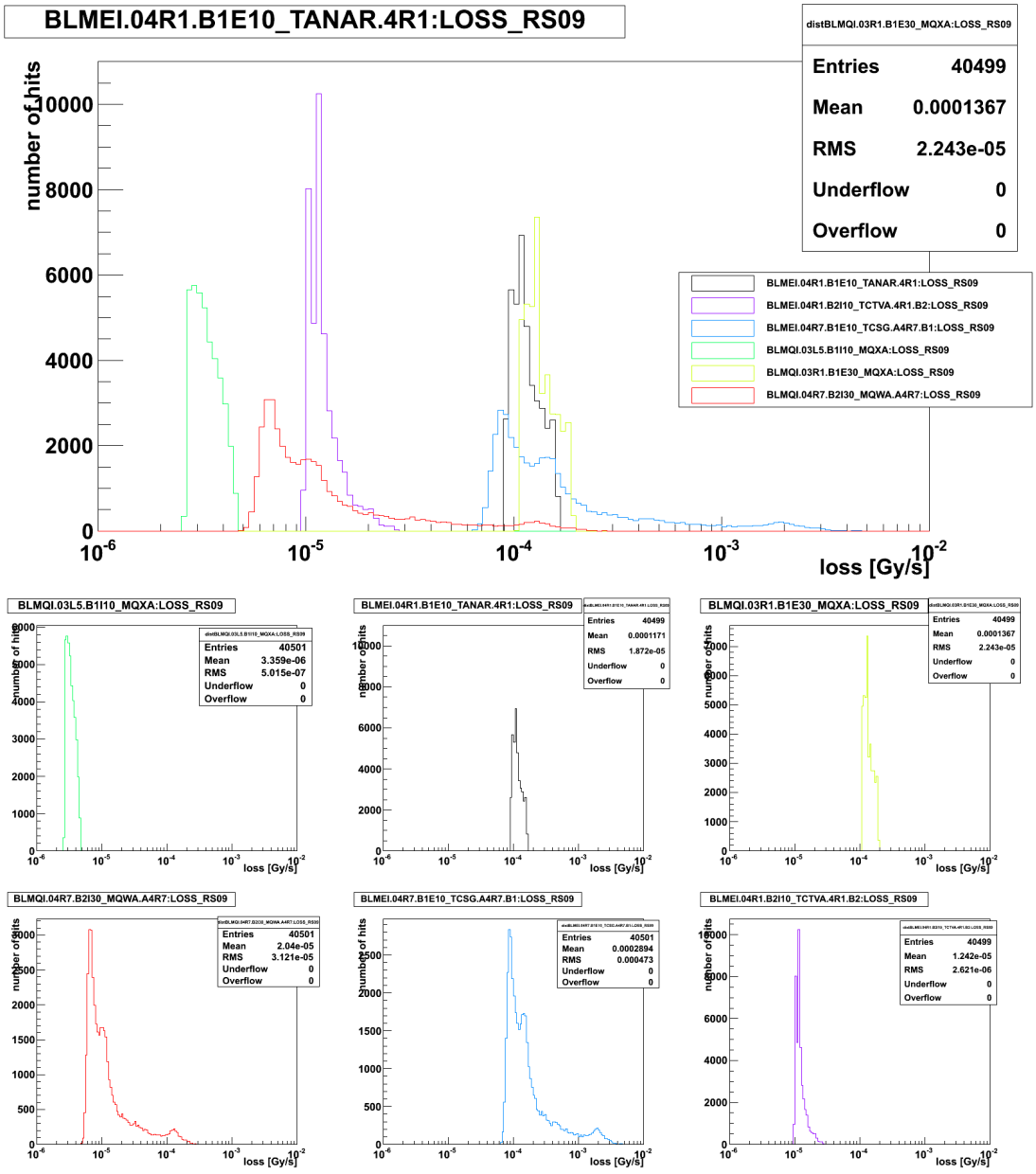

Figure 5.7: Top: Distributions of the signals of monitors showing high losses during stable beams. The data were taken during the stable beam run of the 23^{rd} of July 2011. Bottom: Separated distributions of the signal of monitors with high signal. These plots give the values of average signal and standard deviation. The names of the monitors are given on the top figure, and in *tab. 5.1*. The distributions are not Gaussian, and correspond to losses happening during operations which can't be expressed analytically.

Their names are given in *(cf. tab. 5.1)*. They are found around the interaction points: this is were the collimators and absorbers, which permanently create losses, are installed. These losses correspond to luminosity induced losses in IR1 and IR5, and to cleaning in IR7. The luminosity losses are constant, with a narrow distribution; the collimation losses show more variations even during "stable beams".

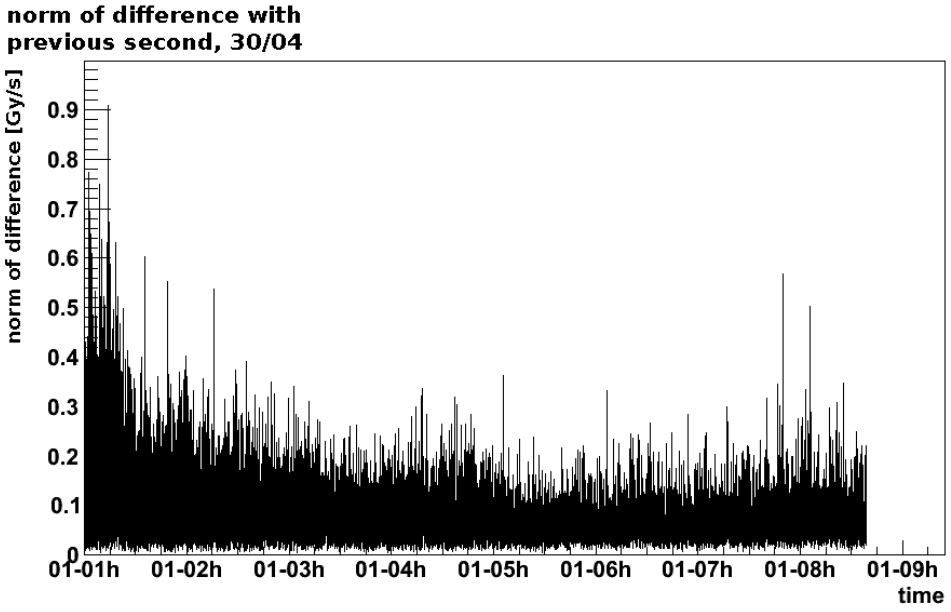

Figure 5.8: Norm of the difference with the previous second during the stable beam of the 30^{th} of April 2011. Even if this is the "stable beam" period, the number of peaks decreases during the first 3 hours. The norm of the difference also decreases in the first 3 hours; this is shown in more detail in *fig. 5.9*.

5.3 Evolution of the overall losses

One way to evaluate the evolution of losses in the LHC is to study the norm of the difference between the normalised loss vector at one second and the normalised loss vector at the previous second. This quantity shows the variations of the "shape" of the vector, regardless of its norm *(cf. § 4.8.2)*, because the vectors are normalised to a euclidean norm of 1. Note that some occasional higher losses still appear as higher value for this quantity: this is because the loss, in addition to being higher in value than the usual loss (but this is not seen due to normalisation), also has a different shape. Higher losses would not appear for this quantity only if all 3600 BLMs considered in

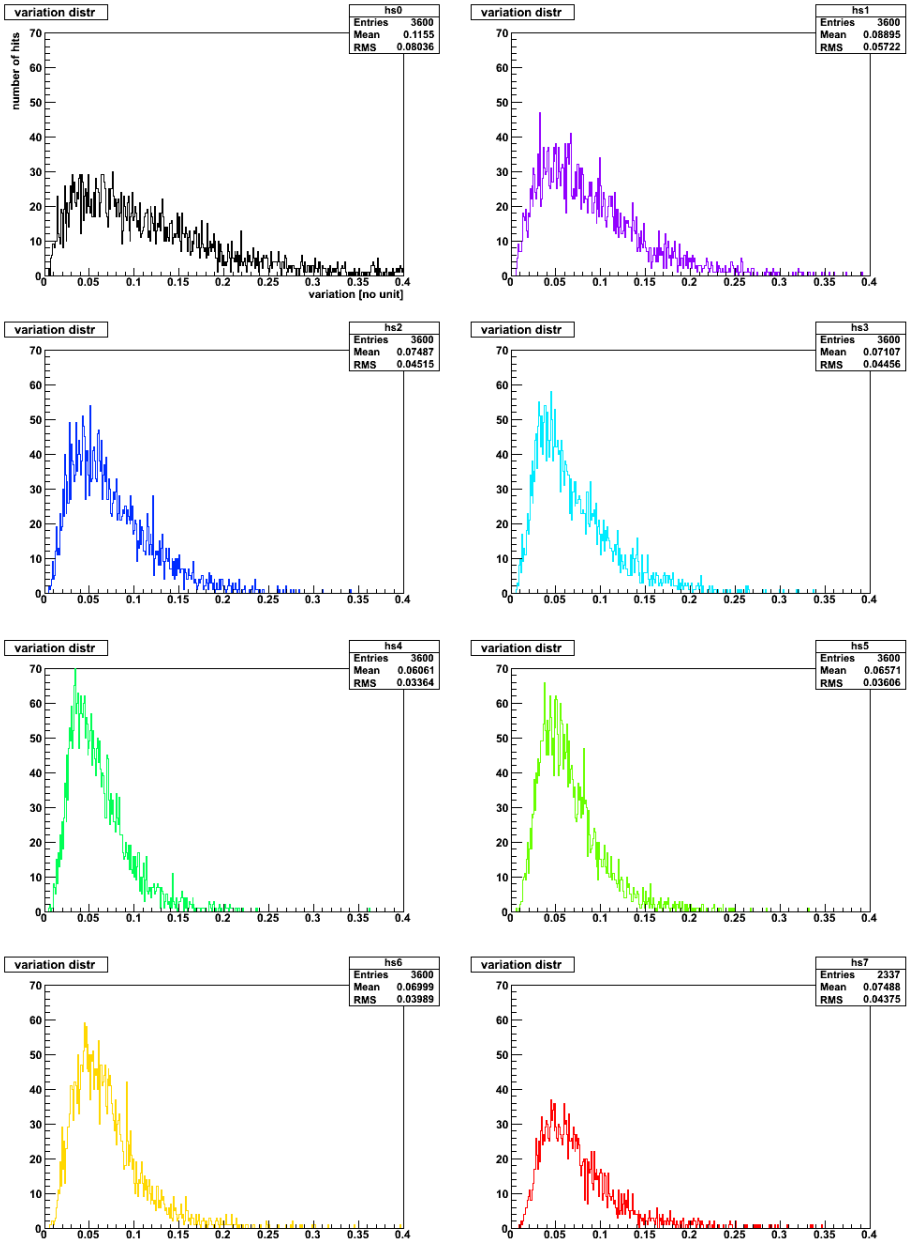

Figure 5.9: Distributions of "time slices" of the norm of the difference between the normalised current loss vector and the normalised loss vector at the previous second. Each histogram has one entry per second, and corresponds to one hour of stable beam except the last one (red) because the beam was dumped. The distributions have less high values and get narrower with time. The X axis is the value of the norm of the difference, and the Y axis is the number of entries per bin. The values of mean and standard deviation are valid in spite of the overflow, because they are calculated numerically with the real value even if it is higher than the maximum bin.

the LHC would see their signal multiplied by the same unique value from one second to another. This is of course unlikely.

All the studied "stable beam" runs showed that this value decreases in the first hours of the run, and that peaks happening during these first hours then tend to decrease *(cf. fig. 5.8)*. This means that the losses in the LHC are more subject to variations during the first hours of the "stable beam".

In order to show this more precisely, the distributions of the norm of the difference along time were calculated *(cf. fig. 5.9)*. The higher values happen when the shape of the loss vector is different from one second to another; the low values happen when the shape of the loss vector at one second is similar to the one at the previous second. *Fig. 5.9* shows that the number of high values decreases with time. The distributions get narrower, with less high values (important changes of shape) and more values around average. The mean value of the distribution, around 0.06, is the average variation of shape of the normalised loss vector.

5.4 Conclusion

In this chapter, several points were validated: a default loss profile could be extracted, and the fact that nearly no losses happen in the arcs (only rare occasional ones) was ascertained. Consequently, the fact that some monitors have a "constant" loss level (standard deviation which is two orders of magnitude lower than their average signal) means that any loss above this level carries the information that non-nominal events happened. No decomposition is therefore needed.

The choices of the losses in IR7 and IR3 as the base for the study were validated by the fact that they are the places in the LHC where the losses have the widest spread; thus, were information can be extracted.

Chapter 6

Spatial distribution and decomposition of the beam loss

In this chapter, the results of the vector decomposition applied to the nominal running conditions will be presented, for vector bases from 2011. These results will be associated to other beam measurements. The way the decomposition is calculated is explained in the previous chapters.

6.1 Results of decomposition

In this section, the results of the decomposition will be presented, as well as the way to display them.

6.1.1 Presentation of the results

For each second of stable beam, the loss vector was created (offset subtracted, normalised) and decomposed using the SVD and Gram-Schmidt algorithms. For each second, the *factors* of the decomposition are calculated: one factor per vector. In addition, the factors are used to recompose the vector, and the *recomposition error* (as described in *§ 3.5*) is calculated: the norm of the difference between the recomposed vector and the current loss vector (both normalised).

For each second, the value of the *centers of mass (cf. § 4.5)* is also calculated. The goal is to give a simple result on the type of loss at the current second, and to allow a comparison.

6.1.2 Displaying the decomposition

Decomposition vs. time

One way to display the decomposition factors is to plot them versus time. Several of these decompositions will be presented in *§ 6.2.* It allows to show how the decomposition evolves with time, and which loss scenario is dominating at each second. Similarly, the factors associated with the tertiary collimators are represented versus time *(cf. fig. 6.4).*

In addition, the decomposition error is displayed, in order to evaluate the accuracy of the decomposition *(cf. § 4.7)*: it evaluates the difference (norm of the subtraction vector) between the original vector and its recomposition using the given factors.

For the centers of mass, the two different aspects (vertical / horizontal, beam 1 / beam 2) are separated *(cf. § 4.5, eq. 4.1, eq. 4.2).* The values of the centers of mass vary between -1 and -0.5 for H/V; between -1 and 1 for B1/B2. Since they are numerical, and are not the product of a decomposition, no decomposition error can be calculated on these values; however, the results have to be interpreted carefully *(cf. § 4.5).* The measurement errors are on the signal of the BLMs.

2-dimensional representation

The two aspects considered here (the transverse planes and the beams) can be put on two different axes. This way, the relative composition of the loss at a time is displayed with one point.

For the centers of mass, the coordinates of a point at one time t are $(CoM_{1|2}(t)$, $CoM_{H|V}(t))$. The time is coded by colour: it starts with purple, and goes to blue, green, yellow and finally red *(cf. fig. 6.1).* This type of display can be useful for a real time calculation and display of the centers of mass. The position of the point includes all the information on the centers of mass.

The same type of display is not as direct for the result of the decomposition because there are as many factors (f_i) as the number of vectors. The four transversal factors could be combined in different ways, such as a Center of Mass, in order to have a 2-dimensional display; it is less straightforward with the 6 vectors.

This problem is not relevant for the interpretation of the result. The choice was made to only use the display versus time, which is sufficient to study the decomposition.

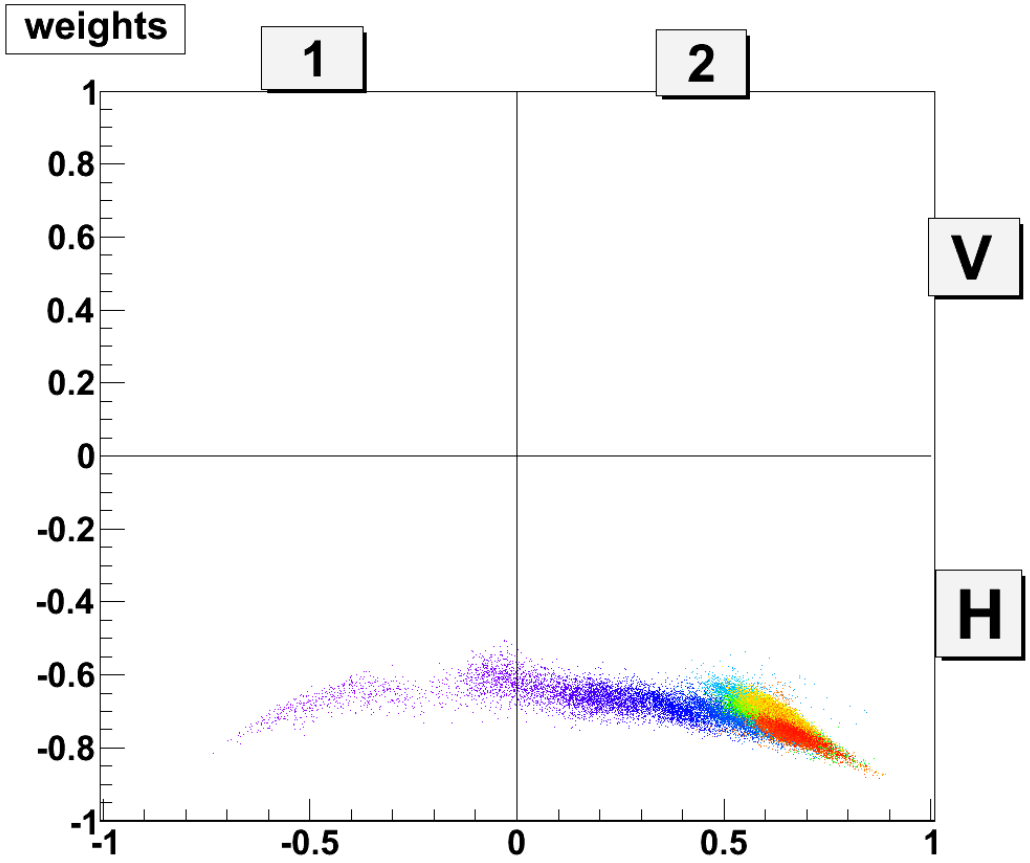

Figure 6.1: 2-dimensional display of the centers of mass. The colour of the points changes with time: purple represents the beginning of the run, then it follows the colours of the rainbow. Red is the end of the run. Most of this run was dominated by losses of type B2H. Points closer to zero for B1/B2 separation or closer to -0.5 for H/V separation show a less clear separation.

6.2 Examples of decomposition versus time

In this section, several examples of the results of the decompositions of complete LHC fills will be presented *(cf. fig.6.2, 6.3 and 6.5)*. The factors associated to the six vectors are plotted versus time, as well as the error on the decomposition. All vectors are normalised before decomposition, so the recomposition should be also normalised. This means that when one scenario is dominating the loss and the associated factor increases, the other factors will decrease, even if the corresponding loss hasn't: only the proportion has changed. Every time, the two decomposition algorithms are presented, SVD and G-S. The factors associated to TCTs *(cf. § 4.4.5)* are represented on a separated plot

(cf. fig. 6.4).

6.2.1 Error propagation for the factors

It was suggested that an error on each decomposition factor could be calculated, in addition to the error on the decomposition *(cf. § 3.5)*. This is achieved by calculating the error propagation in the factors for Gram-Schmidt.

Each of the Gram-Schmidt factors f_i is defined as the result of the scalar product between the corresponding reference vector $\vec{v_i}$ and the vector of the current loss $\vec{X}$. This can be expressed analytically:

$$f_i = \vec{v_i} \cdot \vec{X} = \sum_{j=1}^{m} v_{ij} \cdot x_j \tag{6.1}$$

where (x_j) are the coordinates of $\vec{X}$, and (v_{ij}) the coordinates of the vector $\vec{v_i}$.

The error on x_j, written as σ_{x_j}, is the error on the measure of the BLM. It is known to be proportional to the value of the loss:

$$\sigma_{x_j} = 0.01\, x_j \tag{6.2}$$

The error on the vector $\vec{v_i}$ is written as:

$$\sigma_{v_{ij}} = \sqrt{sys^2 + (0.01\, v_{ij})^2}$$

where sys represents the systematic error on the reference vector. This is known: it is the standard deviation of each coordinate of the reference vector over all loss maps composing this vector. It was calculated when the reference vector was created. It corresponds to the length of the error bar in *fig. 4.3*, and is the RSD of *fig. 4.11, fig. 4.12* and *fig. 4.13* before being divided by the monitor signal. The second term is the error on the measure of the BLM. Both are independent: one is the error on the measure from the physical monitor, the other is the error over the different loss maps. They are consequently summed in square.

Then, the squared error on the factor is calculated as the squared partial derivative with respect to each independent variable T:

$$\sigma_f^2 = \sum_T \left(\frac{\partial f}{\partial T}\right)^2 \cdot \sigma_T^2$$

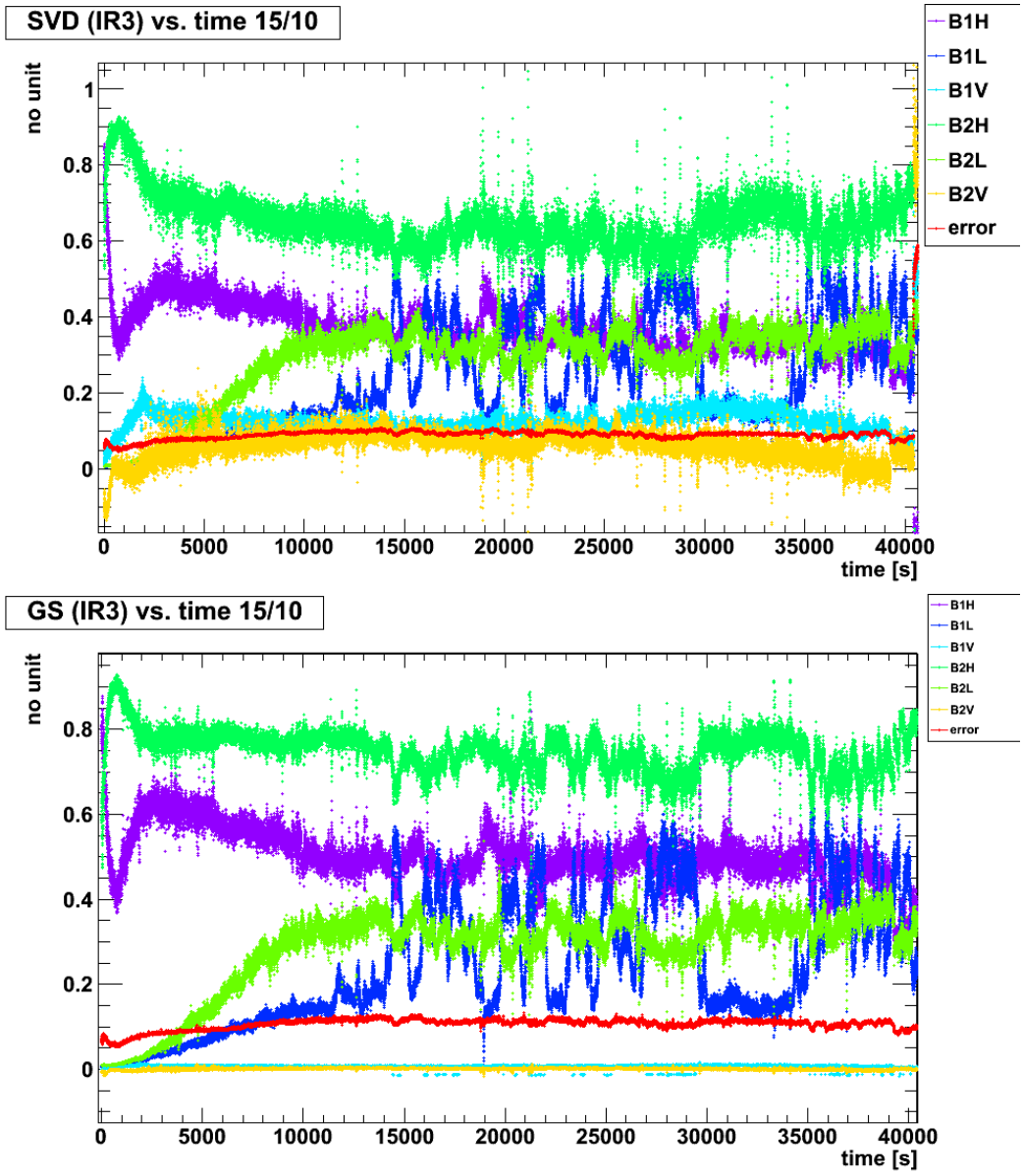

Figure 6.2: Top: SVD versus time, for transversal and longitudinal loss scenarios and the error on decomposition, for the stable beam of the 15^{th} of October 2011. Bottom: Gram-Schmidt versus time. The factors are similar in both cases, and the times at which noticeable changes appear are exactly the same time. The factors for B1V and B2V in G-S are close to zero, because there is nothing left of the vector after the projections. As it is often the case, the factor for the L scenarios are not dominating.

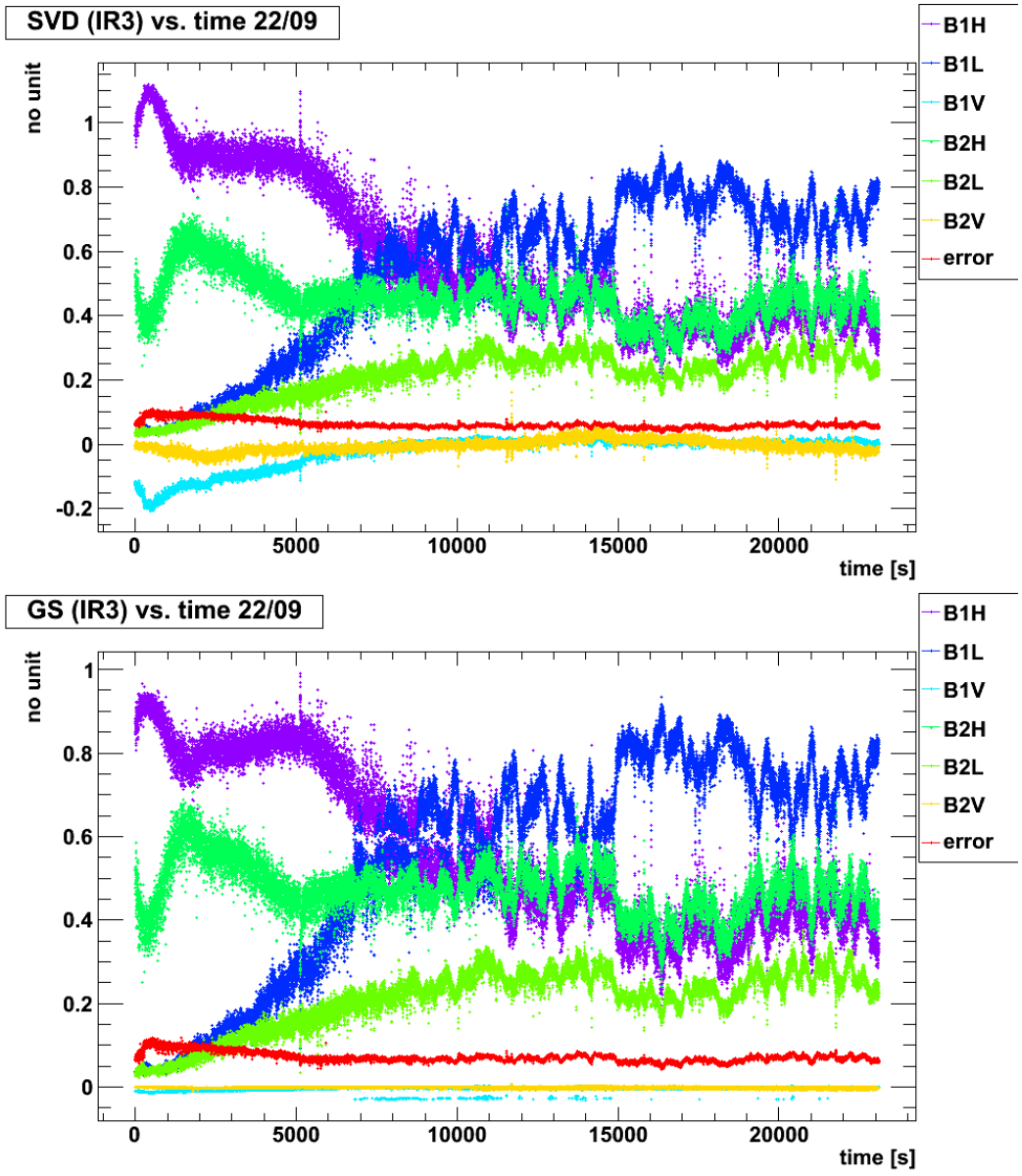

Figure 6.3: Decomposition for transversal and longitudinal loss scenarios and the error on decomposition, for the stable beam of the 22^{nd} of September 2011. Top: SVD versus time, bottom: Gram-Schmidt versus time. The factors are similar in both cases, and the times at which noticeable changes appear are exactly the same time. This is an example when the longitudinal factors actually dominate the decomposition: B1L, dark blue, higher factor at the end of the fill. B2L is the lower green.

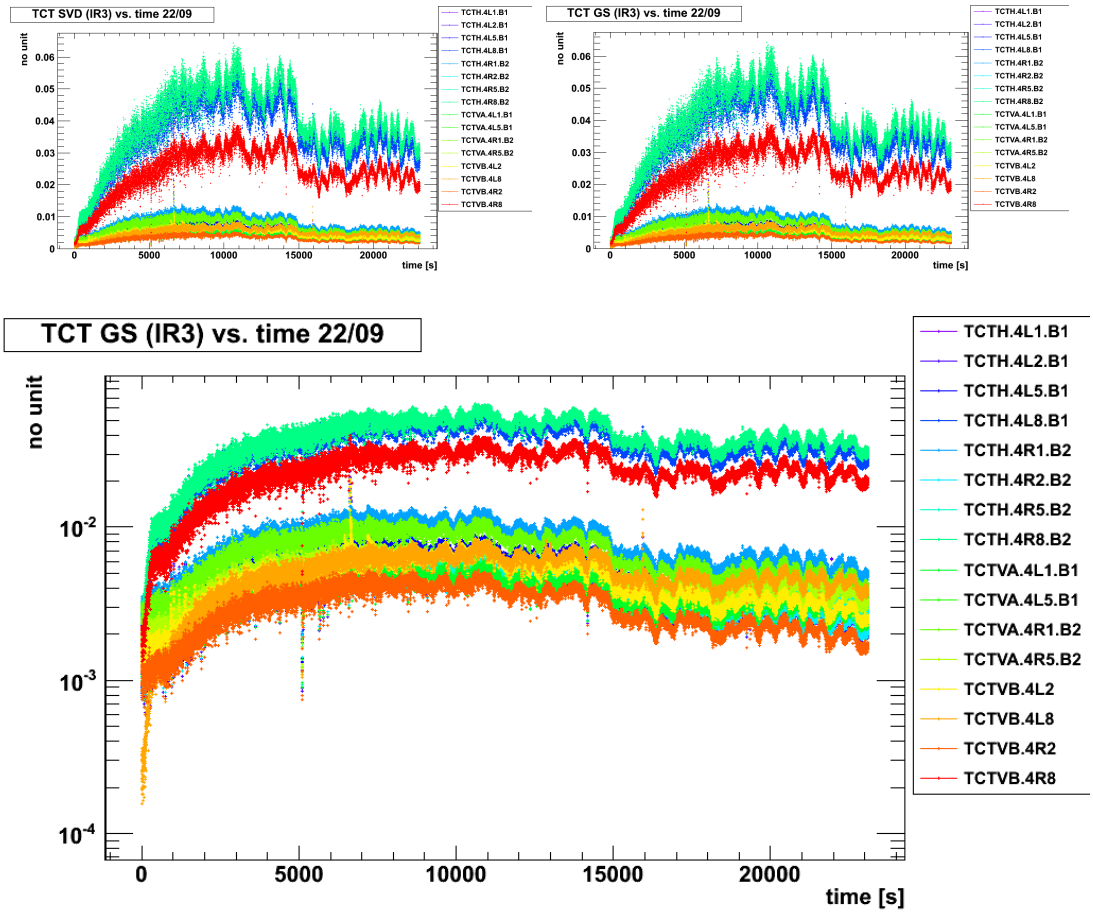

Figure 6.4: Factors calculated for each of the canonical vectors associated to a tertiary collimator (TCT), for the two decompositions of the stable beam of the 22^{nd} of September 2011. The factor correspond to the part of the signal at the TCT that wasn't reconstructed by the reference vectors. Left: for SVD. Right: for Gram-Schmidt. Bottom: decomposition for Gram-Schmidt represented in log scale. The factors in both decompositions are equal to a precision of 10^{-4}, and the times at which noticeable changes appear are exactly the same time. All factors seem to behave similarly *(cf. bottom)*; the different offsets could be due to the different levels of debris coming from the experiments measured at each TCT.

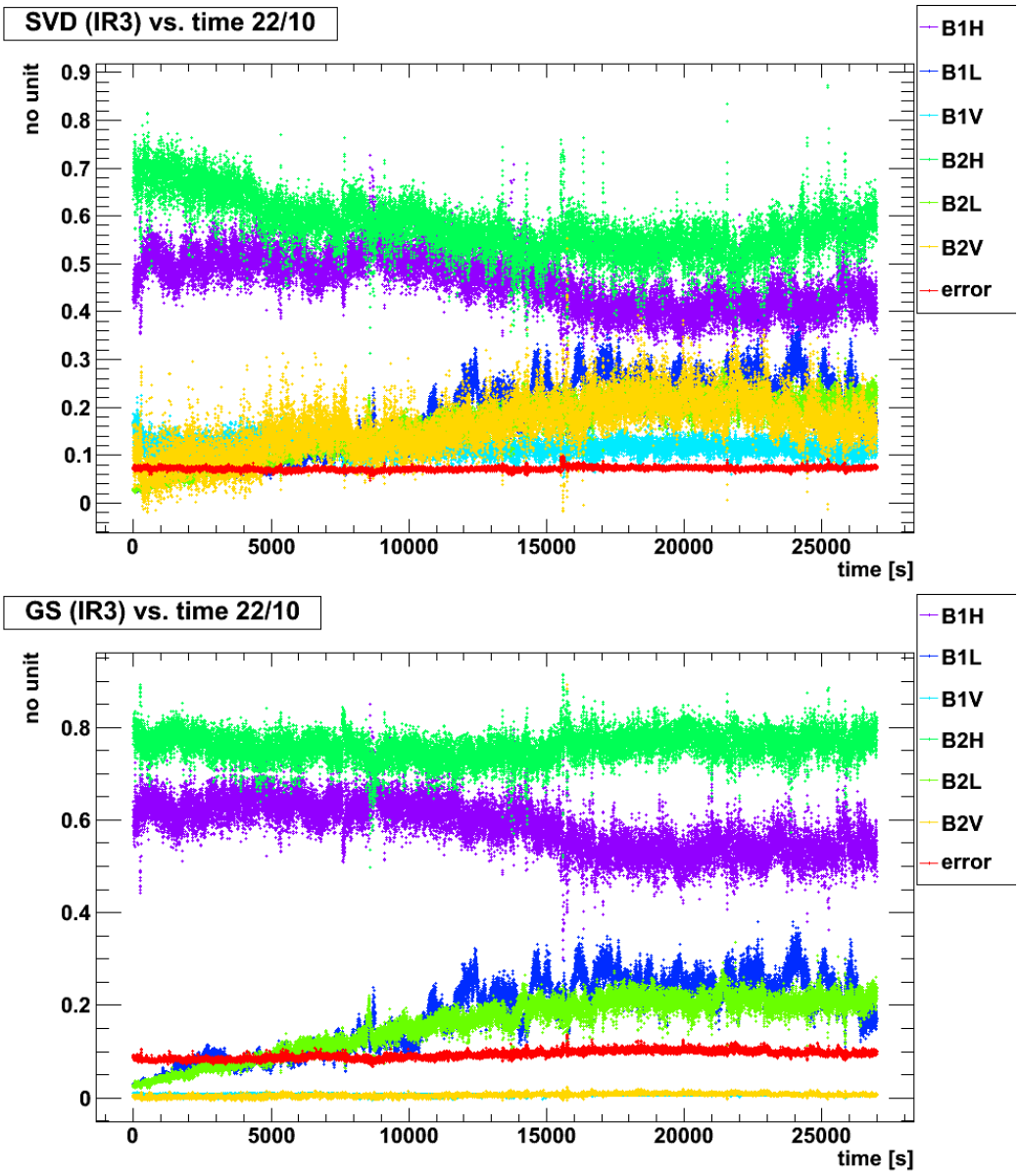

Figure 6.5: Example of almost constant decomposition for transversal and longitudinal loss scenarios and the error on decomposition, for the stable beam of the 22^{nd} of October 2011. Top: SVD versus time, bottom: Gram-Schmidt versus time. This fill was dominated by horizontal losses for both beams. The factors are similar in both cases, and the times at which noticeable changes appear are exactly the same time.

which is calculated as:

$$\sigma_f^2 = \left(\frac{\partial f}{\partial v_{ij}}\right)^2 \sigma_{v_{ij}}^2 + \left(\frac{\partial f}{\partial x_j}\right)^2 \sigma_{x_j}^2 = x_j^2 \cdot \sigma_{v_{ij}}^2 + v_{ij}^2 \cdot \sigma_{x_j}^2$$

The error on each vector coordinate corresponds to an error on the measurement, so is also calculated from *eq. 6.2*.

$$\sigma_f^2 = \sum_{j=1}^{m} x_j^2 \cdot \left(sys^2 + (0.01\, v_{ij})^2\right) + v_{ij}^2 \cdot (0.01\, x_j)^2 \tag{6.3}$$

The error on each factor depends on the current loss vector $\vec{X}$ and and has to be calculated every second. The results are presented in *fig. 6.6*.

The errors, calculated this way, are too small to affect the final decomposition. They are dominated by the error on the loss maps, and are at least 3 orders of magnitude lower than the values of the factors, so they will not be displayed on the results.

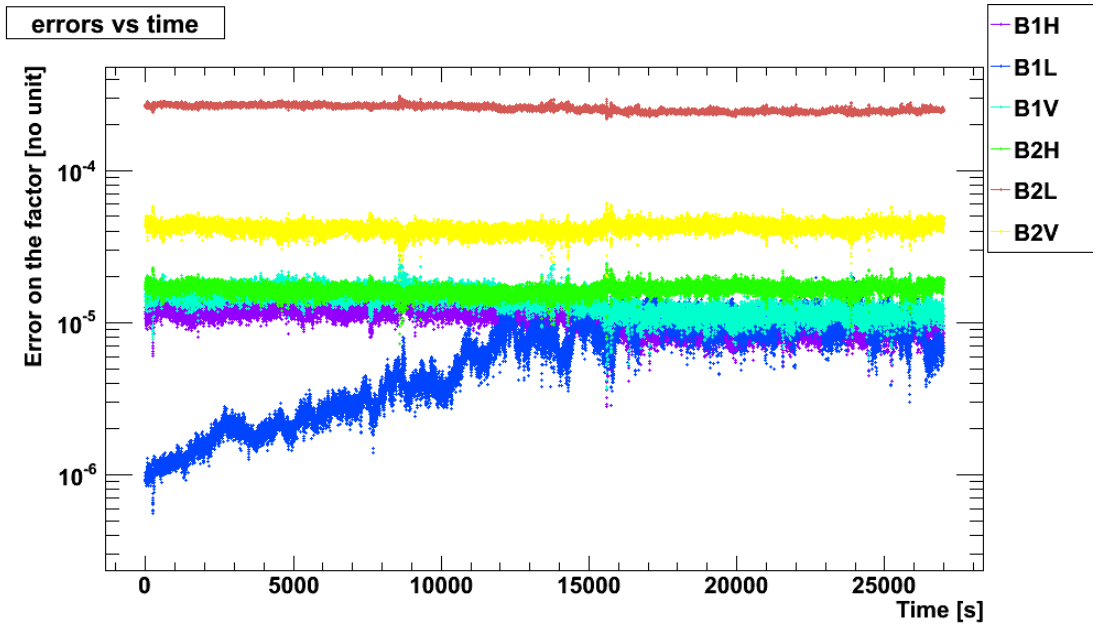

Figure 6.6: Error on the decomposition factors calculated by propagation, for the stable beam of the 22^{nd} of October 2011 *(cf. fig. 6.5)*. The highest error corresponds to the reference vector which had the highest standard deviation: B2L. All the errors are lower than 3 orders of magnitude or more of the values of the factors.

6.3 Validation of results

In this section, we will show how the results of the decomposition can be correlated with other validated machine parameters, such as beam measurements of intensity and emittance.

6.3.1 Beam intensities

All particles measured in the Beam Loss Monitors come from showers initiated by protons lost from the beam. There is a fundamental link between the decrease of *intensity* and the measured losses. However, different events can cause different behaviour: for instance, a non-noticeable part of the overall intensity lost in a short time at one location in the LHC can create losses high enough to trigger a beam dump. In this section, only beam losses having a noticeable effect on the beam intensity are considered.

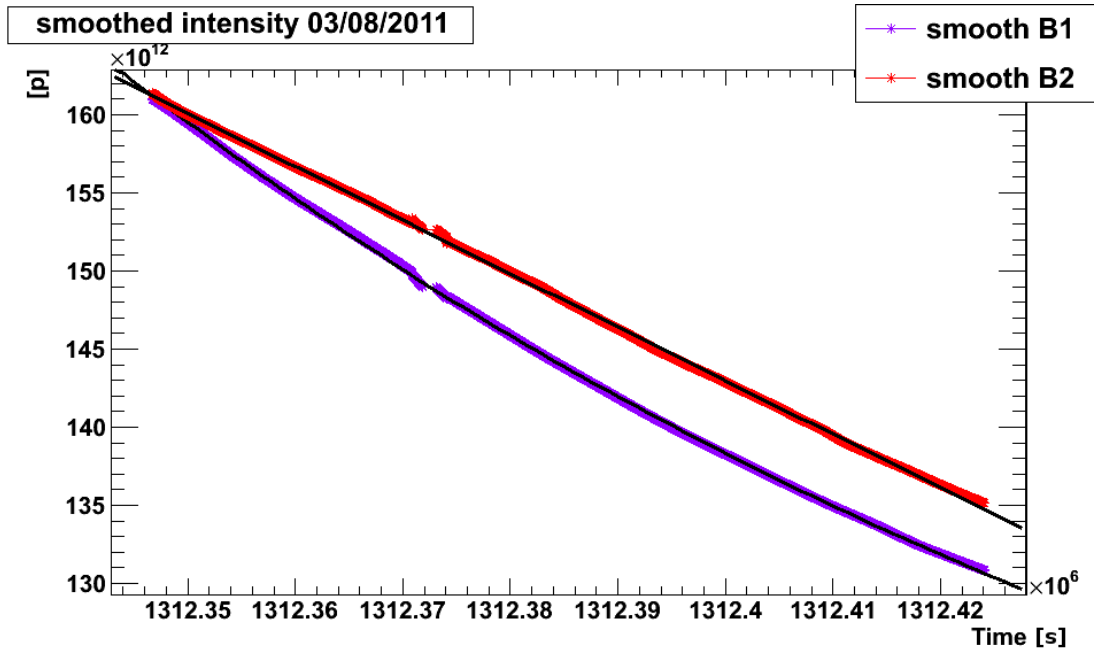

Figure 6.7: Intensity versus time, from the 3^{rd} of August 2011 (fill #2000). This plots shows the readings of the *Fast Beam Current Transformers (FBCT)* for both beams, smoothed with a sliding window of 2001 points. During most of this fill, beam 1 lost more particles than beam 2 (the derivative is given in *fig. 6.9*). The results of the fits are given in *eq. 6.13* and *eq. 6.14*. The different values in the middle are due to a glitch in the FBCTs.

When considering the decrease of intensity with time over entire LHC runs, i.e. for

periods of time longer than the duration of a loss, one of the first observation is that the intensity is decreasing linearly with its derivative (with a possible constant):

$$I(t) \propto \frac{dI}{dt} \tag{6.4}$$

Of course, if the intensity derivative is extremely small, the intensity is nearly constant. This will be shown by measures later *(cf. fig. 6.10)*, but is also rather intuitive: for the same beam characteristics and optics, if the same proportion of the beam is lost per unit of time, a beam with a higher intensity will create more losses. This is true at first order for low values of luminosity, as was the case in 2010. For higher values, at second order, one should consider the square of the intensity.

The *eq. 6.4* can be expressed as a differential equation, with α the proportionality coefficient:

$$I(t) \simeq \alpha \cdot \frac{dI}{dt}$$

$$I(t) \simeq I_0 \cdot e^{-\alpha t} + C \tag{6.5}$$

This result corresponds to what is often observed in the beam intensity in the LHC *(cf. fig. 6.7, beam 1, blue)*. It links to the concept of *beam lifetime*: the time it would take for the intensity to reach $1/e$ of its original intensity. If the constant α is small, the intensity is seen as linearly decreasing at first order (an example of this behaviour will be shown later in *eq. 6.11*):

$$I(t) = I_0 \cdot e^{-\alpha t} + C \quad \sim \quad I_0(1 - \alpha \cdot t) + C = -\alpha I_0 \cdot t + D \tag{6.6}$$

In the case of a decreasing exponential, the beam lifetime would correspond to $\tau = 1/\alpha$. The lifetime calculated for the LHC beams is smoothed to compensate for the small-scale variations of the beam intensity.

Derivative & smoothing

The first step to investigate the validity of this relation is to calculate the *derivative* of the beam intensity. This derivative can be approximated numerically by calculating, for each value $I(t)$ of the intensity:

$$\frac{\delta I}{\delta t} \equiv \frac{I(t+1) - I(t-1)}{(t+1) - (t-1)} = \frac{I(t+1) - I(t-1)}{2} \tag{6.7}$$

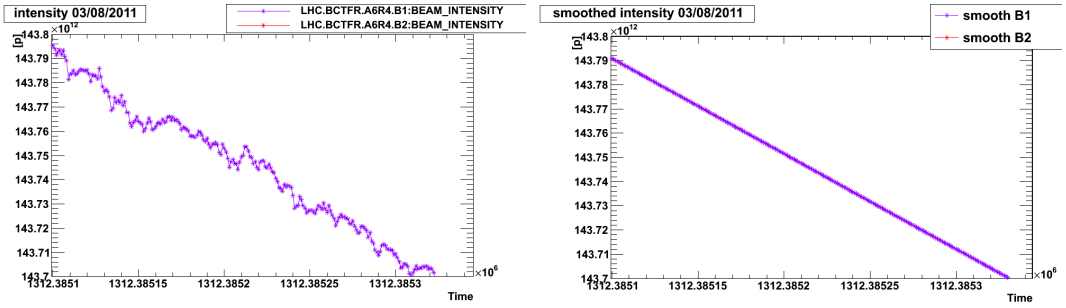

Figure 6.8: Left: short period of evolution of the intensity in the LHC as measured by the Fast Beam Current Transformers, without smoothing, from the 3^{rd} of August 2011. Right: intensity after applying a smoothing with a sliding window of 2001 points. The small variations were suppressed, but not the general trend.

The exact derivative would be the limit of this, for δt approaching 0 (and would then be noted dt). Here, there is only one value per second, so the choice was made to use only this approximation. For simplicity this value will still be noted dI/dt.

The signal measured by the Beam Current Transformers, representing the intensity in the ring, is subject to fluctuations: small scale variations of the measured number of protons, up and down. They should be removed, because they do not correspond to the actual number of protons: an increase of this number would indicate a creation of protons in the ring. Moreover, the calculation of a numerical derivative would give successively positive an negative results: the derivative would not be continuous because of the discrete measurements. The result would not be fit for visualisation.

These variations can be seen as high frequencies, and can be removed by a low-pass filter, also called *smoothing*. The gain from this smoothing is to keep the global decreasing tendency of the beam intensity, which relates to the loss of protons, while removing the fluctuations of the instrument.

One way to achieve this smoothing is via a sliding window: each point $I(t)$ is replaced by the average of all points in the window, noted $\tilde{I}(t)$.

$$\tilde{I}(t) \equiv \frac{\sum_{\tau=t-n}^{t+n} I(\tau)}{2n+1} \tag{6.8}$$

where n is half the length of the sliding window, which holds $2n+1$ points: n points before, the current point at t, and n points after. The higher the number n, the smoother the curve. The numerical derivative can then be calculated with less variations. The results are shown in *fig. 6.8*.

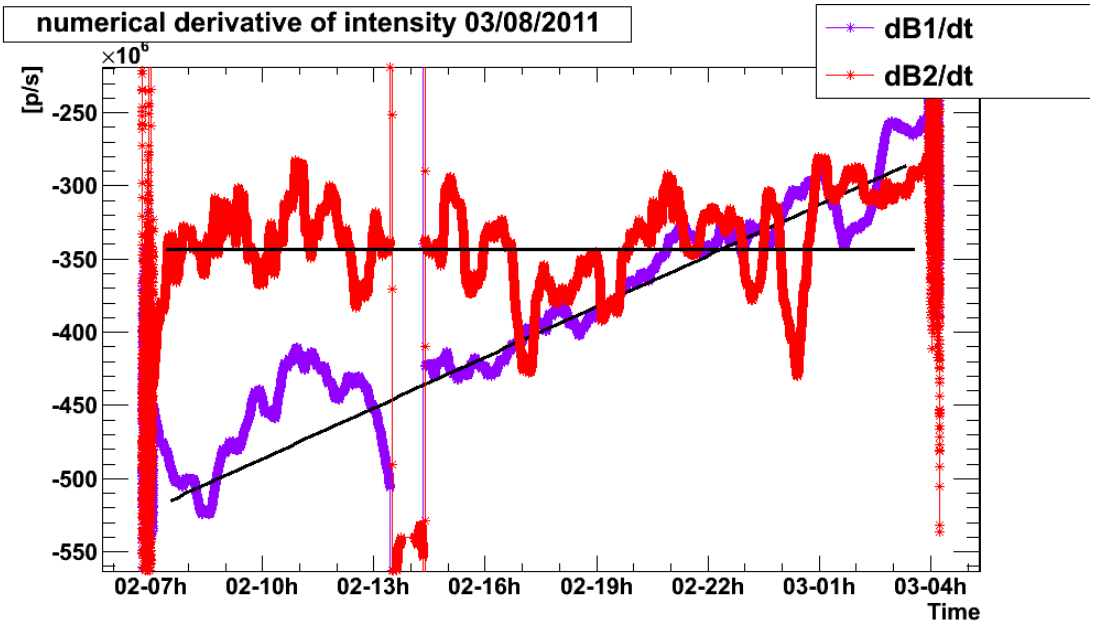

Figure 6.9: Derivative of the beam intensity of the 3^{rd} of August 2011, smoothed by averaging in a sliding window with a small number of points compared to the scale of the variations (201 points). The results of the fits are given in *eq. 6.10* and *eq. 6.11*. Note that variations are still visible, but that both derivatives are clearly negative. The original (non-smoothed) curves were not fit for visualisation: the pedestals of each side correspond to parts of the curves that were smoothed with a smaller window.

Another way to avoid small-scale variation when calculating the numerical derivative is to take a rougher estimation *(cf. eq. 6.8)* of the derivative:

$$\frac{\delta I}{\delta t} \equiv \frac{I(t+n) - I(t-n)}{2n} \tag{6.9}$$

where n is half the length of the sliding window. With a high enough number of points, this restores the continuity of the derivative.

Numerical results

Both techniques lead to very similar results. The evolution of dI/dt versus time is shown in *fig. 6.9*. The derivative of the intensity in beam 1 was fitted with the function:

$$\frac{dI_1}{dt}(t) = A \cdot (t - t_0) + B \tag{6.10}$$

$$A = 3106,31\,\mathrm{p/s^2}$$

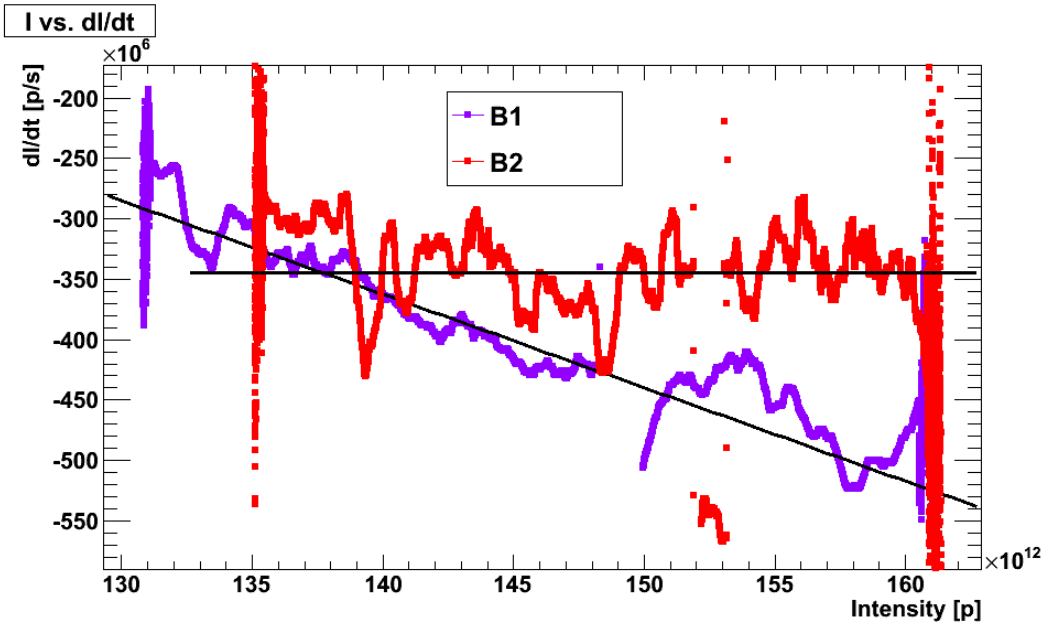

Figure 6.10: Correlation between intensity and its derivative for both beams. The vertical lines at both ends of the curves are numerical edge effects.

$$B = -5,17182 \cdot 10^8 \,\mathrm{p/s}$$

$$EDM = 5.9 \cdot 10^5 \,\mathrm{p/s}$$

where t_0 is the starting time of observation, and corresponds to 1312346700 s since EPOCH (origin of database times), and the *Estimated Distance to Minimum (EDM)* is the average distance between a point and the fitted function. This is an illustration of the 1^{st} order approximation presented in *eq. 6.6*.

The derivative of the intensity in beam 2 was estimated to be a constant:

$$\frac{dI_2}{dt}(t) = -3.44598 \cdot 10^8 \,\mathrm{p/s} \tag{6.11}$$

$$EDM = 47 \,\mathrm{p/s}$$

The fact that the derivative of the intensity in beam 2 can be fitted as a constant justifies the use of a linear function to fit beam 2 in *fig. 6.7*.

To get to the final result, the calculated value of the smoothed derivative at one time t is correlated with the value of the intensity at the same time t. The results

are shown in *fig. 6.10*. The derivative of the intensity in beam 1 was fitted with the function:

$$\frac{dI_1}{dt} = \alpha \cdot I(t - t_0) + \beta \tag{6.12}$$

$$\alpha = -7.73802 \cdot 10^{-6}\,\mathrm{s}^{-1}; \quad \tau = \frac{1}{\alpha} \simeq 35.9\,\mathrm{h}$$

$$\beta = 7.20954 \cdot 10^{8}\,\mathrm{p/s}$$

$$EDM = 3.1 \cdot 10^{4}\,\mathrm{p/s}$$

The derivative of the intensity in beam 2 was estimated to be a constant of the same value as given in *eq. 6.11*.

Knowing this, the derivative equation *6.12* can be solved as:

$$I(t) = K \cdot e^{\alpha \cdot (t - t_0)} - \frac{\beta}{\alpha}$$

which will be simply written as:

$$I(t) = K \cdot e^{-\frac{t - t_0}{\tau}} + C \tag{6.13}$$

where $C = -\alpha/\beta$. The results of the fit *(cf. fig. 6.7)* are:

$$K = 69.3561 \cdot 10^{12}\,\mathrm{p}$$

$$\tau = 1,32969 \cdot 10^{5}\,\mathrm{s} \simeq 36.9\,\mathrm{h}$$

$$C = 91.8838 \cdot 10^{12}\,\mathrm{p}$$

$$EDM = 2.8 \cdot 10^{10}\,\mathrm{p}$$

Note that $K + C = 161.24 \cdot 10^{12}\,\mathrm{p}$, which is the value of the intensity at the beginning of the study *(cf. fig. 6.7)*. The interesting result is that the intensity can be described as a decreasing exponential, but there is an offset in addition.

The intensity in beam 2 was fitted with the function:

$$I_2(t) = A \cdot (t - t_0) + I_0 \tag{6.14}$$

$$A = -3.42158 \cdot 10^{8}\,\mathrm{p/s}$$

$$I_0 = 161,223 \cdot 10^{14}\,\mathrm{p}$$

$$EDM = 1.1 \cdot 10^{8}\,\mathrm{p}$$

The value of A matches the constant found in *eq. 6.11*.

In conclusion, the fact that the beam intensity is evolving linearly with its derivative is a good estimation of the behaviour of the beam.

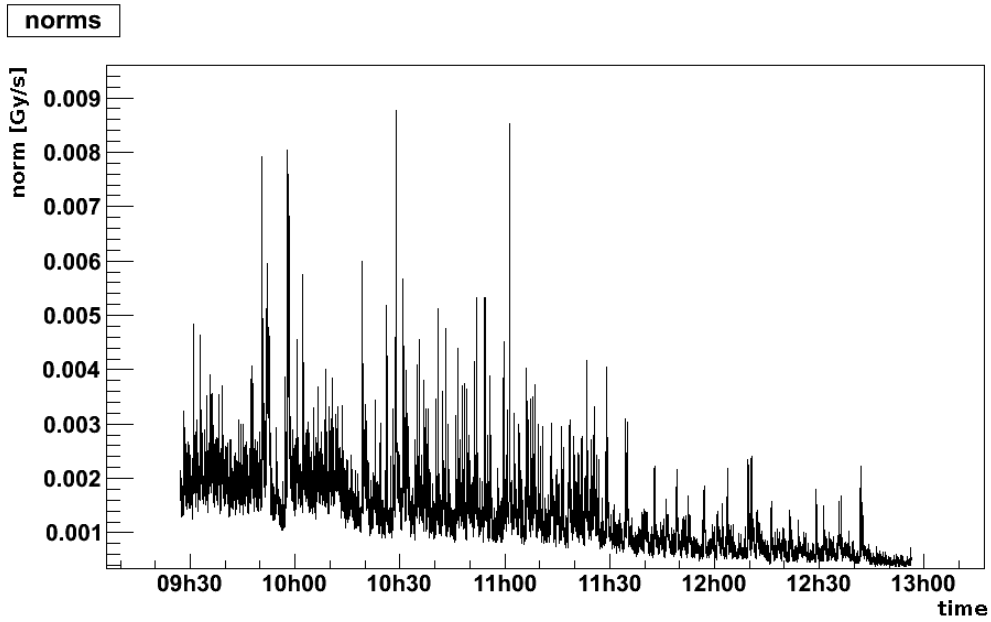

Figure 6.11: Euclidean norm of the loss vector for all BLMs in LHC versus time. The norm decreases with time.

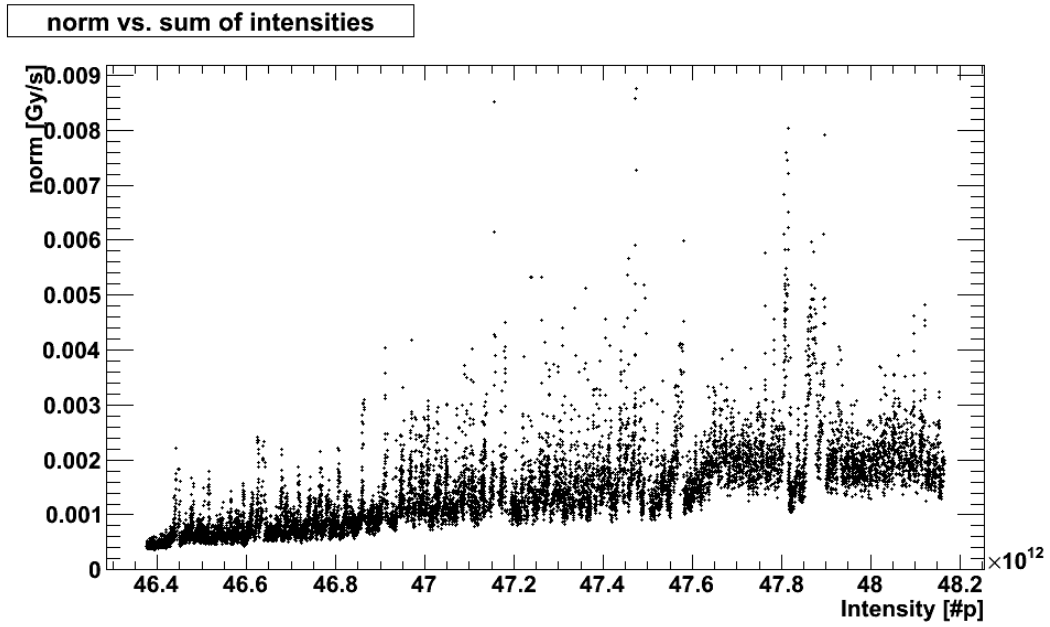

Figure 6.12: Correlation of the norm of the loss versus the sum of the readings of the BCTs. Only the "average" value of the norm correlates with the sum of the two beam intensities. The points for higher values of the norm correspond to occasional higher losses that do not relate to the intensity, by opposition to "regular" losses which increase linearly with the number of protons.

Dependence of the decomposition on the overall loss

All losses measured by the Beam Loss Monitors come from lost protons: the secondary particles detected by the BLMs come from primary particles lost from the beam, mostly on collimators. The norm of the loss vector including all LHC BLMs is shown in *fig. 6.11*. If no important loss location is missed, and not too many losses are double-counted, it should be proportional to dI/dt.

Since the intensity is following linearly to its derivative, the norm of the loss vector for the whole LHC, reflecting all losses in the ring, should vary linearly with the intensity. This can be seen in *fig. 6.12*. Since the BLMs can detect the secondary showers regardless of which beam they come from, the signal of the BCTs were summed up. The figure illustrates how all previous assumptions on the way to evaluate the total loss in the LHC and on the behaviour of the beam are justifiable. It can also be assumed that no important loss location is ignored.

However, this is only true for an average loss and an average intensity: the spikes seen in the norm *(cf. fig. 6.7)* correspond to a number of lost protons that is still small in comparison to the overall number of protons in the beam. The change in intensity is not necessarily visible. They correspond to "occasional" losses that do not happen permanently, so they do not relate directly to the value of the intensity (this corresponds to the cases when big losses are created with little intensity).

6.3.2 Correlation with the result of the decomposition

One simple way to link the results of the decomposition back to direct measurements in the machine is to consider periods of fills during which the two beams behave differently, as shown in *fig. 6.7*: the derivatives of the two beam intensities are different *(cf. fig. 6.9)*. As explained in *§ 6.3.1*, it means that the losses should be dominated by the beam losing more protons (Beam 1 in this case). It should show in the decomposition and the centers of mass.

In order to compare similar values, the center of mass *(cf. § 4.5)* for the derivatives is calculated as:

$$CoM_{\frac{dI}{dt}} = \frac{\frac{dB_1}{dt} - \frac{dB_2}{dt}}{\frac{dB_1}{dt} + \frac{dB_2}{dt}} \tag{6.15}$$

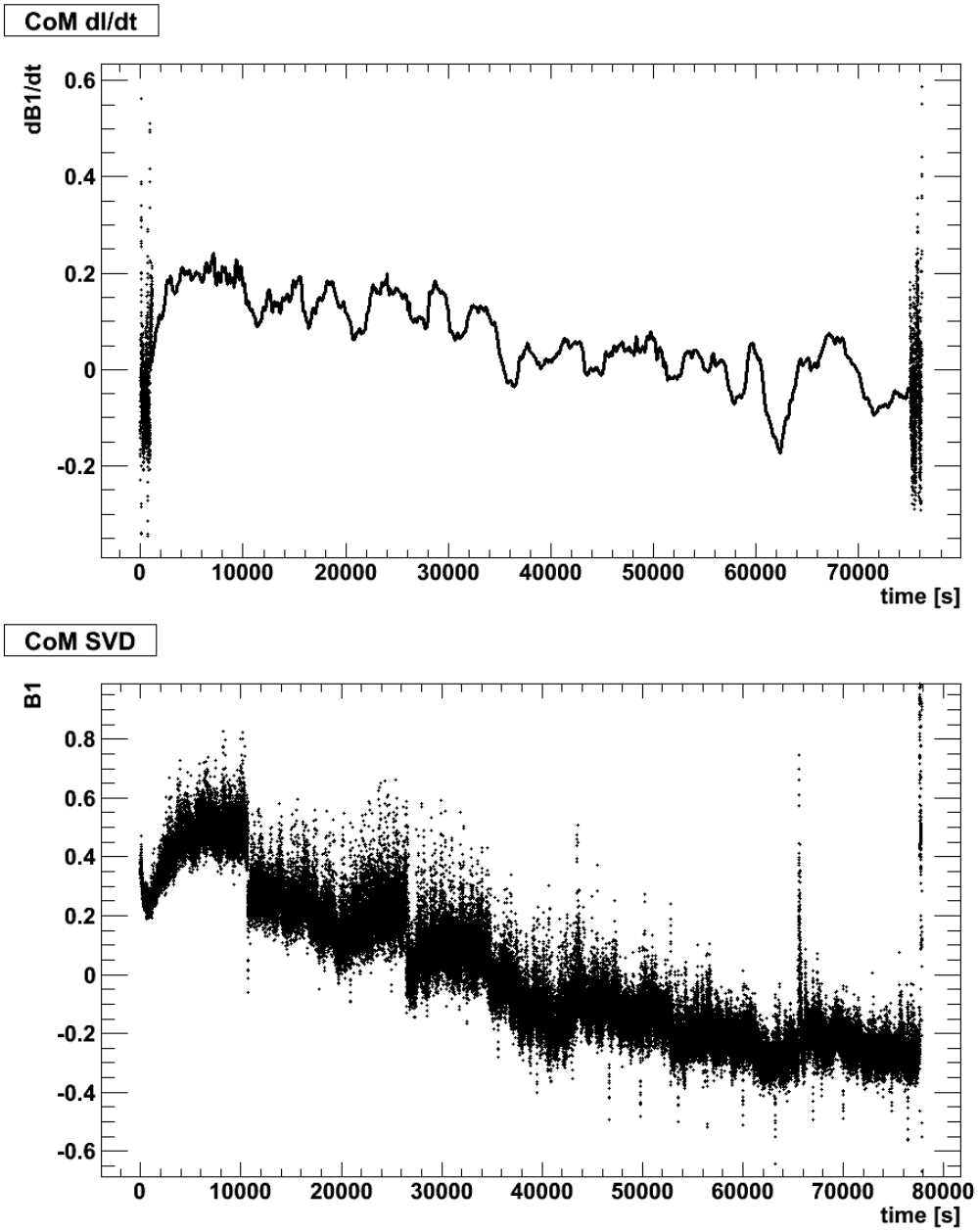

Figure 6.13: Top: Center of Mass calculated for the derivatives of the intensities in both beams *(cf. eq. 6.15)*, for the stable beams of the 3^{rd} of August 2011 (fill #2000). At the beginning of the fill, the overall derivative is dominated by the derivative of Beam 1: the center of mass is positive. The scattered points at the extremities are an edge effect of the smoothing. Bottom: Center of Mass calculated for the SVD factors *(cf. eq. 6.16)*. This is a two step process, used to compare similar quantities. At the beginning of the fill, the decomposition is dominated by the factors associated to beam 1; at the end, the beam 2 factors are more important. The intensity is smoothed over 2000 points but the losses aren't, so the small scale variations can't be correlated.

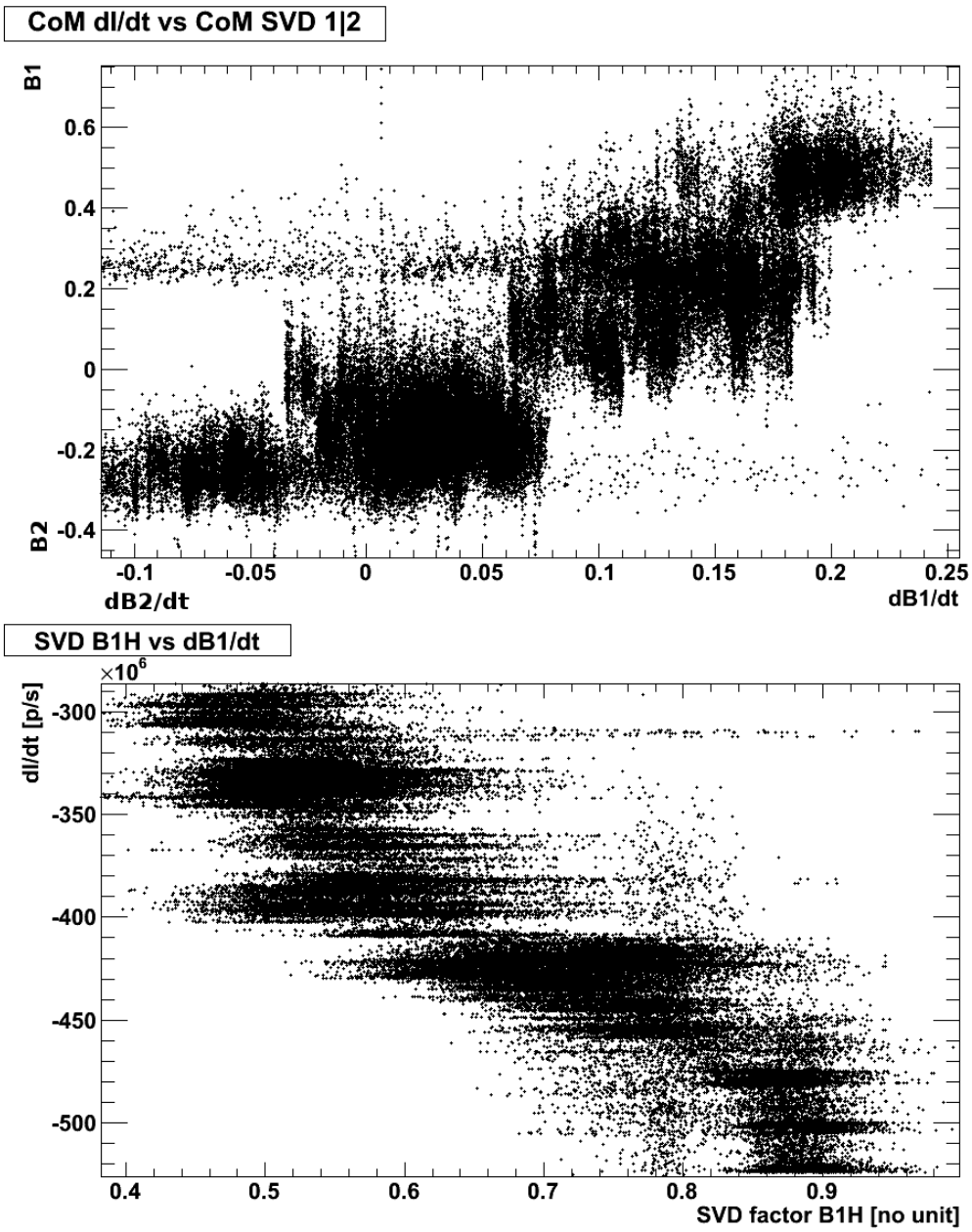

Figure 6.14: Top: correlation between the Center of Mass calculated for the SVD factors (Y axis, *cf. fig. 6.13 bottom*) and the Center of Mass calculated for the derivative of the intensity (X axis, *cf. fig. 6.13 top*). When the derivative of the intensity is dominated by beam 1 (CoM closer to 1), the decomposition is dominated by beam 1 factors (CoM closer to 1). Bottom: correlation between the derivative of the intensity in beam 1 (Y axis) and the SVD factor associated to B1H (X axis). For higher values of the factor, many more protons were lost (higher negative values of derivative).

The results are presented in *fig. 6.13 top*. In this case, the overall derivative is dominated by the derivative of beam 1 at the beginning of the fill: more protons were lost by beam 1 than by beam 2. The same process is applied to the results of the decomposition: a Center of Mass is calculated for the factors of SVD *(cf. eq. 6.16)*. The results are presented in *fig. 6.13 bottom*.

$$CoM_{SVD} = \frac{(h_1 + v_1) - (h_2 + v_2)}{h_1 + v_1 + h_2 + v_2} \tag{6.16}$$

Note that this is not the center of mass calculated for the BLM signal at the primary collimators: this is a two step process, where the SVD decomposition is calculated first, and then a center of mass is calculated from the SVD factors. This verification was also done with the center of mass for the BLM signals, and the following results also apply, but they are not presented here.

The result given by the derivatives of intensities is similar to the result given by the centers of mass for SVD: the losses are dominated by beam 1. Moreover, the two curves can be correlated: the more positive the center of mass for the derivatives is (the more dB_1/dt "dominates" dB_2/dt), the more dominated by B1 the decomposition is *(cf. fig. 6.14 top)*. More simply, the factor h_1 (dominating the decomposition at the beginning of the fill) can be directly correlated with the derivative of the intensity in beam 1, for the entire fill*(cf. fig. 6.14 bottom)* .

6.3.3 Collimator scraping

One of the beam measurement involving the collimators is the collimator scraping, described in *§ 1.4.5*. During these measurements, one collimator is moved in the beam, in order to create high losses. This means that the collimator hierarchy is changed. In the frame of the decomposition, the corresponding loss profile would then not be the same as any of the default vectors, since the collimators are in different respective positions. Conversely, the advantage of this measurement is that the origin of the loss (particularly the beam plane) is known.

This test was performed during the collimator scrapings which took place in the night of the 5^{th} of November 2011 *(cf. fig. 6.15)*. The two beams were scraped in IR7 by their respective horizontal primary collimators. The resulting factors of the decomposition gives the correct beam and plane and the exact time.

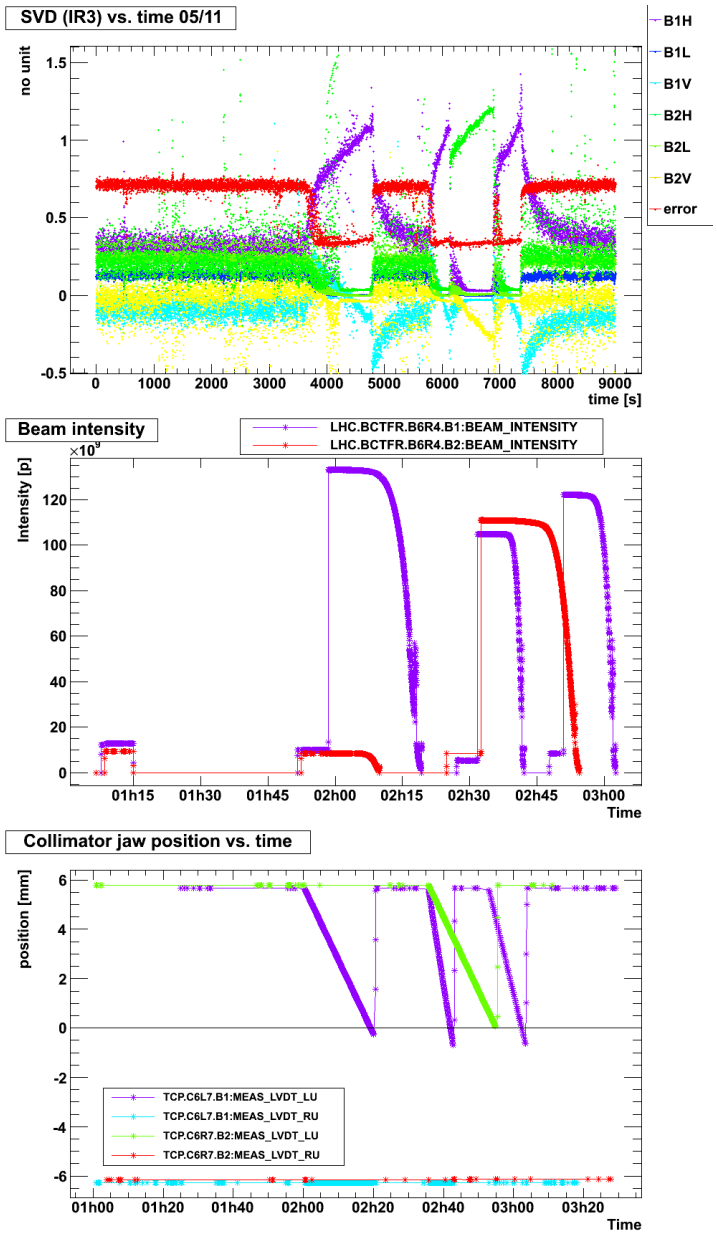

Figure 6.15: Top: Results of the decomposition (SVD) calculated during collimator scrapings performed the 5^{th} of november 2011. Center: Intensity in the two beams at the time of scraping. Bottom: position of the jaws of the two horizontal primary collimators, at the same time. The factors match exactly the type of the TCPs, and the time at which they were moved. The first high values of the B2H factor are due to a scraping with TCLIB.6L8.B2, whose jaw position is not represented. When two scrapings took place at the same time, the decomposition was dominated by the beam losing the more particle (having the bigger derivative).

Further observations show that the observed factor is greater than one. The factor for the same beam, other plane (depending on the case) is lower than zero: these two factors compensate each other. This could be explained by the fact that the losses are higher at the primary collimator than at the other collimators; even higher than in the standard vector. In order to match this coordinate, the decomposition algorithm had to give a factor higher than one to this vector. All other collimators have then a reconstructed signal higher than in the current profile; part of this signal must be subtracted, leading to a negative factor for the vector associated to the other plane.

Another observation is that the value of the error varies a lot. During "normal" losses – that is outside the scrapings – the value of the error is rather high: close to one. This is probably due to the fact that the beam intensity is very slow compared to nominal operation: only one bunch is injected, for loss security reason. The losses are then very low (the offset is subtracted), and can not be very well recomposed. However, during the scraping, the losses increase a lot; and the shape of the vector is then closer to the default ones, and the loss is better recomposed. This shows that the error is an efficient way to evaluate the quality of the recomposition.

Another observation is that, starting at 2:35, two collimator scrapings are taking place at the same time *(cf. fig. 6.15 bottom)*. However, the loss is decomposed in only one vector at a time: B1H, then B2H, then B1H again. The reason for this is visible in the plot of the beam intensity versus time *(cf. fig. 6.15 center)*. As explained in *§ 6.3.1*, the results of the decomposition correlate with the derivative of the beam intensity. *Fig. 6.15 center* shows that there is always one beam losing more protons than the other at a time. This behaviour corresponds to the results given by the decomposition.

6.4 Conclusion

Several very different techniques decomposing an unknown loss profile into a sum of given loss scenarios were presented. All techniques agree with each other. In addition, the results of these theoretical and non-trivial mathematical operations could be linked back to the reality of the LHC, such as the beam intensities and their derivatives. The results were partly confirmed on the scale of the entire LHC, with the tertiary collimators.

Global Conclusion

The goal of this work was to identify patterns in the beam loss profiles, both in their spatial distribution and in their time evolution.

The first part was achieved by considering the profiles as vector, using both vector projection (Gram-Schmidt) and matrix inversion techniques (Singular Value Decomposition). Different studies proved that it was possible to identify patterns in a measured loss profile, considering limitations such as the quality of the recomposition and the choice of the patterns. The extracted information must always be considered with these limitations: a good decomposition on wrong vectors, as well as a bad decomposition on good vectors could lead to wrong conclusions. The selection of the reference vectors proved to be a key aspect. patterns corresponding to specific loss mechanisms were identified: the scenarios corresponding to the 3 planes of the particle coordinates for the 2 beams.

The second part, the time evolution, helped understanding how to consider the difference between vectors. Averaging the monitor signals over a long period of time lead to the creation of a default loss profile. It showed that most Beam Loss Monitors have a rather constant behaviour; the decomposition focuses on the monitors which don't. Most of the non-nominal losses which are not covered by the spatial decomposition could still be noticed by comparison with the default loss profile. A way to evaluate the error on the recomposition was developed, in order to investigate the correctness of a decomposition. It lead to the implementation of a "threshold" between good and bad decompositions. The results were cross-checked with other beam instruments and measurements.

The decomposition techniques have been implemented by other people in a real-time instrument, which can be used to help machine operation, by helping to identify the origin of a loss at a given time and detecting unusual losses. Further work would

include adding more default vectors for different situations. For instance, reference vectors could be created for all possible beam modes in addition to stable beams, and for the ion fills. The decomposition could be performed on all past and future "stable beams" periods, to learn about the global evolution of the behaviour of the LHC. New reference vectors could be produced for other scenarios, such as a breaking of the collimators hierarchy. Implementing the comparison with the default loss profile in real time would help evaluating how "standard" the current loss is.

Different vectors could be produce also by changing the selection of monitors, or using different integration windows. Other decomposition algorithms could be added, such as the Gram matrix, blind signal separation or data fits that would return only positive factors.

Eventually, this tool could be used in other machines having loss monitors and in which loss profiles can be measured. This doctoral work, with its limitations, could help the operation of particle accelerators by extracting information on the beam dynamics from the global beam losses.

Appendix A

Data Access

A.1 Introduction

A.1.1 Beam losses

The Beam Loss section at CERN has installed more than 3600 *Beam Loss Monitors* (BLMs) around the LHC ring, in order to measure the *beam losses* in the LHC. If the losses exceed the set *loss thresholds*, the beam permit is removed, and the beam is removed from the ring and directed towards a beam absorber. The whole process is called a *dump*, and must be triggered in less than one turn of the LHC: 89 μs.

The BLMs are installed in expected loss locations, given by simulation and a good understanding of the beam optics in the LHC. Finding the origin and the reason of a beam loss (whether it lead to a beam dump or not) is crucial to the further understanding of the beam optics, as well as the good functioning of the LHC.

All data produced by the BLMs are used in real time, for threshold comparison; then some is stored in the LHC databases, which will first be further described below. However, the layout of the machine where the loss was produced is just as important as the measured loss itself, and must be understood as well.

A.1.2 Introduction to the Beam Loss Analysis Toolbox

The Beam Loss Analysis *toolbox* was designed to allow the access, processing and display of data in a fast, user-friendly and easy way. This chapter describes the techniques used to access the different databases, to combine the values of losses with the position of the BLMs and magnets, and their display. The ensemble of these techniques is referred

to as a *toolbox*. The toolbox was then expanded to process and display other beam instruments than the BLMs.

The main programing and data analysis framework at CERN is ROOT, a C++ framework providing classes and a C++ interpreter called CINT. Amongst other, ROOT provides objects that can send SQL statements and receive the results.

The choice was made to use Python (2.4) as the developing language (and not CINT), since a true interpreter was desirable. It links easily with ROOT (5.28) objects thanks to the pyROOT project.

The toolbox was developed in a way as object–oriented as possible. It is made of several *modules*, holding different *classes* and *functions*. The classes hold *methods* that are functions bound to the object, and *attributes* that are variables stored in the object. Additionally, specific structures were created and are common to several objects, simplifying the communication between objects and the understanding of the user.

The main modules are:

- databases;
- analysis;
- display.

The `databases` module provides all the classes to connect to the different databases, and get the data in specific formats. The language used for database access at the time of development was PL/SQL, so the access was first done using *Structured Query Language (SQL)* queries. Then, a new *Application Programing Interface (API)*, written in Java, was implemented for the Logging and Measurement databases by the databases management in order to protect them. It avoids having a direct access of the databases by the user (dangerous for the databases) by implementing a "tier 3" access via a server running the API. The access to the Layout database is still achieved via SQL queries.

The `display` module provides classes taking data in the format returned by the `databases` module, and plots them on screen. It allows a simple management of several graphs in one scope.

The `analysis` module is "wrapping" class that uses classes and methods provided by all the other modules so that the user can display losses in a section the LHC at

one timestamp, in only one command line. It also accesses other modules dedicated to other instruments in the LHC.

A.2 Types of required data and corresponding databases

Before describing the structure of the modules, the different type of data (signal or layout data) must be presented, as well as the storage structure of the different databases holding these data.

A.2.1 Data structure

Running sums

The Beam Loss Monitors are ionisation chambers. The BLM electronics reads the output of the chamber every 40 μs, permanently. These values are then summed up following different integration intervals called *running sums (cf. tab. 2.1)*. The resulting values corresponds to the charge deposited in the chamber after applying conversion factors.

Every second, for each monitor, one value per running sum is selected to be stored in the Measurement database. For the running sums shorter than one second (1 to 8), the selected value is the highest in the last second; for the others (9 to 12), the last value is selected. The running sums are stored under a specific *variable name*: `BLM_EXPERT_NAME:LOSS_RSXX`, where `"BLM_EXPERT_NAME"` is the official name of the BLM following the naming convention, and `"RSXX"` is the running sum name *(cf. tab. 2.1)*.

Two SQL lists are associated to each variable: the list of *timestamps* (date and time at which the data was taken) and the value at that timestamp *(cf. §. A.2.3)*.

Thresholds

The loss thresholds are different from BLM to BLM, depending on the element they protect; they also change depending on 32 levels energy of the beam and the LHC cycle phases.

The current thresholds used at one time are stored in the databases, under a variable name similar to the one of the loss: `BLM_EXPERT_NAME:THRESH_RSXX` where `"BLM_EXPERT_NAME"` is the official name of the BLM, following the naming convention, and `"RSXX"` is the running sum name *(cf. tab. 2.1)*.

A.2.2 Layout database

The Layout database holds most of the layout information about the LHC. In this case, the relevant information includes:

- position of the BLMs;
- position of the beginning and the end of magnets;
- position of the collimators;
- position of other beam instruments;
- optics variables.

This information is essential to the good understanding of the losses, in order to show where it happened, and what element of the LHC can have created it.

The structure of the Layout database is the one of a standard SQL database: several tables hold all related information in different columns. For instance, the collimator positions, in column `TC_POSITION`, are linked with the collimator names in the column `TC_OFFICIAL_NAME`, and they are both stored in the table which is called `COLLIMATOR_STRUCTURES`.

A.2.3 Measurement database and Logging database

Data storage

Two identically behaving databases are used to store the values coming from the beam instruments of the LHC. The first one, called *Measurement database (MDB)*, gives a temporary storage (one week) to all selected data *(cf. § A.3.1)*. Then, an algorithm specific to each system selects which data will be send to the *Logging database (LDB)* to be stored permanently.

For the "loss" values, the data are stored permanently in the *Logging database* after applying a filter: if the difference between two subsequent values is higher than a delta

set per Running Sum, the value is saved; if not, one value per minute is saved. This makes sense because during regular running of the LHC, when the losses are minimal and don't fluctuate much around the basic offset, only a few data are logged. When losses do appear, the values are higher than the basic offset, and it is important to log all of them.

However, one must understand that data from each BLM are not all logged at the same timestamp. This is described in *fig. A.3* and an example is shown in *fig. A.5* where one point corresponds to one logged value: they are not logged at the same second in a minute.

For the "threshold" values, the data are logged "on change": a value is logged only if it differs from the previous one, and once per day if they don't change.

Data types & views

Because of their sizes, of the fact that they are written and read permanently, and contrary to layout data, the measurement data do not follow the basic table / column / element structure. They are stored following their *data type* in different tables called *views*. The views are different ways of getting the same data, e.g. all data in the time range, or only last data in the time range. All possible views are described in (16).

Each table only has few columns, including `UTC_STAMP`, giving the timestamps at which the data was logged, and `VALUE`. The name of the variable itself is not stored there. The variable name and the time range, the *query parameters*, have to be set before requiring the data from the relevant view (17).

A.3 Database Access Techniques

In this section, the module used to access databases is described, as well as the techniques implemented in the tool.

A.3.1 PL/SQL Access

The first way to access the Measurement and Logging databases was via an API written in PL/SQL, providing a direct access to the databases (17).

Connection — passwords and security

In order to access each database with SQL statements, user names and passwords specific to each database must be provided. In addition, the access to Logging and Measurement databases requires a client identification and an application name.

For obvious security reasons, these are not hard-coded in the modules. They are stored in a specific separated file which is not distributed and is specific to each user. The default python module `ConfigParser` (18) provides the retrieving of the values in the file. It is embedded in a method belonging to the superclass of all `databases` classes. The details are stored as attributes of the class and used to open connections. The classes dealing with Logging and Measurement databases leave the opening and closing of connection to the user; all other classes do it automatically.

The connection is opened via an object imported from ROOT and called `TSQLServer` (19). The user and password are passed to the `Connect` method, which returns a pointer to the `TSQLServer` object. It is stored as an attribute called `sqlData` and will be used to send *queries (cf. § A.3.1)*.

For Measurement and Logging databases, the client identification and the application name had to be passed in addition. The SQL query was the following:

```
DECLARE
 l_client_id varchar2(30) := 'YOUR_CLIENT_ID_HERE';
 l_app_name varchar2(30) := 'YOUR_APP_NAME_HERE';
BEGIN data_access.set_client(l_client_id, l_app_name); END;
```

The reason for these classes to be able to open and close connection themselves is that the Logging and Measurement databases are protected in access. One could not open more than 500 "tokens", one token corresponding to the query of one variable. If the user requested more than 500 variables, the connection object would close the connection after 500 variables, and then open a new connection.

Note that after moving to the java command line application to access the Logging and Measurement databases, these operations were not needed any more. The application deals with the opening and closing of connections.

PL/SQL Queries

Once the connection is opened, *queries* can be sent. This is achieved the attribute called `sqlData`. It is used to communicate with the database by sending SQL queries that are automatically constructed as strings, e.g.:

```
select TC_OFFICIAL_NAME, TC_POSITION from COLLIMATOR_STRUCTURES;
```

Sending a query with a `TSQLServer` object returns a `TSQLStatement` object. It can be iterated by the `NextResultRow()` method, and the contents of each row (two in the previous example) are returned by the `GetString(i)` method (19).

The values are always returned in order as strings so the user does not have to change the ROOT method depending on the data. Instead, a function of `databases` will automatically cast it as an integer if possible, or a float if not possible, or leave it as a string if both castings fail.

Query Parameters

For the Measurement and Logging databases, the query parameters have to be set before starting the data query; that is, the time window and the variable names *(cf. § A.1.2)*.

The time window is set by a single method, that sends the following query:

```
begin data_access.SET_TIME_WINDOW(:1, :2); end;
```

where "`:1`" and "`:2`" are the positions of the arguments, coded by an integer in the call of the `TSQLStatement.SetString(i, str)` method. Note that the numbering of the arguments starts at 1 in the SQL query, but starts at 0 in the ROOT function.

The variable names are passed the same way, starting with the query:

```
begin data_access.SET_VARIABLE(:1); end;
```

and followed by the actual variable name is passed with the same TSQLStatement method. Then the actual timestamp and values are requested by the query:

```
select utc_stamp, value from var_numeric_data_v
```

where `var_numeric_data_v` can be any "view" described in (16). Again, the results are returned by the `TSQLStatement.SetString(i, str)` method iterating over all timestamps in the time window.

Variable lists

The database access services provide a way to save *variable lists*, in order to make the querying of repeated series of the same variables easier and faster. Variable lists have to be created beforehand and saved under a user name. However, once created, they are fixed: they won't follow the evolution of the variables in the database.

The querying of variable lists is similar to the querying of separated variables, the differences being: the views (16), and the fact that each variable name has to be queried as well:

```
select variable_name from variable_list_variables_v
```

All lists had to be created by direct SQL access to the databases using `sqlplus`, and where filled using another module which is not described here.

A.3.2 Java access

The current way to access the Logging and Measurement databases is through the provided Java API. It provides an additional layer between the user and the databases, protecting them and dealing with all the security requirements. The Java API is originally designed to write applications in Java. In addition, it allows being called from the command line, thus being more portable: the data are not returned inside one specific application, they are written to the shell standard output.

The use of this command line is further described in (20).

Connection and security

The Java API provides all the opening and closing of connections, so the user does not have to deal with it. It also provides the user names and passwords for the Logging and Measurement databases.

Most of the connection configuration settings, including the client ID and application name, are written in a file called `configuration.properties` (20). A different name can be passed in the command line, allowing different pre-saved configurations. However, rather than having the user edit this file separately, this file is generated automatically. It allows a more advanced behaviour, and backward compatibility. For instance, if the user requires data from the Measurement database, but with a date

older than a week, the tool switches to Logging database automatically, instead of returning empty objects.

Data request methods —
Calling a command line from python

The command line API currently provides two methods to access data: `DS` (DataSet, all data in time range) and `LD` (Last Data during or before the given time range). The "data or last" view in SQL, that was returning all data in range if any, or the last data before range if not, is not implemented.

The time range is passed as two options, `-t1` and `-t2`, and the dates must have the format `"YYYY-MM-DD HH24:MI:SS"`. Dealing with the dates is done with the `Datime.py` module, which was written on purpose.

The standard way to access the data is via the `-O` option. The data are then written in the standard output of the shell. The default python `os` module provides the interaction with the shell from python. The `os.popen` function takes the command line as a string, which allows easy string manipulation. It returns a file iterator, which is the same type as the object return by the default function `open` opening files. The data flow is described in *fig. A.1.*

This object can then be iterated over line by line, since they are strings. The main limitation is the rather small memory limit (with respect to the amount of data considered here) of the Java heap: 250 Mb, which corresponds to only 15 mins of measurement data for the whole ring.

Passing variables is done with the `-VS` option followed by all variables separated by commas. There is apparently no limitation on the number of variables: all BLMs in the LHC can be queried at once. The only limitation is the total size of the data set.

The Java command line API provides an extra functionality: it allows to write the data directly in a file. The filename is passed with the `-N` option, and the type with the `-F` option.

The command line has the ability to cut a dataset into subsets, in order to allow the downloading of amounts of data bigger than the memory limit. This is done using the `-IT` (Interval Type) option, together with the `-NI` (Number of Intervals) option. For instance, passing "`-NI 15 -IT MINUTE`" will cut the dataset in slices of 15 minutes.

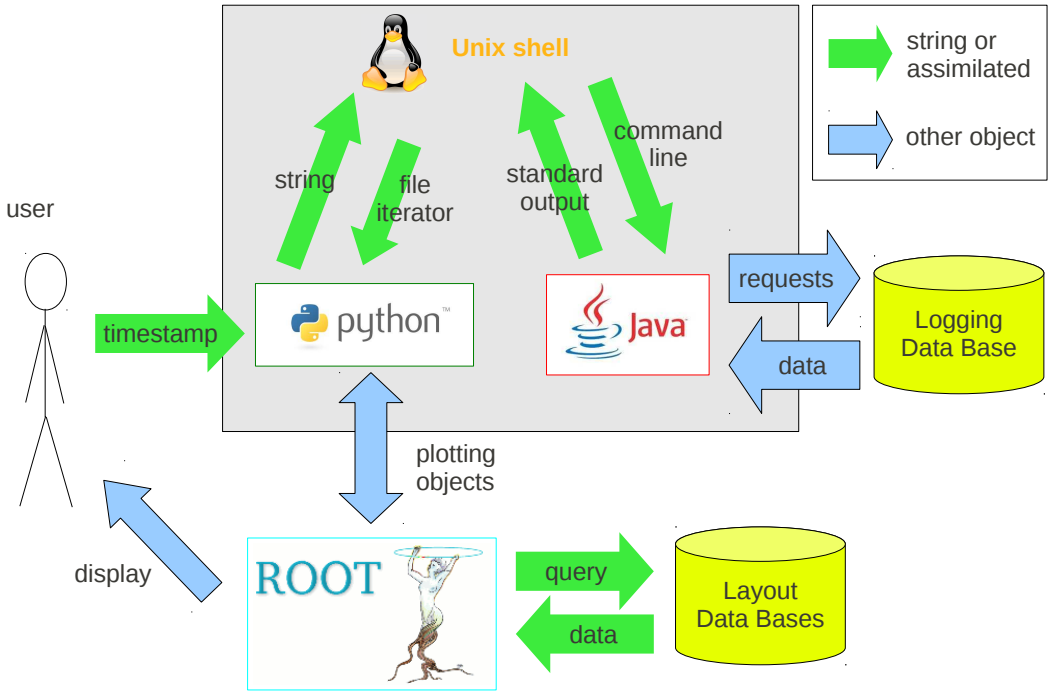

Figure A.1: Data flow in the toolbox, from the user to the databases and back. A timestamp is passed to the python object, which can start the java command line application and request logging and measurement data. The data are returned through the same application. The layout data access and the plotting are done with ROOT objects.

A.3.3 Structure of the returned object

In this tool, different objects were created with structures matching their purpose.

Logging / Measurement databases

Since not all variables are logged at the same timestamp *(cf. § A.2.3)*, the choice was made to associate each value with its timestamp, as it is already done in the database. Timestamps are written as *strings* with the correct format, and values are usually *floats*. The python float type is automatically converted into a C++ float (or ROOT `Float_t`) thanks to the PyROOT project.

The basic structure for one variable is then a *list* of *2-tuples*. Tuples are immutable ordered iterable objects, and are represented by elements between parentheses "( )" separated by commas. Once the tuple is created, it can not be modified. *Lists* are mutable ordered iterables, represented by elements between square brackets "[ ]" and

$$\left\{ \begin{array}{cccc} \texttt{'BLM\_1'} & \texttt{'BLM\_2'} & \cdots & \texttt{'BLM\_m'} \\ \begin{bmatrix} (\text{'t'}, v) \\ (\text{'t'}, v) \\ \vdots \\ (\text{'t'}, v) \end{bmatrix} & \begin{bmatrix} (\text{'t'}, v) \\ (\text{'t'}, v) \\ \vdots \\ (\text{'t'}, v) \end{bmatrix} & \cdots & \begin{bmatrix} (\text{'t'}, v) \\ (\text{'t'}, v) \\ \vdots \\ (\text{'t'}, v) \end{bmatrix} \end{array} \right\}$$

Figure A.2: Global structure of the signal dictionary. 'BLM_m' is the expert name of a BLM (string), 't' is a timestamp (string), v is the signal of the BLM at that timestamp. Note that the lengths of the lists (in square brackets) can be different, and that the timestamp are all different.

$$\left\{ \begin{array}{cccc} \texttt{'BLM\_1'} & \texttt{'BLM\_2'} & \cdots & \texttt{'BLM\_m'} \\ \begin{bmatrix} \\ (\text{'}t_1\text{'}, v_1) \\ \\ (\text{'}t_2\text{'}, v_2) \\ \end{bmatrix} & \begin{bmatrix} (\text{'}t_3\text{'}, v_3) \\ \\ (\text{'}t_4\text{'}, v_4) \\ \\ (\text{'}t_5\text{'}, v_5) \end{bmatrix} & \cdots & \begin{bmatrix} \\ (\text{'}t_6\text{'}, v_6) \\ \\ (\text{'}t_7\text{'}, v_7) \\ \\ \end{bmatrix} \end{array} \right\}$$

Figure A.3: Structure of the signal dictionary for the Logging database. The vertical spaces between 2-tuples indicate the lack of data between two timestamp and show that all timestamp are different.

separated by commas. Lists can be modified: a new element can be *appended* to the list.

In order to associate the list of values to the name of the variable, a mapping is done thanks to a *dictionary* object. Dictionaries are non-ordered mutable iterable, where the elements, called *values*, are referred to by a *key* instead of an index (as it would be the case in a list). This way, the variable name (the key) can be associated easily with the tuple list (the value). Dictionaries are represented in curly brackets "{ }".

This way, no information is repeated: in the case of logging data, the size of the object is minimal, and reflects the database structure *(cf. fig. A.2, A.3)*. In the case of Measurement database, where variables have values every second, this structure is not optimal: the timestamps are repeated since they are the same for each value *(cf. fig. A.4)*. A more size–efficient structure could have been created, by recording the

$$\left\{ \begin{array}{cccc} \texttt{'BLM\_1'} & \texttt{'BLM\_2'} & \cdots & \texttt{'BLM\_m'} \\ \begin{bmatrix} (\text{`}t_1\text{'}, v) \\ (\text{`}t_2\text{'}, v) \\ \vdots \\ (\text{`}t_n\text{'}, v) \end{bmatrix} & \begin{bmatrix} (\text{`}t_1\text{'}, v) \\ (\text{`}t_2\text{'}, v) \\ \vdots \\ (\text{`}t_n\text{'}, v) \end{bmatrix} & \cdots & \begin{bmatrix} (\text{`}t_1\text{'}, v) \\ (\text{`}t_2\text{'}, v) \\ \vdots \\ (\text{`}t_n\text{'}, v) \end{bmatrix} \end{array} \right\}$$

Figure A.4: Structure of the signal dictionary for the Measurement database. Note that all timestamps in each "line" are the same; all values are different.

timestamps separately, but it would have implied a different processing of measurement and logging data. The choice was made to keep the same structure for both databases.

This object is referred to as *signal dictionary (cf. fig. A.2, fig. A.3)*.

The non-ordering of dictionaries is part of the characteristics of the object, and done on purpose by a randomization of the keys to insure that one is never in the worst case (in an algorithmic efficiency point of view) when accessing elements. However, the list of keys can be ordered.

Layout databases

In the case of layout databases, several columns can be queried at once. In this case, the `get_from_layout` method returns a dictionary with one key per column, associated to a list of the values returned by the database *(cf. § A.3.1)*. The fact that all lists have the same length is insured by the structure of the database. The structure of the object reflects the structure of the database.

This structure is general but not the most adapted to all situation. New and more adapted objects are created later. For instance, in the case of magnets, three variables are required: the magnet name, the magnet start and the magnet end. The reconstructed object is a dictionary where the key is the magnet expert name and the value is the 2-tuple (start, end).

A.4 Display

In this section, the different objects in the `display` module are described. This objects are made to take the objects returned by other functions and classes in other modules.

A.4.1 Plotting with ROOT

When the modules were developed, the best option to produce plots and graphs was to use ROOT objects. ROOT provides graphical objects that are straightforward to use in a global scope, i.e. in a ROOT script interpreted by CINT or in the python interpreter; however, using them in functions and classes requires more care.

The main object for scatter plots is called `TGraph` (21). The latest versions of ROOT do not require to know the number of points beforehand any more; the points can be set on the fly. The object corresponding to the window on the screen is called `TCanvas`. Both the `TGraph` and `TCanvas` object must exist in the current scope for the graph to be seen.

The `TGraph::Draw()` method will automatically create a TCanvas if no one has been created before. However, this specific TCanvas is not returned: if this method is called in any other scope than the global one, the TCanvas will consequently be deleted when exiting the current scope. Moreover, if another TCanvas was created before, and held a different graph, its graph will be replaced.

If the TCanvas is returned, but not the TGraph, the graph will be deleted when exiting the scope, thus disappearing from the TCanvas, leaving and empty window.

The correct way to proceed is to first create a TCanvas, then draw the TGraph on it, and return or save both. This way, they stay visible for the user as long as the code is running. The choice was made to store them as attributes of the different plotting classes. This way, the user can have several instances of the class achieving the same type of display.

A.4.2 Signal vs. time

Reflecting the data structure — multigraphs

The first plot (and most related to the database structure) is the display of all data versus time. It is created from the *signal* dictionary *(cf. § A.3.3)*. One TGraph object is associated to each variable.

For each 2-tuple of the list associated to each variable, a `Datime.datime` object is created, corresponding to the current timestamp. This object has a `Convert()` method that returns the number of seconds since *epoch* at that time. This is used as the X coordinate, the Y coordinate being the second element of the 2-tuple. The axes of the

TGraph have a `TAxis::SetTimeDisplay()` method that will convert this number back into human-readable time and date.

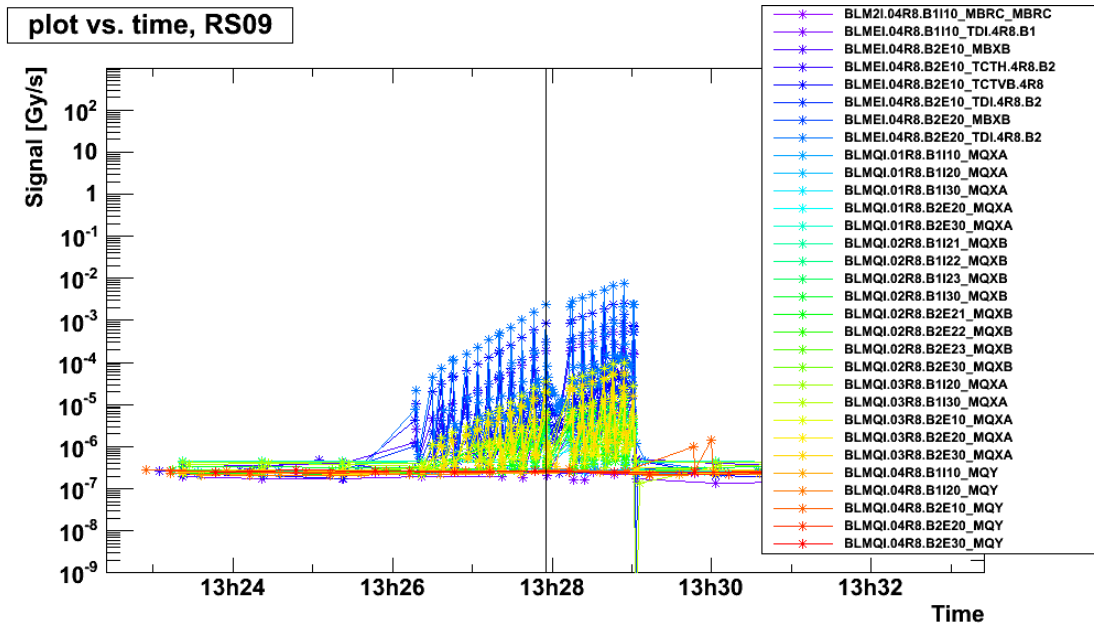

Figure A.5: Example of "plot_time" object: signal of BLMs versus time. One graph and one colour is associated to each BLM. The X axis displays date and time in human-readable format. The BLMs are ordered in the legend, and in colours. One specific timestamp can be indicated on the plot by a vertical line; the requested timestamp is displayed by default.

All the TGraphs are stored in an attribute of the object: a dictionary called *graph-dict*, where the key are the variables, and the values are the TGraphs. All TGraphs are gathered in a `TMultiGraph` object. Each TGraph gets a specific colour as different from the others as possible. All this and the creation of the `TLegend` is done by the `display.rainbowplot` function.

Rainbow plots

In ROOT, colours are coded as integers. The first integers (0-9) give a range of basic colours, but higher values (51-100, 200-228) give a smoother colour range. In order that all graphs have colours as different to each other as possible, the colour range is divided into $n-1$ ranges of equal lengths, where n is the number of graphs. For instance, if there are 3 graphs, the first graph gets the first colour of the range, the second gets

the colour of the middle of the range, and the third gets the last colour. Graphs can be ordered for clarity: in this case, an ordered list of names has to be passed.

The legend is created at the same time, its length depending on the number of graphs. If there is only one graph, the colour is black.

A.4.3 Plotting the LHC

One of the current main application of the toolbox is a longitudinal loss profile of a section of the LHC at a requested timestamp. This needs the position of the magnets and collimators, obtained from the Layout database. The signal of the BLMs is mapped to their longitudinal position in the LHC, called *DCUM*, which are obtained from the same database. The results are shown in *fig. A.7*.

Format of the "plot_LHC" data

The format of the data taken by this plot is the following: the basic 2-tuple (couple) of values is: (DCUM, value of the loss at the displayed timestamp). The names of the BLMs are not displayed, but they contain all relevant information: type of monitor (*Ionisation Chamber (IC)* or *Secondary Emission Monitor (SEM)*), associated beam (B1 or B2), injection or extraction line. The sorting of the monitors according to these criteria will be described in *§ A.5.2*.

The structure of the data object, called *plotdict (cf. fig. A.6)*, reflects this sorting: to each graph name is associated a list of 2-tuples: (DCUM of the monitor, signal of the monitor at the plotting time). The creation of this object is done in the `process` module *(cf. § A.5.2)*.

$$\left\{ \begin{array}{lll} \texttt{'name\_of\_graph\_1'}, & \texttt{'name\_of\_graph\_2'}, & \cdots \\ \begin{bmatrix} (dcum_1, v_1) \\ (dcum_2, v_2) \\ \vdots \end{bmatrix}, & \begin{bmatrix} (dcum_3, v_3) \\ (dcum_4, v_4) \\ \vdots \end{bmatrix}, & \cdots \end{array} \right\}$$

Figure A.6: Global structure of "plotdict" object. $dcum_1$ is the position of BLM_1, and v_1 the signal of BLM_1 at the plotting time.

Because of the very wide dynamic range of the BLMs (10^6), the signal (Y axis) is nearly always displayed in logarithmic scale. However, for some reason, this is a method

of the `TCanvas` object and not of the `TAxis`, regardless if the canvas holds a graph or not. The canvas being stored as an attribute, this method can still be accessed.

The plotting time is an important value that is displayed in the title of the plot.

The thresholds can be displayed on the same plot. They have the same structure, and will be plotted on the same scale, with the same X coordinate (DCUM) of the BLM they correspond to, in a different colour (green).

The colours of these graphs follow the plotting convention of the LHC: graphs related to beam 1 are plotted in shades of blue, and those related to beam 2 in shades of red. The `plot_LHC._set_graphs_with_conventional_colours` method holds all the mapping of the different graph names to the correct colour.

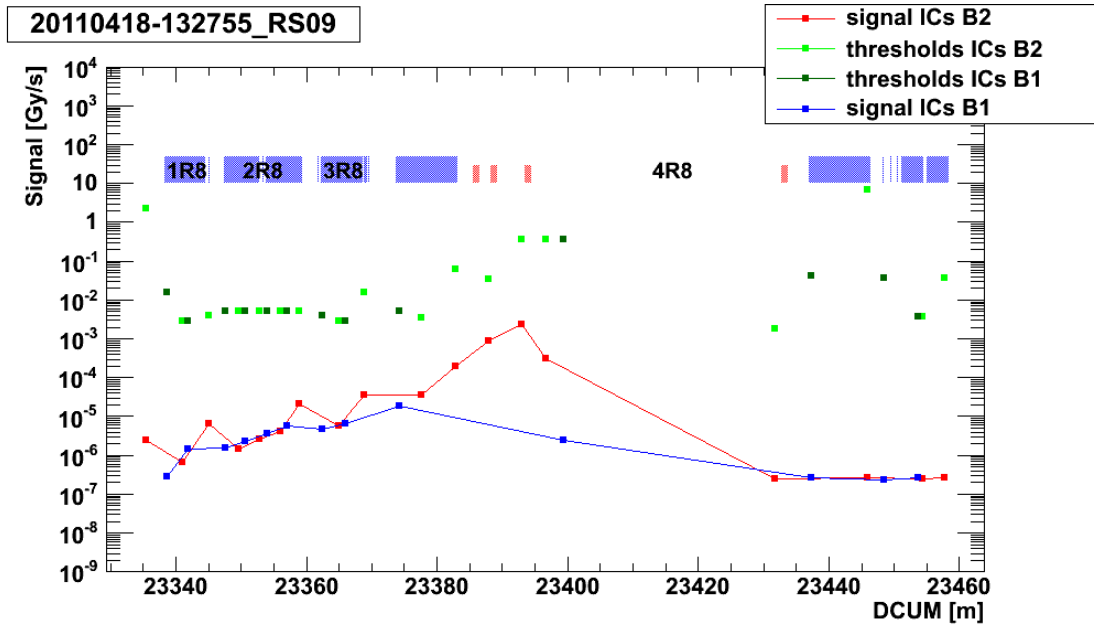

Figure A.7: Example of "plot_LHC" object: longitudinal loss at one timestamp (given in the title). The X coordinate gives the longitudinal position of one BLM; the Y coordinate gives the value of the signal or threshold of this BLM. The plot is only made of four graphs: two for the BLM signals and two for the thresholds. The magnets are displayed as blue boxes, the collimators as red ones. The plotting time and the running sum are displayed in the title.

In addition, the object must have the position of all collimators in DCUM range, and the positions and lengths of all magnets in range. They can be passed in the constructor; if not, the object has the possibility to create a `databases.ConnectionToLayout` object

(cf. § A.3.1) that will get the details of all collimators and magnets in the DCUM range.

Display of the magnets and collimators

Magnets and collimators are displayed on the graph using the ROOT `TBox` objects. The constructor takes the coordinates of top left an bottom right corners, and these coordinates can be expressed in the same range as the coordinates of the graphs: the TBoxes will then follow the zooming in and out in the plot. Magnets are plotted with their real lengths, since it provided in the database, whereas collimators just have one position recorded in database. They are all plotted with an arbitrary length of 1 m, which is close to reality. Magnets are displayed in blue, and collimator as smaller red boxes.

The Y coordinate of magnets and collimators can be specified so they are conveniently displayed whatever the scale of the plot is. By default for LHC losses, the boxes are arbitrarily displayed between 10 and 50 Gy/s.

Display of the cell names

Another information to display would be the cell name. It tells which half-octant of the LHC is considered, and the number of the cell in this half octant. A cell is the basic pattern which is repeated in the arcs to create the whole ring: that is, three dipoles and a quadrupole. The ROOT object to display text, the `TPaveText`, can be created the same way as a TBox, following the plot coordinates; however, once created, it will not follow the zooming in and out of the plot. It can only be seen when a small portion of the LHC is requested: the cell names are only displayed if the displayed section corresponds to less than 30 cells.

A.4.4 XY plots

The `display` modules provides a class creating a scatter plot, with the same conventions, attributes and method as the other plots. The data as passed in a `plotdict` dictionary, where the key is the name of the plots and the value is a list of 2-tuples, each 2-tuple being the coordinate of one point.

$$\left\{\begin{array}{lll} \texttt{`name\_of\_plot\_1'}, & \texttt{`name\_of\_plot\_2'}, & \cdots \\ \begin{bmatrix} \text{RS01} \\ \text{RS02} \\ \vdots \\ \text{RS12} \end{bmatrix} & \begin{bmatrix} \text{RS01} \\ \text{RS02} \\ \vdots \\ \text{RS12} \end{bmatrix} & \cdots \end{array}\right\}$$

Figure A.8: Global structure of the running sums dictionary. RS01, ..., RS12 are the values of the twelve running sums; usually, a plot will display all running sums for one monitor, or the thresholds of a family of monitors.

A.4.5 Plotting Running Sums

The display in one graph of all the running sums of the same monitor versus the corresponding integration duration is a recurrent requirement. A class has been specifically designed to fulfill this requirement.

Format of the RS data

The duration of each running sum is a fundamental value of the BLM system *(cf. § A.2.1)*. These values are hard-coded in a list, which is a global variable for the module and can be accessed all the time. The number of the running sum is coded by its position in the list. For human-readability purposes, the indexing of the running sums starts at 1, matching their names (the first element of the list is zero).

The structure of the data object is a dictionary, where the key is the name of the graph, and the value is the list of values for each running sum, coded by position.

Conventions for plotting

The conventions for plotting running sums are the following: the duration is represented on the X axis in logarithmic scale; the dose per second is represented on the Y axis in logarithmic scale. The 12 dots are linked by a line.

This way, a flat line represents a constant dose per second deposited in the ionisation chambers, while the loss is occurring; a line of slope -1 shows that all the dose was deposited, and that the same deposited dose is being integrated over longer and longer integration windows.

A.4.6 Methods shared by all plots

All plots inherit from the same class, called `superclass_plot`. This class has several methods.

Title & plotting time

The smallest piece of information to describe a loss is its timestamp: it is unique for each loss. It is thus displayed in the title. The `Datime.datime` object provides different formats to print a timestamp, one of them being called the "short" format: `YYYYMMDD-HHMMSS` (returned by the `datime.print_short` method). This format is used in the title. If no title is specified, one is automatically created, being the short format of the plotting time. The user has the possibility to add more details about the loss: the type of loss, the section of the LHC that is displayed, or anything passed as a string in the argument called `additional`.

Saving

All plots come with a `save` method, in order to make the saving of plots easy for the user. This method will automatically generate a meaningful file name, matching the title of the plot, and save it in the `~\public` folder.

In the simplest of cases, the method `myplot.save()` can just be called and the plot will be saved just as it is seen on screen, with a unique and relevant name. An additional string and a saving path can be specified.

A.5 The wrapping module: analysis

In order to avoid having to create many different objects, call many different methods and use different attributes, and wrapping class has been created called `analyse`, in the `analysis` module. It creates automatically all the different connection objects, gets the relevant data in the correct format, passes the data objects to the plot objects, and holds the resulting plots as attributes. All these attributes are described in *tab. A.1.*

A.5.1 Basic behaviour

Introduction: list of arguments

The basic behaviour of the `analyse` class is to display the longitudinal development of one loss appearing at one timestamp in a section of the LHC, getting the data from the Logging database *(cf. § A.2.3)*. The constructor needs to take at least one argument: the time of the loss, called *plotting time*. The time range for data download is centered around that time.

A specific section of the LHC can be specified by passing two values of DCUM. Only the data concerning the BLMs, magnets and collimators within this DCUM range will be downloaded. The number of the running sum can be specified, as well as *flags* (boolean values that are only *true* or *false*) controlling the inclusion of thresholds or SEMs.

All the actions described in this section are performed automatically.

Creation of the list of BLMs

When plotting only a section of the LHC, there is no point requiring all monitors in the ring, as it is a time-consuming operation. Only the monitors within the specified DCUM range are required. The choice was made that the user only passes the DCUM range as an extra argument; if no range is passed, the default value of the arguments selects all BLMs.

At the beginning of the run of the LHC, the list of BLMs details in the databases was updated regularly. The choice was made to not have the list of BLMs written in a file, but to generate it from the database once per day. This list (ordered by DCUM) is downloaded from one of the layout databases called MTF. If no list was created that day, the tool creates the list and saves it in a temporary file holding the date. If the file already exists and has the correct date, the tool reads the data from the file. The list is not generated every time for speed reasons.

Once the list is generated, the names of the BLMs in the DCUM range are selected and stored as an attribute.

Data query

Once the list of BLMs is created, a connection object is created *(cf. § A.1.2)*. The default is a connection to the Logging database, but the user can ask to connect to the Measurement database. The data are queried with the current time window, the current list of BLM, and the given running sum value. The returned object is called "signal" dictionary. The structure of the signal dictionary is described in *fig. A.2*. The next step is to extract the signal of the chambers at the required time.

Getting the exact second — Case of the Logging database

Once the data are downloaded, the losses as the specified time must be extracted. This extraction is achieved by the `process` module. The corresponding algorithms are described in *§ A.5.2*.

Preparation of the data for plotting versus DCUM

Plotting all BLM signals together versus BLM position would not display relevant information. The BLMs have to be separated depending on their type: if they are ionisation chambers or second emission monitors, if they belong to beam 1 or beam 2, or if they belong to the dump line or not. The corresponding thresholds are sorted accordingly. The sorting is done in the `process` module. The structure of the "plotdict" object is described in *fig. A.6*.

Plotting

Once all the data are gathered and put in the proper formats, they are displayed on screen.

The `analyse.Signal` object *(cf. fig. A.2)* is passed to a `display.plot_time` object *(cf. § A.4.2)*, and the result is stored in the attribute `analyse.TimePlot`.

The `plotdict` object *(cf. fig. A.6)* is passed to an object of type `display.plot_LHC` *(cf. § A.4.3)* and stored in the attribute `analyse.LHCPlot`.

The plotting can be disabled for speed purposes by passing a the default argument `PlotOut` as `False`.

A.5.2 Process

Most of the data processing required in order to display a loss in a section of the LHC is done in the `process` module: finding the value of the loss at the plotting time, creating the "plotdict" object holding the data *(cf. fig. A.6)* and sorting the BLMs by type.

Weighted averages

As explained in *§ A.2.3*, BLMs don't have data logged every second in the Logging database. If a big loss (bigger than the set delta) occurred at the time of plotting, data will be recorded for this specific second; but if no loss appeared on some BLMs, only one data per minute is recorded. In case of no loss, the choice was made to use a linear interpolation between the previous and the next recorded values. This makes sense because the fact that no data was recorded is a proof that the signal did not change more than the delta. The difference between the real signal and the recalculated signal is within the fluctuations of the signal, thanks to the tuning of this delta.

The choice of the algorithm finding data at a timestamp in a list of tuples or calculating the linear interpolation is very crucial, as it is heavily used in certain analyses looping many times over the same dataset.

Linear interpolation. The first algorithm was one that can be used both on measurement and logging data. It takes the reference timestamp, a list of tuples, and progresses through the list. If the same timestamp is found, the value (second element of the tuple) is returned. If not, the next (and newer) timestamp is taken, and the linear interpolated is calculated, following:

$$v_{req} = \frac{v_2 - v_1}{t_2 - t_1} \cdot t_{req} + \frac{t_2 \cdot v_1 - t_1 \cdot v_2}{t_2 - t1}$$

where t_{req} is the reference time; v_{req} is the value at t_{req}; (t_1, v_1) are the timestamp and value of the point (tuple) before t_{ref}; (t_2, v_2) are the timestamp and value of the point (tuple) after t_{req}.

The result returned is the maximum between the signal and a non-zero value (usually set at 10^{-9}, lower than the lower possible signal) in order to avoid zero values, which can not be displayed in logarithmic scale. All results are gathered in a *One Value Dictionary (OVD)*, where keys are BLM names and values is the calculated signal at the plotting time.

Speed. The speed of this algorithm is roughly $O(m \cdot n)$, where m is the number of monitors (the algorithm has to loop over monitors) and n is the index of the second (the algorithm has to go through all tuples from the beginning till the tuple holding the proper timestamp). For speed reasons, the algorithm does not go through all seconds every time: when the next timestamp has been found, the looping stops.

The processing time is dominated by the data access time in the case of the Logging database, when only one second is requested in a time range composed of a few tuples. Very big time windows are rarely requested. However, during statistical analysis, when all seconds are considered, the running time diverges when reaching the last seconds of the dataset.

Different consideration of Measurement database. Searching for a specific second doesn't make sense for the Measurement database: when no data management error appears, all seconds are in the dataset. Using the previous algorithm, the number of operations would become $m \times \frac{N \cdot (N+1)}{2}$ where N is the total number of tuples (seconds) in the requested time range: the processing time would dominate the access time. Moreover, all lists of tuples have the same length. Thus, only one index is enough to represent one second of data for all BLMs: the index of the 2-tuple holding the reference time.

The algorithm can then be highly simplified, by going only once through all seconds from the beginning of the time range until the tuple holding the proper timestamp is found, and then just keeping its index. In this case, the speed of the algorithm becomes $O(m)$.

Improved algorithm for Logging database. Looping over all seconds from the beginning of the time range must be avoided when looping several times over the same dataset. In this purpose, the index of the tuple holding the last timestamp before reference time can be saved for each monitor. This requires the creation of a new object mapping the name of the BLMs to the corresponding index. In this case, the algorithm must only check that the timestamp at the index is before the reference time, and that the next tuple is after the reference time.

The algorithm has to go through all BLMs two times, and its speed is $O(2m)$.

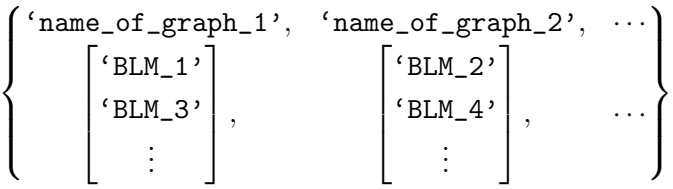

Figure A.9: Global structure of "checkdict" object. The name of the graph describes the criteria validated by the BLMs in the list, e.g. "Ionisation chambers for beam 1"; and the value is a list of BLM expert names validating the criteria. Note that all BLMs of one list are different from the BLMs of the other lists: a monitor can only appear in one list.

Sorting of the BLMs

The BLMs have to be separated depending on the following criteria: if they are ionisation chambers or second emission monitors, if they belong to beam 1 or beam 2, or if they belong to the dump line or not. All these details are coded in the BLM expert name. The logical progression for one criterion is the following:

- if the criterion is not considered:
  - take all BLMs regardless of their type for this criterion;
- if the criterion has to be considered:
  - create two separated list for the two possibilities (criterion is true or false);
  - check if BLM verifies criterion:
    - if yes, add it to one list;
    - if no, add it to the other.

It must be repeated for each criterion, conserving the previous results. The validation of the criteria is done by an object called `type_check`.

All results are stored in the `checkdict` attribute of the process object: a dictionary where the key is the name of the type of BLMs (name of the graph, e.g.: "Ionisation chambers for beam 1"), and the value is a list of BLM expert names *(cf. fig. A.9)*.

Creation of the "plotdict" object

The "plotdict" object is created from the "checkdict" object, the "OneValueDict" object, and the list of the position (DCUM) of each BLM. For each graph name in checkdict is associated a list of 2-tuples. Each 2-tuple is (DCUM of BLM, signal of BLM at plotting time) where the BLMs names are in the list associated to the graph name in "checkdict", and the value comes from the "OneValueDict" object.

This object can be passed to a `display.plot_LHC` object *(cf. § A.4.3)*, which is saved as an attribute. This is done automatically by the wrapping module.

A.5.3 Advanced functionalities

The "analyse" object has more than the basic functionalities. In order to help the studying of beam losses, it can display the loss thresholds. It can also access and display other beam instruments.

Thresholds

The display of thresholds can be enabled by passing the default argument `thresholds` in the object constructor as `True`. In this case, the value of the last threshold of each BLM at the time of plotting will be downloaded from the database and stored as an attribute *(cf. tab. A.3)*

When required, the thresholds are automatically added to the LHC plot *(cf. § A.4.3 and fig. A.7)*. This shows how close each monitor is to its corresponding threshold.

Ratio Signal / Threshold

The display of the value of the threshold may not be enough to find easily the position of a loss. The most relevant information is often "which monitor is closest (or above) threshold". It can be easily retrieved by calculating the ratio signal over thresholds for each monitor. Any ratio above 1 means that the monitor sent a dump request.

It is requested by calling the `ratio_signal_threshold` method. The result of all ratios is stored in the `OneRatioDict` attribute, and is displayed by a `display.plot_LHC` object stored as the `RatioPlot` attribute.

Once the ratio was calculated, the results can be printed on terminal and written in a file. The monitors are sorted by closeness to threshold, and the longitudinal position

Type	Name of attribute	Description
single values	`a.DB`	Name of the selected database.
	`a.dcum1`	Starting position (DCUM) of the displayed LHC section (default is 0).
	`a.dcum2`	End position (DCUM) of the displayed LHC section (default is 27000).
	`a.PloTime`	Current plotting time: the only necessary argument.
	`a.RSnum`	Number of the selected running sum (default is 1).
	`a.plus_minus_x_mins`	Width of time window, in minutes (default is 3).
	`a._Thresholds_BackInTime`	Number of minutes to go back in time to be sure to find at least one value for the thresholds (default is $-1500 =$ 25 hrs)
iterable	`a.BLMs`	List of all BLM in the selected LHC section, in DCUM order.
	`a.Collimators`	Collimator names and positions (DCUM) in the selected LHC section.
	`a.Magnets`	Name, start and end positions (DCUM) of the magnets in the selected LHC section.
	`a.Signal`	Signal of all BLMs at the selected time range in the selected LHC section.
booleans	`a.Dump_flag`	`True` if the BLMs of the dump line are required (default `False`).
	`a.ICs_flag`	`True` (default) if ionisation chambers are to be displayed.
	`a.PlotOut`	`True` (default) if plots are to be displayed on screen.
	`a.SEMs_flag`	`True` if Second Ionisation Monitors are to be displayed (default `False`).
	`a._TwoBeams_flag`	`True` (default) if the two beams must be separated.
objects	`a.LHCPlot`	*cf. A.4.3.*
	`a.Processor`	*cf. A.5.2.*
	`a.TimePlot`	*cf. A.4.2.*

Table A.1: Description of the basic attributes of the "analyse" object. All these attributes are automatically created when creating the object.

(DCUM) is also given. It is done by calling the `get_monitors _close_to_threshold` method.

Intensity

The value of a loss depends on the intensity in the ring. The value of the intensity (in number of protons) at the plotting time must be taken into account as a normalization factor when studying losses happening in similar conditions.

The `plot_intensity` method will access all *Beam Current Transformers (BCT)* in the ring and display their reading, store the data in the `IntDict` attribute, and display them with the `IntPlot` attribute, which is an object of type `display.plot_time` *(cf. fig. A.10)*.

The reading of the BCT is different depending on their type: if they are fast BCTs, direct current BCTs or injection line BCTs. When calling the `get_intensity` method, `plot_intensity` is called, and the different readings at the plotting time are printed on terminal; however, the choice of the correct value is left to the user. Note that this stops the running of the code: it waits for the answer of the user.

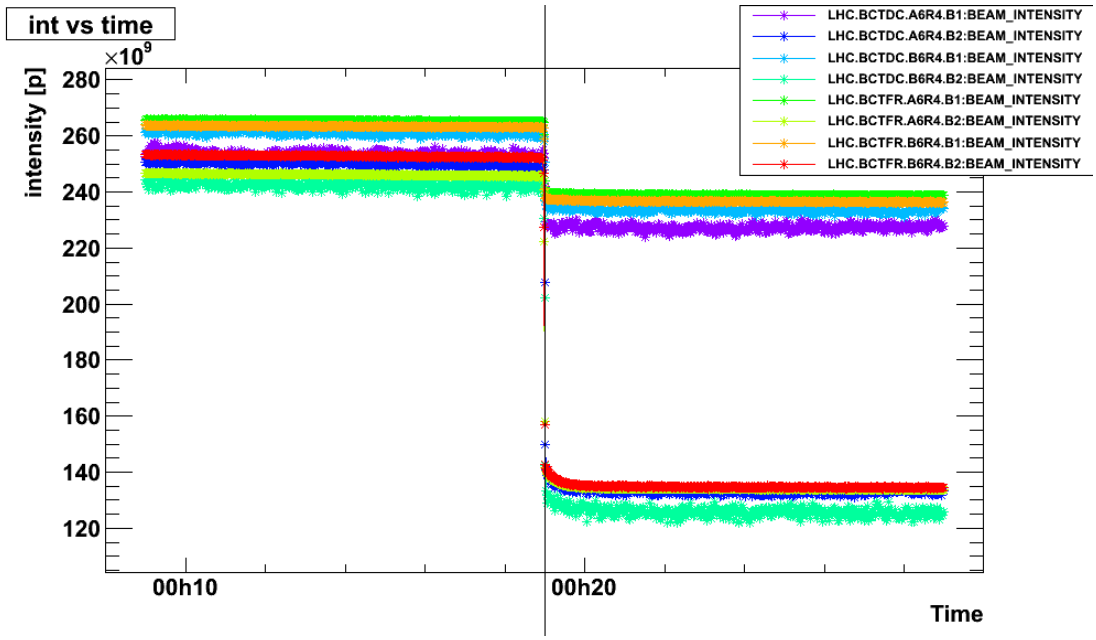

Figure A.10: Example of the plot of intensity versus time during sudden loss mainly in beam 2. The vertical black line indicates the time at which values are given on terminal. Note that the BCTs have different value and different dispersion according to their type.

The tool provides another functionality in the `normalise_to_intensity` method. In addition to calling the two precedent methods, it expresses the closeness to threshold of each monitors in number of extra protons in the beam that would have made the signal reach the threshold. This is done by dividing the calculated intensity by the ratio signal / threshold. This can be seen as a security margin: for instance, if the ratio is $\frac{1}{2}$, there is enough margin for a total of twice the current number of protons. If the ratio is $\frac{2}{3}$, there is only margin for an extra half of the number of protons in the ring. Once calculated, these values are written in a file.

Position of collimator jaws

The collimators are some of the elements of the LHC that can create the biggest losses during normal operation. Knowing the position of their jaws can explain losses around them. The `collimators_vs_time` method creates the list of variables corresponding to the jaws of the collimators in the DCUM range; then, it creates a connection object and requires the data. The data are stored in the `ColPos` attribute, and displayed in the `ColPlot` attribute *(cf. fig. A.11)*, which is a `display.plot_time` object.

Beam Position Monitors (BPMs)

The position of the beam itself, linked with the value of the aperture, can be a reason for a loss. The BPMs are separated into two types, depending on the plane in which they measure the position of the beam: vertical or horizontal.

The display of the signal of the BPMs requires a similar process to the BLMs one. The main difference is that the BPM can't be required independently: all values except two are stored in one vector, in the *vectornumeric* format. The two extra BPM are situated in the dump line and must be ignored. There is only one dataset every ten seconds. The mapping of the value with the name and the position has to be done after the data query.

Like the BLM data, the BPM data are first stored and displayed against time by the `plot_BPMs_vs_time` method; then, a `process` object is created to display the values versus position (DCUM) by a method called `plot_BPMs`. All data and plots are stored as attributes *(cf. tab. A.3)*.

Name of method	Description
a.collimators_vs_time	plots the position of the jaws of the collimators in the considered LHC section versus time.
a.get_intensity	returns the readings of all BCTs during the time range.
a.get_monitors_close_to_threshold	takes an integer n, and returns the n BLMs closest to their corresponding threshold, ordered accordingly.
a.get_thresholds	returns the dictionary of the thresholds of all considered BLMs at the timestamp.
a.load	takes a filename corresponding to the result of the `save` method, and loads it.
a.normalise_to_higher	finds the BLM with highest signal and calculates, for each BLMs, its signal normalised to the highest one. The results are plotted in a `display.plot_LHC` object and written in a text file.
a.normalise_to_intensity	creates lists of monitors, sorted by different criteria. See text.
a.plot_BPMs	creates a longitudinal plot of the reading of the BPMs at a timestamp.
a.plot_BPMs_vs_time	plots the readings in the time range of all BPMs.
a.plot_LHC	displays the longitudinal loss at the given timestamp, or at PloTime if no timestamp is passed.
a.plot_all_RS	takes a list of BLM names, gets the signals in all running sums, and plots them in a `display.plot_RS` object.
a.plot_aperture	plots the values of the aperture of the beam pipe (from a file) for considered section of the LHC.
a.plot_dcum	plots a vertical line at a given DCUM on a given `LHC_plot` object.
a.plot_intensity	plots the readings of all BCTs during the time range.
a.plot_optics	produces longitudinal plots of the beta function, the alpha function and the dispersion for the considered LHC range.
a.plot_vs_time	takes a time (in the time range) and calculates and plots the longitudinal loss at this time.
a.print_elements	prints in terminal the name of all BLMs, collimators and magnets
a.ratio_signal_threshold	calculates the ratio between the signal and the threshold of every monitor, and displays it in a separated `plot_LHC` object.
a.remove_absent_entries	takes to iterables, and remove the entries of the first iterable that are not in the second one.
a.remove_empty_entries	removes variable names with no entries (empty lists) from any signal dictionary.
a.run	"buffer" methods allowing different constructor behaviours, and data loading.
a.save	creates a file holding all attributes containing data. The entire object can be created from this file without accessing databases.
a.sort_by_type	executes the sorting by type of the BLM provided by the `process` module.

Table A.2: Description of the methods of the "analyse" object. Note that, when running interactively, the "help" function can be called on every method, giving the list of arguments and a little explanation text.

Type	Attribute	Type	Description
single value	`a.Intensity`	float	– Overall number of protons in the ring.
iterables	`a.Alpha`	PlotDict	– Values of the α function at each corrector.
	`a.Aperture`		– Values of aperture at every point of the LHC, assuming that all aperture changes correspond only to steps in the transversal plane (no slopes).
	`a.Beta`		– Values of the β function at each corrector.
	`a.Disp`		– Values of the dispersion at each corrector.
	`a.ColPos`	Signal dict.	– Positions of both jaws of the selected collimators versus time.
	`a.BPMH`		– Readings of the vertical BPMs versus time.
	`a.BPMV`		– Readings of the horizontal BPMs versus time.
	`a.IntDict`		– Readings of all BCTs versus time.
	`a.Thresholds`	OneValueDict	– Value of the threshold of each BLM.
	`a.OneRatioDict`		– Value of the signal-over-threshold ratio of each BLM.
objects	`a.AlphaPlot`	TimePlot	– Display of the values of the α function versus time.
	`a.BetaPlot`		– Display of the values of the β function versus time *(cf. fig. A.13)*.
	`a.DisPlot`		– Display of the values of dispersion versus time.
	`a.Colplot`		– Display of position of the collimator jaws versus time *(cf. fig. A.11)*.
	`a.IntPlot`		– Display of the readings of the BCTs versus time *(cf. fig. A.10)*.
	`a.BPMTimePlotH`		– Display of the readings of the horizontal BPMs versus time.
	`a.BPMTimePlotV`		– Display of the readings of the vertical BPMs versus time.
	`a.BPMPlot`	LHC Plot	– Longitudinal plot of the positions and readings of the BPMs.
	`a.AperturePlot`		– Longitudinal plot of the aperture restrictions in the LHC.
	`a.RatioPlot`		– Longitudinal plot of the position and the signal-over-threshold ratio of each BLM.

Table A.3: Description of the advanced attributes of the "analyse" object. All these attributes are only created when calling related methods.

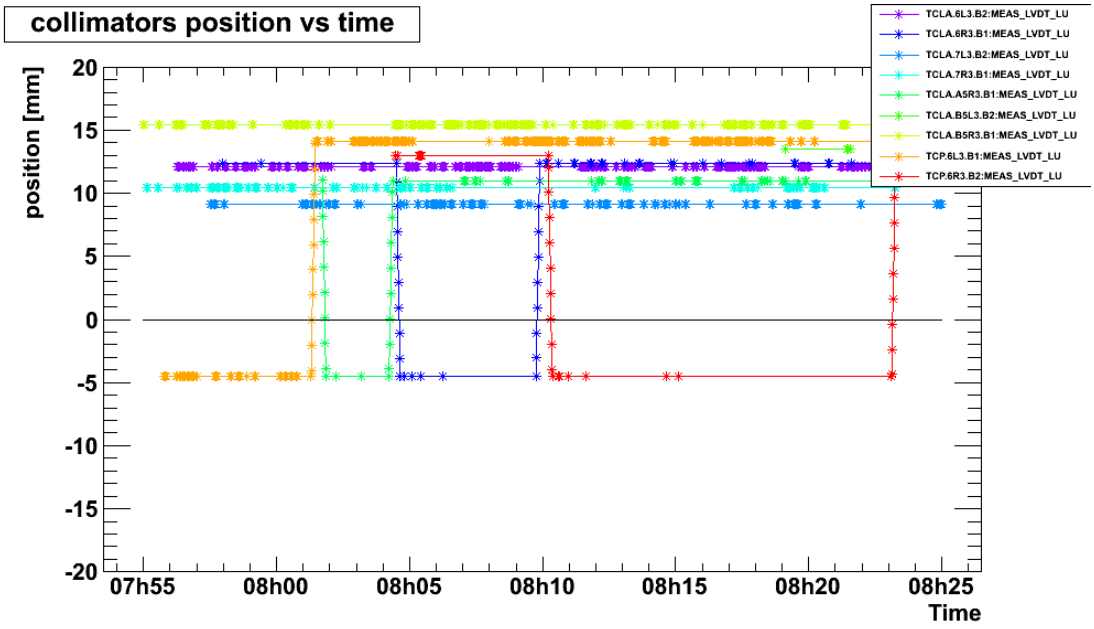

Figure A.11: Movement of different collimator jaws versus time during direct shots on collimators. The left jaws of four collimators were moved in then out successively. The zero represents the middle position of the two jaws of each collimator. Note that each jaw can move further than the middle.

Optics

The main optics functions of the LHC can be displayed for the selected section of the ring: the β function, the α function, and the dispersion. All other optics function can be displayed but no automatic display is implemented. The method is `plot_optics` and the processing is done by the `optics` module. The data and plots are stored as attributes *(cf. tab. A.3 and fig. A.13)*.

Saving

When displaying a loss, the limiting factor in running time is the downloading of data from database. In order avoid having to download the same dataset several time, the tool provides the option to *save* the dataset.

In order to allow maximum flexibility, the choice was made to save the dataset itself, instead of the processed objects such as plots. This way, the only difference in behaviour is that the data have to be loaded from file instead of downloaded; all other

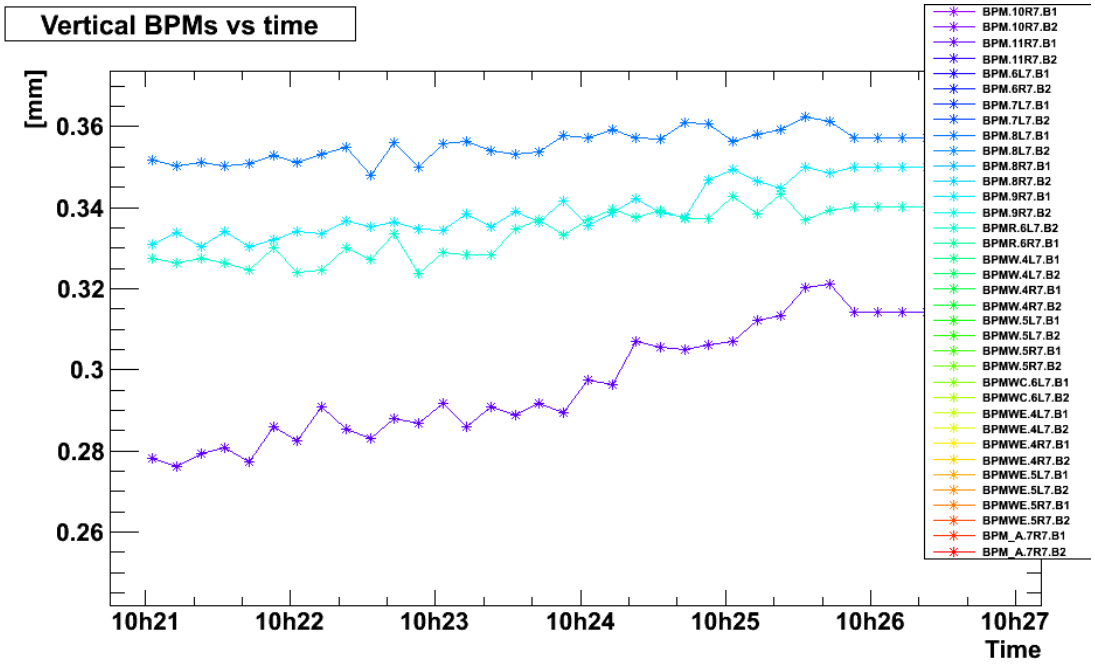

Figure A.12: Evolution of the position of the beam during a collimator scraping. The plot is zoomed on four relevant BPMs. The evolution can be correlated with the position of the collimator jaw.

functionalities remain unchanged.

The choice was made to us the default python module *shelve* to store the data (22). It creates a binary object with a dictionary structure. All relevant attributes describing the object are stored in one file. The file name is made of the plotting time printed in short format, the running sum and any additional string provided by the user. This is done by the `save` method. All files are saved in a folder called `[working_folder]\databank`.

In order to load saved data, an empty "analyse" object must be created by passing no argument. Then, the `load` method must be called, with the name of a saved file as argument. The automatic behaviour starts.

Others: printing elements, cleaning, hidden methods

It is possible to print the list of the elements ordered by DCUM on the terminal by calling the `print_elements` method, that is: the magnets, the collimators and the

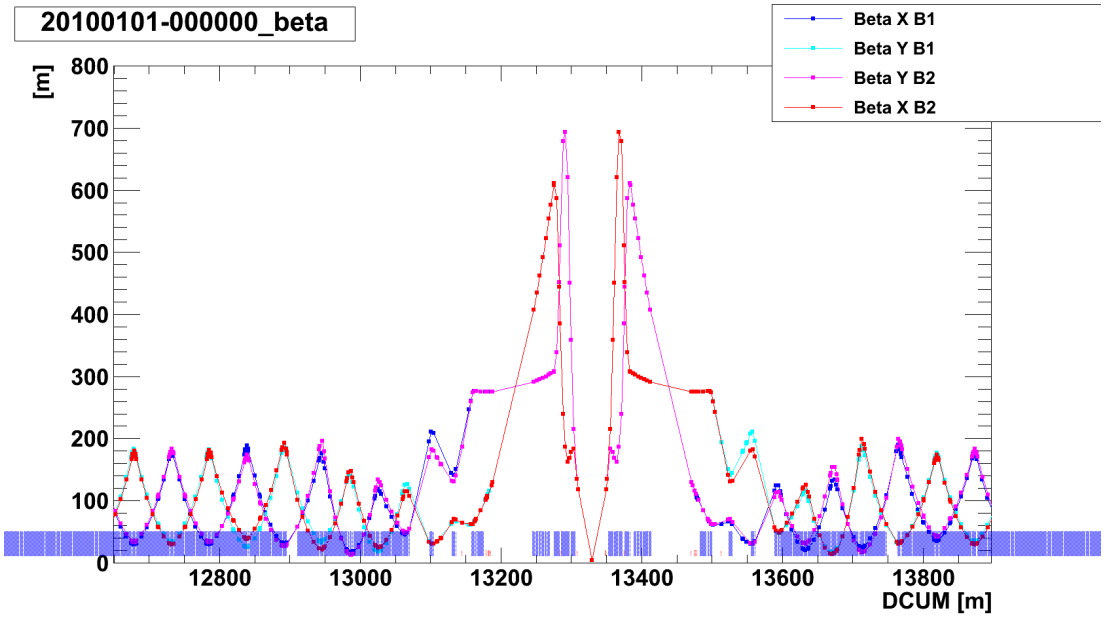

Figure A.13: β function around IP4. The periodicity in the arcs corresponds to the periodicity of the LHC cells. Note that the two planes X and Y are opposite (A quadrupole focusing in one plane is defocusing in the other), and that the two beams are opposite due to the way the field lines are directed in the magnet.

BLMs. The longitudinal position can then be displayed on the LHC plot by passing it to the `analysis.plot_DCUM` method.

Several "wrong" behaviours can happen when requesting variables: either can be nonexistent in the database, or have no data in time range. The `database` module and the `analysis` module have functions that prevent crashes when requiring fake variable names, and that will suppress variables with no data in time range, and clean the variable lists.

Several methods have a name starting with an underscore '_'. These methods are called by other methods, but are not supposed to be called by the user. When checking the methods of the object in interactive mode, the interpretor displays methods starting with an underscore in a different list, such that the list of methods that can be called by the user is cleaner.

A.6 Conclusion

Most of the objects and methods described here are meant to be ran interactively from the Python interpreter. This way, the user can call the `help` function on a method or object, and get explanations. The interactive environment also provides completion for variables, methods and attributes, and allows the user to access all his objects.

The source code is also accessible and helps understanding.

Appendix B

Cross-checks

B. CROSS-CHECKS

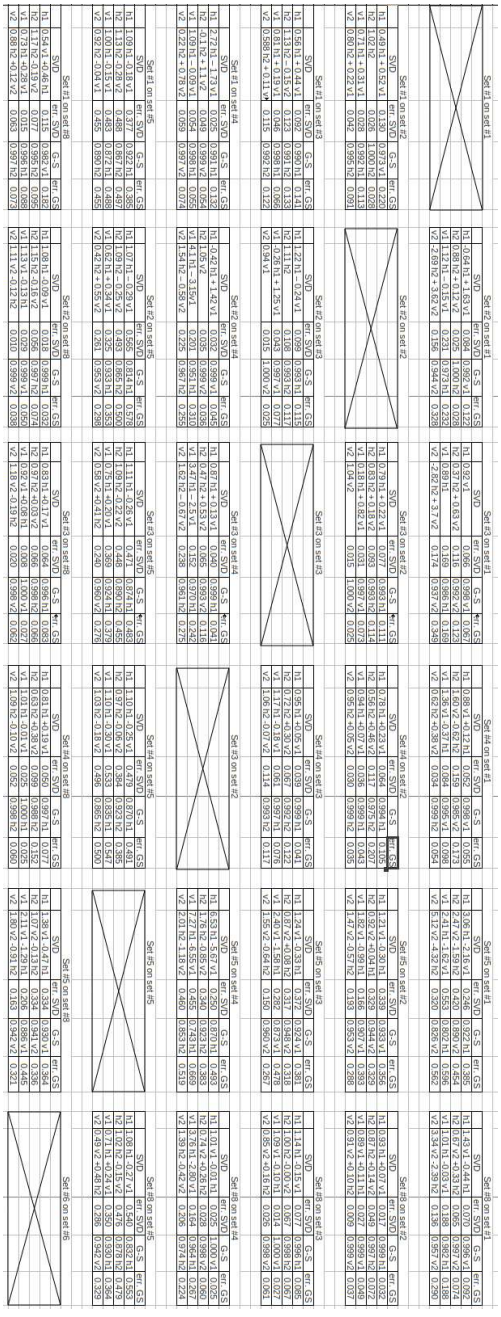

Figure B.1: Factors and error of the decompositions of all sets of loss maps of 2010 on themselves. Only one factor is given for G-S, and two for SVD (the other ones are always close to zero).

Set #1 on selected set

	SVD	err. SVD	G-S	err. GS
h1	0.96 h1 +0.04 v1	0.011	1.000 h1	0.015
h2	0.99 h2 +0.01 v2	0.010	1.000 h2	0.010
v1	1.41 h1 -0.45 v1	0.220	0.969 h1	0.244
v2	1.57 h2 -0.61 v2	0.154	0.977 h2	0.209

Set #2 on selected set

	SVD	err. SVD	G-S	err. GS
h1	1.02 h1 -0.02 v1	0.025	1.000 h1	0.025
h2	1.02 h2 -0.02 v2	0.012	1.000 h2	0.014
v1	1.09 v1 -0.10 h1	0.013	1.000 v1	0.026
v2	0.97 v2 +0.04 h2	0.016	1.000 v2	0.018

Set #3 on selected set

	SVD	err. SVD	G-S	err. GS
h1	0.60 h1 +0.36 v1	0.316	0.945 h1	0.327
h2	0.68 h2 +0.29 v2	0.265	0.962 h2	0.273
v1	2.33 v1 -1.45 h1	0.153	0.923 v1	0.375
v2	2.32 v2 -1.42 h2	0.108	0.935 v2	0.345

Set #4 on selected set

	SVD	err. SVD	G-S	err. GS
h1	0.47 h1 +0.47 v1	0.359	0.926 h1	0.376
h2	0.75 v2 +0.20 h2	0.341	0.939 v2	0.344
v1	2.36 v1 -1.50 h1	0.234	0.902 v1	0.423
v2	2.43 v2 -1.56 h2	0.158	0.916 v2	0.392

Set #5 on selected set

	SVD	err. SVD	G-S	err. GS
h1	1.02 h1 -0.02 v1	0.025	1.000 h1	0.025
h2	1.69 h2 -0.75 v2	0.202	0.963 h2	0.265
v1	1.09 v1 -0.10 h1	0.013	1.000 v1	0.026
v2	0.97 v2 +0.04 h2	0.016	1.000 v2	0.018

Set #6 on selected set

	SVD	err. SVD	G-S	err. GS
h1	1.07 h1 -0.13 v1	0.329	0.944 h1	0.330
h2	0.48 v2 +0.47 h2	0.333	0.936 v2	0.350
v1	1.96 v1 -1.06 h1	0.268	0.929 v1	0.366
v2	2.22 v2 -1.32 h2	0.182	0.932 v2	0.354

Set #7 on selected set

	SVD	err. SVD	G-S	err. GS
h1	0.63 v1 +0.33 h1	0.320	0.944 v1	0.330
h2	0.93 v2 +0.04 v1	0.321	0.947 v2	0.321
v1	1.35 h1 -0.42 v1	0.311	0.945 h1	0.326
v2	1.13 h2 -0.24 v2	0.431	0.900 h2	0.435

Set #8 on selected set

	SVD	err. SVD	G-S	err. GS
h1	1.29 h1 -0.36 v1	0.333	0.939 h1	0.344
h2	0.50 h2 +0.45 v2	0.343	0.933 h2	0.358
v1	2.25 v1 -1.36 h1	0.178	0.927 v1	0.366
v2	2.19 v2 -1.29 h2	0.189	0.933 v2	0.352

Set #9 on selected set

	SVD	err. SVD	G-S	err. GS
h1	0.73 v1 +0.22 h1	0.336	0.940 v1	0.340
h2	1.06 v2 -0.14 h2	0.329	0.944 v2	0.331
v1	2.11 v1 -1.20 h1	0.186	0.938 v1	0.339
v2	1.19 h2 -0.28 v2	0.397	0.916 h2	0.402

Set #10 on selected set

	SVD	err. SVD	G-S	err. GS
h1	1.05 h1 -0.05 v1	0.021	1.000 h1	0.024
h2	0.98 h2 +0.02 v2	0.021	1.000 h2	0.022
v1	0.57 v1 +0.43 h1	0.051	0.993 v1	0.114
v2	1.54 h2 -0.58 v2	0.144	0.980 h2	0.197

Set #11 on selected set

	SVD	err. SVD	G-S	err. GS
h1	0.96 h1 +0.04 v1	0.011	1.000 h1	0.015
h2	0.99 h2 +0.01 v2	0.010	1.000 h2	0.010
v1	1.41 h1 -0.45 v1	0.220	0.969 h1	0.244
v2	1.57 h2 -0.61 v2	0.154	0.977 h2	0.209

Set #12 on selected set

	SVD	err. SVD	G-S	err. GS
h1	1.36 h1 -0.40 v1	0.191	0.977 h1	0.213
h2	1.40 h2 -0.42 v2	0.064	0.993 h2	0.117
v1	1.02 h1 -0.04 v1	0.185	0.983 h1	0.185
v2	0.78 v2 +0.22 h2	0.060	0.997 v2	0.079

Set #13 on selected set

	SVD	err. SVD	G-S	err. GS
h1	1.20 h1 -0.26 v1	0.324	0.944 h1	0.330
h2	0.88 v2 +0.08 h2	0.300	0.954 v2	0.301
v1	1.91 v1 -0.98 h1	0.158	0.959 v1	0.279
v2	2.04 v2 -1.11 h2	0.109	0.959 v2	0.278

Set #14 on selected set

	SVD	err. SVD	G-S	err. GS
h1	0.75 v1 +0.19 h1	0.348	0.936 v1	0.351
h2	0.89 v2 +0.05 h2	0.319	0.947 v2	0.320
v1	1.87 v1 -0.95 h1	0.245	0.942 v1	0.332
v2	2.15 v2 -1.25 h2	0.190	0.936 v2	0.344

Set #15 on selected set

	SVD	err. SVD	G-S	err. GS
h1	0.84 v1 +0.09 h1	0.362	0.932 v1	0.362
h2	1.24 v2 -0.31 h2	0.321	0.944 v2	0.329
v1	1.78 v1 -0.87 h1	0.259	0.943 v1	0.330
v2	2.29 v2 -1.40 h2	0.155	0.931 v2	0.357

Set #16 on selected set

	SVD	err. SVD	G-S	err. GS
h1	1.16 h1 -0.25 v1	0.388	0.920 h1	0.392
h2	0.80 v2 +0.14 h2	0.334	0.942 v2	0.335
v1	2.37 v1 -1.51 h1	0.229	0.902 v1	0.423
v2	2.37 v2 -1.49 h2	0.174	0.919 v2	0.385

Set #17 on selected set

	SVD	err. SVD	G-S	err. GS
h1	1.38 h1 -0.41 v1	0.184	0.978 h1	0.208
h2	0.89 h2 +0.12 v2	0.019	0.999 h2	0.033
v1	1.04 v1 -0.04 h1	0.016	1.000 v1	0.019
v2	1.05 v2 -0.05 h2	0.035	0.999 v2	0.038

Set #18 on selected set

	SVD	err. SVD	G-S	err. GS
h1	1.22 h1 -0.31 v1	0.382	0.921 h1	0.389
h2	0.67 v2 +0.28 h2	0.342	0.938 v2	0.347
v1	2.38 v1 -1.51 h1	0.202	0.908 v1	0.409
v2	2.36 v2 -1.48 h2	0.173	0.920 v2	0.383

Set #19 on selected set

	SVD	err. SVD	G-S	err. GS
h1	0.78 v1 +0.17 h1	0.344	0.938 v1	0.346
h2	0.99 v2 -0.05 h2	0.329	0.944 v2	0.329
v1	2.16 v1 -1.27 h1	0.184	0.934 v1	0.350
v2	2.08 v2 -1.18 h2	0.195	0.940 v2	0.333

Set #20 on selected set

	SVD	err. SVD	G-S	err. GS
h1	0.85 v1 +0.09 h1	0.347	0.937 v1	0.348
h2	1.10 v2 -0.16 h2	0.327	0.944 v2	0.329
v1	2.22 v1 -1.33 h1	0.174	0.930 v1	0.359
v2	2.42 v2 -1.55 h2	0.165	0.916 v2	0.392

Set #21 on selected set

	SVD	err. SVD	G-S	err. GS
h1	1.34 h1 -0.38 v1	0.208	0.974 h1	0.226
h2	1.02 h2 -0.02 v2	0.025	1.000 h2	0.025
v1	1.06 v1 -0.06 h1	0.023	1.000 v1	0.027
v2	1.13 v2 -0.13 h2	0.043	0.999 v2	0.053

Set #22 on selected set

	SVD	err. SVD	G-S	err. GS
h1	1.03 h1 -0.03 v1	0.010	1.000 h1	0.013
h2	1.21 h2 -0.22 v2	0.059	0.997 h2	0.078
v1	1.10 v1 -0.10 h1	0.010	1.000 v1	0.025
v2	1.16 h2 -0.17 v2	0.034	0.999 h2	0.051

Set #23 on selected set

	SVD	err. SVD	G-S	err. GS
h1	0.98 h1 +0.02 v1	0.005	1.000 h1	0.006
h2	1.06 h2 -0.06 v2	0.014	1.000 h2	0.019
v1	0.86 h1 +0.14 v1	0.127	0.991 h1	0.131
v2	1.52 h2 -0.57 v2	0.208	0.969 h2	0.246

Set #24 on selected set

	SVD	err. SVD	G-S	err. GS
h1	1.01 h1 -0.01 v1	0.011	1.000 h1	0.011
h2	0.98 h2 +0.02 v2	0.004	1.000 h2	0.007
v1	1.40 h1 -0.44 v1	0.205	0.973 h1	0.230
v2	1.49 h2 -0.53 v2	0.199	0.972 h2	0.233

Set #25 on selected set

	SVD	err. SVD	G-S	err. GS
h1	0.96 h1 +0.04 v1	0.011	1.000 h1	0.015
h2	0.99 h2 +0.01 v2	0.010	1.000 h2	0.010
v1	1.41 h1 -0.45 v1	0.220	0.969 h1	0.244
v2	1.57 h2 -0.61 v2	0.154	0.977 h2	0.209

Set #26 on selected set

	SVD	err. SVD	G-S	err. GS
h1	1.33 h1 -0.36 v1	0.177	0.980 h1	0.195
h2	1.50 h2 -0.54 v2	0.173	0.977 h2	0.213
v1	0.75 v1 +0.26 h1	0.027	0.998 v1	0.066
v2	1.11 v2 -0.12 h2	0.012	1.000 v2	0.030

Figure B.2: Factors and error of the decompositions of all loss maps of 2011 on the average set of selected loss maps used for decomposition of real data. Only one factor is given for G-S, and two for SVD (the other ones are always close to zero).

Glossary

`API`: Application Programming Interface. Ensemble of codes and functions used to create related softawre applications.

`BCT`: Beam Current Transformer. Beam instrument measuring the intensity in one beam pipe.

`BLM`: Beam Loss Monitor. Any monitor, sensitive to a secondary shower of mixed particles coming from protons lost in the LHC. Each monitor is associated to a specific loss location.

`BPM`: Beam Position Monitor.

`DCUM`: Longitudinal coordinate [m] along the LHC describing the position of every element. It is calculated from the interaction point #1 clockwise.

`G-S`: Gram-Schmidt process. Vector manipulation process creating an orthonormal set of vectors *(cf. § 3.3)*.

`LHC`: Large Hadron Collider *(cf. § 1.2)*

`IRX`: Insertion Region #X. Short parts of the accelerator where the majority of the beams operations take place (collision, acceleration, cleaning, measurements...) by opposition to the arcs, where the beam is carried. There are 8 IRs in total.

`PL/SQL`: Procedural Language / Structured Query Language. Oracle Corporation's procedural extension language for SQL and the Oracle relational database.

`RS`: Running Sum. Predefined integration interval used as a sliding integration window by the BLM electronic to evaluate the time duration of a beam loss *(cf. tab. 2.1)*.

`RSD`: Relative Standard Deviation [no unit]. Standard deviation of a distribution divided by the average of the same distribution.

`SQL`: Structured Query Language. An international standard for database manipulation.

`SQL`: Singular Value Decomposition. Matrix inversion technique used in this work *(cf. § 3.2)*.

`TCP`: Primary collimator. Element of the accelerator which is the closest to the particle beam.

`TCT`: Tertiary collimator.

`Timestamp`: Association of a date and a time (with a precision of one second) corresponding to one value in a database.

Bibliography

[1] "LHC Design Report", CERN-2004-003-V-1. p 3

[2] E. B. Holzer, B. Dehning et al. "Beam Loss Monitoring for LHC Machine Protection", proceedings, TIPP 2011. p 11

[3] R. Alemany, M. Lamont, S. Page, "LHC MODES", Functional specification, 11-2007, LHC-OP-ES-0005. p 8, 9

[4] B. Puccio, R. Schmidt, J. Wenninger "Beam interlocking strategy between the LHC and its injector", proceedings, ICALPECS 2005. p 11

[5] R. Assman *et al.*, "The final collimation system for LHC", CERN-LHC-Proj.-Report-919, 2006. p 11, 13, 15, 16

[6] R. Bruce, R. Assmann, "Collimator settings in 2012", presented at the LHC Machine Committee, 28/03/2012. p 14, 15

[7] Markus Stockner, "Beam Loss Calibration Studies for High Energy Proton Accelerators". PhD thesis, CERN-THESIS-2008-099 . p 22

[8] A. Arauzo and C. Bovet, "Beam loss detection system in the arcs of the LHC". Technical Report, CERN-SL-2000-052 BI. p 22

[9] D. Kramer, "Design and Implementation of a Detector for High Flux Mixed Radiation Fields". PhD thesis, CERN-THESIS-2008-090. p 3, 23, 24

[10] C. Zamantzas, "The Real-Time Data Analysis and Decision System for Particle Flux Detection in the LHC Accelerator at CERN", CERN-thesis-2006-037. p 29

[11] E. Nebot et al., "Handling of BLM abort thresholds in he LHC", IPAC 2011, WEPC170. p 29

[12] Todd Will, UW-La Crosse, "Introduction to the Singular Value Decomposition" http://www.uwlax.edu/faculty/will/svd/index.html p 37

[13] B. Autin, Y. Marti, "Closed orbit correction of A.G. Machines using a small number of magnets". Technical report, CERN-ISR-MA-73-17. p 43

[14] "LHC e-Logbook", LHC operation group, BE-OP, CERN https://ab-dep-op-elogbook.web.cern.ch/ab-dep-op-elogbook/elogbook/eLogbook.php p 49

[15] "Horizontal and vertical blow-ups", private communication with Daniel Wollmann, BE-APB, CERN. p 49

[16] All available views, C. Roderick, BE–CO–DM, http://lhc-logging.web.cern.ch/lhc-logging/software/public_data_access_views.jpg p 133, 135, 136

[17] LHC Logging Project, C. Roderick, BE–CO–DM, http://lhc-logging.web.cern.ch/lhc-logging/software/default.htm p 133

[18] ConfigParser module, python documentation, http://docs.python.org/library/configparser.html p 134

[19] TSQLServer, ROOT documentation, http://root.cern.ch/root/html528/TSQLServer.html p 134, 135

[20] Logging Data Extraction Client, Command Line API, https://espace.cern.ch/be-dep/CO/DM/CALS/other/CommandLineManual.pdf p 136

[21] TGraph, ROOT documentation, http://root.cern.ch/root/html528/TGraph.html p 141

[22] shelve module, python documentation, http://docs.python.org/library/shelve.html p 160